Mesoscopic Simulation of Droplet Dynamics in Confinements and Porous Media Flows

A thesis submitted in partial fulfillment of the requirements for the

degree of

DOCTOR OF PHILOSOPHY

By

Saurabh Bhardwaj

DEPARTMENT OF MECHANICAL ENGINEERING
INDIAN INSTITUTE OF TECHNOLOGY GUWAHATI
GUWAHATI 781039, INDIA
November, 2018

CERTIFICATE

It is certified that the work contained in the thesis entitled **"Mesoscopic Simulation of Droplet Dynamics in Confinements and Porous Media Flows"** by **Saurabh Bhardwaj**, has been carried out under my supervision and that this work has not been submitted elsewhere for a degree.

(Amaresh Dalal)
Associate Professor
Department of Mechanical Engineering
Indian Institute of Technology Guwahati

November, 2018

ABSTRACT

Multiphase-multicomponent flows in its general form can be defined as any fluid flow which is having two or more phases or components and their interaction influences the interface between them. The topic of multiphase-multicomponent flows is having a vast field of application owing to the fact that it is ubiquitous in industry as well as in nature. Some practical examples of multiphase fluid problems are liquid water transport in the catalyst layer during fuel cell operation, recovery and enhanced recovery of petroleum resources from reservoirs, non-aqueous phase liquid contamination of groundwater, soil water behavior and surface wetting phenomena. Therefore, it is worth reflecting the diverse and universal challenges of multiphase flows. In several multiphase-multicomponent applications, the presence of a solid wall is frequently observed and it makes the physics of multiphase flow more complex. The property which primarily affects the fluid flow characteristics on solid wall is known as wettability i.e., the ability of any solid surface to attract or repel the fluid and allows the fluid to spread or contract on the solid surface. In context to multiphase-multicomponent flows, the study of fluid flow through porous media has always been an important field of research. The flow of immiscible fluids through porous media e.g., fuel cell, as compared to single-phase flow, is much more complicated and is still not well understood in many areas due to the complex interactions of different fluid phases in porous media.

The present research is a step put forward to extensively explore the detailed insight of flow of immiscible liquids inside a channel. A lattice Boltzmann Shan-Chen model is implemented to carry out the study because of its ability to capture multi-fluid physics including phase-change and interfacial dynamics with relative ease. In addition, the lattice Boltzmann method algorithm can be easily parallelized which allows larger problems to be simulated quickly. A very few researchers have focused on the complex physics of droplet flow dynamics inside a channel and considered the effect of surface wettability. Moreover, most of the studies available in the literature considered the two-dimensional domain for the analysis. Therefore, it is important to investigate the droplet dynamics inside a three-dimensional wetted channel in detail considering all aspect of physical problem. With this motivation, the objective of the present work is to study the effect of surface characteristics of channel wall

on the droplet displacement and spreading behavior in different scenarios and to investigate the dynamics of droplet deformation through a partially obstructed pore confinement as well as to analyze the behaviour of two-phase flow passing through a porous domain under different conditions.

Firstly, the numerical analysis of the dynamic behavior of sliding droplets on a wall of a rectangular channel considering wetting effects has been investigated. The study includes the coalescence of two equal size droplets placed on a channel wall along its length under the action of gravitational force. The effects of center distance between the droplets and capillary number have been illustrated in the form of evolution of wetted area and wetted length. The main focus of this study is to investigate the time taken by the two droplets to start coalescence for different parameters. In this study, it is revealed that the type of wettability plays a crucial role in the coalescence of two droplets in a channel wall. In addition to this, it is also noticed that the two droplets coalesce more quickly in case of mixed wettability compared to uniform hydrophilic wettability for a certain capillary number. Another investigation which is carried out is to examine the effect of center distance between two droplets and it is observed that an increase in center distance increases the time of coalescence.

In microfluidic applications, sometimes a condition arises when the surface is not completely smooth throughout the domain but it is having some irregularities. One of the different types of irregularities can be assumed as groove on the flat surface. The effect of these grooves is that it behaves as an irregularity in the path of fluid flow and the fraction or complete fluid may get entrapped inside the groove which is highly undesirable in the application of ink-jet printing, spray painting and coating etc. An investigation has been conducted to study the dynamic droplet behavior on a wetted flat vertical wall as well as grooved wall of a rectangular microchannel. The study reveals that in case of flat vertical wall, as the viscosity ratio increased, the displacement of droplet on hydrophobic surface is faster and more deformation of the droplet occurs, and finally droplet gets detached from the wall. A reverse effect is observed in the case of hydrophilic wall surface. The investigation also shows that as the capillary number increased, the displacement of droplet on the surface is much faster than the low capillary number. Additionally, an attempt has been made to sweep out the trapped volume of droplet fluid inside groove. To explore the physics associated with sweeping phenomena, a parametric study has been carried out to explore the physics of sweeping of the previously entrapped fluid out of the groove created on one of the walls of a three-dimensional duct. The analysis shows that the sweeping of entrapped fluid out of the groove largely depends on the groove surface wettability, capillary number and groove height.

The distortion of an immiscible liquid droplet in a stream of another liquid has been a major fluid mechanics issue for last 100 years . It is to be noted that in

a wide-range of industrial applications, the phenomenon of droplet dynamics past solid obstacles can be found very frequently and thus, the study of the droplet past a solid target has recently been an active field of research for its great importance in many fields. This study presents droplet dynamics due to the capillarity-wettability interaction through a partially obstructed channel confinement based on a mesoscopic, two-phase lattice Boltzmann model. To explore the dynamic behavior of droplet motion past an obstruction, the effect of capillary number and surface wettability, including obstruction size and architecture, are elucidated. In this work, single spherical obstruction, and different spherical agglomerate structures are considered. The mesoscale simulations exhibit interesting two-phase flow physics and pattern formations due to droplet pinching, break up, and surface adherence owing to the underlying wettability-capillarity characteristics. This study further reveals an interesting trade-off, between the time required for the bulk droplet fluid to pass by and/or through the obstruction and the fraction of droplet fluid volume adhering to the surface, depending on the combination of the capillary number and surface wettability.

The fundamental study of fluid flow inside porous media being an important topic of research has attracted many researchers to explore the physics. The flow through porous media is critically important to many scientific and engineering applications such as petroleum engineering, groundwater hydrology, carbon capture utilization and storage and specifically in fuel cells. A number of investigations can be found in literature describing fluid flow through porous media but still there is large scope for further exploring the physics associated with fluid flow through packed-bed porous medium. Therefore, the aim of the present problem is to analyse the advancement of fluid front through pores created between porous beds and drain out the other fluid. The effects of pressure difference, porosity and different wetting conditions have been explored.

Finally, the thesis concludes with a summary of the main findings and recommendations for future work.

Dedicated to my Father

Acknowledgements

My deep gratitude goes first to Prof. Amaresh Dalal, who expertly guided me throughout the course of Ph.D. and who shared the excitement of four years of discovery. His unwavering enthusiasm for physics and publications kept me constantly engaged with my research and his personal generosity helped make my time at IIT Guwahati.

I would like to express the deepest appreciation to my Doctoral committee chair, Prof. Gautam Biswas, who has the attitude and the substance of a genius. He continually and convincingly conveyed a spirit of adventure, encouragement and knowledge in regard to research. Without his guidance and persistent help this dissertation would not have been possible. I would also like to thank Prof. Anoop K. Dass and Prof. Subrata K. Majumdar for their service on my doctoral thesis committee and for their suggestions and insightful comments on my work.

I am very grateful to Professor Partha P. Mukherjee from Purdue University, USA for a fruitful discussion on lattice Boltzmann method and helping me to understand the complex methodology and physics related to LBM and porous media flows. My sincere thanks goes to Prof. Arnab De and Prof. Ganesh Natarajan for making me understand the basic concepts of fluid mechanics and CFD as a part of my course work at IIT Guwahati. My special thanks goes to Prof. Pitambar Randive for introducing me to LBM and encouraged me to take LBM as a simulation tool for conducting research. He helped me a lot in the initial phase of my Ph.D. when I was new to the field of LBM. I also extend my thanks to all staff members and Research Scholars of Department of Mechanical Engineering, IITG for helping me one way or another.

These acknowledgements would not be complete without mentioning my research

lab colleagues Preetirekha, Mukul, Vinod, Subrat and all M.Tech. students of Anupravaha Lab. Special thanks also goes to Dr. Sathisha H. M. and Dr. Jai Manik for the personal and professional discussion on various topics. It was really a great pleasure working with all of them. A person, who is not directly involve to my Ph.D. research but made my stay at IITG memorable and homely, is Mrs. Soumita Dalal wife of Prof. Amaresh Dalal. She has always been there for me with her supporting hands whenever I needed it the most during various fastivals and occassions. She always treated us like her family member and provide us homely atmosphere at IITG Campus.

Finally, I take the opportunity to thank my many friends and family members whose support and encouragement was worth more than I can express on paper. I am especially grateful to my parents, who supported me emotionally and financially. I always knew that you believed in me and wanted the best for me. I would also like to thank my wife for motivating and supporting me in all phase of my life. I am very grateful to my elder brother who supported my decision to quit a regular job and join IITG for my Doctorate. He is like a father to me who was always there for me in all ups and downs in the journey of my Ph.D.

Saurabh Bhardwaj

Contents

List of Figures

List of Tables

Nomenclature

a_0	Initial droplet height
A	Wetted area
$\frac{A}{A_0}$	Dimensionless wetted area
b	Wetted length
$\frac{b}{b_0}$	Dimensionless wetted length
c	Lattice speed
C_d	Center distance between droplets
f_i	Probability density function
f_i^{eq}	Equilibrium density function
$\mathbf{g}$	Acceleration due to gravity
g_{1w}	Interactive force strength between non-wetting phase and wall
g_{2w}	Interactive force strength between wetting phase and wall
g_k	Interactive strength between the component k and wall
$G_{k\bar{k}}$	Interactive potential
M	Viscosity ratio
Ma	Mach number
n_w	Number density of the wall
Q	Collision integral
R	Droplet radius
r	Obstruction radius
t	Lattice time
t_{ps}	Passing time
$\mathbf{u}$	Macroscopic velocity of particle
V_f	Deposited droplet fluid volume fraction

Greek Symbols

ϕ	Porosity
θ	Contact angle
μ	Dynamic viscosity
ν_k	Kinematic viscosity of k^{th} component
δt	Change in time
ρ_k	Density of k^{th} component
σ	Surface tension
τ	Relaxation parameter
ψ_k	Effective mass density function
ω	Collision frequency
Ω	Collision operator

Abbreviations

BGK	Bhatnagar-gross-Krook
BCC	Body centered cubic
Ca	Capillary number
CFD	Computational fluid dynamics
CE	Chapman-Enskog
CL	Catalyst layer
EOR	Enhanced oil recovery
FCC	Face centered cubic
FDM	Finite difference method
FVM	Finite volume method
FEM	Finite element method
GDL	Gas diffusion layer
LB	Lattice Boltzmann
LBM	Lattice Boltzmann model
LBE	Lattice Boltzmann equation
LGA	Lattice gas automata

LGCA	Lattice gas cellular automata
MPI	Message passing interface
MD	Molecular dynamics
N-S	Navier-Stokes
NWP	Non-wetting phase
PDE	Partial differential equations
PEFC	Polymer electrolyte fuel cell
PEMFC	Proton exchange membrane fuel cell
S-C	Shan and Chen model
SC	Simple cubic
WP	Wetting phase

Chapter 1

Introduction

Multiphase-multicomponent flows in its general form can be defined as any fluid flow which is having two or more phases or components and their interaction influences the interface between them. Multiphase-multicomponent phenomena and flows can involve single component multiphase fluids, e.g., water and its own vapour, and multi-component multiphase fluids, e.g., oil/water. The topic of multiphase-multicomponent flows is having a vast field of applications in different technological and engineering disciplines as well as natural phenomena [1]. Some practical examples of multiphase flow problems are the recovery and enhanced recovery of petroleum resources from reservoirs, non-aqueous phase liquid contamination of groundwater, soil water behaviour, surface wetting phenomena, fuel cell operation, and the movement and evolution of clouds [2]. In a more realistic condition, every processing technology must deal with the multiphase flow, for example, cavitating pumps, turbines, electrophotographic processes, papermaking etc. So, it is important to clearly predict the fluid flow behaviour of these processes in contrast to the efficiency and effectiveness of those processes. For example, the effective flow of toner is a major factor in the quality and speed of electrophotographic printers. Multiphase flows can also be found universally in our environment whether one considers rain, snow, fog, mudslides, sediment transport, debris flows, and countless other natural phenomena. The very critical biological and medical flows are also multiphase, from blood flow to semen. So it is worth to say that multiphase-multicomponent flow has a very wide area of application for having an attention from a research point of view.

In the context of multiphase-multicomponent flows, the study of flow through porous media has always been an important field of research. Moreover, it can also be identified, in nature as well as technology, in several phenomena during flows in material that can be designated as porous media. The filtration of water in the soil, as well as the flow of groundwater in aquifers, are first straightforward examples. In petroleum engineering, the rocks of an oil reservoir can be considered as a porous medium, as they have some void space and they are not consolidated. Thus, in this field, the understanding of the fluid transport inside the reservoir is fundamental to figure out the amount of unrecovered oil and the technical parameters to be used in the design of the extraction system. Accordingly, the study of flows in oil reservoir has been subject of strong research in literature [3] and it has been definitely the field of application, which has given the greatest contribution in the development of porous media theory. A further and captivating application of porous media theory in energy engineering is the study of flows through the porous electrodes of fuel cells [4]. In case of multiphase flows in a porous medium, the Darcy law can be extended by means of the concept of relative permeability, which tries to take into account the effect of the presence of the other fluids. In this case, an important effect is given by the wetting conditions of the porous medium, and also by other dimensionless parameters.

1.1 Lattice Boltzmann method

Transport equations in fluid flow and heat transfer can be simulated by different modes of scales (e.g., macroscopic scale, microscopic scale and mesoscopic scale). In a conventional mode of numerical analysis or in computational fluid dynamics (CFD), transport equations are solved on a macroscopic scale and partial differential equations (PDE) like Navier-Stokes (N-S) equations are used. These equations are very difficult to solve due to non-linearity involved in convective terms. The different numerical schemes are used to solve these equations e.g., finite difference method (FDM), finite volume method (FVM) and finite element method (FEM); PDE is converted to a system of algebraic equations and solve these equations iteratively. The major issue in these numerical methods is to maintain the stability of the system. These are highly unstable schemes.

As it is well known that any medium is considered to be made of small particles such as atoms and molecules and these particles continuously interacting with each other in the form of collisions. Molecular dynamics (MD) is a microscopic approach where the fluid dynamics is modelled based on the collisions and other interactions between the individual molecules. The basic governing equation in this approach is Hamilton's equation. In this approach, location and velocity of each particle are identified at each time step. One can recover the macroscopic properties of these models by using statistical mechanics. But by doing so one has to deal with the too much data to solve a problem that is interesting on a macroscopic scale and hence the major drawback in MD models is the excessive computational resources and data reduction process, otherwise MD is simple and can be used to handle the complex problems without using any extra ingredients.

The approach which bridges the gap between previously defined two approaches

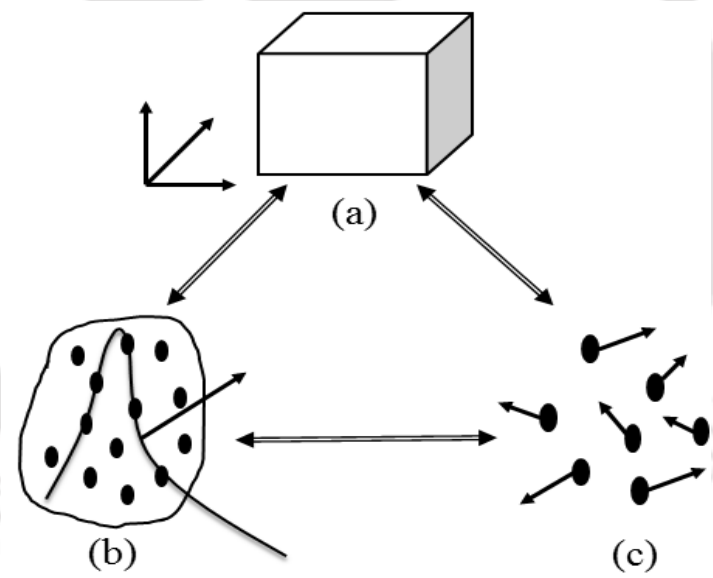

Figure 1.1: Different scale models, (a) Macroscopic scale, (b) Mesoscopic scale, (c) Microscopic scale

(macro and micro-scales) is known as the mesoscopic scale. In this approach, neither continuum approach nor tracking of individual particles is required but the behaviour of a collection of particles as a unit is considered. This collection of particles is represented by the property called as a distribution function. The method which is used to connect the macro-scale and micro-scale is known as the lattice

Boltzmann method (LBM). It is based on microscopic models and mesoscopic kinetic equations. The fundamental idea of the LBM is to construct simplified kinetic models that incorporate the essential physics of microscopic processes so that the macroscopic averaged properties obey the desired macroscopic equations.

1.2 Comparison of LBM with N-S equations solver

The LBM is based on discrete equations derived from the well known Boltzmann equation in kinetic theory. The basic quantity in LBM is the single point distribution function whose evolution is governed by the corresponding equation. The discretization in LBM is chosen in such a way that the resulting relevant hydrodynamics does not suffer any discrete lattice effects. The Navier-Stokes equations are shown to be a result of this kinetic description of a fluid at the so-called hydrodynamic regime, with sufficiently long spatial and temporal variations. Once this quantity is solved, the familiar hydrodynamic quantities (such as the fluid velocity, density and pressure) can be obtained via similar post-processing. The advantages of the LBM over the N-S equations based solver are given below.

1. N-S equations contain nonlinear convection terms whereas the convection terms in LBM are linear.

2. N-S equations are second order PDEs whereas LBM consists of a set of first-order PDEs (kinetic equations).

3. To obtain pressure, CFD solvers use the pressure Poisson equation. In LBM, the pressure is calculated locally via an equation of state.

4. LBM depends on lattice structure; N-S equations are in vector form which does not depend on the coordinate and grids.

5. Lattice Boltzmann Equation (LBE) is basically the discretized kinetic equation and N-S equations, however, can take integral or differential forms.

6. The N-S solver normally uses an iterative procedure to obtain a converged solution; the LBM is explicit in form and does not require iterative procedures.

7. The Boltzmann equation is kinetic-based, and small-scale details can be dealt with in this method. Boundary conditions can be intuitively specified and expressed in the form of particle distribution functions.

8. The scheme being local in space and explicit in time, LBM is scalable for parallel computing.

Adding to all these advantages to LBM, some limitations of LBM are also there. Regular square grid and numerical instabilities for small viscosity are the major limitations of LBM and also, it is difficult to analyze the high Mach number flows with LBM.

1.3 Literature review

In recent years, the improvement of the calculating capacity of computers and the development of new numerical schemes have made it possible to approach the study of fluid dynamics problem by solving directly the governing equations. The latest class of algorithm to solve fluid flow is a lattice Boltzmann method which is based on the kinetic theory of gases.

1.3.1 Review on lattice Boltzmann method

LBM works as a mediator between the macroscopic and microscopic scale approach. Thus, the LBM provides a lower level description compared to the N-S equations, but a higher level description with respect to molecular dynamics, in which the particle collisions are directly taken into account. Therefore, LBM is known as a mesoscopic model. Historically, Broadwell [5] performed the study by considering the discrete velocity models for the first time in this direction, where the velocity is discrete but space and time are still continuous. Later, Kadanoff and Swift [6] introduced a master equation with a continuous time and leading to sound waves. In 1973, a fully discrete model (HPP) on a square lattice was defined by Hardy et al. [7, 8] which allows the complex analyses of fluid flows. However, the HPP model was not able to reproduce the non-linear term as well as the dissipative term of the N-S equations due to a lack of isotropy of the lattice. This drawback of the HPP model was first resolved by Frisch et al. [9] for the two-dimensional case and then

for the three-dimensional case by d'Humires et al. [10]. There are two possibilities which can define the evolution rules, named as lattice gas automata (LGA) and the lattice Boltzmann equation (LBE). The roots of LBM has been found in the model developed in the seventies which is known as lattice gas automata [7, 9, 11]. It is a kinetic model with discrete lattice and discrete time.

LGA is an approach in which the variables are the boolean populations. These boolean variables indicate the presence or the absence of particles in the link of the lattice. The evolution is essentially defined by a set of collision and streaming rules, possessing suitable conservation laws. Moreover, lattice models are extensively used for parallel processing due to the locality of the updating rules. The microscopic nature of the LGA resulted in the simulations to be intrinsically noisy [12, 13] and proved to be costly in terms of memory and time taken for the computations. McNamara and Zanetti [12] were the first to introduce the LBM in 1988. Their main focus was to overcome the main drawback of LGA, i.e., statistical noise which was achieved by replacing the boolean variables with the single particle distribution functions. With this replacement, the statistical noise is removed because the distribution function is by definition an ensemble averaged which is a smooth quantity [14]. In this approach, individual particle motion and correlations among them are neglected and distribution functions in the kinetic equations are introduced, which make LBM numerically much more efficient than their statistically noisy cellular automata counterparts. They also presented an estimate, according to which LBM is computationally efficient in the low Reynolds number region. But, no direct generalization to the three-dimensional face-centred-hyper-cubic (FCHC) has been achieved and change in viscosity is not possible by this method since it uses the collision rules from lattice gas cellular automata (LGCA) models. In the LBM approach, the collision parameter is replaced by a Bhatnagar-Gross-Krook (BGK) collision term [15] with one parameter called relaxation parameter. Use of this lattice BGK model makes the computations more efficient and allows flexibility of the transport coefficients. This is the first sign of the connection between BE and LBE. In addition to this, He and Luo [16, 17] have shown that the LBE is a special type of discretization of the BE. Another problem is to recover the macroscopic equations from LBE which is made possible by Chapman-Enskog (CE) expansion [18].

LBM mesoscopic approach has been adopted by many researchers to analyze

the multiphase-multicomponent flows. The main advantage of using LBM is that it is not required to track the interface location but it is inherently being tracked from the underlying lattice if a proper interaction between particles is taken into account. Many models have been proposed by many researchers for the analyses of multiphase flows. The very first method to analyze multiphase-multicomponent flow with LBM was given by Gunstensen et al. [19] which was based on the model given by Rothman and Keller [20]. The density and viscosity variations were considered by Grunau et al. [21] which was the extension of [19]. This model is also known as a colour model because, in this model two, red and blue, particle distribution functions were considered to represent two fluids. But, the major drawbacks of the model proposed by Gunstensen et al. [19] were the time-consuming calculations of local maxima due to redistribution of coloured density at each node and another was the anisotropic surface tension due to perturbation step with the redistribution of coloured distribution functions which induces the unphysical vortices near interfaces. This model is further modified by D'ortona et al. [22] in 1994 by replacing the recolouring step by an evolution equation. A very simplified model for multiphase-multicomponent flows has been given by Shan and Chen [23] which is based on a fictitious interaction potential. This model has been revised by Shan and Doolen [24] in 1995. In this model, microscopic interactions have been used to modify the surface tension related collision operator. This model improves the isotropy of the surface tension and the separation of fluid phases or components is automatic [25]. This has proved to be a better numerically efficient model compared to original LBM multiphase models. Swift et al. [26, 27] have proposed a model using the free energy approach in 1995 in which equilibrium distribution can be defined consistently based on thermodynamics. It is an important improvement compared to previous models that are based on phenomenological models of interface dynamics and suitable for isothermal multicomponent flows. Both models (Shan-Chen and free energy) shared similar drawbacks: spurious currents at the interface and limited density ratios. Sbragaglia et al. [28] has proposed an improvement in Shan-Chen model to overcome its drawback by extending the range of the interactions and according to Yuan and Schaefer [29], improvement can be made by changing the form of the interaction potential. An improvement in the free energy model was suggested by Zheng et al. [30] by solving the original problem of the violation of Galilean invariance.

Although each of the above LBM multiphase models was built on different physical pictures and each has a quite different appearance, a recent study by He et al. [31] showed that all of them have an origin in the kinetic theory. To be specific, all these models can be derived by discretizing the continuous Boltzmann equation with certain approximations. Some of these approximations turn out to be unphysical and lead to certain unsatisfactory features, such as the spurious current around interfaces and the lack of Galilean invariance. He et al. [32] further suggested that an improved LBM scheme for multiphase flow can be derived by systematically removing these unphysical approximations. In this model, single particle distribution function is replaced by two distribution functions: one for tracking the pressure and velocity fields and the other for the density field. In this way, this model proved to be a more numerically and thermally stable and consistent model. It is already mentioned above that these LBM models are limited to small density ratios less than 10 due to numerical instability. High density and viscosity ratios can be achieved by considering models given by Inamuro et al. [33] and Lee and Lin [34] by improving the models given by Swift et al. [26, 27] and He et al. [32] respectively but the drawback of these models is higher complexity and more computational cost.

1.3.2 Review on droplet displacement

Several studies have been conducted to understand the physics of displacement of a three-dimensional immiscible droplet on a wettable surface by many researchers experimentally as well as numerically. The phenomenon of displacement of immiscible fluid has attracted many researchers due to its application in enhanced oil recovery. The effect of capillary number, droplet sizes and different wettability scenarios have been examined on the displacement of three-dimensional immiscible droplet keeping viscosity ratio constant. Till now, a very few studies have been performed to see the effect of different viscosity ratios on the displacement of a three-dimensional immiscible droplet on a wettable wall through a duct. The notable work in this context has been done by Dimitrakopulos and Higdon [35]. In their study, a series of numerical experiments have been conducted to investigate the displacement behaviour of three-dimensional fluid droplets in a flow which is driven by the pressure gradient. The three values of viscosity ratio (i.e., 0,1 and 10) have been considered for this study. In this analysis, it was observed that the droplet displaces easily as

the viscosity of the droplet increases and the high flow rate is required to displace the droplet when the viscosity of the droplet is zero. Schleizer and Bonnecaze [36] have analyzed the dynamic behaviour of a two-dimensional immiscible droplet attached to a wall. The flow is driven by shear or pressure gradient considering negligible inertial and gravitational forces. The effect of capillary number, droplet size and viscosity ratio have been studied in this analysis. The effect of three different viscosity ratios (i.e., 0.125, 1 and 8) have been considered to study the displacement of the droplet. It was found that as the viscosity ratio increases, the deformation of the droplet also increases but up to a point beyond which an infinite viscosity ratio can be considered. It was also observed that as the capillary number increases the deformation of the droplet also increases until a critical value. Recently, Randive and Dalal [37] have simulated the displacement of a three-dimensional immiscible droplet on various wettabilities in a microchannel by S-C lattice Boltzmann method using gravitational force as the driving force. The physics of the droplet motion explored considering various parameters such as capillary number, droplet size and viscosity ratios. In this study, the viscosity ratios are considered in the range of 1-5. They have found that the displacement of a droplet on the hydrophobic surface for higher values of viscosity ratios is faster. It was also observed that the effect of viscosity ratio on the displacement of the droplet depends on capillary number also. For low values of capillary number, the effect of viscosity ratio is not sufficient to cause droplet movement and for higher values of capillary number, the higher values of viscosity ratio enhance the movement of droplet causing reduced wetted area. Kang et al. [38] have studied the displacement of a two-dimensional immiscible droplet in a channel. They have seen the effect of different viscosity ratio and different density ratio on the droplet displacement behaviour. In addition to that an extensive research has been done to explore the physics of liquid droplet spreading and displacement on the wetted flat wall of microchannels and duct [39–44].

The surface characteristics play a major role in the displacement or spreading of the droplet on the channel wall. The main characteristic of the surface is its roughness. Many researchers have focused on the analyses of droplet displacement on the rough or grooved surface. In the context of that Huang et al. [45] have studied the displacement of the droplet in a grooved channel using LBM for high-density ratios. In their study, the effect of wettability and geometric properties of the surface has been studied on the velocity of the droplet and flow pattern. The

analysis shows that the movement of the droplet is faster in the grooved hydrophobic surface compared to the hydrophilic surface. It is also observed that the aspect ratio of the groove majorly affects the motion of the droplet. The displacement of the droplet on a single grooved wall of a two-dimensional channel has been studied by the Son et al. [46] under the action of gravitational force. The Shan and Chen lattice Boltzmann method was adopted to analyze this problem for high-density ratios using the Carnahan-Starling equation of state. In their study, the effect of groove height and wetting condition on the droplet displacement have been studied. Wang et al. [47] have analyzed the dynamic behaviour of the droplet displacement on an inclined micro-grooved surface under the influence of gravitational force. It is reported that the displacement and wetting of the droplet on the micro-grooved surface are greatly affected by the area covered by the groove and its width. Fan et al. [48] investigated the contact line dynamics of immiscible fluid displacement on an ideally smooth wall of a two-dimensional channel using a lattice Boltzmann model.

The two-phase lattice Boltzmann method (LBM) has been used by [49] to simulate the droplet flows with coalescence and breakup. It has been found that the interfacial area during coalescence decreases and then increases. A very few studies have been conducted to understand the physics of droplets coalescence on a wettable surface by many researchers experimentally, theoretically and numerically. Basically, two stages are encountered during the process of coalescence of droplets; the first one is an initial growth of the meniscus junction between two droplets and the second is the slow conversion of elliptic shape to the circular shape of the combined droplet at longer times. Earlier work in this context involves the investigation of the coalescence dynamics of two spreading droplets on a highly wettable substrate experimentally as well as numerically by Ristenpart et al. [50]. In this analysis, it has been observed that the width of the meniscus junction between two droplets follows power law behaviour. Later, an LBM based single phase free surface model has been developed by Xing et al. [51] to study the interfacial dynamics of coalescence of two droplets. Nilsson and Rothstein [52] have investigated the effect of contact angle hysteresis on the dynamics of coalescence of sessile drops. In this study, three superhydrophobic surfaces have been investigated keeping advancing contact angle same and varying contact angle hysteresis. It is observed that there are three different regimes of coalescence which is a function of both Weber number

and impact angle. It is to be noted that the thermal characteristics of the coalescence process are also a major concern which is analyzed by Xie et al. [53]. In this study, an experimental investigation has been performed to study the thermal characteristics in the interaction process of water droplets on a hydrophobic insulator surface under high direct current voltage. Yeh et al. [54] have conducted an experimental study to investigate the influence of surface tension on the mixing and coalescence of droplets on a wettability gradient surface. It has been found that for droplets with identical surface tension, a larger surface tension caused stronger recirculation flow in a coalesced droplet; for droplets with distinct surface tensions, the coalescence and mixing behaviour is dominated by the arrangement of the two droplets. Moghtadernejad et al. [55] have analyzed the shedding behaviour of a single and two droplets coalescence on hydrophilic and superhydrophobic surfaces. In the support of this context, Fakhari and Rahimian [56] have been carried out an investigation on falling droplet by using LBM for a range of Eotvos and Ohnesorge numbers. Many different micro and nanoscale problems like rarefied [57] and bubbly [58] flows have been performed using LBM. A detailed review of LBM studies concerning microfluidics has been reported by Zhang [59].

1.3.3 Review on droplet moving past a solid cylinder

The droplet impact on an arbitrarily shaped substrate has been simulated by Pasandideh-Fard et al. [60]. In this study, experimental as well as numerical results of the impact of a water droplet on stainless steel tubes have been presented. The droplet diameter was considered to be constant throughout the study but the diameter of the tube is varied. As a result, it is reported that the surface area of the droplet impact on the tube affects the droplet breakup and the formation of daughter droplets after impact. Link et al. [61] experimentally analyzed the breaking of the large droplet into precisely controlled daughter droplets using two different configurations of the channel i.e., T-junction and flow past an isolated obstacle. It was reported that the transverse positioning of the square-shaped obstacle allows the proper control over the breakup and the relative size distribution of spreading. An experimental and theoretical study has been conducted by Bakshi et al. [62] to see the effect of the impact of a droplet on a spherical shape target. The diameter of the spherical target has been varied for the study. Depending on the film thickness, it was found

that there are three different phases are present, namely the initial drop deformation phase, the inertia dominated phase, and the viscosity dominated phase. It was also observed that the thinning process of the liquid film is slower when the target size is increased compared to droplet size. Chung et al. [63] numerically analyzed the droplet dynamics passing through a solid circular cylindrical obstruction in a confined micro-channel. The analysis was aimed to study the effect of droplet size and capillary number on the droplet dynamics for both Newtonian as well as viscoelastic fluids. The analysis showed that the breakup of the droplet in the Newtonian fluid passing through the obstruction depends on the size of the droplet whereas in case of a viscoelastic fluid, the normal stress difference evolved in the droplet or medium is a key factor on the breakup or merger of the droplets. In another study which is the extension of their previous research, Chung et al. [64] investigated the droplet dynamics passing through a more complex and complicated obstruction in a two-dimensional channel. They have studied this problem numerically as well as experimentally. The study was focused on the effect of different shapes of obstruction (i.e., cylinder and square), droplet size and capillary number. It was observed that the performance of cylindrical obstruction is much better than the square obstruction owing to the fact that in the square obstruction, more non-trivial daughter droplets are generated and an additional dead zone id observed near the front stagnation point.

Protiere et al. [65] explored the dynamics of a droplet past a circular cylinder and aimed at the capillary effects. In this study, a one-dimensional model is developed to elaborate the experimental phenomena and observed that the breakup occurs owing to the surface-tension-driven instability as well as variation of the axial gaps. The importance of wettability in order to obtain high-quality prints studied extensively by Do-Quang et al. [66]. In this work, two- and three-dimensional numerical experiments of ink droplets impacting on a paper-like surface have been conducted. It was found that only by changing the wettability of the fibres, droplets were either deposited on the paper or could bounce off. To explore the impact behaviour between a droplet and a target with different shapes, an extensive study has been conducted by Gac and Grado [67] and Juarez et al. [68]. The former investigation indicated two kinds of splashing regimes which depend on the number of the target vertices, while the latter work found that the behaviour of a head-to-head collision is almost independent of the target shape and drop splashing can be potentially controlled

by geometric features of the target. Salkin et al. [69] theoretically and experimentally studied the break-up phenomena of drops and bubbles passing through a linear micro-obstacle, unlike the previous studies where circular or square cylinder were considered an obstruction. This study considered the hidden nature of viscosity contrast between dispersed and transporting phases to identify the critical drop size and critical capillary number for the breakup. A more detailed discussion on droplet deformation, spreading and breakup in a channel has been reported by Chakraborty [70] and Chakraborty et al. [71].

1.3.4 Review on flow through porous media

The fundamental study of fluid flow inside porous media is an important topic of research has attracted many researchers to explore the physics. The flow through porous media is critically important to many scientific and engineering application specifically in fuel cells [72], petroleum engineering [73], carbon capture utilization and storage [74] and groundwater hydrology [75], etc. A number of investigations can be found in the literature describing fluid flow through porous media but still, there is a large scope for further exploring the physics associated with fluid flow through the packed-bed porous medium. In this context, Owens and Archer [76] experimentally represented the fluid flow data that describe the preferential characteristics of rock wetting in a core has a remarkable effect on the oil-water relative permeability relationship. An investigation showing the effect of the structure of pores on two-phase capillary pressure hysteresis and relative permeability of strongly-wetted system at low capillary number performed by Jerauld and Salter [77]. In this experimental analysis, it is found that the aspect ratio of pore-body to pore-throat is an extremely important structural determinant of the hysteresis behaviour. Oostrom and Lenhard [78] performed a study to compare the results of numerical multiphase flow and transport simulator (STOMP) with the experimental results. The prime objective of their study was to examine and evaluate the ability of often used constitutive relations to forecast the multiphase flow in a variably water-saturated porous media with an invariable water table. The coupled dissolution and precipitation process in a simplified porous medium has been investigated using LBM by Kang et al. [79]. The Shan-Chen lattice Boltzmann approach was utilized to simulate the immiscible two-fluid-phase flow in a porous medium domain by Pan et al. [80]. In this

investigation, a closely packed spherical particle system was designed to represent the laboratory experiments and the study was performed to evaluate the capillary pressure-saturation relationship.

Fuel cells, owing to their high energy efficiency, environmental friendliness and low noise, are widely considered as the 21st-century energy-conversion devices for mobile, stationary and portable power. Among the several types of fuel cells, the polymer electrolyte fuel cell (PEFC) has emerged as the most promising power source for a wide range of applications. Despite tremendous recent progress in enhancing the overall cell performance, a pivotal performance limitation in PEFCs is manifested in terms of mass transport loss originating from suboptimal liquid water transport and resulting flooding in the constituent components [81, 82]. Liquid water blocks the porous pathways in the CL and GDL thereby causing hindered oxygen transport to the reaction sites as well as covers the electrochemically active sites in the CL leading to increased surface overpotential. This phenomenon is known as flooding and is perceived as the primary mechanism leading to the limiting current behaviour in the cell performance. The catalyst layer and gas diffusion layer, therefore, play a crucial role in the PEFC water management aimed at maintaining a delicate balance between reactant transport from the gas channels and water removal from the electrochemically active sites. In this context, several researchers conducted numerical experiments to explore the physics of two-phase flow through porous medium associated with fuel cells. Zhu et al. [83] numerically analyzed the dynamic behaviour of liquid water entering a PEMFC gas flow channel through a GDL pore. The simulations are conducted using the volume of fluid method for explicitly tracking the liquid-gas interface. The objective of the study was to see the effect of pore size, channel size and coalescence of droplets. Gostick et al. [84] developed a pore network model to analyze the GDL in a PEMFC. The pore network model was used to measure the limiting current in a PEM fuel cell under operating conditions for which transport through the GDL dominates mass transfer resistance. In order to investigate the wettability and structure influence on the liquid water transport in the PEFC CL and GDL, a two-phase lattice Boltzmann method with microstructure reconstruction model is developed by Mukherjee et al. [85]. The invasion of the liquid waterfront is captured in CL and found a transition from capillary fingering to stable displacement patterns. The study also considered the effect of different wetting conditions. Hao and Cheng [86] investigated the dynamic

behaviour of a droplet formation and its detachment in a micro gas flow channel of PEMFC. The free-energy LBM is used to simulate the problem. The study focuses on the size of the detached droplet and the time taken by the water removing out of the channel under various gas flow velocity. Detailed analyses on two-phase flow through porous media of a PEMFC have been done by Hao and Cheng [72, 87, 88]. An investigation has been done to see the effect of water droplet behaviour in a fuel cell channel for different droplet positions, gas channel wall wettability and gas channel heights by Salah et al. [89]. To show the water drainage performance, the droplet velocity and pumping efficiency have been calculated. Cho et al. [90, 91] studied the droplet dynamics in a micro-duct through theoretical, experimental and numerical analysis. These studies are focused on the examination of the forces on a water droplet, droplet deformation and detachment. Chukwudozie and Tyagi [92] used lattice Boltzmann method to study the flow through BCC sphere packs of varying roughness and a real porous media. In this analysis, the permeability, tortuosity and beta factor were calculated for the interpretation of the simulated results. Liu et al. [93] investigated the flow through porous media for high-density ratio using stabilized lattice Boltzmann diffuse interface model. A new wetting boundary treatment for convex and concave corners was proposed which can also be extended to more complex geometries along with curved boundary. Using this method, the effect of viscosity ratio, Bond number, capillary number and contact angle have been investigated to simulate gas displacement of liquid in a 2D pore network.

1.4 Motivations and research objectives

The multiphase-multicomponent flows are extensively analyzed by several researchers in different scenarios and conditions owing to its The The multiphase-multicomponent flows are extensively analyzed by several researchers in different scenarios and conditions owing to its existence in nature and industrial fields. A detailed literature review on multiphase-multicomponent flows shows that the droplet displacement and spreading on channel wall is an important and emerging topic of research due to its wide area of application. However, a very few studies are conducted on droplet displacement and spreading behaviour on the channel wall considering different wetting characteristics of the surface. Moreover, most of the studies on this topic have

been performed considering a single hemispherical droplet on a two-dimensional channel wall. In addition to that these studies considered the droplet displacement and spreading on a flat wall of the channel whereas in nature or in some of the industrial application, irregularities can be found on the surface of the channel wall. These irregularities sometimes hamper the behaviour or displacement of the droplet and affect the efficiency of the whole system. The researchers, in the past, tried to replicate this irregularity in terms of small grooves on the surface of the channel wall. But, previous pieces of literature show that the physics of droplet displacement on grooved channel wall is still unexplored completely and there is a scope to analyze thoroughly the droplet dynamics on the grooved wall under the consideration of wall wettabilities and various physicochemical parameters.

A critical review of the literature on multiphase-multicomponent flows shows that the multiphase-multicomponent flow can be extensively found in porous media flows or flow through pore confinements inside a channel. Researchers have focused on the droplet moving past an obstruction inside the channel but the droplet flow through pore confinements is still not considered for the study. However, immiscible fluid flows or primary drainage of wetting phase fluid by the flow of non-wetting phase fluid under various wetting conditions of the pore structures are still unexplored. However, several researchers tried to completely describe the physics of fluid flow through porous media. The literature review also shows that the porous structure inside a domain plays a crucial role in the fluid flow. Therefore, it is important to analyze the capillarity-wettability interactions in an immiscible fluid flow through a complex porous medium. The present simulations are inspired from the two-phase (PEFC) channels and porous structures [94]. The two-phase (water and air as the fluids couple) transport in the PEFC is capillarity driven and characterized by low capillary number and low Reynolds number. The parameters are chosen accordingly as given in Table A.1 and Table A.2.

With this motivation, the overall research objective of this work is to analyze the behaviour of two immiscible fluids interaction using the Shan-Chen lattice Boltzmann method. The specific research objectives of the present study can be described as below.

- To investigate the coalescence of two immiscible droplets adhering on a verti-

cal wettable wall in a three-dimensional rectangular channel.

- To investigate the effect of low viscosity ratio on the dynamic behaviour of the displacement of a droplet on a vertical wettable wall in a three-dimensional rectangular channel.

- To investigate the droplet displacement and spreading behaviour on the grooved wetted wall of a three-dimensional channel under various physicochemical conditions.

- To analyze the droplet dynamics due to the capillarity-wettability interaction through a partially obstructed three-dimensional channel confinement.

- To explore the physics of two-phase flow through porous domain represented by packed bed spherical particles.

1.5 Thesis outline

The overall structure of the present thesis is organized as follows.

The introduction and relevant application areas of multiphase-multicomponent flow and lattice Boltzmann method are described in Chapter 1. The present chapter also contains a thorough review of available literature on LBM, droplet motion on channel walls and two-phase flow through the porous domain. The formulation of lattice Boltzmann method and Shan-Chen model is discussed in detail in Chapter 2. The different boundary conditions available in LBM and validation of code are also presented in Chapter 2.

Chapter 3 discusses the dynamic behaviour of droplets sliding on a wall of a rectangular channel considering wetting effects. The study includes the coalescence of two equal size droplets placed on a channel wall along its length under the action of gravitational force. The effects of centre distance between the droplets and the

capillary number have been illustrated in the form of evolution of wetted area and wetted length. The study is focused on the time required for merging two droplets with the variable centre distance between the two droplets. The effect of low viscosity ratio on the dynamic behaviour of the droplet displacement on a wetted wall of the three-dimensional channel is presented in Chapter 4. The wetted wall of the channel is considered to be flat as well as grooved in two different cases and a comparison of droplet displacement and spreading behaviour is done. In the grooved wall case, it is assumed that the channel wall on which droplet is moving has only one groove. Chapter 5 describes the effect of the wettabilities of the groove, location of the groove and number of grooves on the displacement and entrapment of the droplet fluid. In Chapter 6, an attempt is made to sweep out the fluid which gets entrapped inside the groove of the three-dimensional channel wall. To sweep out the entrapped fluid, a large size three-dimensional immiscible droplet is allowed to slide down on the three-dimensional channel wall above the groove.

Chapter 7 discusses the dynamic behaviour of the droplet moving under gravity in a three-dimensional channel where the path of the droplet is restricted by wetted solid spherical obstruction pore confinement. Therefore, the study also considers the direct impact of droplet and obstruction as well as the spreading behaviour of droplet fluid over the solid obstruction. To explore the complex physics of the present problem, the study is conducted to analyze the effect of capillary number, surface wettability, obstruction size and different structures of pore confinements. Chapter 8 is devoted to understand and investigate the behaviour of two-phase flow inside a porous domain. To represent a porous structure inside a domain, a packed bed spherical particles are considered and primary drainage phenomena in fuel cells are investigated. The front invasion of fluid through porous media is captured and shown in terms of displacement and percentage saturation.

Finally, the main findings and suggestions for further work are summarized in Chapter 9.

Chapter 2

LBM Formulation

2.1 Introduction

The lattice Boltzmann method is a technique or class of mesoscopic particle-based approach for the computational modelling to simulate complex fluid flows including single and multiphase flows. It is basically a discrete computational method based upon a simplified, fictitious molecular model known as lattice gas automata. In LBM, a fluid element is to be considered which consists of a collection of fictitious particles. These particles are represented by a particle velocity distribution function for each and every fluid component at each grid point. Under the action of applied forces, these fluid particles collide with each other after streaming as per their discrete velocity and finally, get new velocities. These particles are convected from one lattice to the other in discrete time steps.

2.2 Lattice structure

In LBM, all the particles are assumed to be residing at the fixed location called as nodes of a lattice. These lattices are the regular arrangement of the particles in the domain and hence all particles should follow or move along these fixed paths thereby reducing the degree of freedom of the system. All particles should be streamed along these lattice links and collide at lattice sites. The common terminology is to refer to the dimension of the system and the number of velocity vectors commonly represented as DnQm where 'n' represents the number of dimensions of a system and

'm' represents the speed model, i.e., number of linkages of a node.
In the literature, square and hexagon are the two generally used lattice structure in two-dimensional situations. Depending on the number of particles speed at lattice node, the square lattice can have 4-speed, 5-speed, 8-speed or 9-speed models and the hexagonal lattice can have 6-speed and 7-speed models. In three-dimensional situations, cubic lattice structures are commonly used e.g., a three-dimensional (D3Q19) lattice structure with rest particle is shown in Fig. 6.1. By including rest particle in a discrete velocity set, the computational stability and reliability are improved. Each node with crystal shape can stream particles to each of the six neighbouring

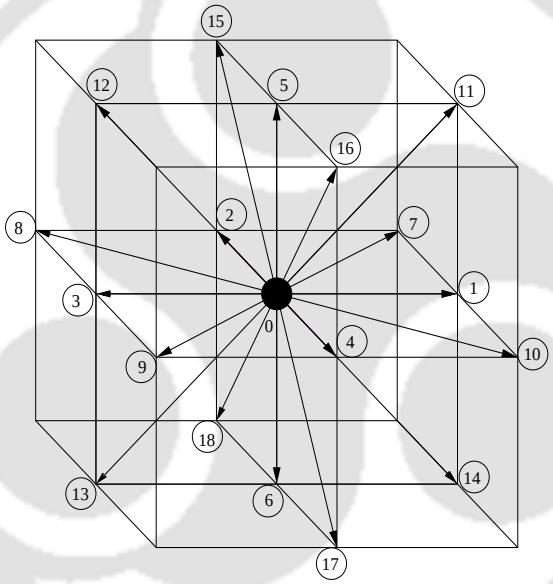

Figure 2.1: D3Q19 lattice structure

nodes which share a surface. The eight neighbouring nodes share a corner and itself. Mostly the simulations using LBM, δ_x is taken as a basic unit for lattice spacing. If the length of the domain is L and has N lattice units along its entire length, the space unit is defined as $\delta_x = L/N$. Speeds in LB simulations are described in terms of the lattice speed. The discrete time unit can therefore be given as $\delta_t = \frac{\delta_x}{c}$, where the denominator c is the lattice speed.

2.3 Boltzmann transport equation

2.3.1 Background of LBM

The LBE model historically is originated from a Boolean fluid model known as the Lattice Gas Cellular Automata (LGCA), which simulates the motion of fluids by particles moving and colliding on a regular lattice. The averaged fluid variables, such as mass density and velocity, are shown to satisfy the Navier-Stokes equations. It has been proved that the LBE could be derived from the continuous Boltzmann equation directly as a discrete equation, in which velocity space is discretized with the minimum set of values. The simulation of fluid flows by using the LBE method is based on kinetic equations and statistical physics, unlike those of conventional methods which are based on continuum mechanics.
The LBE method eliminates the time consuming statistical averaging step in the original LGCA due to its kinetic nature. Therefore, the LBE method is able to simulate the complicated fluid flows such as multiphase flows, chemically reacting flows, visco-elastic non-Newtonian flows. In addition, simplified collision models are developed and used to replace the collision operator derived from the LGCA to improve both the computational efficiency and accuracy. It is worth noting that the simple collision model of Bhatnagar, Gross, and Krook (BGK) was applied to the LBE and yielded the so-called lattice BGK model. Since the extra flexibility in this approach is to allow the removal of the artefacts of the LGCA (i.e., the lack of Galilean invariance and the dependence between velocity and pressure in LGCA), eventually this method was numerically found to be at least as stable, accurate, and computationally efficient as traditional CFD methods for simulation of simple single-phase incompressible fluid flows. More importantly, the microscopic physics of the fluid particles could be incorporated as easily as in other particle collision methods since fluid motion is simulated at the level of distribution functions. Due to interparticle interactions such as capillary phenomena, multiphase flows and non-linear diffusion, many complex fluid phenomena could be simulated naturally by LBE model.

2.3.2 Boltzmann transport equation

The Boltzmann equation gives the probability of the particles positions in the phase space. A statistical description of a system can be given by distribution function $f(\mathbf{r}, \mathbf{c}, t)$ where $f(\mathbf{r}, \mathbf{c}, t)$ is number of particles at a time t located between $\mathbf{r}$ and $\mathbf{r}+d\mathbf{r}$ which have velocities between $\mathbf{c}$ and $\mathbf{c}+d\mathbf{c}$. An external force $\mathbf{F}$ acting on a gas molecule of unit mass changes the velocity of the molecule from $\mathbf{c}$ to $\mathbf{c}+ \mathbf{F}dt$ and its position from $\mathbf{r}$ to $\mathbf{r} + \mathbf{c}dt$ as shown in Fig. 2.2. The number of molecules, $f(\mathbf{r}, \mathbf{c}, t)$, before the application of external force is equal to the molecules after disturbances, $f(\mathbf{r} + \mathbf{c}dt, \mathbf{c} + \mathbf{F}dt, t + dt)$, if no collisions take place between the molecules. Hence,

$$f\left(\mathbf{r} + \mathbf{c}dt, \mathbf{c} + \mathbf{F}dt, t + dt\right) d\mathbf{r}d\mathbf{c} - f\left(\mathbf{r}, \mathbf{c}, t\right) d\mathbf{r}d\mathbf{c} = 0. \tag{2.1}$$

If collision takes place between the molecules, the number of molecules will be

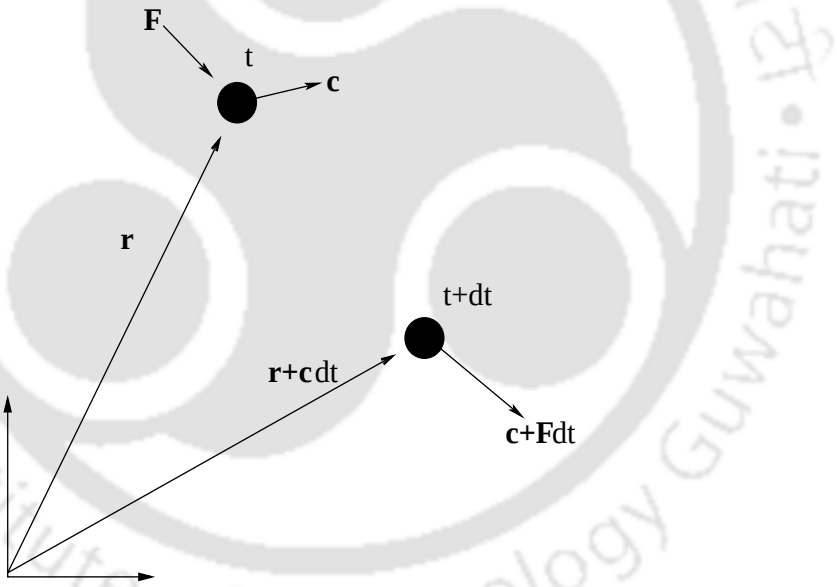

Figure 2.2: Position and velocity vector before and after applying force

different at a location in the interval $d\mathbf{r}d\mathbf{c}$. The collision operator (Ω) gives the rate of change between the final and initial status of the distribution function. Hence, the equation for the evolution of the number of the molecules can be given as,

$$f\left(\mathbf{r} + \mathbf{c}dt, \mathbf{c} + \mathbf{F}dt, t + dt\right) d\mathbf{r}d\mathbf{c} - f\left(\mathbf{r}, \mathbf{c}, t\right) d\mathbf{r}d\mathbf{c} = \Omega(f) d\mathbf{r}d\mathbf{c}dt. \tag{2.2}$$

Dividing the above equation by $dtd\mathbf{r}d\mathbf{c}$ and as the limit $dt \longrightarrow 0$ gives,

$$\frac{df}{dt} = \Omega(f) \tag{2.3}$$

The above equation gives the total rate of change of the distribution function is equal to the rate of collision. Since f is a function of $\mathbf{r}, \mathbf{c}$ and t, the total rate of change can be expressed as,

$$df = \frac{\partial f}{\partial \mathbf{r}} d\mathbf{r} + \frac{\partial f}{\partial \mathbf{c}} d\mathbf{c} + \frac{\partial f}{\partial t} dt \tag{2.4}$$

For the system, without external force, the Boltzmann equation can be stated as,

$$\frac{\partial f}{\partial t} + \mathbf{c} \cdot \nabla f = \Omega\left(f_1, f_2\right) \tag{2.5}$$

where collision operator Ω is given by

$$\Omega\left(f_1, f_2\right) = \int \int \sigma\left(\alpha\right) \ \left|\mathbf{u} - \mathbf{v}\right| \ \left[f_1\left(\mathbf{u}'\right) f_2\left(\mathbf{v}'\right) - f_1\left(\mathbf{u}\right) f_2\left(\mathbf{v}\right)\right] d\mathbf{v} d\alpha \tag{2.6}$$

Here $\sigma\left(\alpha\right)$ is differential collision cross section for the two-particle collision which transforms the velocities from $\mathbf{u}, \mathbf{v}$ (incoming) into $\mathbf{u}', \mathbf{v}'$ (outgoing). The position in physical space is denoted by $\mathbf{x}$ and the velocity in the momentum (or velocity) space is denoted by $\mathbf{u}, \mathbf{v}$. α is the solid angle in which the particles are scattered.

2.3.3 BGK model equation

The collision operator Ω mentioned before is in general a complex non-linear integral. The idea is to linearize the collision term around its local equilibrium solution. Ω is often replaced by the so-called BGK (Bhatnagar, Gross, Krook [15]) collision operator

$$\Omega = \omega(f^{eq} - f) = \frac{1}{\tau}(f^{eq} - f) \tag{2.7}$$

where $\omega=\frac{1}{\tau}$, ω is called as collision frequency and τ is called as relaxation time factor. Inserting BGK approximation the Boltzmann equation can be written as,

$$\frac{\partial f}{\partial t} + \mathbf{c} \cdot \nabla f = \frac{1}{\tau} \left(f^{eq} - f \right) \tag{2.8}$$

The discrete Boltzmann equation can be written along a specified direction as given below

$$\frac{\partial f_i}{\partial t} + \mathbf{c}_i \cdot \nabla f_i = \frac{1}{\tau} \left(f_i^{eq} - f_i \right) \tag{2.9}$$

The above equation replaces the Navier-Stokes (N-S) equations in CFD simulations. It is possible to derive the N-S equations from Boltzmann equation from a Chapman-Enskog expansion [9]. Equation 2.9 can be discretized as

$$f_i \left(\mathbf{r} + \mathbf{c}_i \Delta t, t + \Delta t \right) = f_i \left(\mathbf{r}, t \right) + \frac{\Delta t}{\tau} \left[f_i^{eq} \left(\mathbf{r}, t \right) - f_i \left(\mathbf{r}, t \right) \right] \tag{2.10}$$

Complicated collision integral is replaced by a single time relaxation term.
The main advantage of above equation is simplicity. Adding the force term is also straightforward. Equation 2.10 is usually solved in two sub-steps. Like in the case of LGA, here also streaming and collision steps need to be solved. Collision ,in this case, is not defined explicitly any more as in LGA. In LBM, collision of the fluid particles is considered as relaxation towards a local equilibrium.

2.3.4 Streaming and collision steps

Streaming is the process where each portion of the distribution function is advected to nearby neighbors. By considering a finite number of directions, it is assumed that the portion of the distribution function is advected in the $\mathbf{c}_i$ directions contains many molecules all with the instantaneous characteristic velocity direction $\mathbf{c}_i$ (Fig. 2.3). It can be observed that, the particles of the middle cell moved to the neighboring cells whereas the particles of the neighboring cells moved to the middle cell. The process of modifying the distribution function for all fluid particles after arriving at new cell is known as collision. Collision of the fluid particles is considered as relaxation towards a local equilibrium. It is assumed that the collision takes place between two particles approaching each other (exclusion principle) at node only (not in between

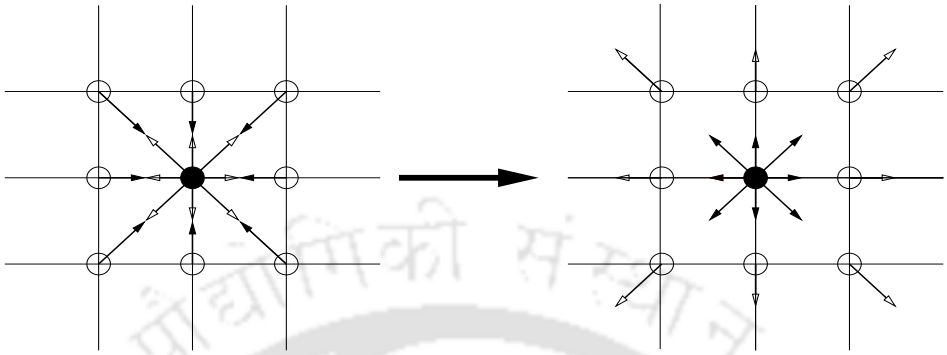

Figure 2.3: Pre-streaming and post-streaming conditions in LBM

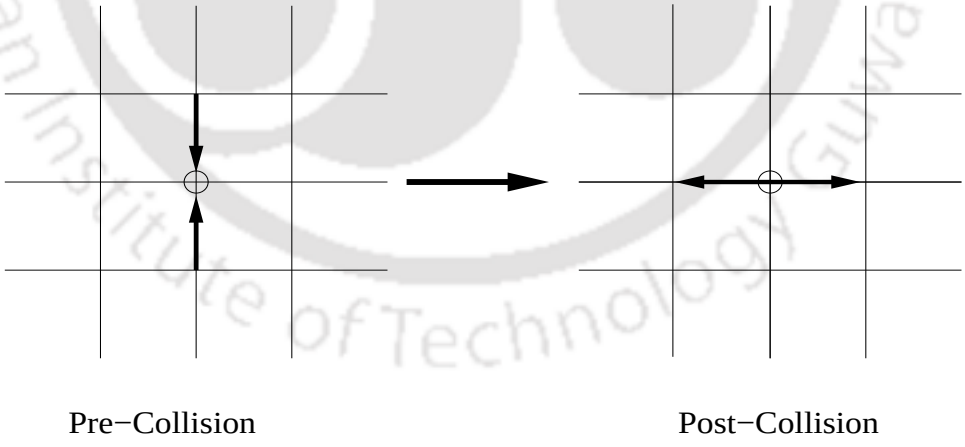

Figure 2.4: Pre-collision and post-collision conditions in LBM

the nodes) (see Fig. 2.4). The particles change their velocity i.e., momentum during collision before they finally reach equilibrium. The process of collision is local with respect to each lattice site and hence can be executed in parallel. Therefore, the discretized LBE can be split into two parts, i.e., streaming and collision as given below.

Streaming step:

$$f_i\left(\mathbf{r}+\mathbf{c}_i\Delta t, t+\Delta t\right) = f_i\left(\mathbf{r}, t+\Delta t\right) \tag{2.11}$$

Collision step:

$$f_i\left(\mathbf{r}, t+\Delta t\right) = f_i\left(\mathbf{r}, t\right) + \frac{\Delta t}{\tau}\left(f_i^{eq} - f_i\right) \tag{2.12}$$

2.3.5 Equilibrium distribution function

Determining a suitable local equilibrium function plays an essential role in the LBM. It is this function that decides what flow equations are solved by means of the LBE. Equilibrium distribution function, f^{eq} , which appears in the BGK collision operator, is basically an expansion of the Maxwells distribution function for low Mach number, Ma.

$$f = \frac{\rho}{\frac{2\pi}{3}} e^{-\frac{3}{2}(\mathbf{c}-\mathbf{u})^2} \tag{2.13}$$

Above equation can also be written as

$$f = \frac{\rho}{\frac{2\pi}{3}} e^{-\frac{3}{2}\left(\mathbf{c}^2\right)} e^{3\left(\mathbf{c}\cdot\mathbf{u}-\frac{\mathbf{u}^2}{2}\right)} \tag{2.14}$$

where $\mathbf{c}$ = lattice speed and $\mathbf{u}$ = macroscopic velocity of particle. Hence, Maxwell equation can be expanded around stationary state as,

$$f = \frac{\rho}{\frac{2\pi}{3}} e^{-\frac{3}{2}\left(\mathbf{c}^2\right)} \left[1 + 3\left(\mathbf{c}\cdot\mathbf{u}\right) - \frac{3}{2}\mathbf{u}^2 + ...\right] \tag{2.15}$$

The general form of equilibrium distribution function can also be written as,

$$f_i^{eq} = \Phi\omega_i\left[A + B\mathbf{c}_i\cdot\mathbf{u} + C\left(\mathbf{c}_i\cdot\mathbf{u}\right)^2 + D\mathbf{u}^2\right] \tag{2.16}$$

In above equation A, B, C, D are the constants which can be calculated by conservation of mass, conservation of momentum and conservation of energy. Φ is scalar parameter such as density (ρ), temperature (thermal energy density), or species concentration. Summation of all of these parameters is equal to one.

$$\Phi = \sum_{i=0}^{i=n} f_i^{eq} \tag{2.17}$$

$$f_i^k\left(\mathbf{x} + \mathbf{c}_i\delta_t, t + \delta_t\right) - f_i^k\left(\mathbf{x}, t\right) = -\frac{f_i^k\left(\mathbf{x}, t\right) - f_i^{k(eq)}\left(\mathbf{x}, t\right)}{\tau_k} \tag{2.18}$$

For D3Q19 model $f_i^{k(eq)}$ has the following form.

$$f_i^{k(eq)} = d_k n_k - \frac{1}{2} n_k \mathbf{u}_k^{eq} \cdot \mathbf{u}_k^{eq} \quad \text{for} \quad i = 0 \tag{2.19}$$

$$f_i^{k(eq)} = \frac{1 - d_k}{12} n_k + \frac{1}{6} n_k \left(\mathbf{c}_i \cdot \mathbf{u}_k^{eq}\right) + \frac{1}{4n_k}\left(\mathbf{c}_i \cdot \mathbf{u}_k^{eq}\right)^2 - \frac{1}{12} n_k \mathbf{u}_k^{eq} \cdot \mathbf{u}_k^{eq} \tag{2.20}$$

for i=1,2,3,...6

$$f_i^{k(eq)} = \frac{1 - d_k}{24} n_k + \frac{1}{12} n_k \left(\mathbf{c}_i \cdot \mathbf{u}_k^{eq}\right) + \frac{1}{8} n_k \left(\mathbf{c}_i \cdot \mathbf{u}_k^{eq}\right)^2 - \frac{1}{24} n_k \mathbf{u}_k^{eq} \cdot \mathbf{u}_k^{eq} \tag{2.21}$$

for i=7,8,.....18

$$\mathbf{c}_i = \begin{cases} (0,0,0) & i = 0 \\ (\pm 1, 0, 0), (0, \pm 1, 0), (0, 0, \pm 1) & i = 1 - 6 \\ (\pm 1, \pm 1, 0), (\pm 1, 0, \pm 1), (0, \pm 1, \pm 1) & i = 7 - 18 \end{cases}$$

$$\left(c_s^k\right)^2 = \frac{(1 - d_k)}{2} \tag{2.22}$$

where d_k is a free parameter, which relates to speed of sound c_s^k of pure k^{th} component. It should be noted that the macroscopic quantities like density and mean velocity are calculated by taking the moments of the distribution function as given

below.

$$n_k = \sum_i f_i^k \tag{2.23}$$

where n_k is the number density of k^{th} component. The macroscopic density and momentum density of each component are calculated as below.

$$\rho_k = m_k n_k = m_k \sum_i f_i^k \tag{2.24}$$

$$\rho_k \mathbf{u}_k = m_k \sum_i \mathbf{c}_i f_i^k \tag{2.25}$$

The kinematic viscosity in lattice unit is

$$\nu_k = \frac{(2\tau_k - 1)\,(c_s^k)^2}{6} \tag{2.26}$$

where c_s is the speed of sound of a region of pure k^{th} component, m_k is mass of k^{th} component and τ_k is relaxation parameter. The total density and momentum density of multicomponent flow are given by

$$\rho = \sum_k m_k \sum_i f_i^k \tag{2.27}$$

$$\rho \mathbf{u} = \sum m_k \rho_k \mathbf{u}_k \tag{2.28}$$

When the local equilibrium distribution is properly chosen through the Chapman-Enskog expansion, one can recover governing continuity and Navier-Stokes equations from Eq. 2.18 [95].

2.4 Boundary conditions in LBM

One of the major and most crucial issue of any numerical approach is the accurate modeling and implementation of the boundary conditions. Modeling and implementation of boundary conditions accurately in LBM is an important part and no application can be discussed without specifying them. Implementing boundary conditions in the LBM is difficult because there is no one-to-one mapping between the

variables of the algorithm, the so-called particle distributions, and the predetermined hydrodynamic macro quantities given at the boundary. In LBM, appropriate equations are to be determined for calculating distribution functions, f at the boundaries. The possible different boundary conditions in LBM are described below.

2.4.1 Periodic boundary condition

Periodic boundary condition is the simplest condition in LBM which is applied to isolate a repeating flow conditions. In this condition, system becomes closed by the edges being treated as if they are attached to opposite edges. Figure 2.5 shows the

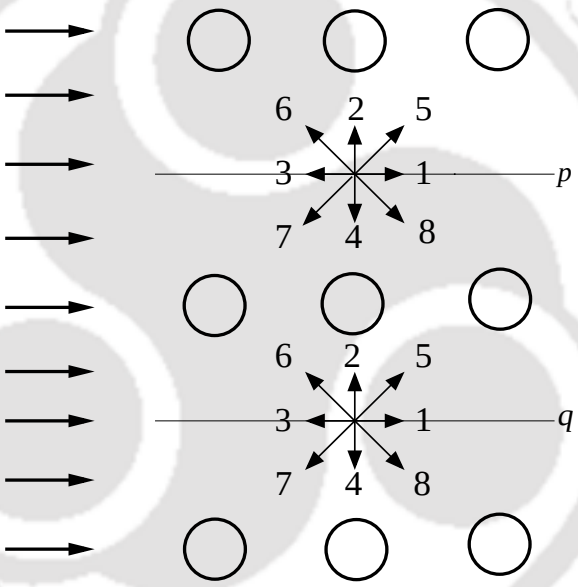

Figure 2.5: Periodic boundary condition in LBM

implementation of the periodic boundary condition in a flow over bank of tubes. Here, the flow condition above the line p and below the line q are same. So, it is not necessary to model complete flow but it is sufficient to model the flow between these two lines and use periodic boundary condition along these boundaries. For this situation, the periodic boundary condition in terms of distribution functions are as follows.

along line p: $f_{4p}=f_{4q}$, $f_{7p}=f_{7q}$, $f_{8p}=f_{8q}$

along line q: $f_{2q}=f_{2p}$, $f_{5q}=f_{5p}$, $f_{6q}=f_{6p}$

2.4.2 Bounce back boundary condition

Bounce back is used to model solid stationary or moving boundary condition, non-slip condition, or flow over obstacles. The name implies that a particle coming towards the solid boundary bounces back into the flow domain. Two different schemes are suggested regarding the position of the solid wall. In one of the schemes, it is suggested to place a solid in the middle of the lattice nodes whereas in other scheme, it is suggested to place a solid on the nodes. It has been shown that the first scheme is second-order in terms of numerical accuracy, whereas the second scheme is only first-order. If we want particles to bounce back from a solid, we have to change certain values of distribution functions f_i. In one time step a fluid particle goes to the boundary site, reverses its velocity and comes back. For example, consider a solid boundary (Fig. 2.6) where there is no streaming from a solid. So, there are three unknown distribution functions f_2, f_5 and f_6, which can be defined as.

$$f_2{=}f_4, \quad f_5{=}f_7, \quad f_6{=}f_8$$

Particles bounce back to the node from which they were originally streamed. It is important, that streaming process is executed before applying boundary conditions.

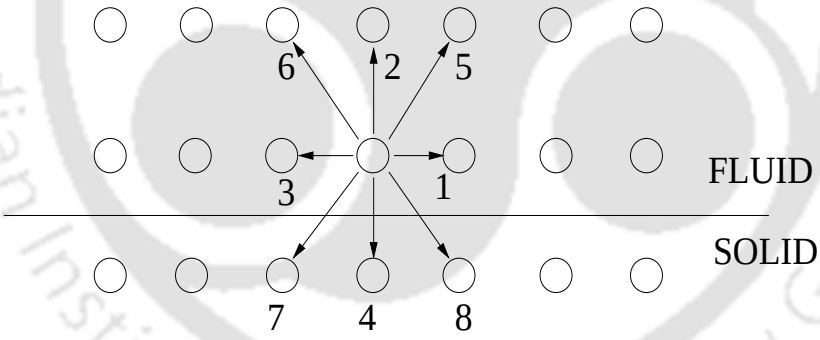

Figure 2.6: Bounce back boundary condition in LBM

2.4.3 Mirror/symmetry boundary condition

In some situations, the advantage of symmetry can be taken to significantly reduce the computation requirement. In LBM, one can just imagine that the fluid properties (actually, the distribution function f's) on one side of symmetric plane are mirror reflection of those on the other side (see Fig. 2.7). The distribution functions from

the image sites are set to be equal to their images on boundary sites $f_3 = f_1$, $f_4 = f_2$, and $f_6 = f_5$.

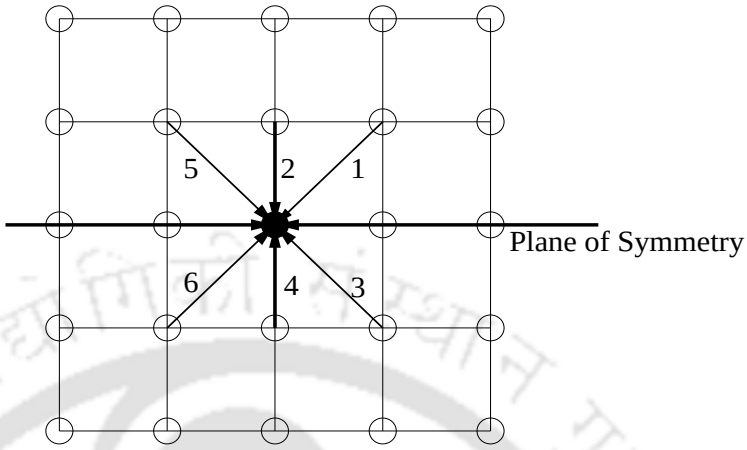

Figure 2.7: Mirror boundary condition in LBM

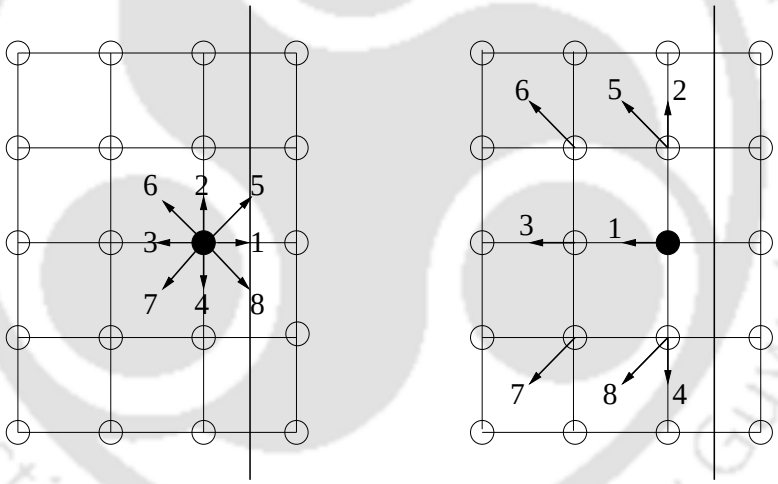

Figure 2.8: Free-slip boundary condition in LBM schematic

2.4.4 Free-slip boundary condition

Since boundary cells can not have fluid neighbor cells on one side, the streamed particles are reflected in their component normal to the wall (free slip boundary condition) as shown in Fig. 2.8. In this case, the tangential motion of the fluid

on the wall is free and no momentum exchange with the wall takes place along the tangential component.

2.5 LB models for multiphase flow

2.5.1 Shan and Chen model

The use of LBM to study multiphase flow can be dated back to the early days of the lattice gas automaton. Shan and Chen [23] proposed a multiphase-multicomponent model using interparticle potentials. Although a similar concept had been proposed earlier in the framework of the lattice gas automaton by Chen et al. [96]. In Shan-Chen model, to incorporate the effect of the intermolecular potential, nearest-neighbor interaction model has been used. Interparticle potential is basically the long range interparticle forces between the fluid molecules due to the mixing or separation of the phases as a result of interactions of molecules at the microscopic level. Interaction potentials for each of the components control the form of the equation of state of the fluid. The interactions between the particles of different components are incorporated in the kinetics through a set of potentials. It may be noted that the collision operator does not conserve total particle momentum at each site owing to the inclusion of interparticle interactions,. However, the total momentum of the whole system remains conserved.

The multicomponent multiphase LBE model by Shan and Chen [23] also considers the BGK collision term. Main distinction lies in determination of equilibrium velocity to include the interaction between different fluid component. The separation of fluid phases or components in the Shan-Chen model is automatic. This is significant improvement in numerical efficiency as compared to original LBM multiphase models. This model improves the isotropy of the surface tension and is preferred because of its convenience in handling fluid/solid interaction. It is important to mention here that although LBM has made great progress in multiphase-multicomponent flow modelling, the classical S-C LBM is limited to small density ratios less than 10 because numerical instability may appear in cases of large density ratio. However, when using the SC two-component multiphase LBM, the viscosity ratio M is also limited to less than 5 due to numerical instability. Therefore, in the present study keeping this fact into mind, the density and viscosity ratio values are

considered to represent fluid assuming it can reflect the same behaviour as a real fluid for low viscosity regimes.

2.5.1.1 Force inclusion

The original inclusion of Shan-Chen force is by using an altered velocity in the equilibrium distribution function. The new momentum taking the interaction force into account is given by the parameter $\mathbf{u}_k^{eq}$ which is determined by the following relation.

$$\rho_k \mathbf{u}_k^{eq} = \rho_k \mathbf{u}' + \tau_k \mathbf{F}_k \tag{2.29}$$

where $\mathbf{u}'$ is an extra component on the top due to inter particle interaction which is added for each component. Total force acting on the k^{th} component is given by the following equation.

$$\mathbf{u}' = \left(\sum_{k=1}^{s} \frac{\rho_k \mathbf{u}_k}{\tau_k} \right) / \left(\sum_{k=1}^{s} \frac{\rho_k}{\tau_k} \right) \tag{2.30}$$

The interaction force between the particles of k^{th} component at location $\mathbf{x}$ and $k'^{\,th}$ component at location $\mathbf{x}'$ is assumed to be proportional to the product of their effective mass $\psi\ (\rho_k)$.

$$\mathbf{F}_{1k}(\mathbf{x}) = -\psi_k(\mathbf{x}) \sum_{\mathbf{x}'} \sum_{k=1}^{s} G_{k\bar{k}}(\mathbf{x}, \mathbf{x}')\, \psi_{\bar{k}}(\mathbf{x}')\, (\mathbf{x}' - \mathbf{x}) \tag{2.31}$$

where $G_{k\bar{k}}(\mathbf{x}, \mathbf{x}')$ is called as the Green's function such that

$$G_{k\bar{k}}(\mathbf{x}, \mathbf{x}') = G_{k\bar{k}}(\mathbf{x}', \mathbf{x}) \tag{2.32}$$

In a multi-phase system, the coexistence of both phases is possible only at critical temperature whereas for the multicomponent case, the components are immiscible i.e., do not mix up in the absence of diffusion in the system, i.e., for null or negative diffusion coefficient. In the interaction force these aspects are modeled with the help of the Green function. The Green function is defined as follows in D3Q19.

$$G_{k\bar{k}}(\mathbf{x}, \mathbf{x}') = g_{k\bar{k}} \quad \text{for} \quad |\mathbf{x} - \bar{\mathbf{x}}| = 1 \tag{2.33}$$

$$G_{k\bar{k}}(\mathbf{x}, \mathbf{x}') = \frac{g_{k\bar{k}}}{2} \quad \text{for} \quad |\mathbf{x} - \bar{\mathbf{x}}| = \sqrt{2} \tag{2.34}$$

$$G_{k\bar{k}}(\mathbf{x},\mathbf{x}') = 0 \quad \text{otherwise} \tag{2.35}$$

$G_{k\bar{k}}(\mathbf{x},\mathbf{x}') > 0$ leads to repulsion and $G_{k\bar{k}}(\mathbf{x},\mathbf{x}') < 0$ leads to attraction between the particles. While a large value of $G_{k\bar{k}}(\mathbf{x},\mathbf{x}')$ makes the interface sharper, it can lead to numerical instabilities since it increases the interaction force and thus the spurious velocities. Interaction potential $V(\mathbf{x},\mathbf{x}')$ can be expressed in terms of Greens' Function as

$$V(\mathbf{x},\mathbf{x}') = G_{k\bar{k}}(\mathbf{x},\mathbf{x}')\,\psi_{\bar{k}}(\mathbf{x}')(\mathbf{x}'-\mathbf{x}) \tag{2.36}$$

The interactive force between the fluid and wall is given as

$$\mathbf{F}_{2k}(\mathbf{x}) = -n_k(\mathbf{x})\sum_{\mathbf{x}'} g_{kw} n_w(\mathbf{x}')(\mathbf{x}'-\mathbf{x}) \tag{2.37}$$

where
n_w= number density of the wall, which is a constant at the wall and zero otherwise.
g_{kw}= interactive strength between the component k and the wall.
$\mathbf{F}_{2k}$ is the force that is perpendicular to the wall. Hence, it does not affect the no-slip boundary condition. g_{kw} is negative for wetting fluid and positive for non wetting fluid. Body force is given by,

$$\mathbf{F}_{3k} = \rho_k \mathbf{g} = m_k n_k \mathbf{g} \quad \text{if the driving force is gravity}$$

$$\mathbf{F}_{3k} = \rho_k \mathbf{W}(t) \quad \text{if the driving force is acoustic excitation}$$

where

$$\mathbf{W}(t) = \mathbf{W}(0) + \delta\mathbf{W}(t)$$

where $\mathbf{W}(0)$ and $\delta\mathbf{W}(t)$ are constant body force and perturbation, respectively.
It may be noted that equation of state is used to calculate pressure as given below.

$$P = \sum_k \frac{(1-d_k)\,m_k n_k}{2} + 3\sum_{k,\bar{k}} g_{k,\bar{k}}\psi_k\psi_{\bar{k}} \tag{2.38}$$

Total force can be calculated as

$$\mathbf{F}_k = \mathbf{F}_{1k} + \mathbf{F}_{2k} + \mathbf{F}_{3k} \tag{2.39}$$

where,
$\mathbf{F}_{1k}$ =Fluid-fluid interaction
$\mathbf{F}_{2k}$ =Fluid-solid interaction
$\mathbf{F}_{3k}$ =External force

2.5.1.2 Effective mass

Other vital parameter of the Shan-Chen model is the effective mass of the phase or component. It is basically a function of the density and so far no direct derivation from physical laws has been found like fluid-fluid interaction parameter G_c has been related to the temperature or the diffusion coefficient. There is currently no deterministic way to map the fluid properties to a given effective mass. Although each fluid should theoretically have a different effective mass, Shan and Chen [23] proposed

$$\psi(\rho) = \rho_0 \left[1 - e^{-\frac{\rho}{\rho_0}}\right] \tag{2.40}$$

which simplifies by assuming $\rho_0 = 1$ to $\psi_k = f(\rho_k(x))$ which is a function of x through its dependency on n_k. For Shan-Chen model, a two components system can basically be modeled in following ways.

1. The molecules of the same substance attract each other then g_{kk} not equal to 0. If molecules have no interaction with the molecules of the other substances then $g_{kk'} = 0$. As stated above an attraction is modeled by a negative value of $G_c = g_{kk'}$

2. The molecules of the same substance have no interaction with each other, then $g_{kk} = 0$ and repel the molecules of the other substances when $g_{kk'} \neq 0$. So a repulsion is modeled by a positive value of $G_c = g_{kk'}$.

3. The molecules of the same substance interact with each other then $g_{kk} \neq 0$ and as well as with the ones of other substances $g_{kk'} \neq 0$.

2.6 Wettability on solid surfaces

The wettability of a liquid in contact with a solid surface is an important factor to analyze the multiphase-multicomponent fluid flow in many industrial, geological and biological applications. Wettability is defined as the ability of a solid surface to reduce the surface tension of a liquid in contact with it such that it spreads over the surface and wets it. The simplest method to evaluate the wettability and solid surface tension is contact angle measurement. The basic equation which measures the contact angle is known as Young's equation [97]. For a given drop resting on a solid surface, Young's equation can be written as given below (see Fig. 2.41).

$$\gamma_{lv} \cos\theta = \gamma_{sv} - \gamma_{sl} \tag{2.41}$$

where, γ refers the interfacial tension and subscripts lv, sv and sl are liquid-vapor,

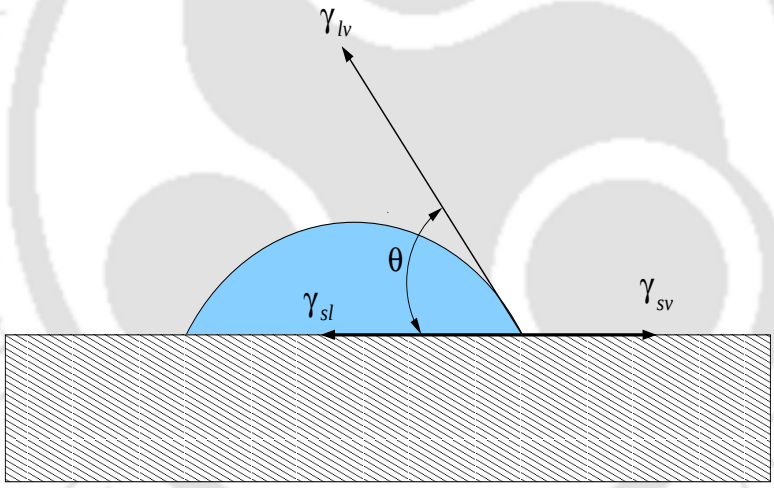

Figure 2.9: Contact angle of a liquid droplet wetted to a solid surface

solid-vapor and solid-liquid interfaces, respectively. The symbol θ is the contact angle at a location where the tangent along a liquid-vapour interface intersects the solid surface. Based on the contact angle, the different solid surface can be defined. A wettable surface can be termed as 'hydrophilic' when contact angle θ is less than 90° and a non-wettable surface is termed as 'hydrophobic' when the contact angle is greater than 90°. There are surfaces for which the contact angle is very high ($\theta > 150°$); these surfaces are known as 'superhydrophobic' surfaces.

2.7 Validation of LBM code

The present LBM code has already been used to analyze multiphase-multicomponent flow problems by Mukherjee [98] and Randive [37]. In these studies, a detailed validation of the present code has been done and discussed in details. In the present work, the same code is used and modified for the problems studied in this thesis. So, for brevity, a detailed discussion on validation has not been given here and only relevant validation of static droplet test has been conducted and discussed.

Before applying the present code for analyzing the different flow problem, it is necessary to calibrate the accuracy and correct implementation of the multiphase model. The two most important parameters which need to evaluate are fluid/fluid and fluid/solid interaction parameters. Fluid-fluid interaction parameter results in surface tension force and the fluid-solid interaction parameter gives rise to the wall adhesion force. For achieving this task, a static droplet test has been conducted and present results are compared with the results of Mukherjee et al. [85].

The fluid-solid interaction parameter basically controls the wall wettability effect through the resulting contact angle at the interface of solid-fluid-fluid. To perform the static droplet test, the presence of a solid wall is required. A D3Q19 lattice model is adopted for this analysis. A half liquid droplet of radius $10lu$ (lattice unit) is placed at the geometric centre of the bottom solid wall. The computational domain is having $50 \times 50 \times 50$ (in lattice units) grid size. The boundary conditions are considered to be of periodic in x-direction and wall BCs in the y- and z-directions. The bounce-back scheme is used on the walls to obtain no-slip boundary condition. No body force is applied in the present simulation.

The model input parameters for static droplet test are: initial densities, ρ_1 and ρ_2, of the wetting phase and non wetting phase outside and inside the bubble respectively, the relaxation times, τ_1 and τ_2, and fluid-fluid interaction coefficient, $g = g_{12} = g_{21}$ and $g_{11} = g_{22}$=0 . It should be noted that all the units are in lattice units unless otherwise stated specifically. The initial fluid densities were specified as ρ_1=150 and ρ_2=0. The relaxation times, τ_1=1 and τ_2=1.42 are considered. In addition to that, fluid/solid interaction parameters are $g_{1w} = -g_{2w}$ that are varied in the present study to obtain the steady droplets with different contact angles.

When a static droplet is formed, the contact angle is evaluated from the final steady state values of the droplet radius R, droplet height a_0, and wetted length of the droplet b_0, as shown in Fig. 2.10 using the following relation [99].

$$\tan(\theta_2) = \frac{b_0}{2(R - a_0)} \tag{2.42}$$

The final radius R, is evaluated from a_0 and b_0, using the following expression

$$R = \frac{a_0}{2} + \frac{{b_0}^2}{8a_0} \tag{2.43}$$

Hereafter, θ_2 is referred to as the contact angle, θ for simplicity. The values of fluid-

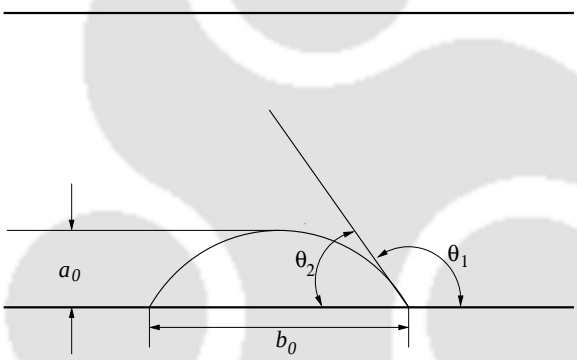

Figure 2.10: Static droplet after steady state

solid interaction parameter g_{2w} are varied from -0.02 to 0.16 to obtain various values of contact angle θ. Simulations were carried out for 40000 time step to get the steady state results. The droplet gets detached at g_{2w} =0.16. The variation of contact angle for various values of g_{2w} is shown in Fig. 2.11. The result is comparable with good agreement with Mukherjee et al. [85]. A negative value of g_{2w} gives rise to a contact angle less than 90° indicating that the phase 2 tends to wet the surface leading to hydrophilic wettability. A contact angle greater than 90° is formed when g_{2w} is positive; indicating that the phase 2 is non-wetting and the wettability condition is termed as hydrophobic. For $g_{2w} = 0$, neither of the phases exhibits preferential wetting to the surface, which is defined as neutrally wet situation.

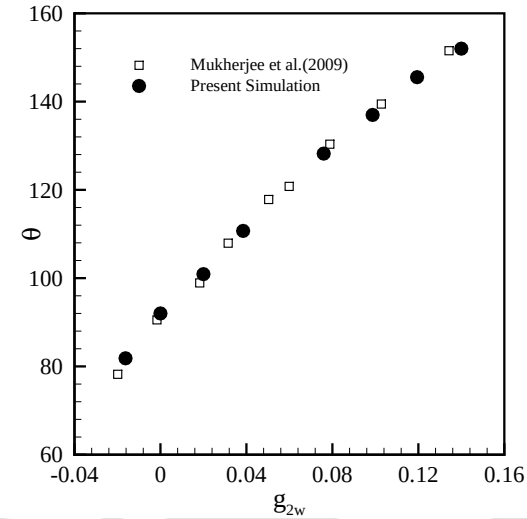

Figure 2.11: Variation of contact angle with g_{2w}

2.8 Summary

A detailed theory of lattice Boltzmann method has been discussed in this chapter. The mathematical formulation of basic lattice Boltzmann equation along with the models incorporating multiphase-multicomponent fluid flow have been presented. The Shan-Chen model has been incorporated in LBE for analyzing multiphase-multicomponent flows in the present thesis. The different boundary conditions (e.g., bounce-back, periodic, free-slip and mirror) in LB framework have been discussed. The validation of the present LBM code has been done and solid droplet test results have been compared with the results of Mukherjee et al. [85].

Chapter 3

The Coalescence of Two Droplets on a Rectangular Channel Wall Considering Wetting Effects

3.1 Introduction

The coalescence of droplets plays a significant role in fluid flow applications and attracted many researchers in the past few years. The application areas of coalescence of droplets cover the nature and engineering systems, e.g., solid inkjet printing, rapid prototyping, spray coating, micro fabrications, water and ice accumulation, erosion and electronic packaging [100]. Most of the researchers analyzed the coalescence of droplets without considering the wettability effect of the channel walls. However, it is observed that this characteristic of the wall strongly affects the behaviour of the droplets coalescence and spreading. The main aim of the present study is to investigate the dynamic behaviour and time of initiation of the coalescence of two droplets on wettable channel wall.

The objective of the present study is to numerically analyze the dynamic behaviour of sliding droplets on a wall of a rectangular channel considering wetting effects. The study includes the coalescence of two equal size droplets placed on a channel wall and droplets move along its length under the action of gravitational

force. The effects of centre distance between the droplets and the capillary number have been illustrated in the form of evolution of wetted area and wetted length. The time taken by the two droplets for different parameters to start coalescence is also investigated.

3.2 Problem specification

The current work studies the coalescence of two droplets adhering on a vertical wettable wall in a rectangular channel as shown in Figs. 3.1(a)-(b). The simulations are carried out in a rectangular channel having length, width and breadth as 300, 41 and 81 lattice units (lu), respectively. The problem considers the two immiscible fluids in which droplets (fluid 2) are placed in the domain filled with displacing fluid (fluid 1). The radius of the droplets is considered to be 18 lu. The upper droplet is positioned at 251 lu in positive z-direction and the distance between the centres of two droplets (C_d) is varying. The study is focused on the time required for merging two droplets with the variable centre distance between the two droplets. The fluid or droplet motion has been governed by the gravitational force that is applied in the negative z-direction. The two different wall wettabilities (e.g., hydrophilic and mixed wettability) have also been considered to analyze the dynamic droplets behaviour on the channel wall. The periodic boundary condition is applied in the z-direction and no slip (i.e., bounce back) boundary condition has been applied at all walls located in x- and y-directions.

3.3 Results and discussion

In the present investigation, a parametric study has been carried out to visualize the effect of varying centre distance (C_d) between two droplets residing on a wall of a vertical rectangular channel as well as the time of coalescence of two droplets. The centre distance (C_d) has been varied from 47 to 55 lu. The two wetting conditions (i.e., hydrophilic (i.e., g_{2w}=-0.02) and mixed wettable (i.e., g_{2w}=$\pm$0.05)) has been considered for the present analysis where g_{2w} represents the interaction parameter of droplet fluid to the wall. The initial densities of wetting and non-wetting phase fluids are considered as 0.035 and 0.965. The results are demonstrated in the form of wetted area and wetted length of the droplet on the channel wall.

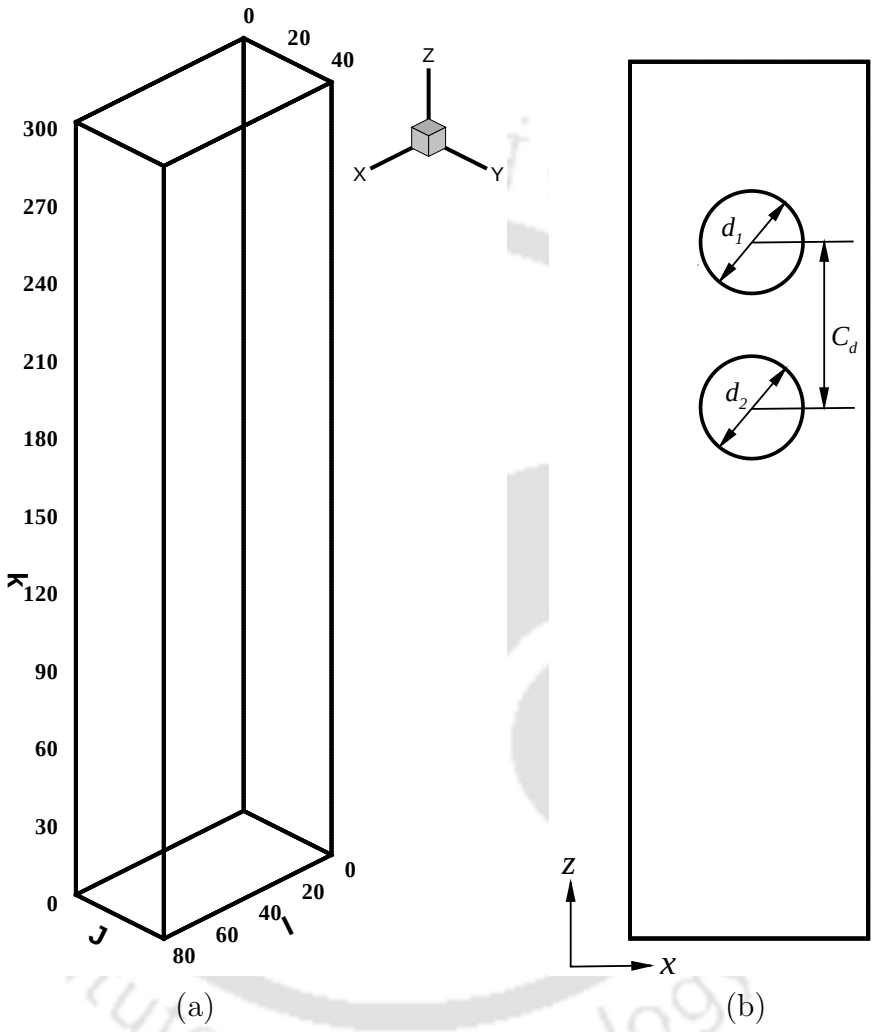

Figure 3.1: (a) Computational Domain, (b) Section of the domain

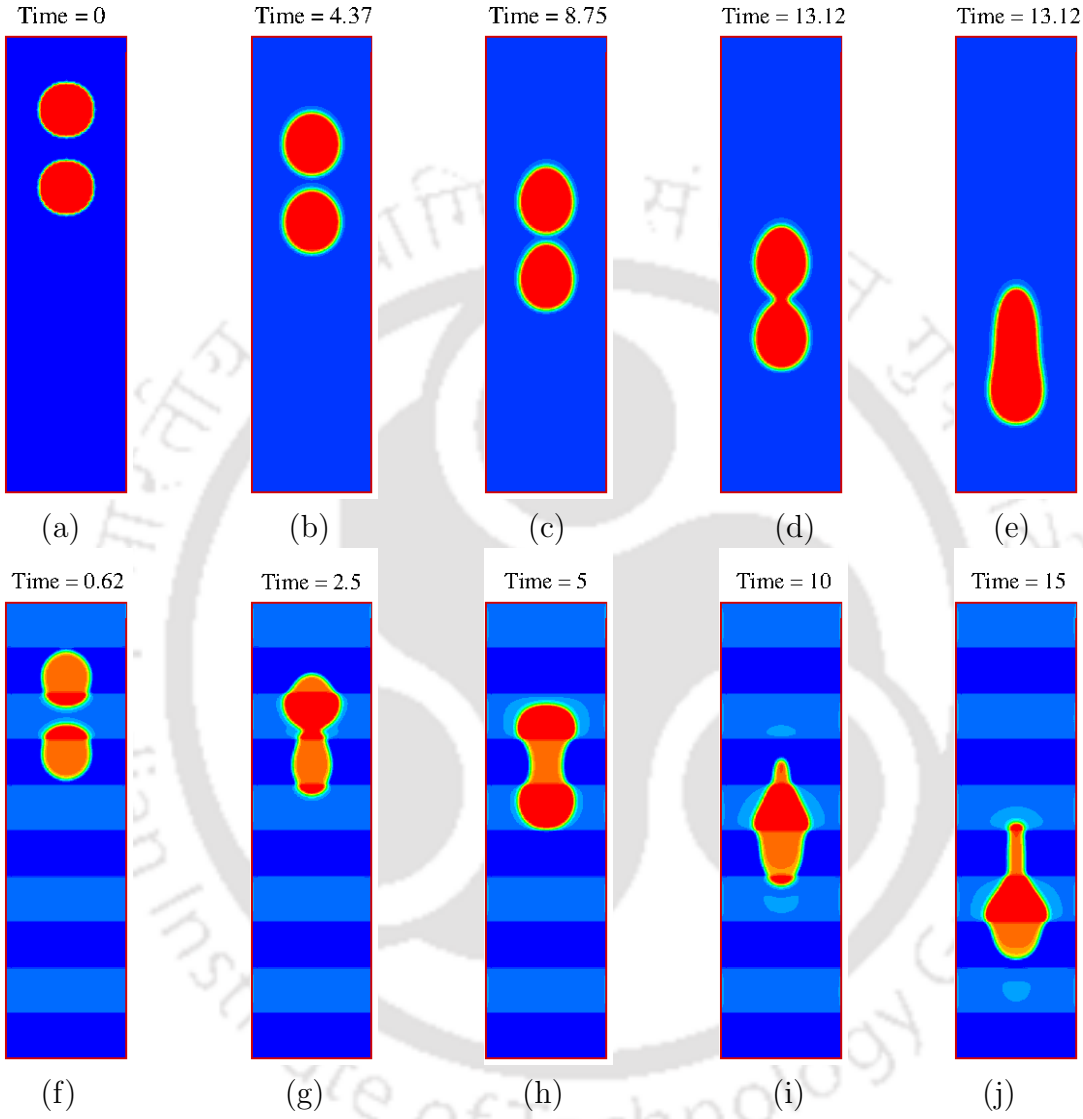

Figure 3.2: Sectional view (i.e., $x - z$ plane) of dynamic behavior of the droplet falling under gravity at Ca = 0.35, C_d=51 lu for hydrophilic surface g_{2w} = -0.02 at Time (a) 0, (b) 4.37, (c) 8.75, (d) 13.12, (e) 17.5, and for mixed wettable surface $g_{2w} = \pm 0.05$ at Time (f) 0.62, (g) 2.5, (h) 5.0, (i) 10.0, (j) 15.0

3.3.1 Effect of centre distance on the coalescence

Figures 3.3-3.4 depicts the evolution of the dimensionless wetted area and wetted length between the droplets and the wall at the capillary number, $Ca = 0.35$ for different values of centre distance, C_d. The plots are demonstrated for the wall having hydrophilic wettability and mixed wettability. It is to be noted that the time is made dimensionless by characteristic time which can be defined as l/U where, l is the length of the channel and U is the characteristic velocity, $U = \frac{\rho_2 g h^2}{\mu_2}$. The basic feature which is observed in the coalescence of droplets is that the two or more droplets come in contact with each other and form a single droplet. When two liquid droplets touch each other, a liquid bridge is formed between the two droplets due to the van der walls forces. Due to this liquid bridging, a negative curvature has been formed at the point where two droplets are touching. This liquid bridge due to interfacial stress expands quickly and finally, two droplets after merging completely form a larger droplet. The similar phenomenon is observed in the present study as shown in Figs. 3.2(a)-(j). Here, two droplets initially placed at a certain distance away from each other and after application of force and as time progresses, droplets start forming a bridge and then merge into a single droplet with deformed structure in both uniform hydrophilic surface (see Figs. 3.2(a)-(e)) as well as mixed wettable surface (see Figs. 3.2(f)-(j)). In the hydrophilic surface channel wall as shown in Figs. 3.3(a)-(b), a single peak for each C_d value is observed which is the point at which the two droplets start merging into a single droplet. The time at which the two droplets start merging is found to be 7.5, 13.12 and 39.37 for centre distance (C_d) equal to 47, 51 and 55 lu, respectively. It is observed that as the distance between the centres of the droplets increases, the time is taken for merging also increases. This fact can be elaborated in a way that in the hydrophilic surface the droplet spreads out on the surface because it has more affinity towards the surface and hence slows down the motion of the droplet. But the upper droplet experiences more gravitational force than the lower one and hence has more moving speed on the surface. The advancement of the upper droplet is more than the advancement of the lower droplet, but the time taken by the upper droplet to approach the lower droplet is more as C_d increases. If we look into the wetted area and wetted length, it is observed that both wetted area and wetted length increase initially up to the point of coalescence of two droplets and after this point it starts decreasing in the case of the hydrophilic surface. It is also observed that when two droplets merge completely

into a single droplet, the wetted area and wetted length again start increasing and reaches steady-state.

In most of the practical situations, we can hardly find the uniform wettable surface. So, it is important to study the effect of centre distance and capillary number on the coalescence of droplets on the mixed wettable surface. Basically, the mixed wettable surface is a combination of hydrophilic and hydrophobic surfaces where hydrophobic and hydrophilic wettable strips are placed alternatively in the domain. In the present problem, the height of each strip is taken as 30 lu. Both the droplets are placed such that it covers part of both types of strips. This is considered so that the droplets behaviour can be studied for both types of wetting characteristics. The spreading behaviour on both the strips is different due to a different wetting structure which can be seen in Figs. 3.2(f)-(j). Figures 3.4(a)-(b) show the wetted area and wetted length of droplets on the mixed wettable surface. When the droplet is moving on the hydrophilic region, it tries to spread on the surface due to wetting tendency and when it moves on the hydrophobic surface, it tries to contract. This is the prime reason of getting the periodic behaviour in the wetted area and wetted length in the case of mixed wettable surface case. As in the present case, most of the area of the droplets fall in the hydrophobic region, the coalescence occurs in the hydrophilic region due to more spreading of the droplets. This happens due to the large stretching of the droplet when it crosses the hydrophobic region and enters into the hydrophilic region in the case of the upper droplet and hydrophilic region to hydrophobic region in the case of the lower droplet. As the centre distance increases, the area of the lower droplet which falls in the hydrophilic region keeps on reducing and hence time taken for coalescence is more. It is observed that the time of coalescence of two droplets is less in the mixed wettable surface compared to the uniform hydrophilic surface.

3.3.2 Effect of the capillary number on coalescence

Figures 3.5-3.6 show the effect of the capillary number on the wetted area and wetted length on the hydrophilic and mixed wettable surface at a centre distance, C_d=51 lu. The capillary number is the ratio of viscous force to interfacial force which can be defined as, $Ca = \frac{\rho_2 g V_2}{\sigma h}$, where V is the volume of the droplet, h is the width of the channel, σ is the surface tension, ρ_2 is the density of droplet fluid and g is the gravitational factor.

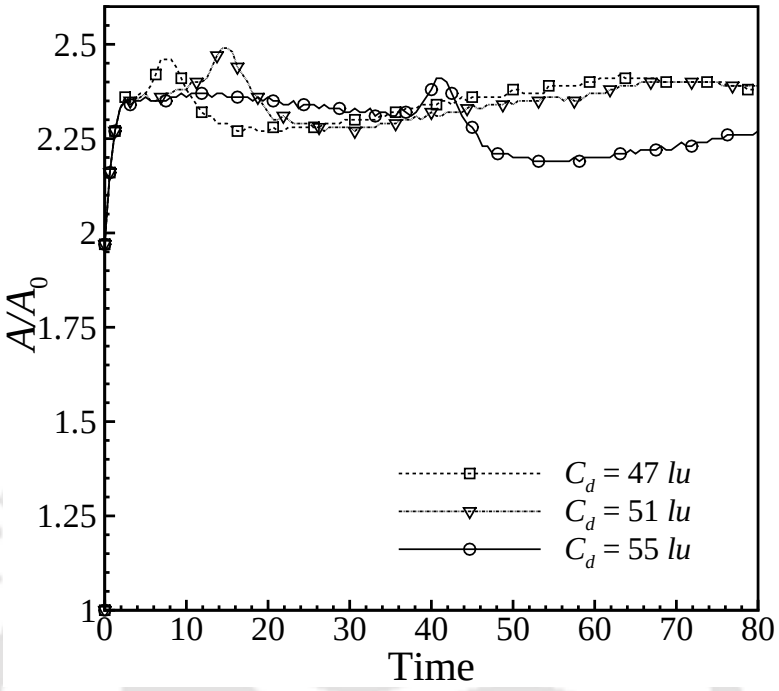

(a)

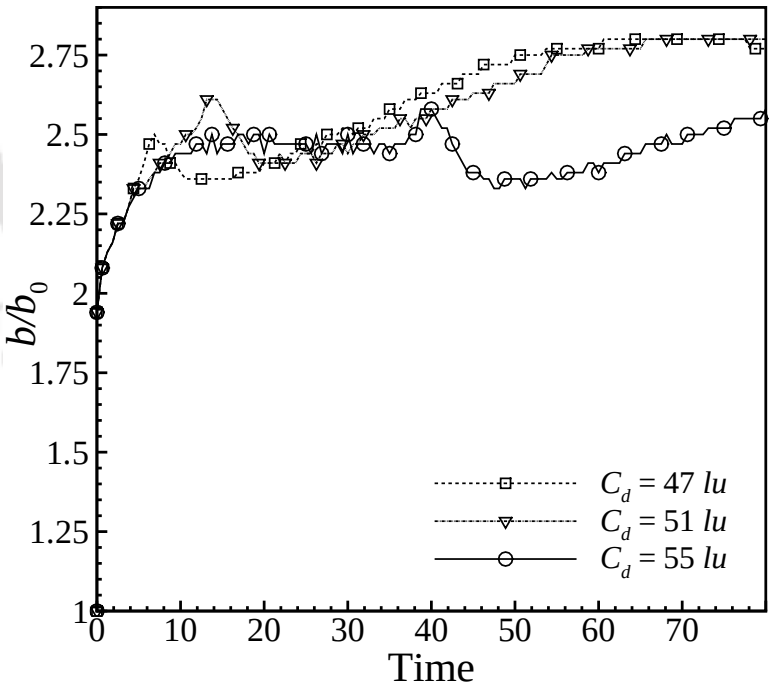

(b)

Figure 3.3: The effect of center distance between the droplets (C_d) at Ca=0.35 on hydrophilic surface (a) wetted area, A/A_0 (b) wetted length, b/b_0

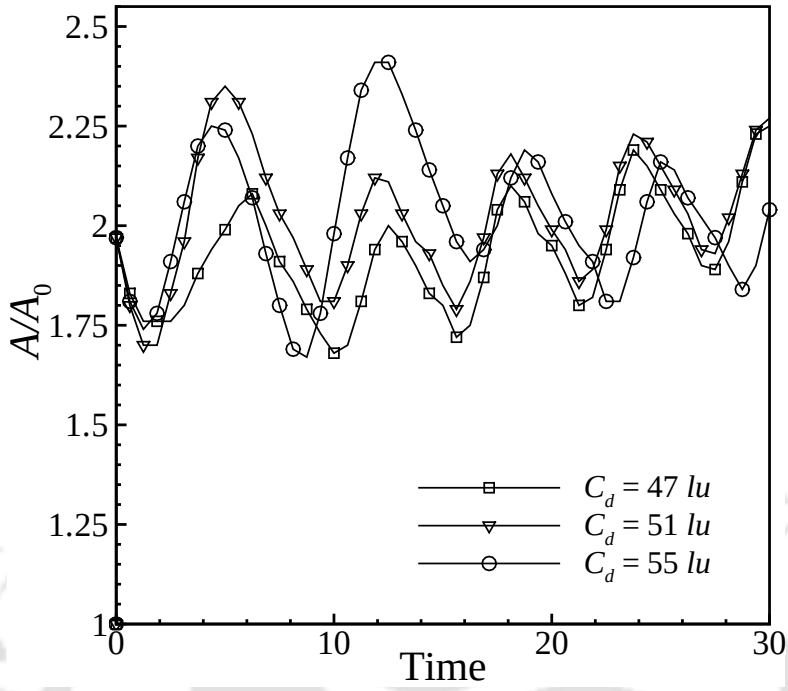

(a)

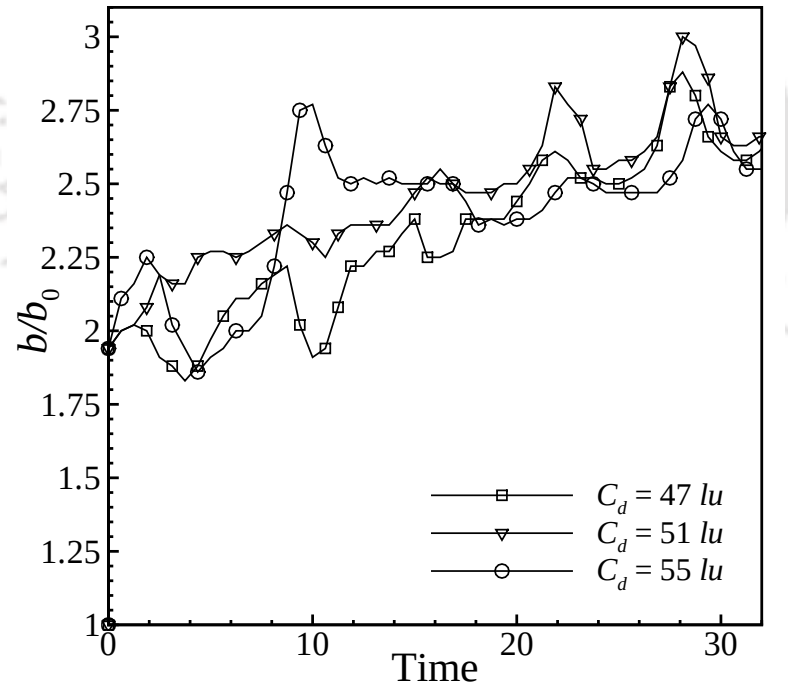

(b)

Figure 3.4: The effect of center distance between the droplets (C_d) at Ca=0.35 on mixed wettable surface (a) wetted area, A/A_0 (b) wetted length, b/b_0

The different capillary number can be obtained by changing the gravitational factor (g), droplet size and surface tension (σ), but the most appropriate way of changing capillary number is the gravitational factor, g. So, in the present study, three different capillary numbers (i.e., Ca=0.35, 0.50, 0.81) have been obtained by changing the gravitational factor, g. The wetted area and wetted length increase gradually as capillary number increases in the case of the hydrophilic surface as shown in Figs. 3.5(a)-(b). As capillary number increases, the viscous stresses along the interface increase which in-turn increase the deformation of droplets. It is also observed that the increase in wetted area is less than the increase in the wetted length. The time at which the droplets start to coalesce is found to be equal to 13.12, 12.5 and 8.69 for capillary number 0.35, 0.50 and 0.81, respectively. Figures 3.6(a)-(b) show the wetted area and wetted length on the mixed wettable surface for three capillary numbers. It is observed that the interface between the wall and the droplets deforms from its initial round shape. It is also observed that this deformation keeps on increasing as capillary number increases. The time taken to start coalescence in the mixed wettable surface at $C_d = 51$ lu is found to be equal to 2.5, 3.12 and 5.79 for capillary number 0.35, 0.50 and 0.81 respectively. In this case, the wetted length keeps on increasing due to the elongation of the droplet at the junction of the hydrophilic and hydrophobic region whereas, wetted area decreases. Figures 3.7(a)-(b) show the comparison of magnitude and behaviour of wetted area and wetted length between the sliding droplet and channel wall considering different wettabilities (i.e., hydrophilic and mixed wettability) at $C_d = 51$ lu and Ca=0.35. It is found that in the case of uniform hydrophilic wettability, the wetted area and wetted length both increase with time initially and after coalescence decreases and again increases to a steady state. Whereas, in mixed wettability case the wetted length increases due to the large elongation of the droplet during the motion but wetted area reduces at a time when droplet crosses the hydrophilic-hydrophobic junction region. It is also observed that the magnitude of the wetted area is more in the uniform hydrophilic case compared to mixed wettability case.

3.4 Summary

A numerical analysis has been carried out to investigate the implications of the dynamic behaviour of the coalescence of two droplets placed on a rectangular channel

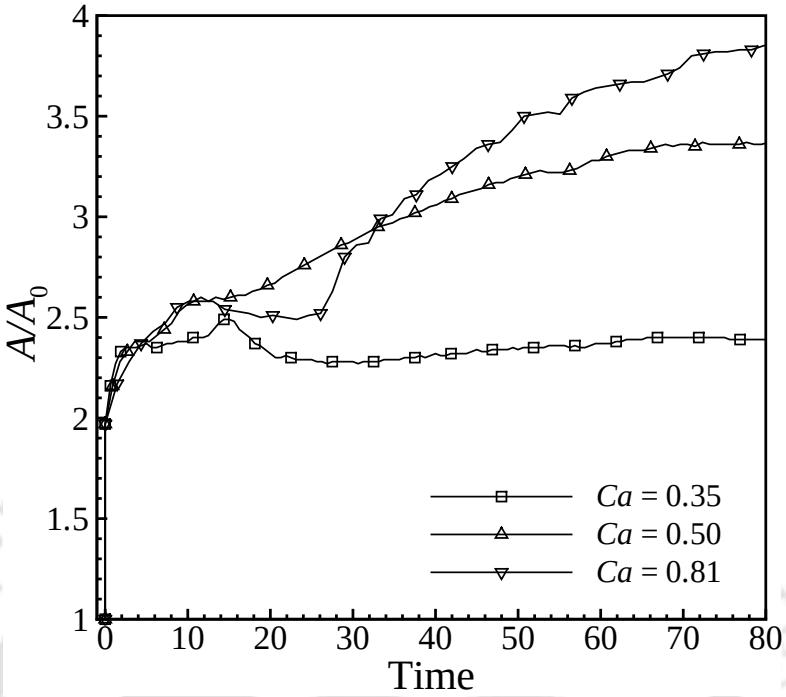

(a)

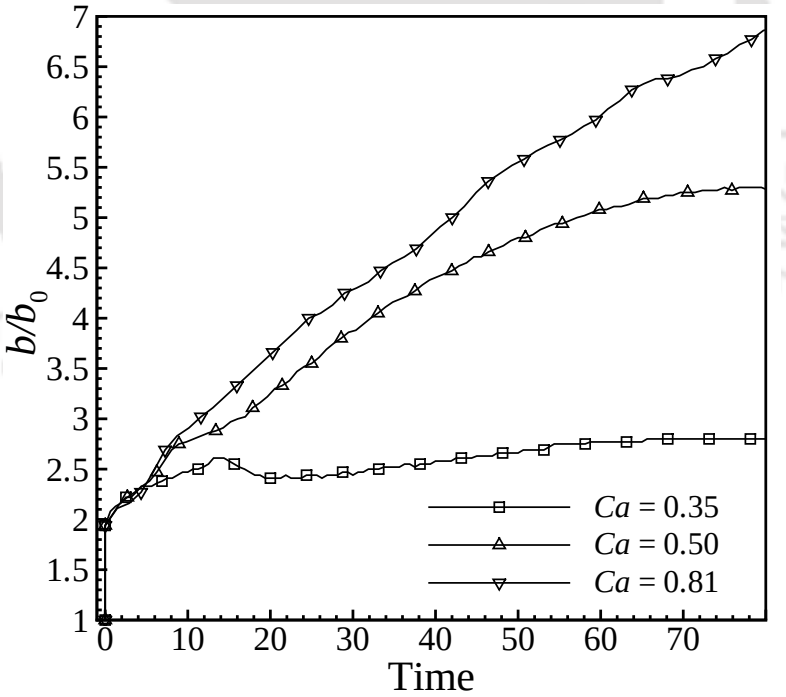

(b)

Figure 3.5: The effect of capillary number (Ca) at $C_d = 51$ lu on hydrophilic surface (a) wetted area, A/A_0 (b) wetted length, b/b_0

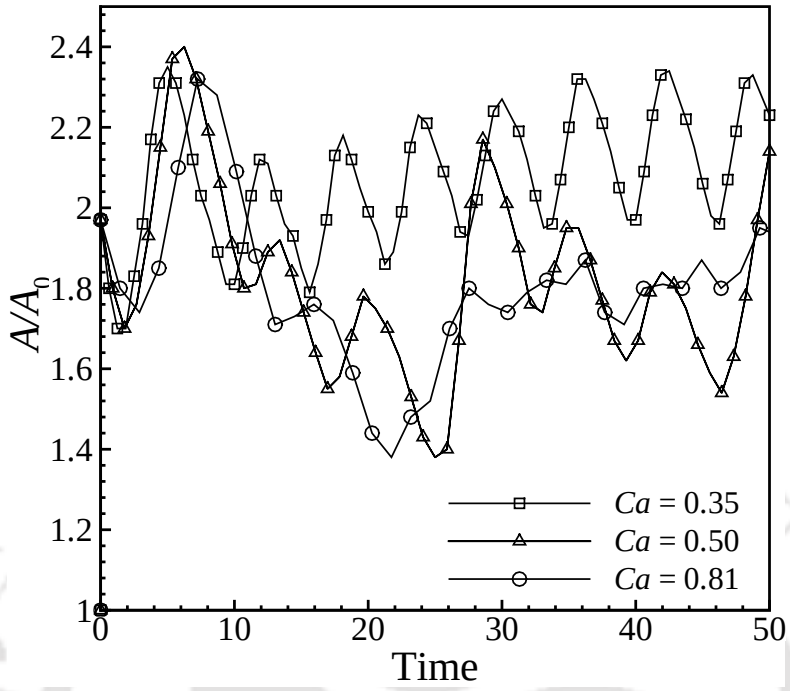

(a)

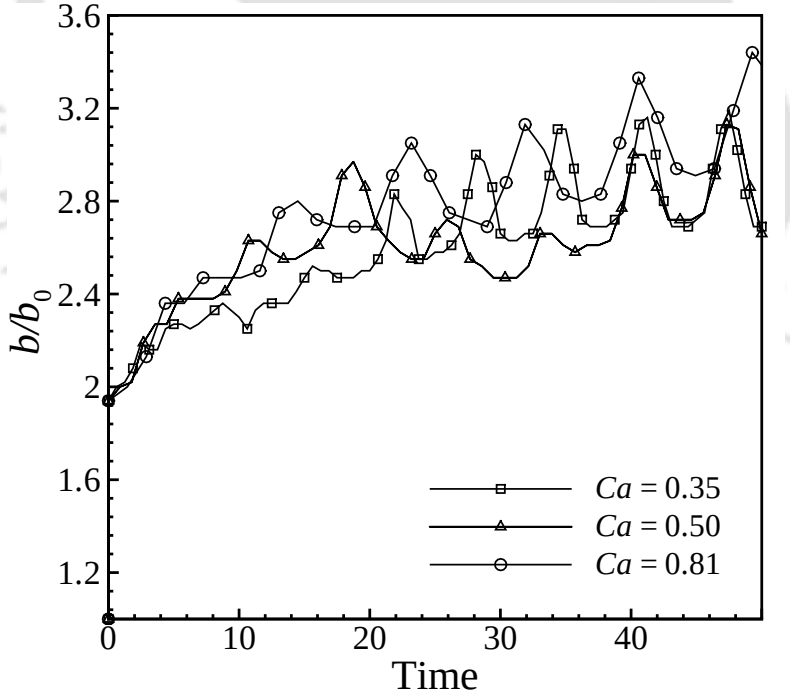

(b)

Figure 3.6: The effect of capillary number (Ca) at $C_d = 51$ lu on mixed wettable surface (a) wetted area, A/A_0 (b) wetted length, b/b_0

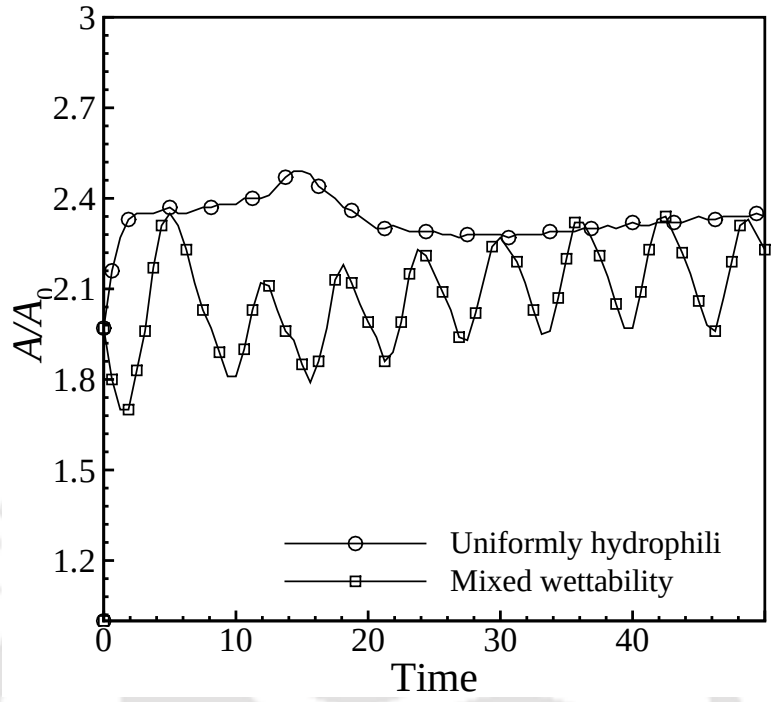

(a)

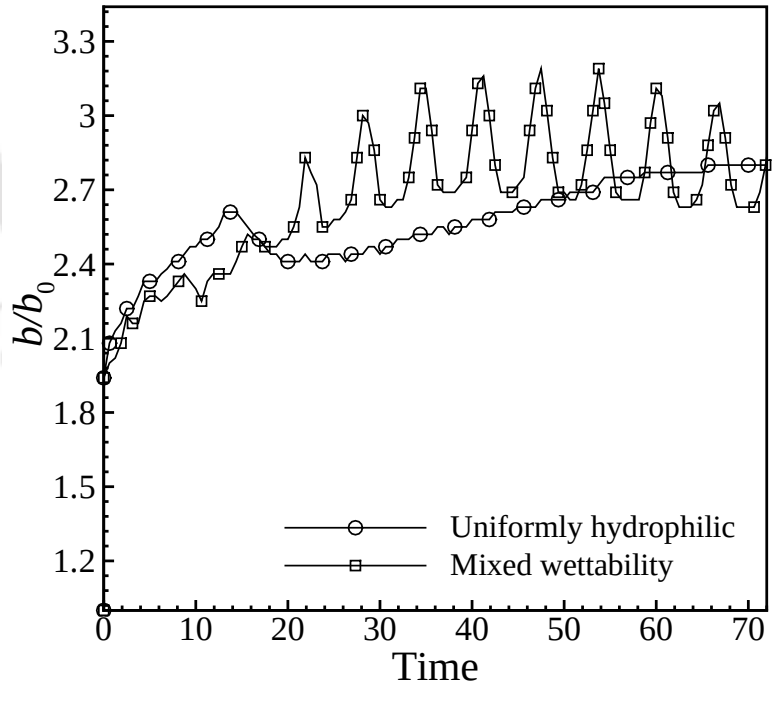

(b)

Figure 3.7: The evolution of wetted area and wetted length between the sliding droplet and channel wall considering different wettabilities at C_d = 51 lu and Ca=0.35, (a) wetted area, A/A_0 (b) wetted length, b/b_0

wall considering wetting effects. In order to asses the effects of centre distance between the droplets on the displacement in the form of wetted area and wetted length, a time study has been performed. It is noteworthy to mention that the time of coalescence of droplets is sometimes a major factor in several engineering and nature applications. In the present study, it is revealed that the type of wettability plays an important role in the coalescence of two droplets in a channel wall. In addition to this, it is also noticed that the two droplets coalesce more frequently in the case of mixed wettability compared to uniform hydrophilic wettability for a certain capillary number. An interesting feature to be observed is that the increase in capillary number increases the time taken by the droplets to start merging in mixed wettability case. Another investigation which is carried out is to examine the effect of centre distance between droplets and concluded that an increase in centre distance increases the time of coalescence.

Chapter 4

Dynamic Droplet Behavior on Wetted Flat and Grooved Surface of Channel For Low Viscosity Ratio

4.1 Introduction

Several studies have been conducted to understand the physics of displacement of a three-dimensional immiscible droplet on a wettable surface by many researchers experimentally as well as numerically. The phenomenon of displacement of immiscible fluid on a flat as well as rough surfaces or surfaces having groove has attracted many researchers due to its application in inkjet printing, coating, enhanced oil recovery etc. The effect of capillary number, droplet sizes and different wettability scenarios have been examined on the displacement of three-dimensional immiscible droplet keeping viscosity ratio constant. Till now, a very few studies have been performed to see the effect of different viscosity ratios on the displacement of a three-dimensional immiscible droplet on a wettable wall through a duct. The surface characteristics play a major role in the displacement or spreading of the droplet on the channel wall. The main characteristic of the surface is its roughness. Many researchers have focused on the analyses of droplet displacement on the rough or grooved surface.

4.2 Problem specification

The present work studies the influence of wettability and low viscosity ratio on the droplet spreading behaviour adhering on a vertical wettable wall in a rectangular microchannel as shown in Fig. 4.1. The simulations are carried out in a rectangular microchannel having length, width and breadth as 300, 41 and 81 lattice units (lu), respectively in case of flat wall and 300, 61 and 81 lu, respectively in a grooved wall case. The problem also considers the two immiscible fluids in which droplet (fluid 2) is placed in the domain filled with displacing fluid (fluid 1). The radius of the droplet is considered to be 18 lu. The droplet is initially placed at $z = 251$. The fluid or droplet motion has been governed by the gravitational force which is applied in the negative z-direction. The dynamics of droplet is explored over range of viscosity ratio for different contact angles, i.e., $\theta = 78°$ (hydrophilic), 118° (hydrophobic) and also for Ca = 0.1, 0.35, 0.66. The periodic boundary condition is applied in the z-direction and no slip (i.e., bounce back) boundary condition has been applied at all walls located in x- and y-directions.

4.3 Results and discussion

The present work deals with a parametric study to see the effect of low viscosity ratio, $M \leq 1$ on the displacement of three-dimensional immiscible droplet adhering to the wetted wall of a rectangular microchannel. In some situations of enhanced oil recovery (EOR), the viscosity ratio of fluids become very important. Thus, it is necessary to explore the physics of capillarity-wettability interactions along with low viscosity ratios in droplet dynamics inside a microchannel. In the present analysis, the three different capillary numbers, i.e., Ca= 0.1, 0.35 and 0.66, have been considered with two wetting conditions, i.e., hydrophobic ($g_{2w} = 0.05$) and hydrophilic ($g_{2w} = -0.02$), to study the droplet displacement behavior. Time is made dimensionless by characteristic time $\frac{l}{U}$, where l is characteristic length and U is defined as characteristic velocity, $U = \frac{\rho_2 g h^2}{\mu_2}$ [101]. The other parameters considered in the present analysis are as follows: initial density of fluid 1, $\rho_1 = 0.035$, initial density of fluid 2, $\rho_2 = 0.965$, relaxation time for fluid domain, $\tau_1 = 0.75$. The motion of the droplet is governed by the gravitational force which is acting in the negative z-direction.

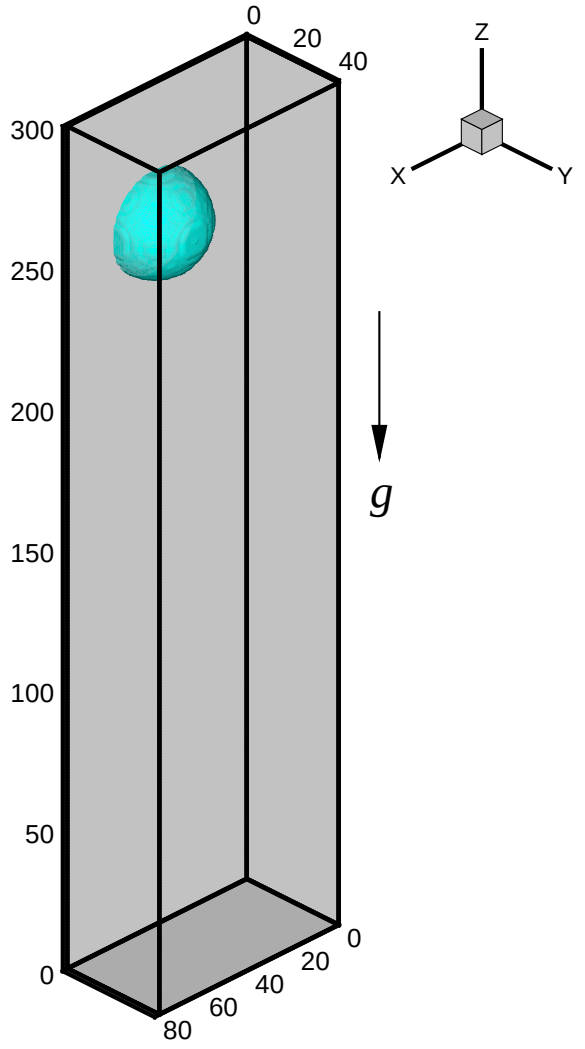

Figure 4.1: Schematic diagram of computational domain

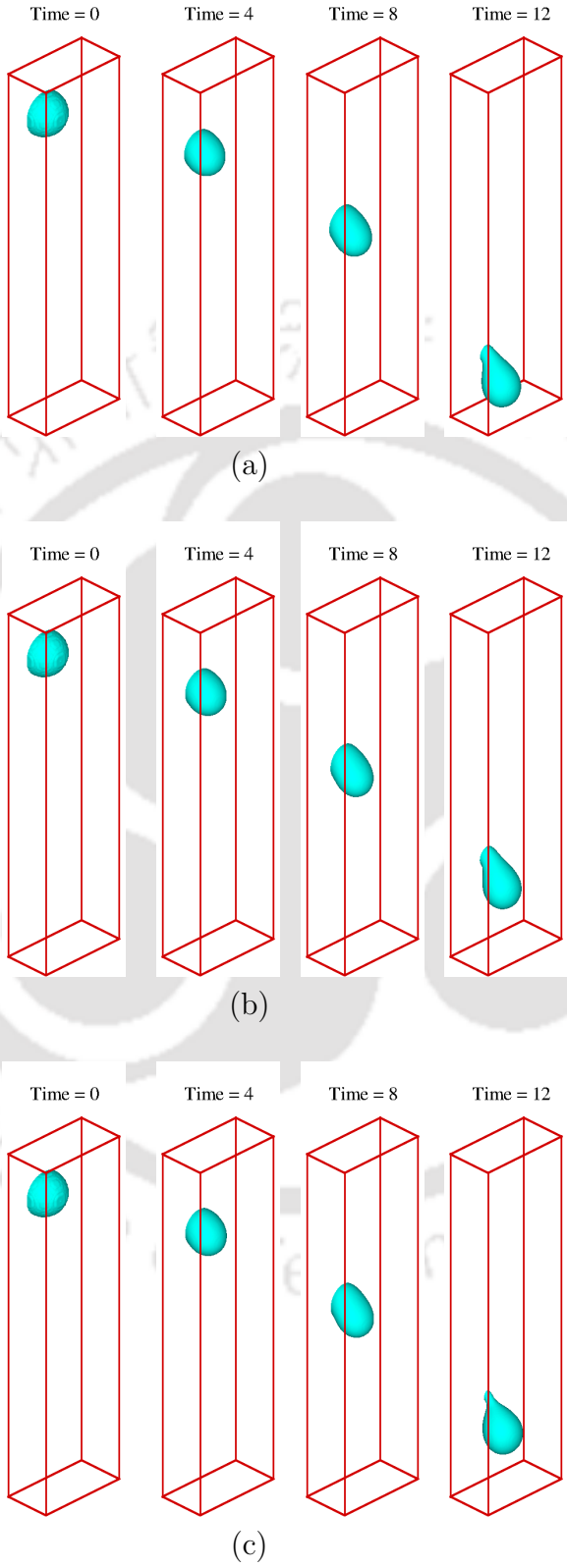

Figure 4.2: Dynamic droplet behavior under gravity with different lattice time at Ca = 0.35, $g_{2w} = 0.05$ and viscosity ratio, (a) $M = 0.7$, (b) $M = 0.8$, (c) $M = 0.9$

4.3.1 Effect of viscosity ratio on droplet displacement behaviour

To investigate the droplet displacement behaviour, two uniform wetting conditions on the wall of the microchannel have been taken. The first wetting condition to be considered is known as uniform hydrophobic and another condition is known as uniform hydrophilic. Basically, wetting or wettability is the property of the surface which defines the ability of a fluid to spread on the solid surface. In nature, different types of wetting patterns are found in which uniform hydrophobic and hydrophilic are two of them. It is to be noted that the wettable nature of the solid surface majorly affects the displacement behaviour of the droplet on the wall. In case of the uniform hydrophobic wettable surface, the surface tries to repel the mass of fluid and in case of hydrophilic wettability, the surface tries to attract and make a bond with the mass of fluid. Figure 4.2 shows the dynamic droplet behavior at different lattice time for capillary number, Ca=0.35 and different viscosity ratios (M=0.7, 0.8, 0.9) on a hydrophobic ($g_{2w} = 0.05$) wettable wall. Initially, a spherical droplet is attached to the wall surface. As time increases, a decrease in the contact surface area between the droplet and the wall is observed as shown in Figs. 4.2(a-c). At Time=12, the contact area is found to be very less and after which the droplet gets detached from the wall with the formation of the sharp neck. The contact area between the droplet and wall at M=0.9 and Time=12 is found to be less than the contact area at M=0.7. It is because of the fact that the cohesive forces are strong at high viscosity ratio and hence tries to reduce the contact between the droplet and wall which can also be clearly seen in Figs. 4.3-4.4. The effect of viscosity ratio on the wetted area and wetted length can also be seen in Figs. 4.7(a)-(b). It is found that initially, the viscosity ratio does not affect much the displacement and deformation of the droplet. But as time progresses, the viscosity ratio increases, the displacement of droplet becomes faster and droplet detaches from the the wall in less time. Hence, the wetted area and wetted length of the droplet decrease with time. The main cause of this behaviour is that the hydrophobicity along with cohesive forces help the droplet to move further under the action of gravitational force. Hence, a quicker detachment of the droplet as a whole is observed.

Figures 4.5-4.6 illustrate the shape of droplet in $y - z$ plane at $x = 40$ lu and $x - z$ plane at Ca=0.35, hydrophilic wettable wall ($g_{2w} = -0.02$) and Time=20

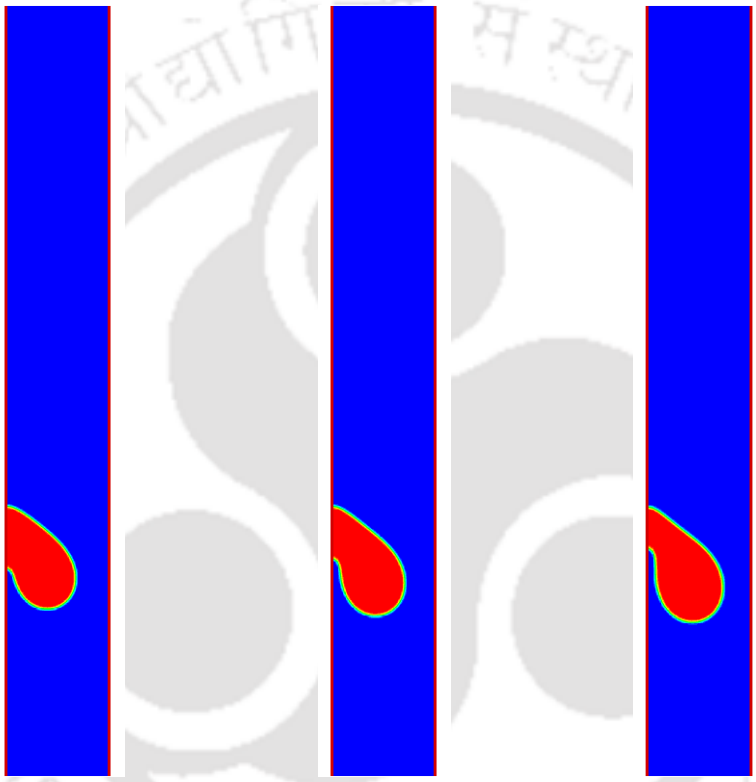

(a) (b) (c)

Figure 4.3: The shape of the droplet in $y-z$ plane at $x = 40$ lu for Ca $= 0.35$, $g_{2w} = 0.05$, lattice Time=8 and viscosity ratio (a) $M = 0.7$, (b) $M = 0.8$, (c) $M = 0.9$

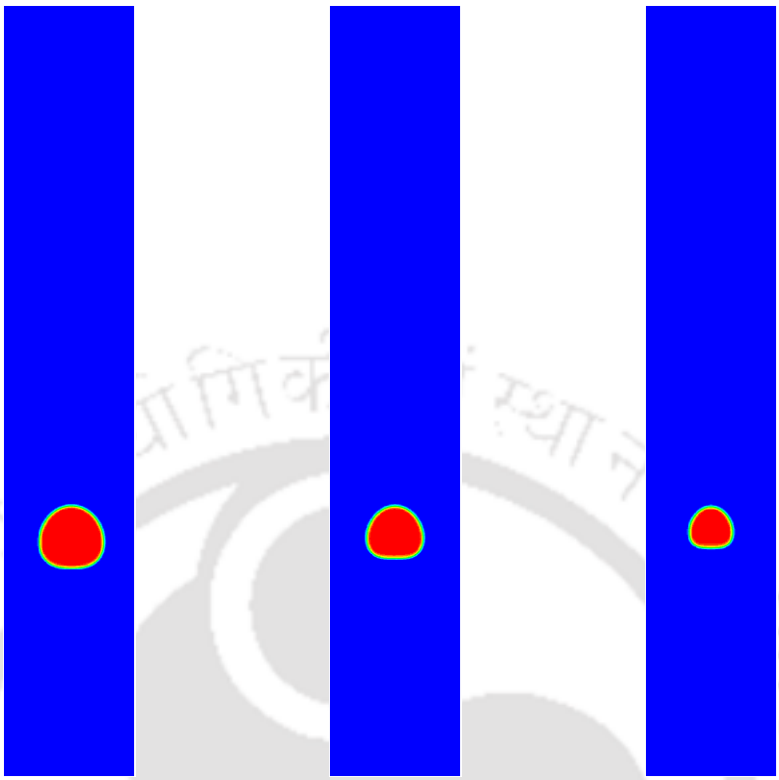

Figure 4.4: The shape of the droplet in $x-z$ plane view at wall for Ca = 0.35, g_{2w} = 0.05, lattice Time=8 and viscosity ratio (a) M = 0.7, (b) M = 0.8, (c) $M = 0.9$

for different viscosity ratio, M. As mentioned earlier, hydrophilic surface allows a droplet of water to spread out. The affinity between liquid and a surface influences not only the behaviour of a static drop of liquid but also greatly affects the motion of a moving droplet. The shape of the droplet deforms due to hydrophilicity, capillary forces and gravitational force. It is seen in Figs. 4.5(a)-(c) that the droplet gets deformed more in the case of large viscosity ratio (Fig. 4.5(c)) although the size of the droplet seems bigger for $M = 0.9$ compared to $M = 0.7$. A clear picture related to the contact surface area of the droplet on the wall has been presented in Figs. 4.6(a)-(c) in which three plots are shown for three different viscosity ratios at a fixed time. It is observed that as viscosity ratio increases at fixed the capillary number in the hydrophilic wall surface, the contact area of the droplet also increases which is the reverse topology compared to the hydrophobic case (see Fig. 4.4). The reason behind this fact is that at very low viscosity ratios, the wetting tendency of the hydrophilic wall dominates on the droplet attached to the wall and hence more

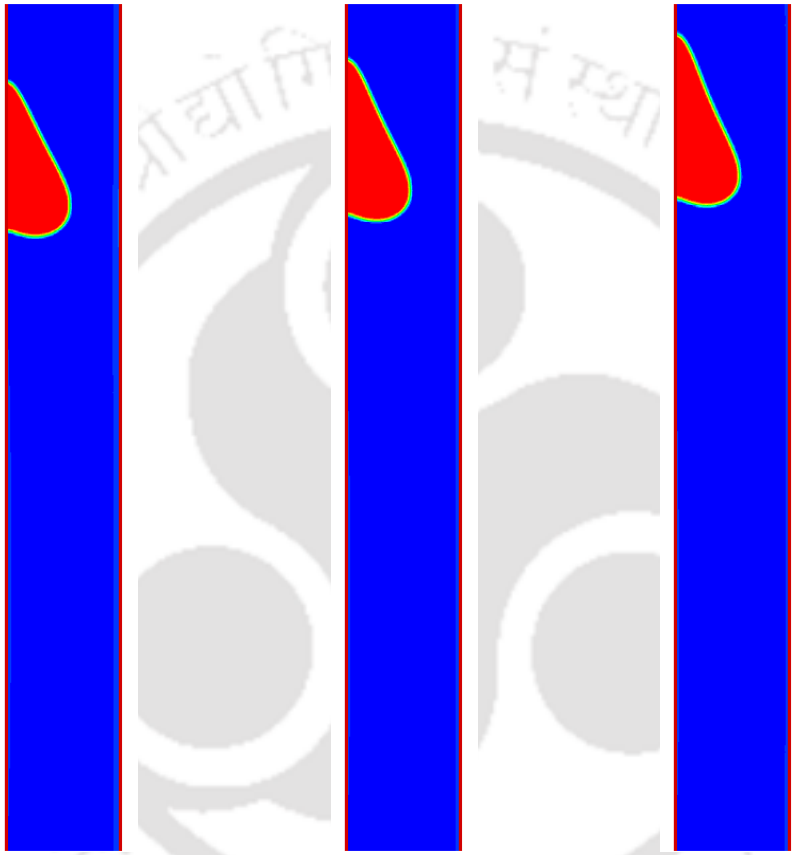

(a) (b) (c)

Figure 4.5: The shape of the droplet in $y-z$ plane at $x = 40$ lu for Ca $= 0.35$, $g_{2w} = -0.02$, lattice Time=20 and viscosity ratio (a) $M = 0.7$, (b) $M = 0.8$, (c) $M = 0.9$

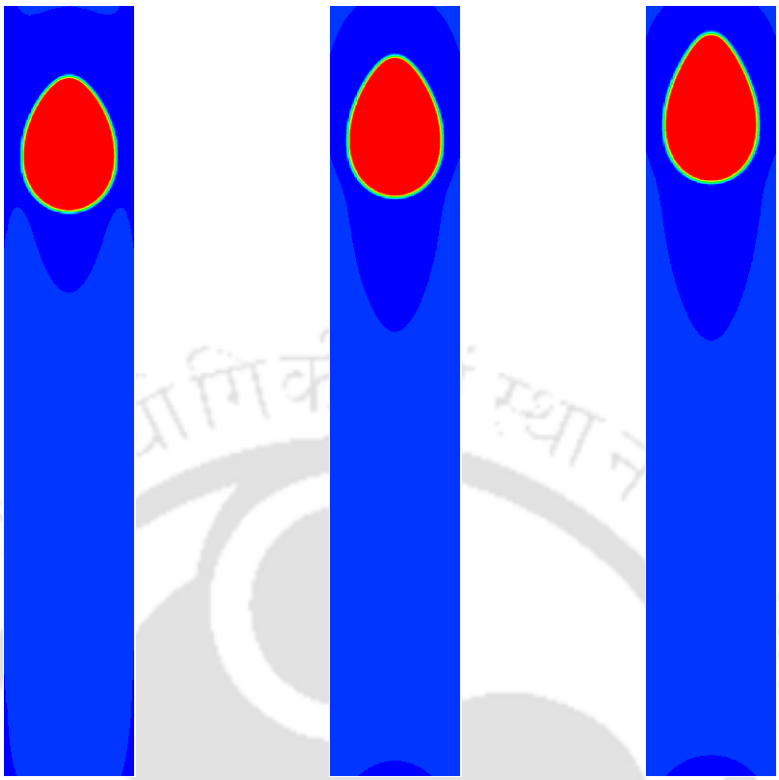

(a) (b) (c)

Figure 4.6: The shape of the droplet in $x-z$ plane view at wall for Ca = 0.35, $g_{2w} = -0.02$, lattice Time=20 and viscosity ratio (a) $M = 0.7$, (b) $M = 0.8$, (c) $M = 0.9$

spreading of the droplet observed on the wall surface and contact area continues to grow. The evolution of the wetted area and the wetted length is shown in Figs. 4.8(a)-(b) for hydrophilic wettability case. It is noticed that both wetted area and wetted length increase monotonically as time progresses. The more spreading of a droplet on the wall surface as the viscosity ratio increases, increase the wetted area and wetted length as shown in Figs. 4.8(a)-(b). More increase in wetted length observed due to the direction of the driving force, i.e., gravitational force in addition to the spreading on the surface. When the viscosity ratio is more, the movement of the droplet becomes slow and the droplet tries to spread more on the wall surface, hence the wetted area and wetted length increase relatively.

For simulating all the cases, a D3Q19 Shan-Chen (S-C) lattice Boltzmann method has been used which is used extensively due to its simplicity and pseudo-potential nature. Another promising feature of this method is the automatic separation of

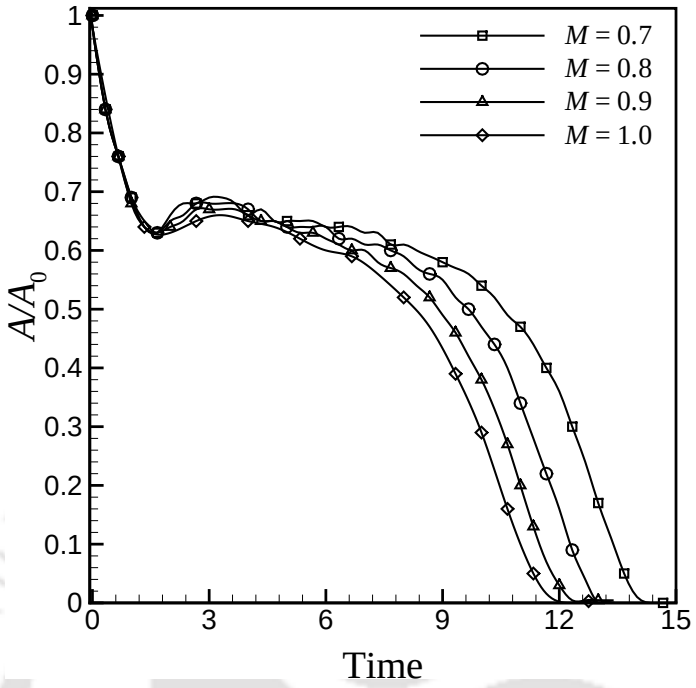

(a)

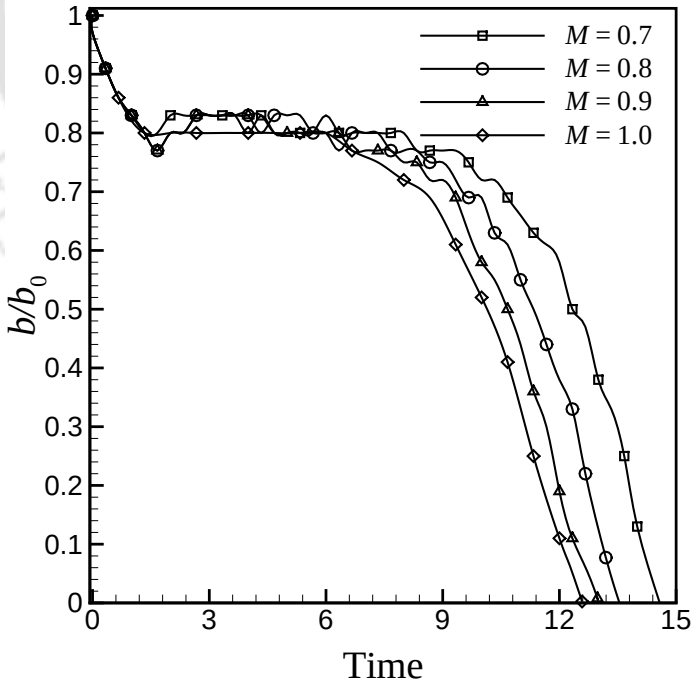

(b)

Figure 4.7: Effect of viscosity ratio at Ca = 0.35 and g_{2w} =0.05, (a) Time evolution of wetted area, (b) Time evolution of wetted length

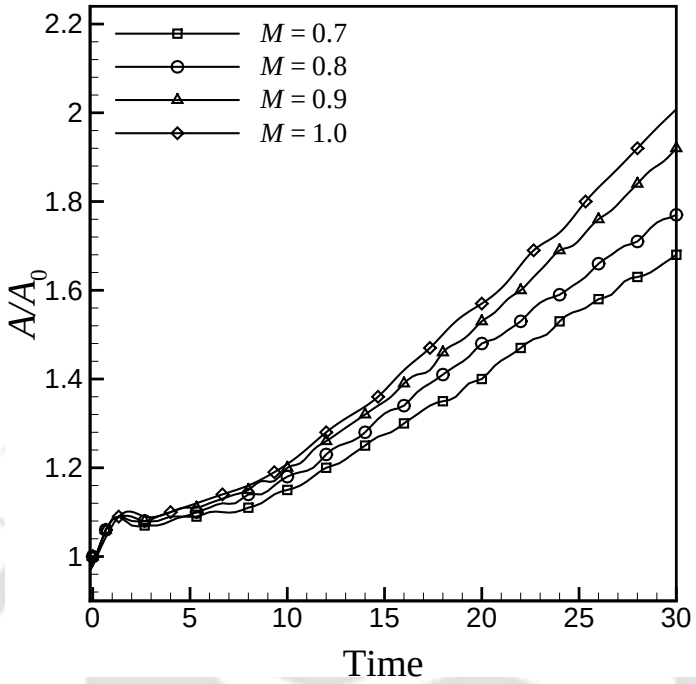

(a)

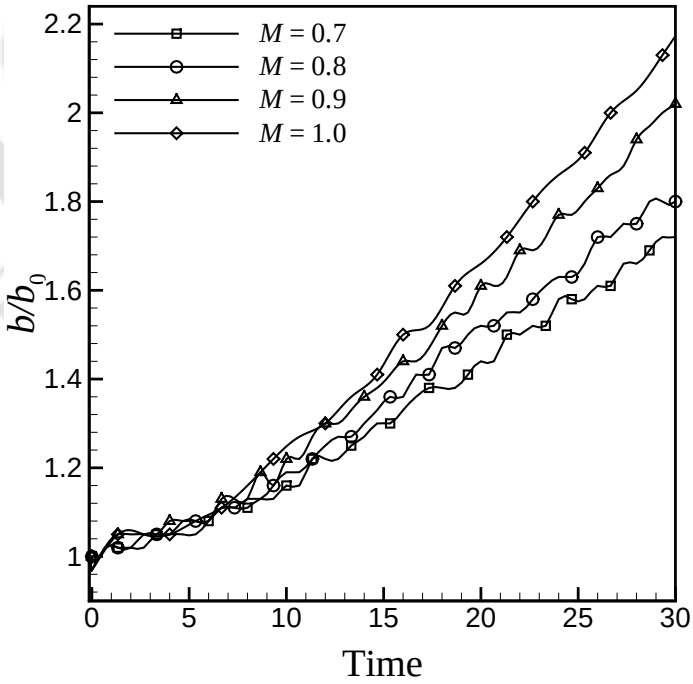

(b)

Figure 4.8: Effect of viscosity ratio at Ca = 0.35 and g_{2w} =-0.02, (a) Time evolution of wetted area, (b) Time evolution of wetted length

two phases and hence, no special interface tracking scheme or method is not required. The main drawback of S-C model is the limitation posed on density ratio and viscosity ratios. In literature, most of the researchers have reported that the S-C model works well for density ratio equal to 10 and viscosity ratio equal to 5. But in literature, only the upper limit of the viscosity ratios has been reported, no literature has talked about the lower limit of the viscosity ratio for below which S-C model works well. In the present analysis, it is observed that for the hydrophilic case, S-C model gives unphysical results for the viscosity ratio below 0.7. This might be the case in which the S-C model does not work well and gives erroneous results due to its lower limit on viscosity ratios.

4.3.2 Effect of the capillary number on droplet displacement behaviour

The effect of the capillary number on the droplet displacement behaviour at a fixed viscosity ratio and time on a hydrophobic wall surface is shown in Figs. 4.9(a)-(c). A capillary number is a non-dimensional number which is nothing but a ratio of viscous force to surface tension force acting across the interface of two immiscible fluids and defined as, Ca=$\frac{\rho_2 g V}{\sigma h}$ where, ρ_2 is the density of fluid 2, g represents the gravitational acceleration, V is volume of spherical droplet, σ is surface tension and h is the width of the rectangular microchannel. It is to be noted that to displace the droplet from its initial position, a greater magnitude of force compared to viscous and surface tension force as a whole is required. From Figs. 4.9(a)-(c), it can be observed that at higher capillary number. Ca=0.66, the extent of deformation of the droplet is more than the low capillary number, Ca=0.1. It is also investigated that as the capillary number increases the displacement of a droplet on the surface is much faster than the low capillary number. The main reason for this behaviour is the combined effect of large gravitational force with the hydrophobic nature of surface and surface tension at the high capillary number. It can also be observed that at the high capillary number, Ca=0.66, a decrease in both the wetted area and wetted length is more compared to a low capillary number, Ca=0.1.

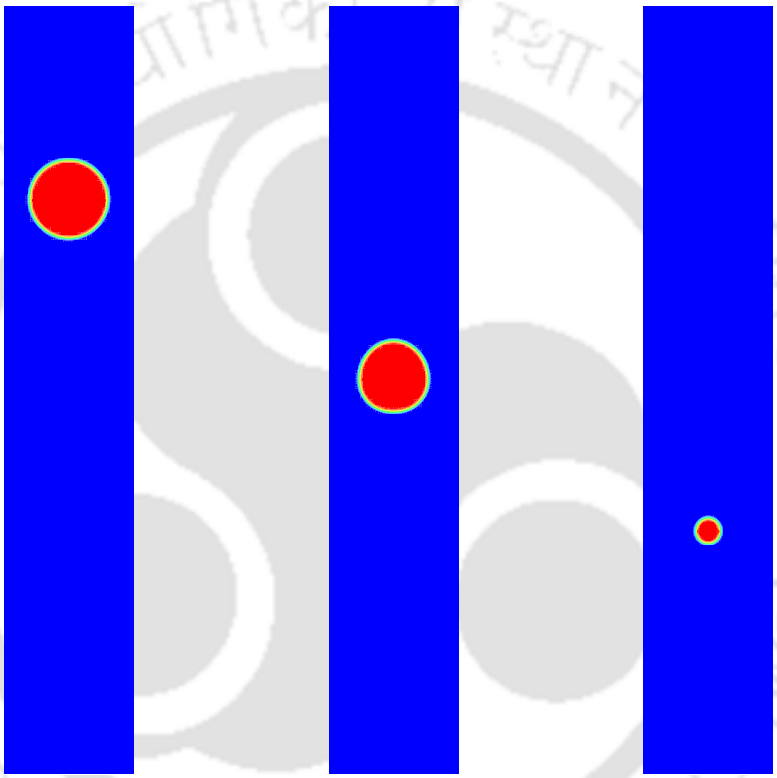

Figure 4.9: The shape of droplet in $x-z$ plane view at wall for $g_{2w} = 0.05$, lattice Time=8 and viscosity ratio, $M = 0.8$ (a) Ca=0.1, (b) Ca=0.35, (c) Ca=0.66

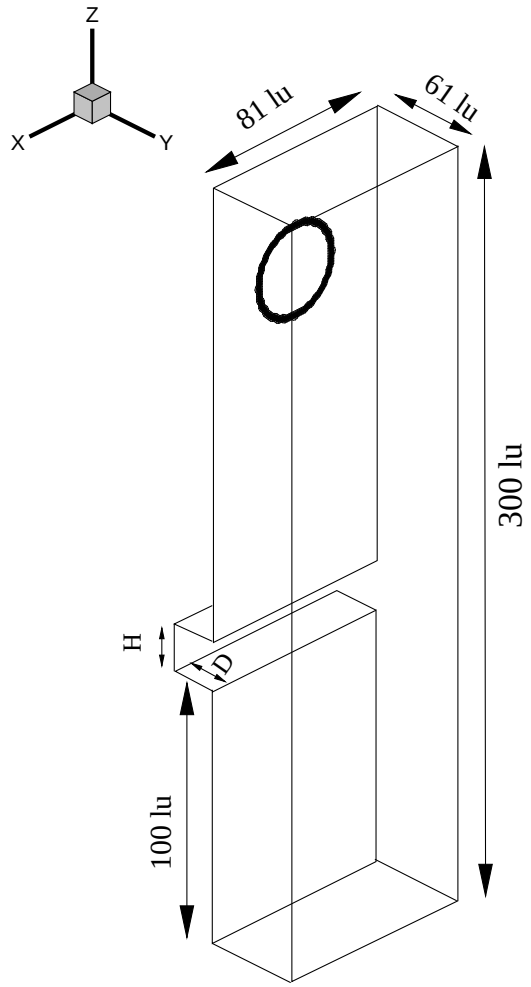

Figure 4.10: Schematic of the grooved surface vertical wall computational domain

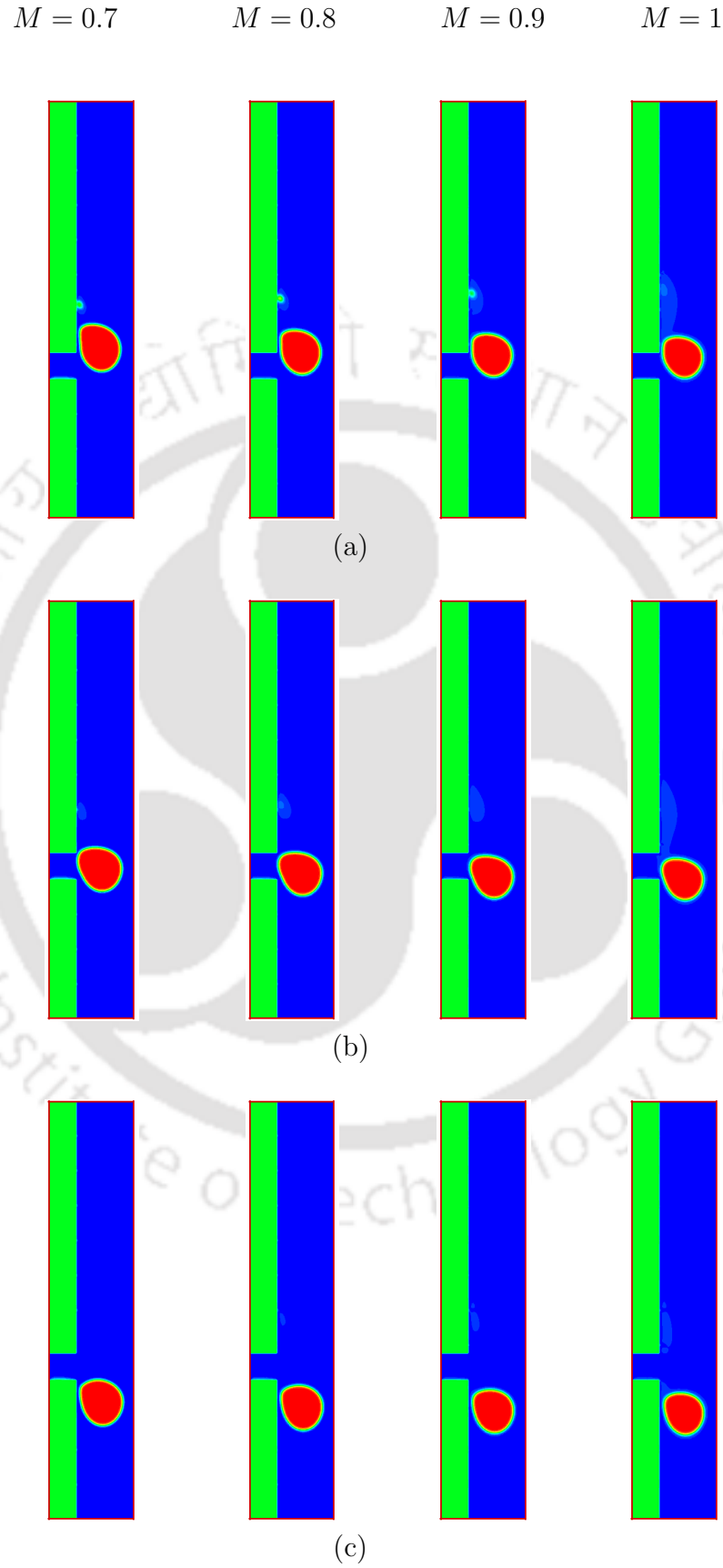

Figure 4.11: Dynamic droplet behavior on grooved wall at Ca = 0.35, groove height=20 lu, $g_{2w} = 0.05$ and non-dimensional time, (a) Time=9.37, (b) Time=10, (c) Time=10.93

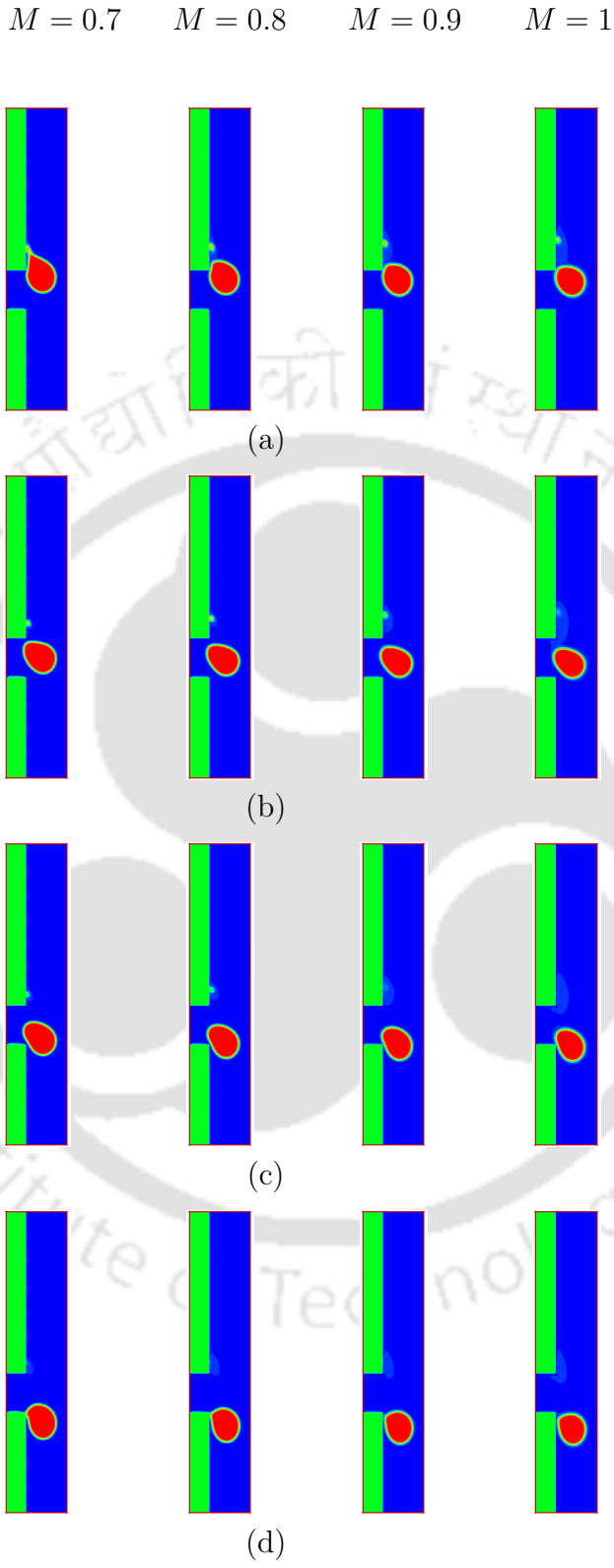

Figure 4.12: Dynamic droplet behavior on grooved wall at Ca = 0.35, groove height=40 lu, $g_{2w} = 0.05$ and non-dimensional time, (a) Time=8.75, (b) Time=9.37, (c) Time=10, (d) Time=10.63

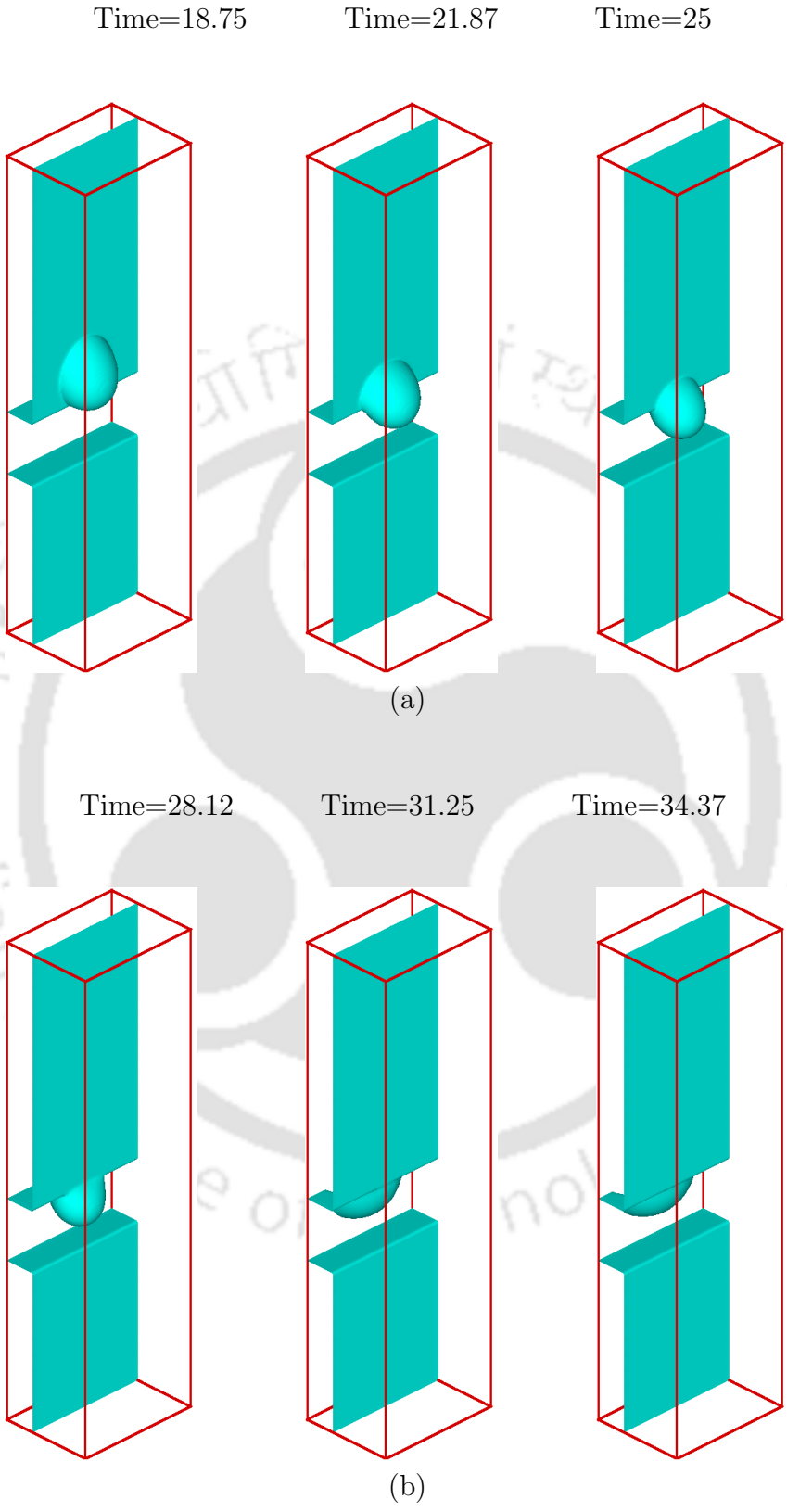

Figure 4.13: Dynamic droplet behavior under gravity on grooved wall at Ca = 0.1, $g_{2w} = -0.02$, viscosity ratio, $M = 1$ and at different lattice time

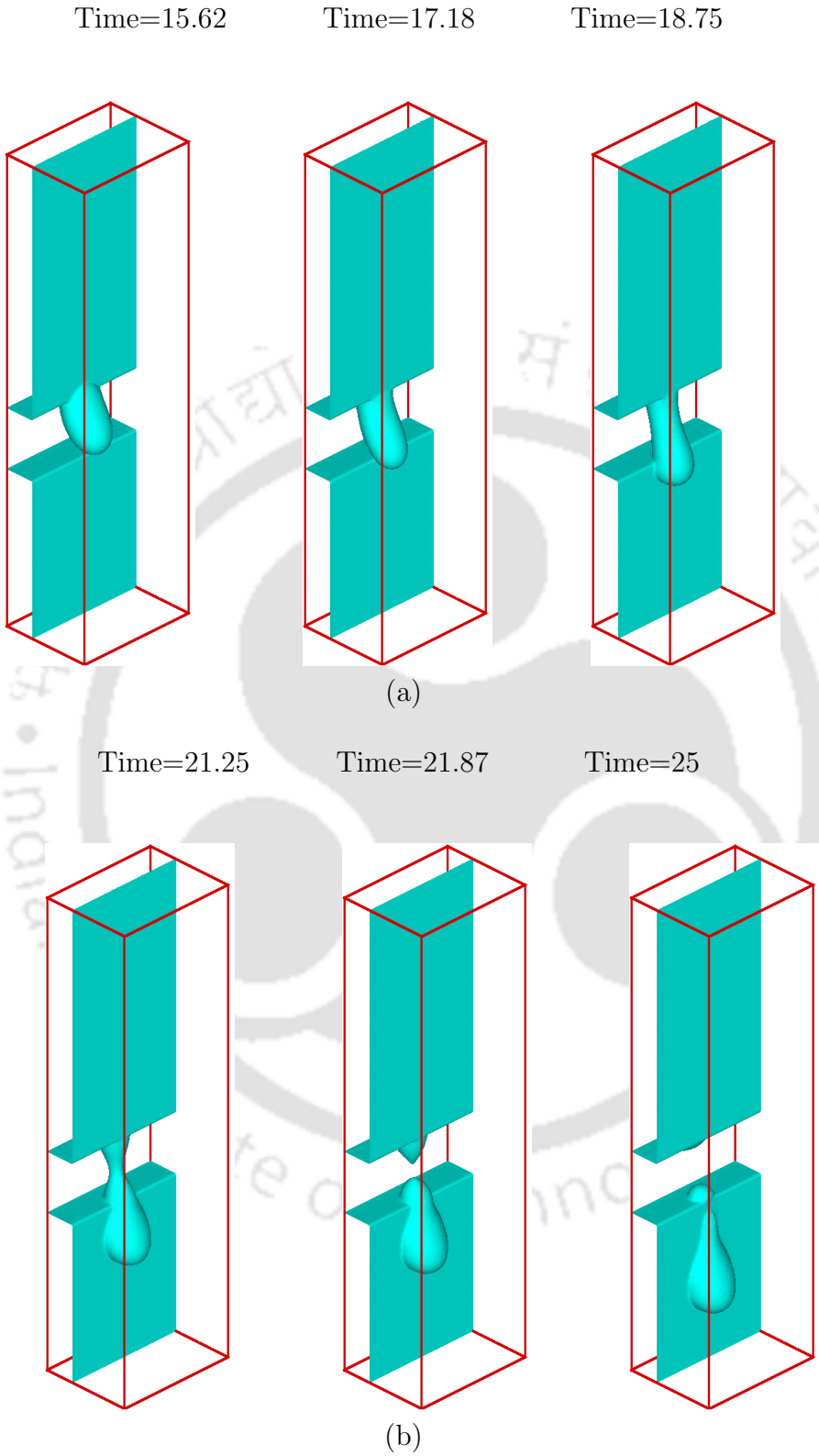

Figure 4.14: Dynamic droplet behavior under gravity on grooved wall at Ca = 0.35, $g_{2w} = -0.02$, viscosity ratio, $M = 1$ and at different lattice time

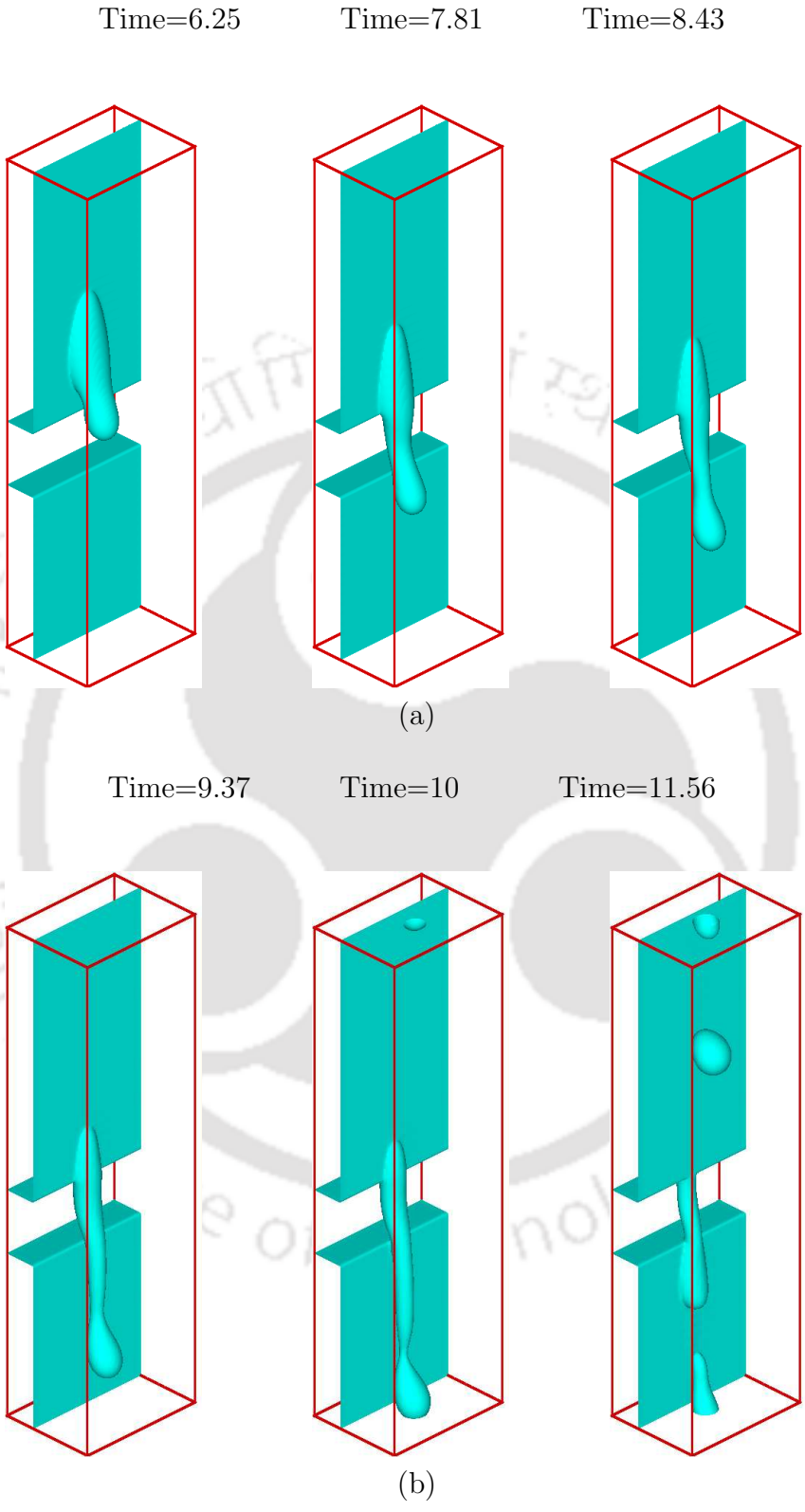

Figure 4.15: Dynamic droplet behavior under gravity on grooved wall at Ca = 0.66, $g_{2w} = -0.02$, viscosity ratio, $M = 1$ and at different lattice time

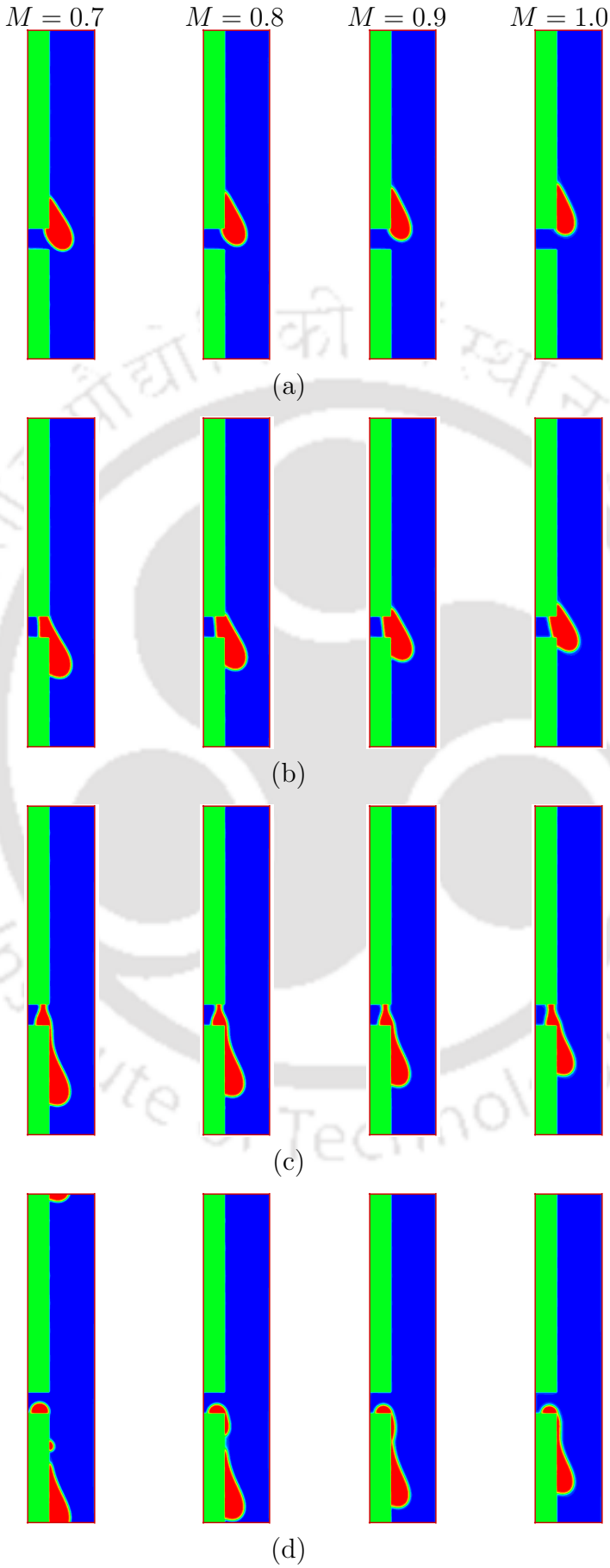

Figure 4.16: Dynamic droplet behavior on grooved wall at Ca = 0.35, groove height=20 lu, $g_{2w} = -0.02$ and non-dimensional time, (a) Time=14.06, (b) Time=17.19, (c) Time=20.31, (d) Time=23.44

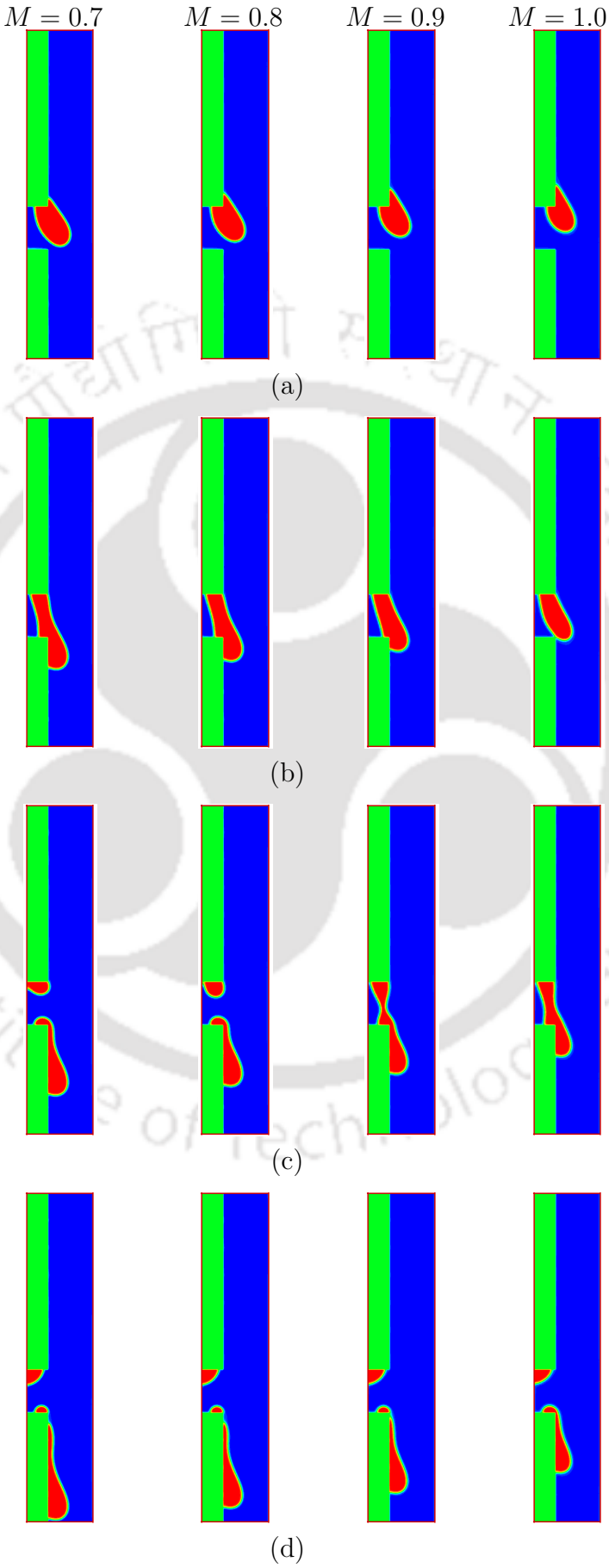

Figure 4.17: Dynamic droplet behavior on grooved wall at Ca = 0.35, groove height=40 lu, $g_{2w} = -0.02$ and non-dimensional time, (a) Time=14.06, (b) Time=17.19, (c) Time=20.31, (d) Time=23.44

4.3.3 Effect of the groove on the vertical wall of channel

In the present analyses, the effect of a single groove of two different sizes ($H \times D$) 20 $\times$ 20 lu and 40 $\times$ 20 lu have been considered for the study of dynamic behaviour of droplet displacement on the wetted wall. The study has been performed for the capillary number, Ca = 0.35. Figure 4.10 shows the geometry of the grooved domain in which a groove of depth, 20 lu at a distance of 100 lu from the bottom of the channel is made. The droplet is placed at 251 lu in positive z-direction and allowed to move in the gravitational-driven flow. The other parameters are taken the same as in the flat vertical wall case. The two wetting conditions, i.e., hydrophobic (θ=118°) and hydrophilic (θ=78°) have been considered on the channel as well as groove walls.

Figure 4.11 shows the dynamic behavior of the droplet displacement for capillary number,Ca=0.35 and viscosity ratio, M=0.7-1.0 for hydrophobic channel wall. It is observed that due to high gravitational acceleration and large hydrophobicity, the droplet detaches from the wall before it reaches the groove as shown in Figs. 4.11(a)-(c). In this case, the groove does not affect the displacement of the droplet. But it is found that the displacement of the droplet is slightly faster as viscosity ration increases from M=0.7 to M=1.0. This is because as viscosity ratio increases the viscosity of the droplet increase and due to higher viscous force, the droplet overcomes the adhesive forces faster under the action of gravitational forces. The groove height is a parameter which plays a crucial role in the displacement of the droplet on the channel wall. In this case, the groove height is considered to be of 40 lu. Similar to the previous case of a hydrophobic wall, in the present case of increased groove height, the droplet detaches from the wall before reaching the groove as shown in Fig. 4.12. The droplet after detachment tries to move towards the groove but due to high gravitational force, it moves past the groove without entrapment. Although droplet touches the lower surface of the groove, the hydrophobic nature of the groove surface does not allow the droplet to adhere on the surface and repels the droplet.

The dynamic behaviour of a droplet on the hydrophilic grooved wall for various capillary numbers (Ca=0.1, 0.35 and 0.66) at several lattice time for groove height, H = 40 lu has been illustrated in Figs. 4.13-4.15. The results are presented at a different time when the droplet passes through the groove on the wall of the microchannel. It can be clearly observed that the capillary number plays a prime

role in the entrapment of the droplet in the groove. In the present study when the capillary number is low (i.e., Ca=0.1), the droplet completely gets entrapped inside the groove and spreads over the upper and back surface of the groove as shown in Fig. 4.13. This is due to the fact that the gravitational force at Ca=0.1 is very low which is not sufficient to largely elongate the droplet and passes through the groove under the influence of hydrophilicity of the wall. As the capillary number increases to Ca = 0.35 and 0.66, the gravitational force is strong enough to elongate the droplet such that it can pass through the droplet with a small fraction of droplet volume entrapped inside the groove, as shown in Figs. 4.14 and 4.15.

In the present investigation, the study of dynamic behaviour of the droplet displacement for the capillary number, Ca = 0.35, and viscosity ratio, M=0.7-1.0, for hydrophobic channel wall has also been conducted. It is observed that due to high gravitational acceleration and large hydrophobicity, the droplet detaches from the wall before it reaches to the groove. In this case, the groove does not affect the displacement of the droplet. But it is found that the displacement of the droplet is slightly faster as the viscosity ratio increases from M=0.7 to M=1.0. This is due to the fact that as viscosity ratio increases, the viscosity of the droplet increases and due to higher viscous force, the droplet overcomes the adhesive force quickly under the action of gravitational force. In the case of the hydrophilic wall as shown in Fig. 4.16, as the droplet moves over the groove, the fraction of droplet liquid remains in the groove and remaining moves past the groove. Due to the smaller size of the groove compared to droplet volume, the larger amount of the droplet crosses the groove and a small amount of droplet fluid is entrapped into the groove. As the droplet reaches the groove, it makes contact with the lower surface of the groove keeping contact with the upper surface. This contact allows the droplet to stretch and forms a bridge. The gravitational force tries to move droplet further and adhesive force tries to attract droplet fluid which in-turn forms a neck formation of the droplet and as a result, drags down a major portion of the fluid from the top surface. A very small fraction of the droplet fluid remain adhered on the upper surface of the groove and a large portion sits on the lower surface of the groove. It is also analysed that as time progresses, the droplet displacement is slower for higher viscosity ratio compared to low viscosity ratio.

The groove height is a parameter which plays a crucial role in the displacement of

the droplet on the channel wall. In the present case, the groove height is increased to 40 lu. Similar to the previous case of a hydrophobic wall, in the present case of increased groove height, the droplet detaches from the wall before reaching the groove in case of hydrophobic surface. The droplet after detachment tries to move towards the groove but due to high gravitational force, it moves past the groove without entrapment. Although droplet touches the lower surface of the groove, the hydrophobic nature of the groove surface does not allow the droplet to adhere on the surface and repels the droplet. When the hydrophilic wettability is considered on the wall keeping groove height equal to 40 lu, the dynamic behaviour of the droplet changes. It is observed that in this case also due to the large groove height, a liquid bridge is again formed and breaks the droplet into two parts. The large fraction of the droplet fluid adhered to the top surface of the groove and remaining fluid moves down the lower surface of the channel wall. It is also found that after the breakup, a small amount of droplet fluid in the form of droplet sits on the lower surface of the groove. The liquid which is entrapped into the groove spreads over the groove surface due to adhesion and remain attached in the upper vertical corner of the groove as shown in Fig. 4.17. It is observed that in this case, the bridge formation and entrapment of the fluid in the groove are much faster in the case of lower viscosity ratio, M=0.7 and slower in lower viscosity ratio, $M = 1.0$. This is due to the fact that lower viscosity ratio signifies a lower viscous force which allows the droplet to move faster on the surface under the action of higher gravitational force.

4.4 Summary

In the present study, the interfacial dynamics of displacement of the three-dimensional spherical droplet on a rectangular microchannel wall considering wetting effects were studied. The aim of this study was to analyze the effect of wettability, low viscosity ratio and capillary number on the displacement of spherical droplet subjected to the gravitational force on the flat as well as the grooved surface of the channel wall. The hydrophobic and hydrophilic nature of wettabilities on wall surface were considered to study for viscosity ratio, $M \leq 1$. The results were presented in the form of temporal evolution of wetted length and wetted area for combined viscosity ratios and wettability scenario. In the present study, it was observed that in dynamic droplet

displacement, the viscosity ratio and capillary number play a significant role. It was found that as viscosity ratio increases, both the wetted area and the wetted length increase and decrease in the case of hydrophilic and hydrophobic wettable wall, respectively. The groove area on the vertical wall tries to entrap fraction of droplet fluid in case of the hydrophilic surface of the vertical wall whereas in hydrophobic case, droplet moves past the groove without entrapment.

Chapter 5

Droplet Displacement on Wetted Grooved Surface of a Rectangular Channel: Effect of Location and Number of Groove

The understanding of the displacement and spreading behaviour of a droplet on a rough surface is an important area of analysis due to its common area of application e.g., inkjet printing, coatings, electronics etc. Several authors have studied the displacement behaviour of the droplet on a uniform and smooth surface of the microchannel in two-dimension only but there are very few studies which were conducted in the three-dimensional microchannel. Only a few authors have taken three-dimensional microchannels as their area of study for exploring physics in the smooth surface of the wall. It is widely accepted in the research community that the roughness on the solid surface plays a major role in the displacement and spreading of fluid; so it is important to analyze the displacement and spreading of the droplet on a rough surface of a three-dimensional microchannel under different wetting conditions.

5.1 Problem specification

The present work deals with the droplet displacement and deformation on a grooved wall of a microchannel. The two types of the domain have been considered for the study i.e., single groove wall and double grooves wall, as shown in Figs. 5.1(a)-(b). The wettability of the solid walls of the microchannel except groove is considered as uniform hydrophilic (g_{2w}=-0.05) whereas three different wettabilities of the groove i.e., hydrophobic (g_{2w}=0.05), hydrophilic (g_{2w}=-0.02) and neutral (g_{2w}=0.0). The simulations are carried out in a rectangular microchannel having length, width and breadth as 300, 61 and 81 lattice units (lu), respectively. The problem also considers the two immiscible fluids in which droplet (fluid 2) is placed in the domain filled with displacing fluid (fluid 1). The radius of the droplets is considered to be 18 lu. The droplet is initially placed at $z = 251$. The fluid or droplet motion has been governed by the gravitational force that is applied in the negative z-direction. The capillary number, Ca and the viscosity ratio, M are taken as 0.35 and 1, respectively. The periodic boundary condition is applied in the z-direction and no slip (i.e., bounce back) boundary condition has been applied at all walls located in x- and y-directions.

5.2 Results and discussion

The effect of surface roughness on the droplet displacement is an important characteristic in the area of fluid flow inside microchannels. In the present study, a parametric study has been performed to study the effect of different wettability of groove surface on the displacement and deformation of the three-dimensional immiscible droplet. The walls of the microchannel except groove surface is considered to be of hydrophilic wettable. The main focus of the present study is to analyze what fraction of droplet volume is entrapped inside the groove and rest passes through the groove. The fraction of entrapped droplet fluid is defined as the ratio of volume of droplet fluid entrapped inside the groove at the end of dynamic process to the initial volume of the droplet fluid. In the present analysis, the capillary numbers, i.e., Ca= 0.35, has been considered with different wetting conditions, i.e., hydrophobic ($g_{2w} = 0.05$), hydrophilic ($g_{2w} = -0.02$) and neutral ($g_{2w} = 0.0$), to study the droplet displacement behavior. Time is made dimensionless by characteristic time $\frac{l}{U}$, where l is characteristic length and U is defined as characteristic velocity, $U = \frac{\rho_2 g h^2}{\mu_2}$

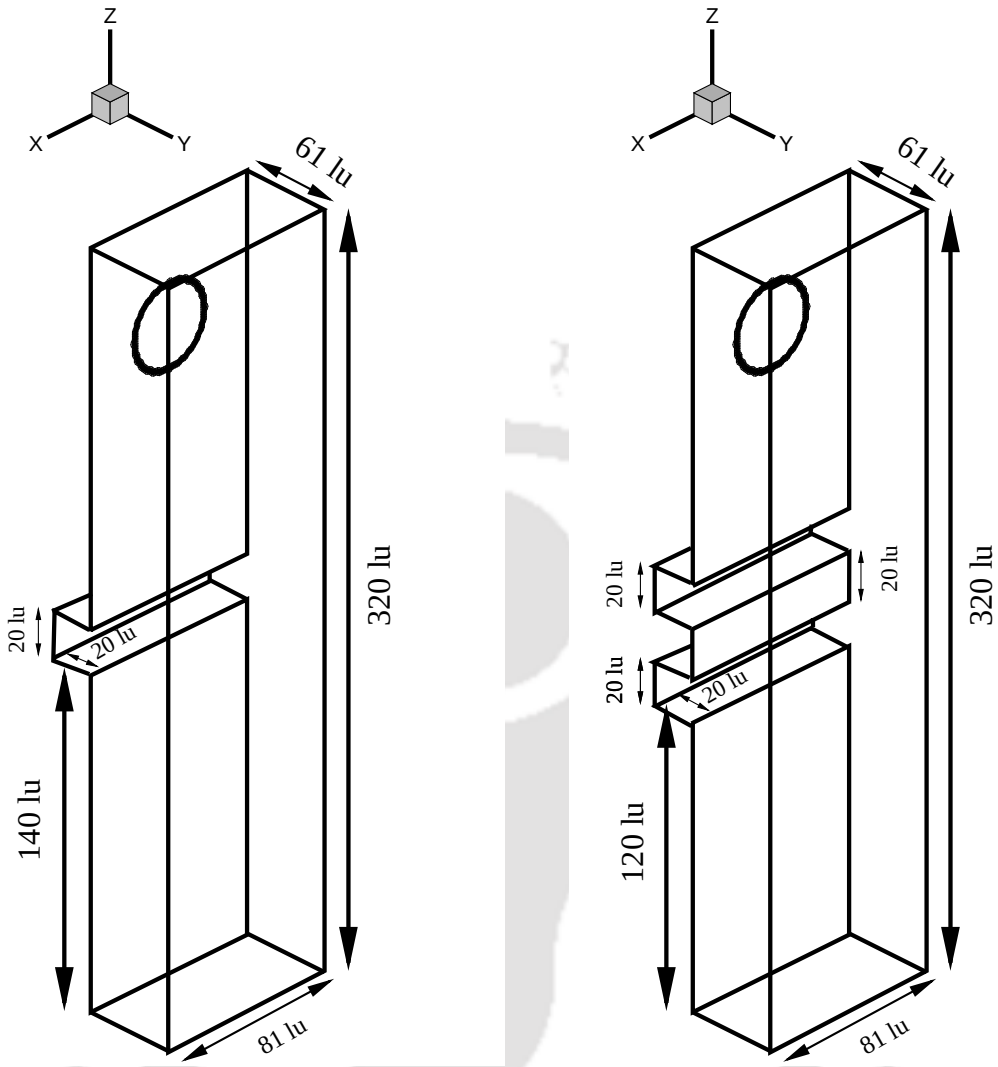

Figure 5.1: Schematic diagram of computational domain (a) single groove (b) double grooves

[101]. The other parameters considered in the present analysis are as follows: initial density of fluid 1, $\rho_1 = 0.035$ and initial density of fluid 2, $\rho_2 = 0.965$. The motion of the droplet is governed by the gravitational force which is acting in the negative z-direction. The height and width of the groove in the present study are considered same which is equal to 20 lu.

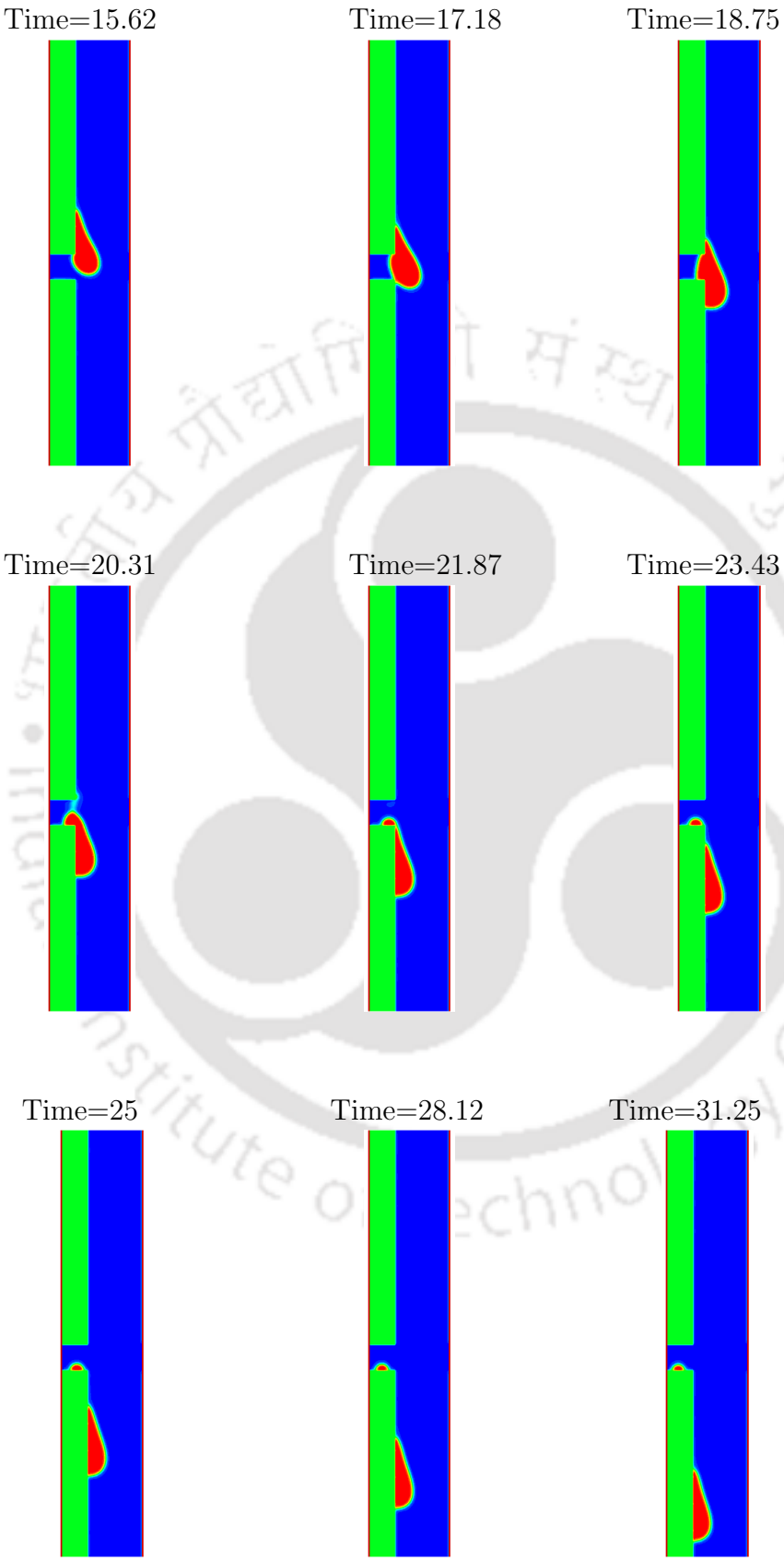

Figure 5.2: The shape of the droplet in $y-z$ plane in single groove (middle) at $x = 40$ lu for Ca $= 0.35$, $g_{2w} = 0.05$ at various lattice time

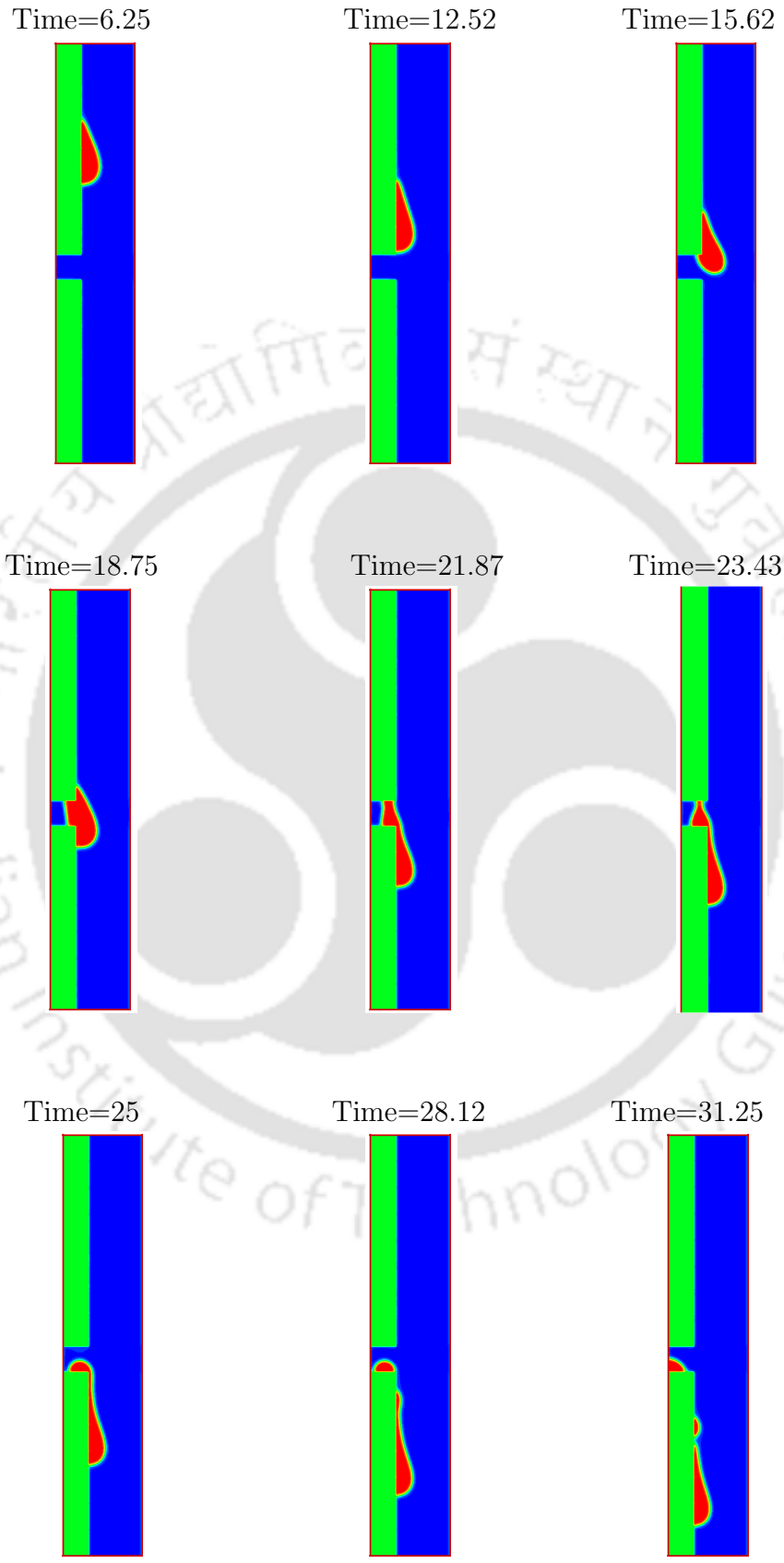

Figure 5.3: The shape of the droplet in $y-z$ plane in single groove (middle) at $x = 40$ lu for Ca $= 0.35$, $g_{2w} = -0.02$ at various lattice time

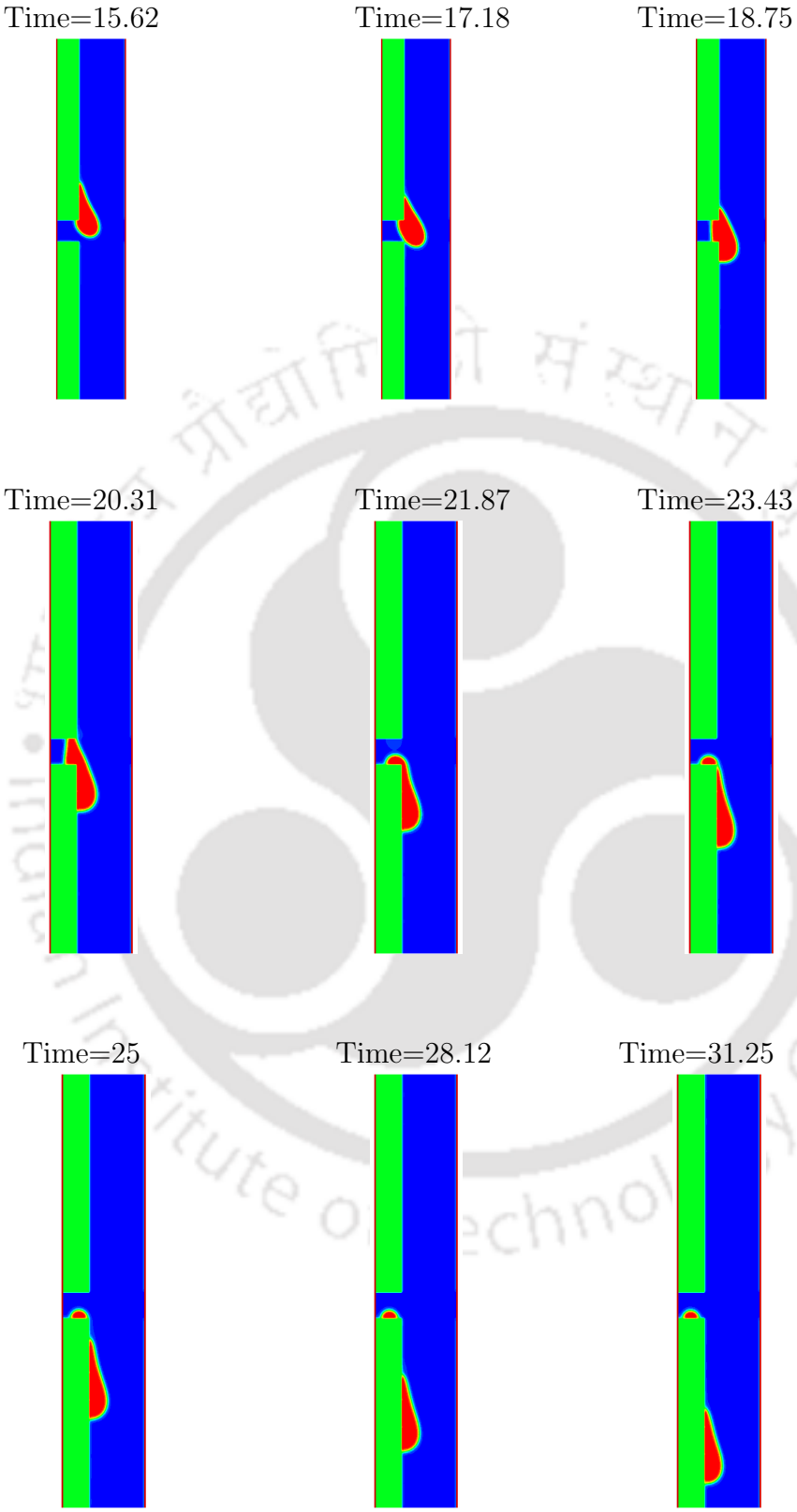

Figure 5.4: The shape of the droplet in $y-z$ plane in single groove (middle) at $x = 40$ lu for Ca $= 0.35$, $g_{2w} = -0.0$ at various lattice time

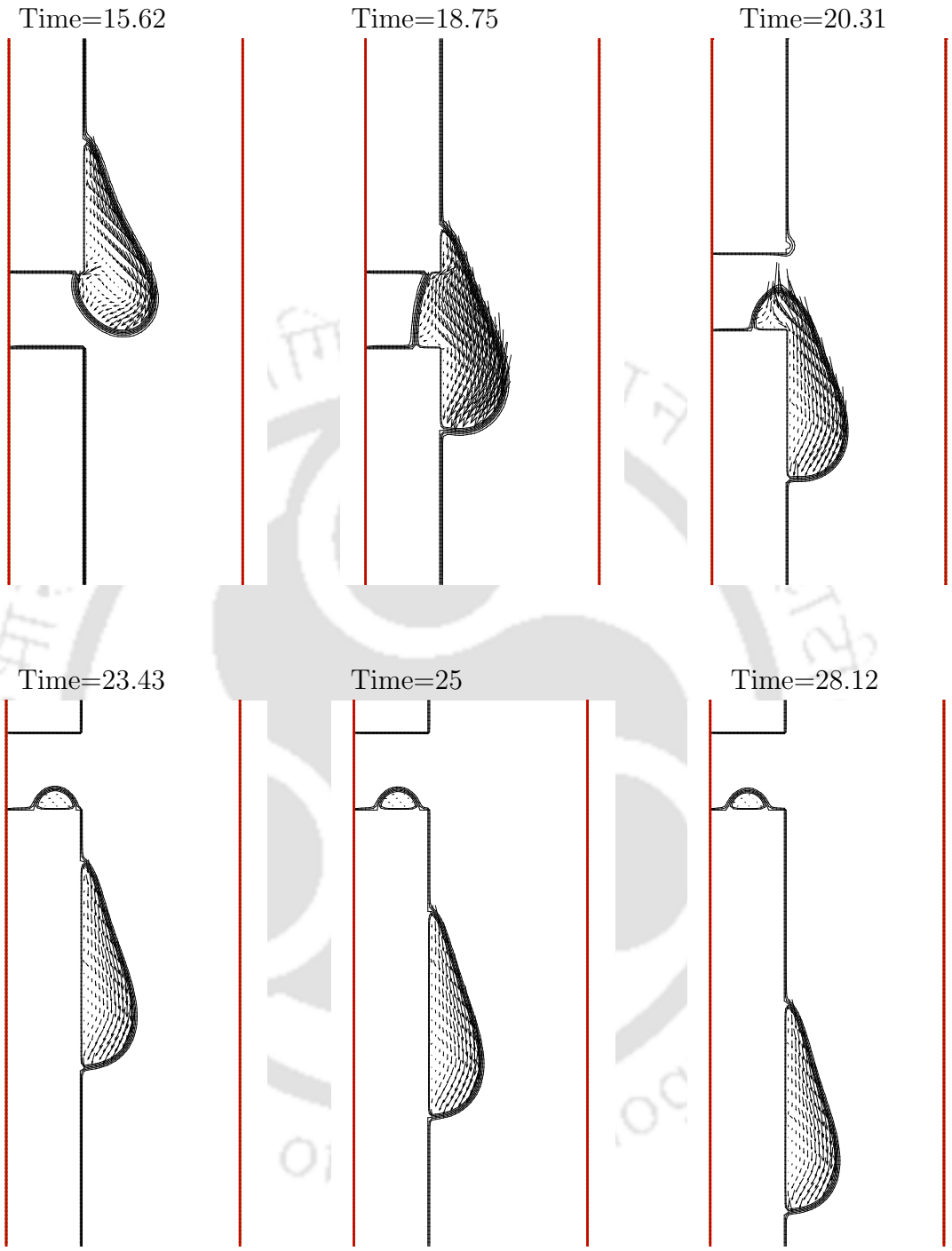

Figure 5.5: Plots showing vectors inside droplet in $y - z$ plane in single groove (middle) at $x = 40$ lu for Ca $= 0.35$, $g_{2w} = 0.05$ ($\theta = 118°$) at various lattice time

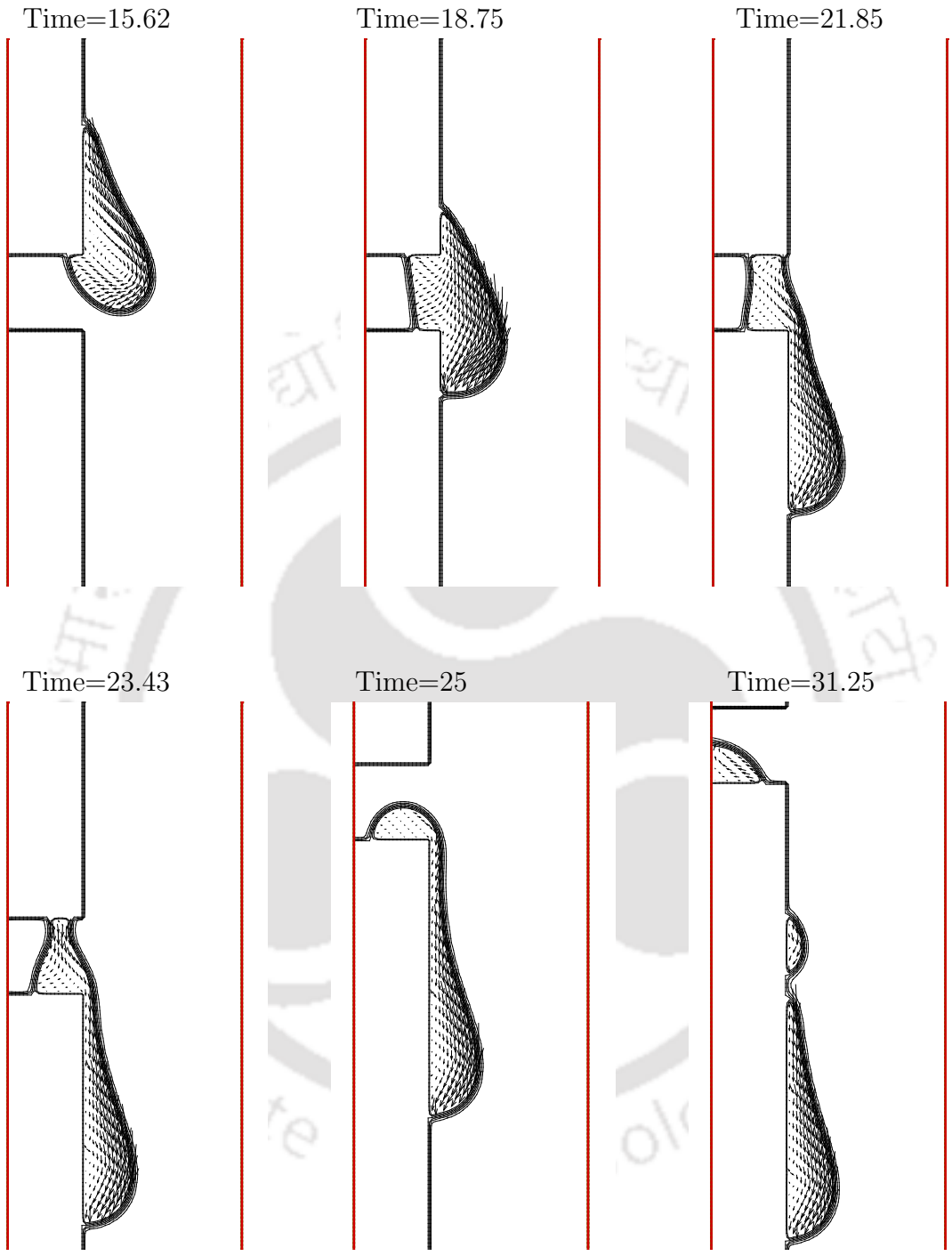

Figure 5.6: Plots showing vectors inside droplet in $y-z$ plane in single groove (middle) at $x = 40$ lu for Ca $= 0.35$, $g_{2w} = -0.02$ ($\theta = 78°$) at various lattice time

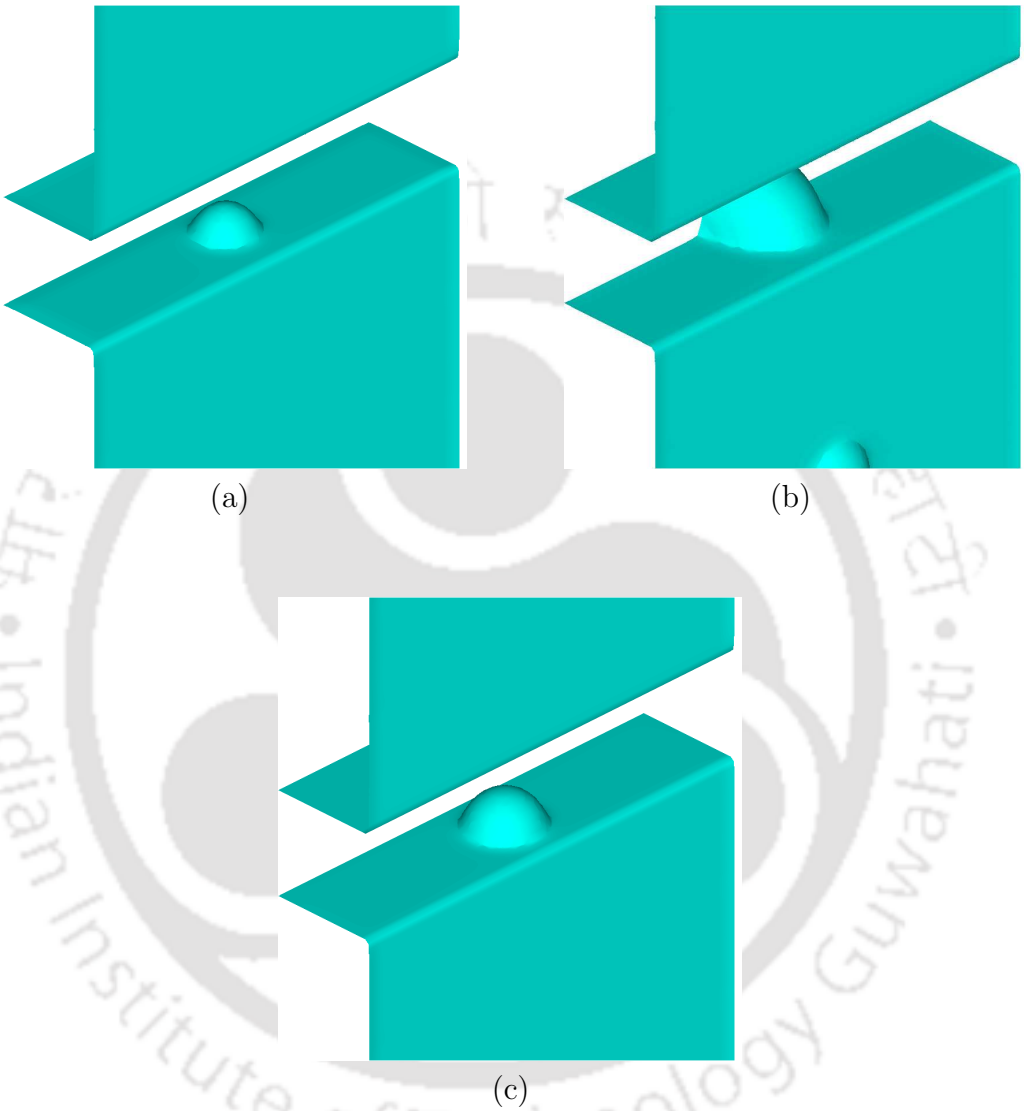

Figure 5.7: The iso surface view of entrapped droplet fluid in the single groove (middle) at Ca=0.35 , Time=31.25 for three wetting conditions (a) hydrophobic, (b) hydrophilic, (c) neutral

Figures 5.2-5.4 illustrate the sectional views of droplet displacement on the different wetting surface of the groove. At a fixed capillary number, Ca=0.35, the droplet starts displacing on the surface of the channel wall. As the wall of the microchannel is hydrophilic, the droplet under the influence of gravitational acceleration spreads over the surface and elongates in length. As time progresses, the elongated droplet displaces on the surface and reaches to the groove which has different wettability compared to the channel wall. In the case of a hydrophobic groove surface as shown in Fig. 5.2, the droplet does not adhere much on the surface of the groove due to the behaviour of the hydrophobic nature of the surface. Due to the hydrophobicity of the surface, the surface repels the volume of droplet fluid and hence, the droplet without affected much attaches to the lower surface of the groove directly. In the transition of a droplet from the upper surface of the groove to the lower surface, a very small fraction of droplet remain attached to the lower surface of the groove and rests there for the whole time. The remaining droplet fluid again starts displacing on the lower half of the hydrophilic surface of the channel wall.

In case of the hydrophilic wetted groove, as the droplet reaches to groove, it got attached to both upper and lower surface of the groove due to the elongation and small height of the groove as shown in Fig. 5.3. The hydrophilic surface of the groove attracts the droplet fluid and allow it to spread over the upper as well as the lower surface of the groove. Due to the attachment of the droplet fluid and gravitational acceleration, droplet tries to elongate and a neck formation generated. As time progresses, this neck formation gets thinner and the droplet breaks into two parts. A very small part of the droplet fluid remain attached to the upper surface of the groove and completely spreads over the surface. The other part of the droplet again breaks into two parts in which major part passes through the groove and continue to displace on the channel wall and the entrapped part continue to spread over the lower surface of the groove. The spreading of the droplet fluid on the lower surface of the groove is three-dimensional and because of that, the entrapped fluid settle down at the backside of the groove. The neutral groove surface behaves similarly to the hydrophobic surface of the groove except for the entrapped volume of the droplet fluid is more than the hydrophilic groove case which can be seen in Fig. 5.4.

Figures 5.5-5.6 show the velocity fields inside the droplet while moving past the

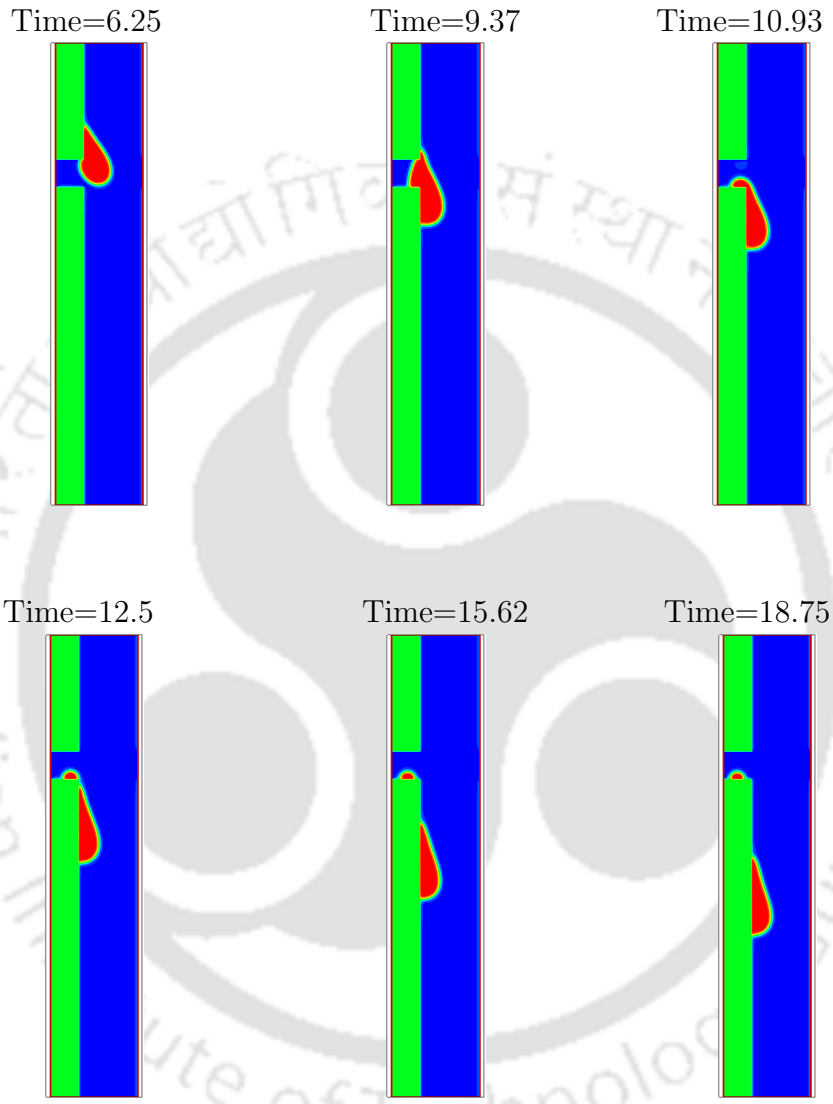

Figure 5.8: The shape of the droplet in $y-z$ plane in single groove (upper) at $x = 40$ lu for Ca $= 0.35$, $g_{2w} = 0.05$ at various lattice time

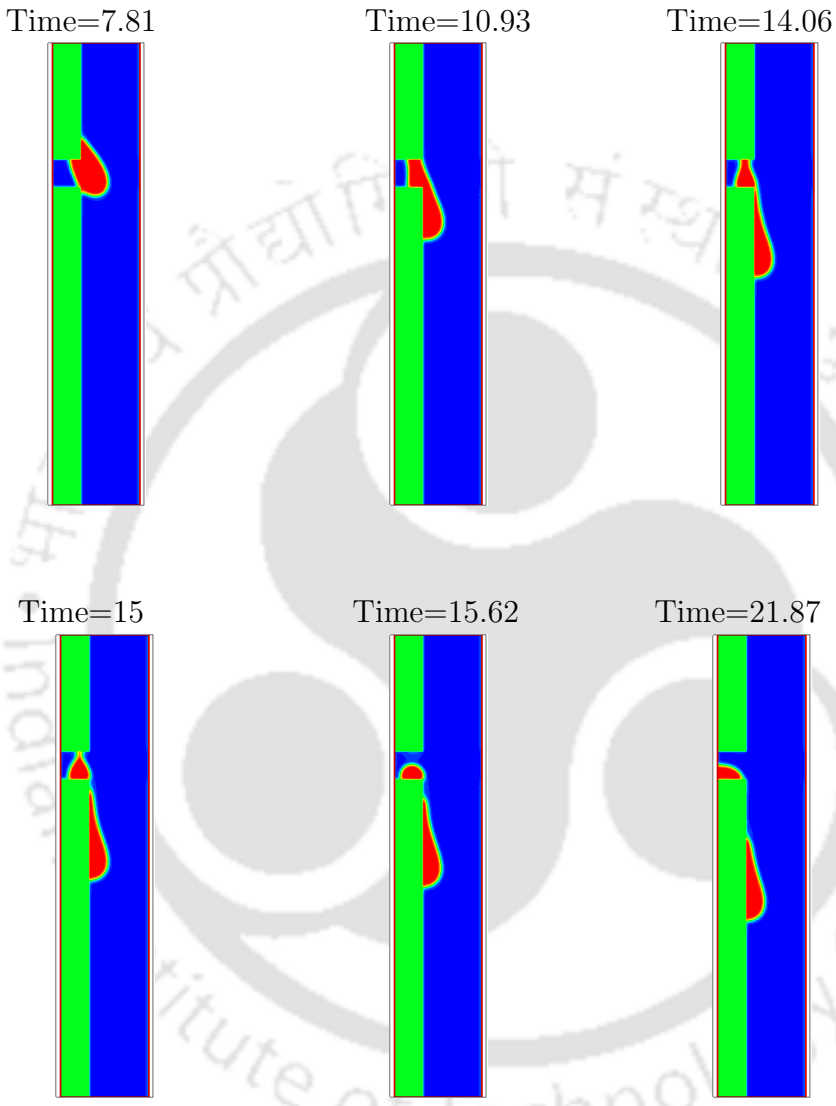

Figure 5.9: The shape of the droplet in $y-z$ plane in single groove (upper) at $x = 40$ lu for Ca $= 0.35$, $g_{2w} = 0.0$ at various lattice time

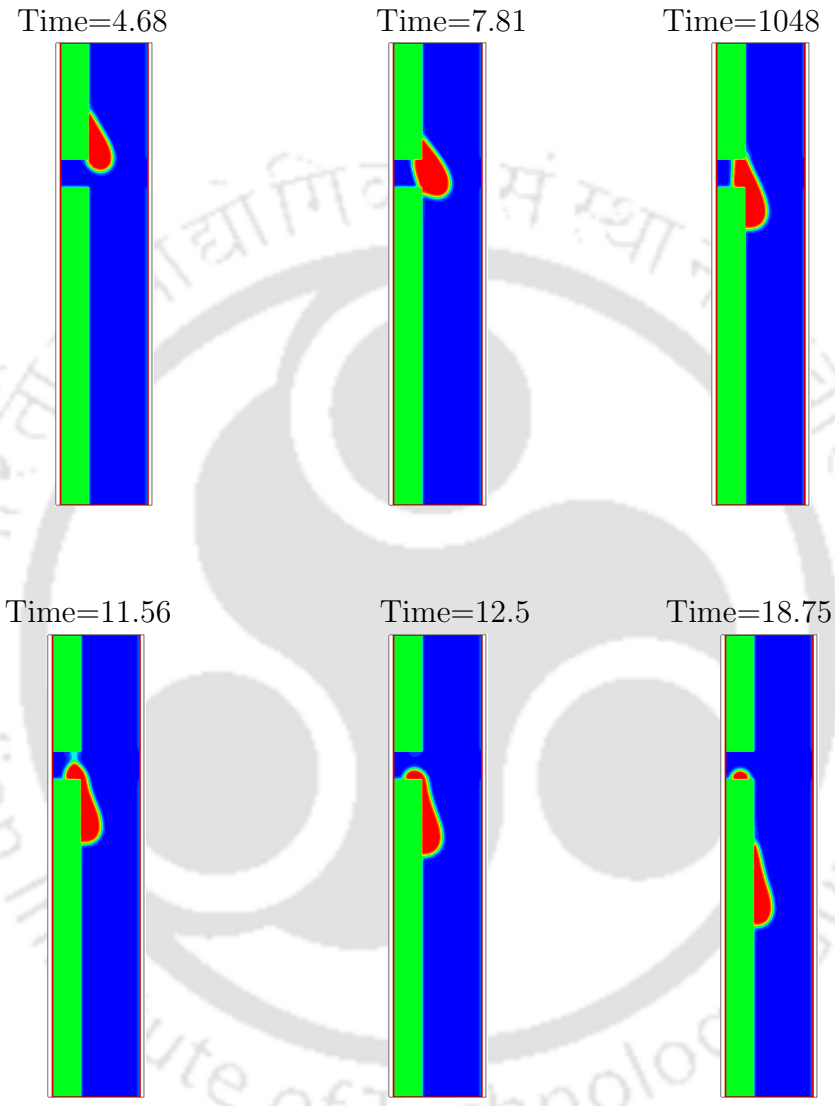

Figure 5.10: The shape of the droplet in $y-z$ plane in single groove (upper) at $x = 40$ lu for Ca $= 0.35$, $g_{2w} = -0.02$ at various lattice time

wetted groove on the channel wall. It is important to note that at the wall, the no-slip boundary condition is satisfied which can be seen by the very low intensity of velocity vectors near to the wall. However, the velocity vectors inside the droplet are not straight and take a curved shape. It is also observed that the velocity inside the outer part of the droplet which is near to the interface is more compared to the inner part of the droplet which is adhered to the wall. When the droplet reaches the groove opening, in the case of the hydrophobic wetted groove as shown in Fig. 5.5, the velocity vectors are such that it tries to push some of the droplet fluid inside the groove but as the groove has hydrophobic wettability, it does not attract more fluid and a very small fraction is entrapped inside the groove. But in the case of a hydrophilic wetted groove as shown in Fig. 5.6, when the droplet reaches the upper surface of the groove, the velocity vectors in the downstream part of the droplet try to push the droplet fluid inside the groove and due to a large adhesion force, when the droplet covers the full opening of the groove, a large amount of droplet fluid enters inside the groove. Later, when the remaining droplet fluid crosses the groove, the velocity in the downstream part of the droplet is more than the upstream part of the droplet and due to that, the droplet pinches off into two parts. One part of the droplet fluid entrapped inside the groove and as time progresses, it settled deep inside the groove and another part of the droplet moves past the groove and displaces on the outer surface of the wall. Figure 5.7 shows the three-dimensional isosurface view of the entrapped droplet in three different wetting condition of the groove surface. It is clearly visualized that the fraction of droplet fluid entrapped inside the groove is maximum in the hydrophilic case. It is interesting to see that for same gravitational acceleration i.e., for the same capillary number, the spreading and displacement in the hydrophilic surface is much more compared to the hydrophobic and neutral surface of the groove cases. This is due to the ultimate effect of hydrophilic nature (or large adhesion forces) of the groove surface.

It is reported in several pieces of literature that the droplet displacement and entrapment have also been affected by the location of the groove on the wall of microchannel majorly. To investigate this effect in the current problem, three different locations of the groove on the channel wall i.e., the distance of grooves from the bottom of the channel in z-direction is 40 lu, 140 lu and 220 lu, have been considered. Figures 5.8-5.10 show the droplet displacement for different wetting conditions of the groove in the case where the groove is located at the upper side of the channel

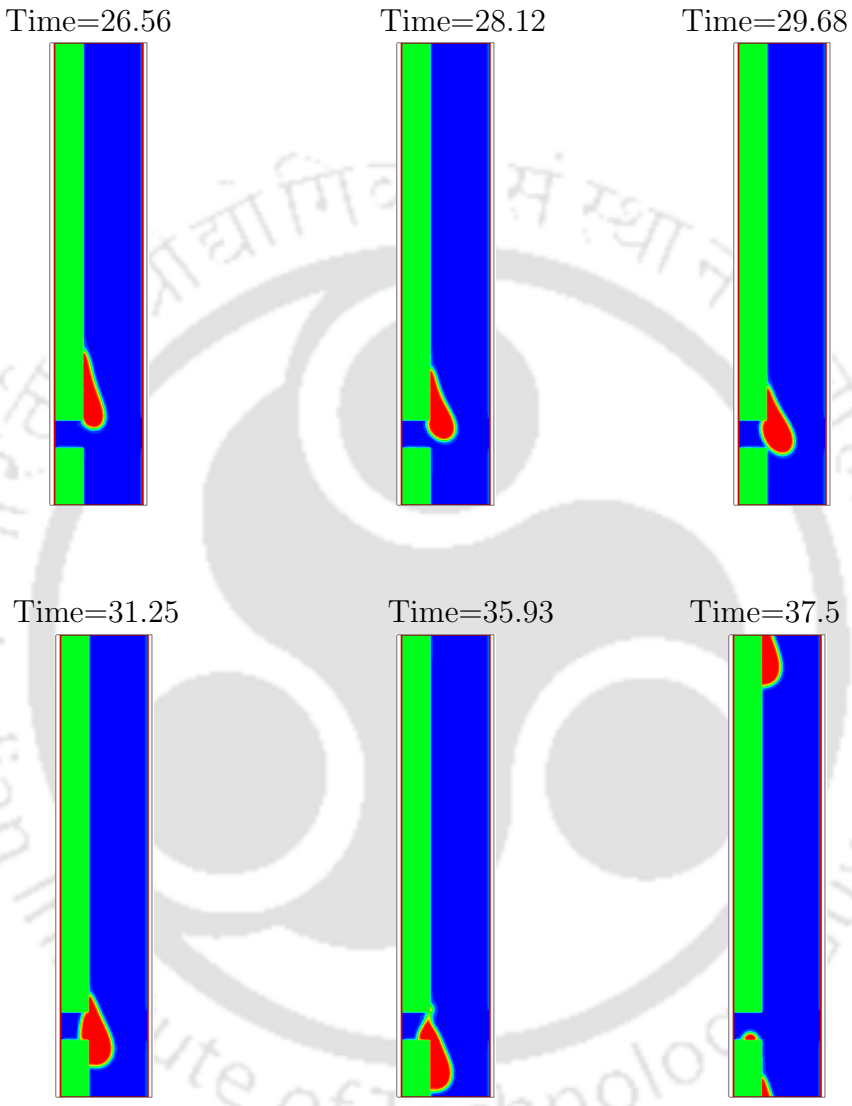

Figure 5.11: The shape of the droplet in $y-z$ plane in single groove (lower) at $x = 40$ lu for Ca $= 0.35$, $g_{2w} = 0.05$ at various lattice time

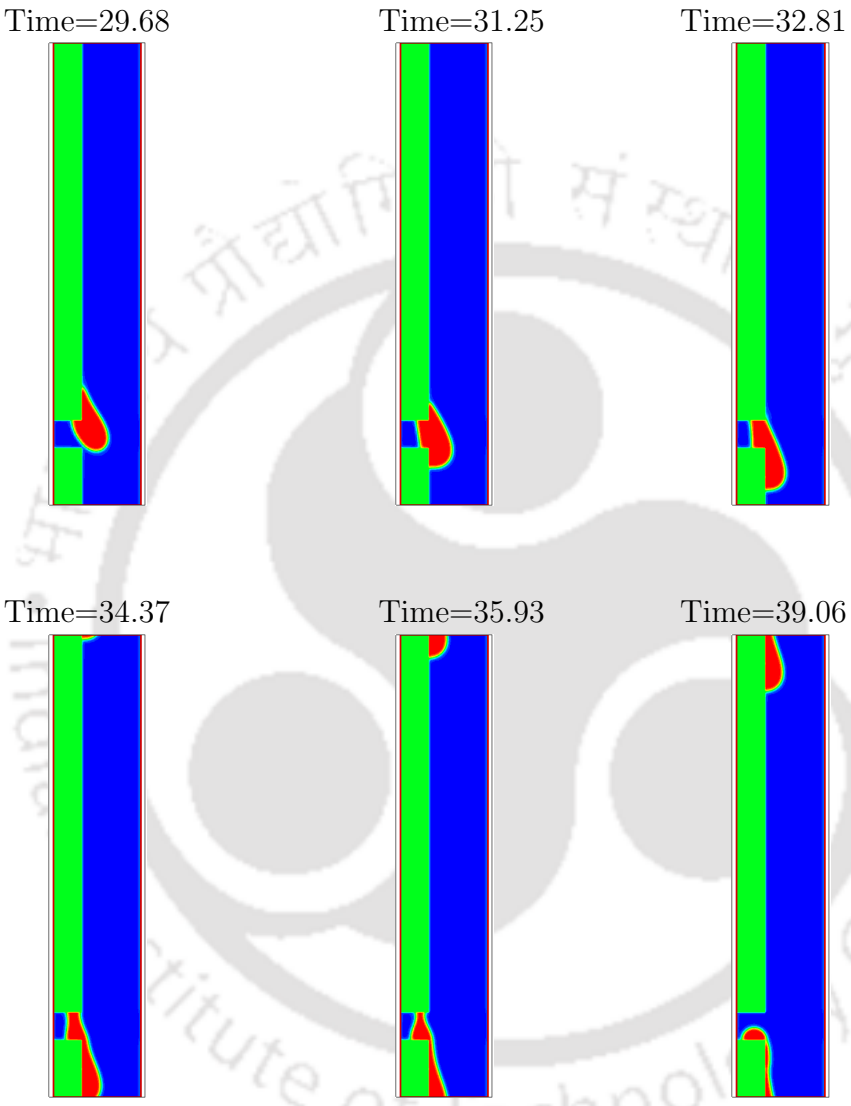

Figure 5.12: The shape of the droplet in $y-z$ plane in single groove (lower) at $x = 40$ lu for Ca $= 0.35$, $g_{2w} = 0.0$ at various lattice time

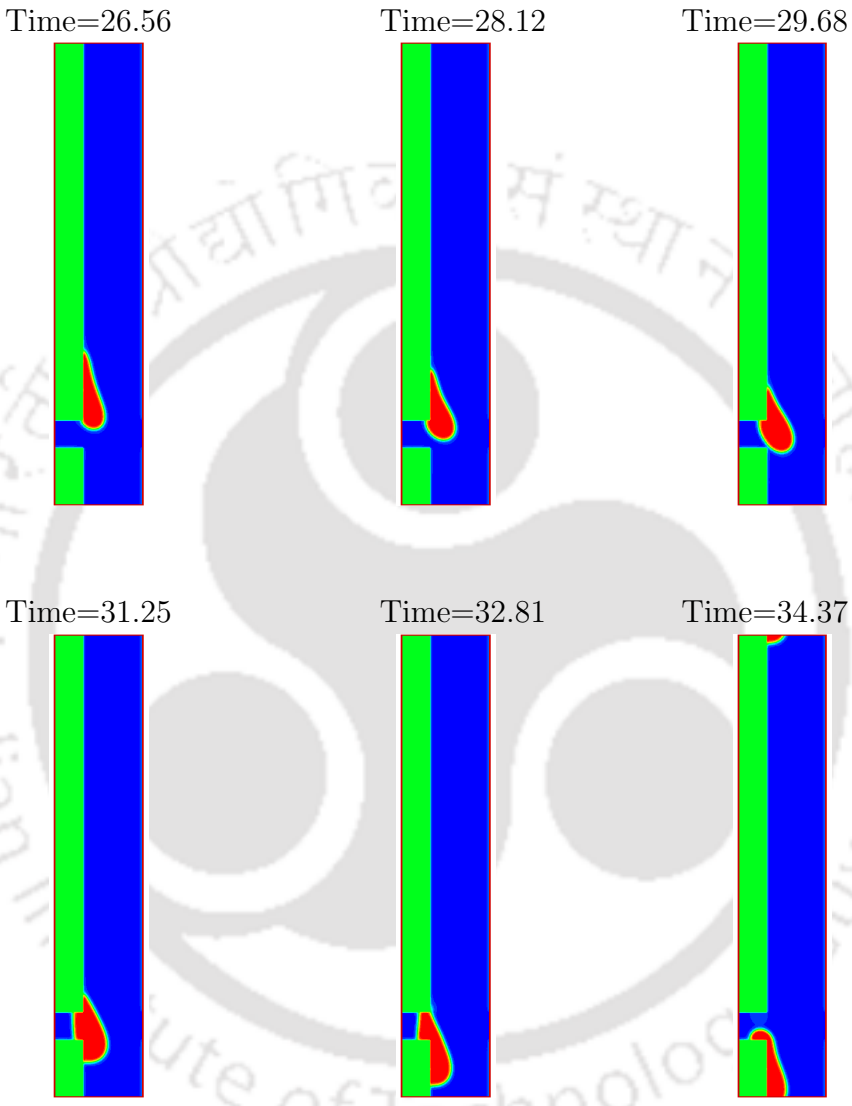

Figure 5.13: The shape of the droplet in $y-z$ plane in single groove (lower) at $x = 40$ lu for Ca $= 0.35$, $g_{2w} = -0.02$ at various lattice time

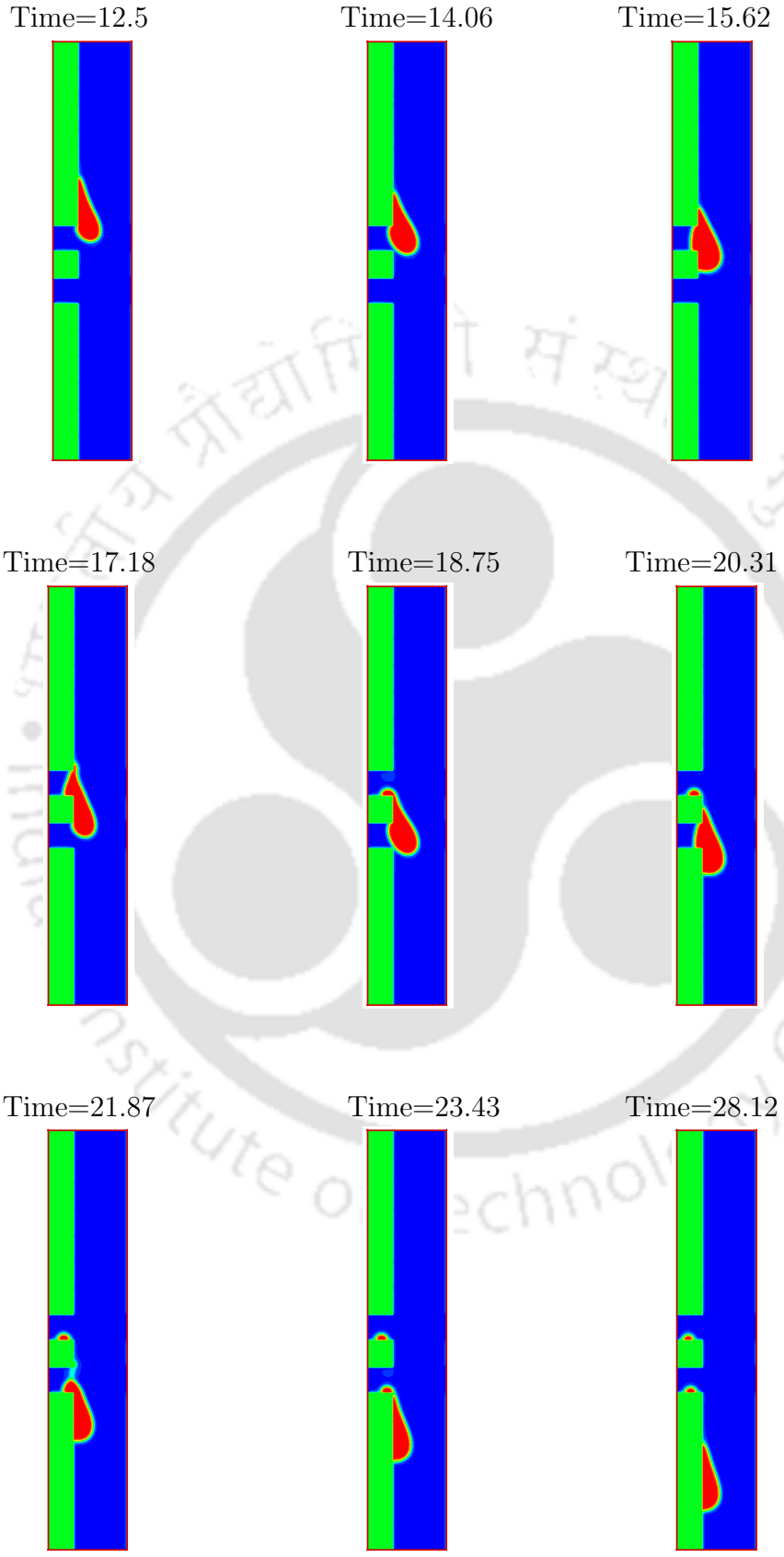

Figure 5.14: The shape of the droplet in $y-z$ plane in double grooves at $x = 40$ lu for $Ca = 0.35$, $g_{2w} = 0.05$ at various lattice time

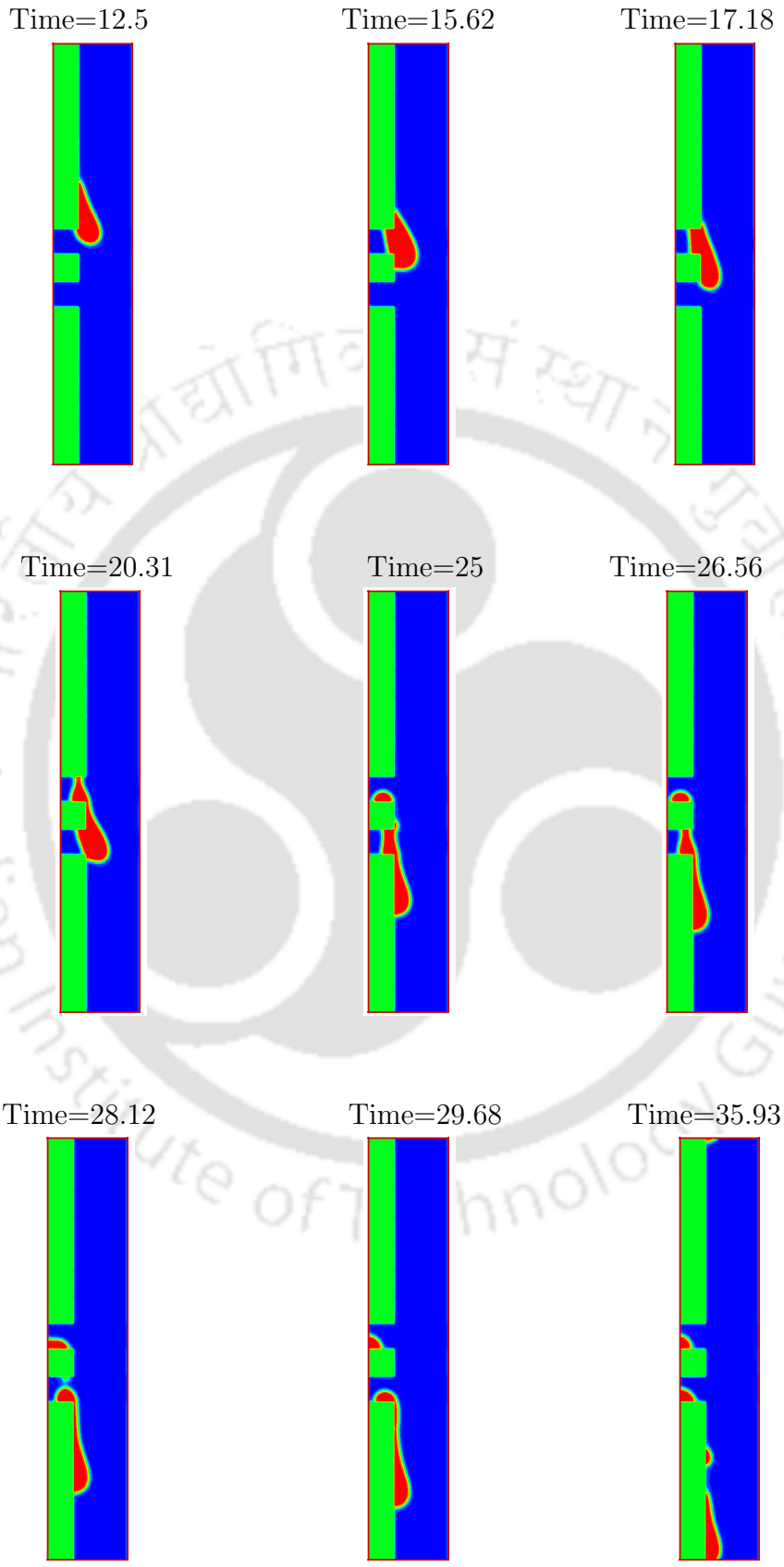

Figure 5.15: The shape of the droplet in $y-z$ plane in double grooves at $x = 40$ lu for $Ca = 0.35$, $g_{2w} = 0.0$ at various lattice time

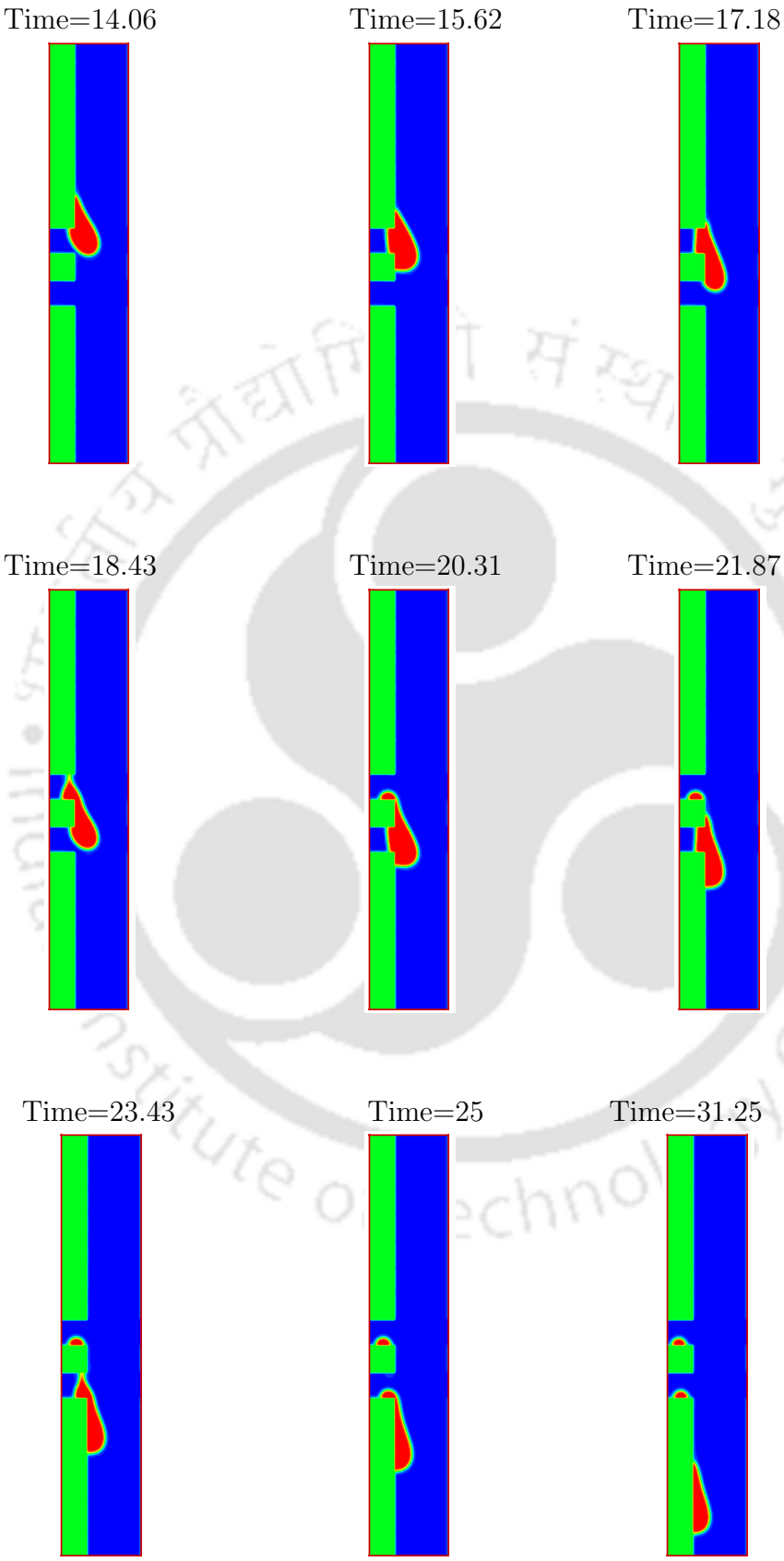

Figure 5.16: The shape of the droplet in $y-z$ plane in double grooves at $x = 40$ lu for $Ca = 0.35$, $g_{2w} = -0.02$ at various lattice time

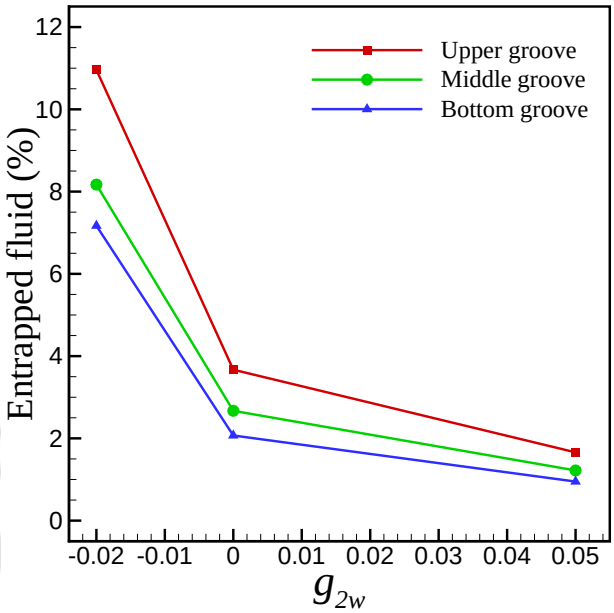

(a)

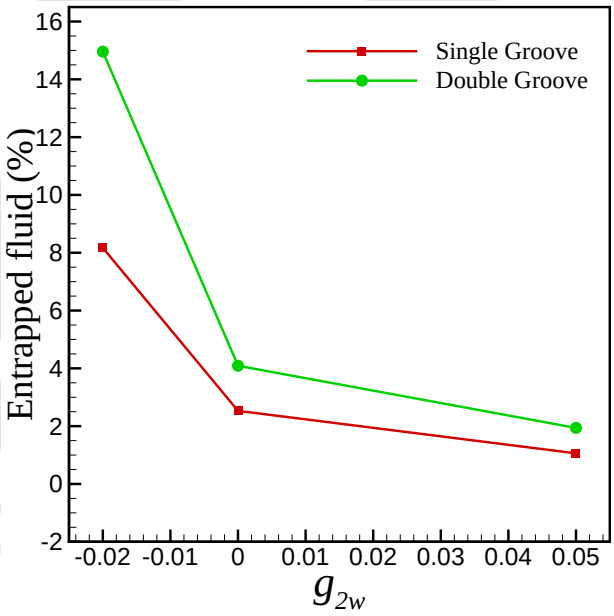

(b)

Figure 5.17: The fraction of entrapped droplet fluid in the groove at Ca=0.35 and at three wetting conditions

(i.e., 220-240 lu). In this case, the droplet initially placed just above the groove such that in the very short time, the droplet passes through the groove. Due to this very less simulation time, the droplet does not elongate much and a large volume

of droplet fluid due to adhesion spreads over the upper surface of the groove and then due to gravitational forces and elongation on the wall, the droplet fluid drips down. In case of hydrophobic groove and neutral groove as shown in Fig. 5.9 and Fig. 5.10, respectively, a negligible amount of fluid remains attached on the upper surface of the groove whereas in hydrophilic case (Fig. 5.8), a small amount of fluid adhered on the upper surface of the groove due to breaking up of the droplet into two parts after forming a liquid bridge and neck formation. It is found that the % fraction of entrapped droplet fluid inside groove is greater than the case in which the droplet is located in the middle of the channel wall i.e., at 140-160 lu distance in z-direction which is clearly seen in Fig. 5.17(a). When the groove is located in the lower side of the channel i.e., at 40-60 lu in z-direction as shown in Figs. 5.11-5.13, it is observed that the volume of droplet fluid which is entrapped in the groove is less than the case where the groove is located at the middle of the channel (see Fig. 5.17(a)). As it is stated earlier that the roughness on the surface plays a major role in the displacement of the droplet, so to create more roughness on the wall of the channel, two grooves have been created in the present case. It is assumed that a number of grooves mean more roughness on the surface. To study this problem, two grooves have been created at a distance of 20 lu as shown in Fig. 5.1(b). All other parameters remain the same as in single groove case. Figures 5.14-5.16 show the movement and shape of the droplet in sectional $y-z$ view for uniform hydrophobic, hydrophilic and neutral groove surface cases. The aim of this study to see the amount of % fraction of droplet fluid entrapped in grooves. Figure 5.17(b) shows that the % fraction of entrapped fluid is almost double in the case of two grooves compared to single groove case for all wettabilities.

5.3 Summary

The present work investigated the droplet displacement and entrapment of the fluid in a grooved wall microchannel under the influence of gravitational force. The groove on the wall was considered to be of different wettabilities under different conditions. The uniform hydrophilic wettability of the channel walls except groove was considered for the study. The study was focused on the effect of the wettabilities of the groove, location of the groove and number of grooves on the displacement and entrapment of the droplet fluid. The analysis showed that the volume of fluid

entrapped in the single groove was maximum in the hydrophilic surface of the groove. It was also found that when the groove is located on the upper side of the domain, the fraction of entrapped droplet fluid is more compared to the groove located in the middle and lower side of the channel wall. In the case of two grooves on the wall, the entrapped fluid is almost double of the single groove case. In all cases, it was observed that the amount of entrapped fluid is maximum in the hydrophilic groove and minimum in the hydrophobic groove.

Chapter 6

Sweeping of the Entrapped Fluid Out of the Groove by Large Droplet in a Channel

6.1 Introduction

In microfluidic applications, sometimes a condition arises when the surface is not completely smooth throughout the domain but it is having some irregularities. One of the different types of irregularities can be assumed as a groove on the flat surface. The effect of these grooves is that it behaves as an obstacle in the path of fluid flow and the fraction or complete fluid may get entrapped inside the groove which is highly undesirable in the application of inkjet printing, spray painting and coating etc. In the present study, an attempt has been made to sweep out the trapped volume of droplet fluid inside the groove. It is to be mentioned here that the present work is the first attempt to sweep out the trapped droplet fluid and no literature is available which analyses the sweep out the phenomenon of the droplet fluid trapped inside the groove on the duct wall. In order to gain a full understanding of droplet fluid entrapment inside groove and sweeping-out of that entrapped fluid, it is necessary to have comprehensive studies of such multiphase fluid systems. However, there is a large number of experimental and numerical studies available which analyses the liquid droplet spreading and displacement phenomenon on the flat surface.

The prime aim of this study is to sweep-out the fluid which is somehow entrapped

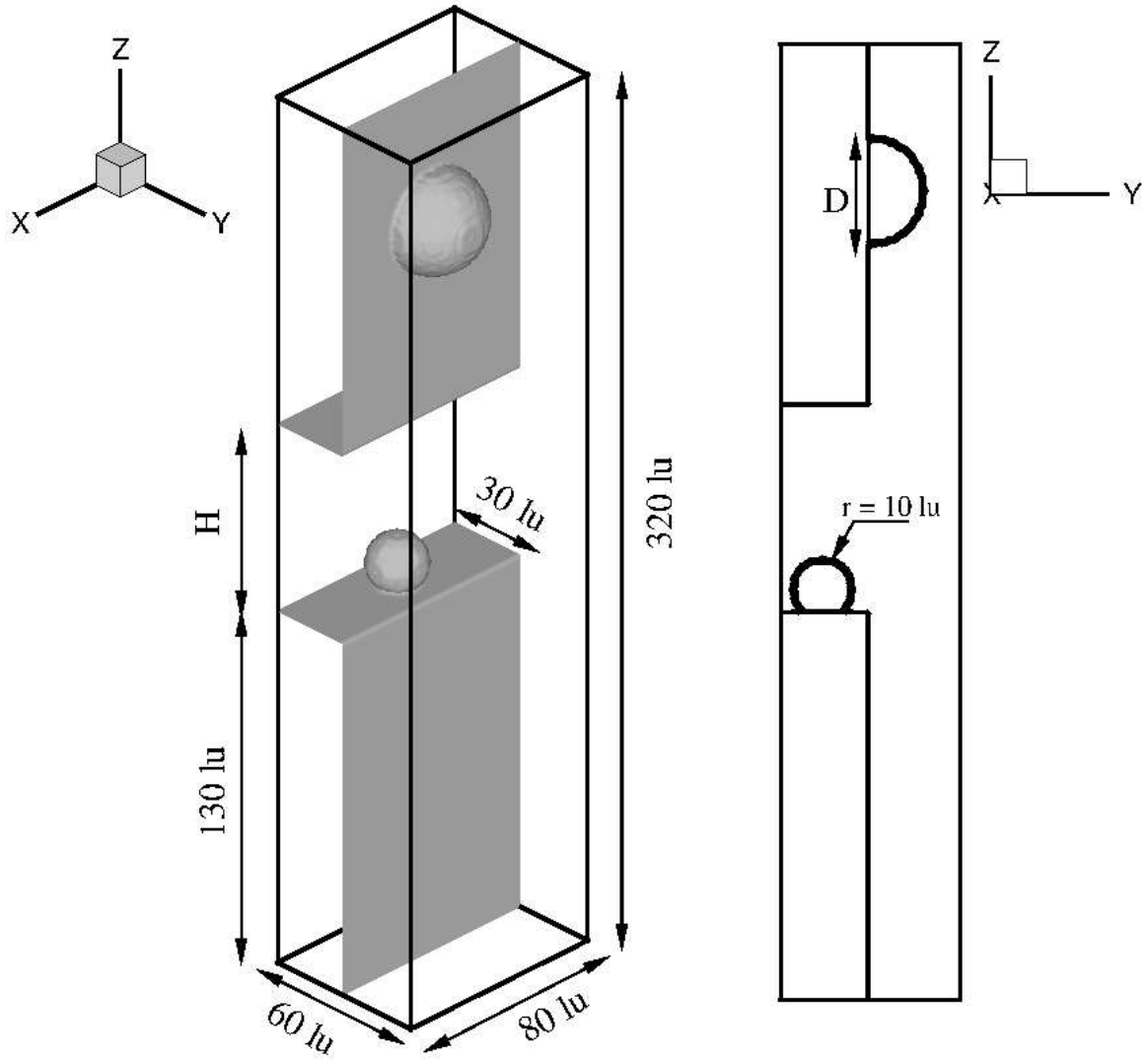

Figure 6.1: Schematic diagram of computational domain

inside the groove of the duct wall. To sweep-out the entrapped fluid, a large size three-dimensional immiscible droplet is allowed to slide down on the duct wall above the groove. It is important to mention here that it is the first study on sweeping the entrapped fluid out of the groove on the duct wall to our best knowledge. The results are shown in the form of isosurface plots, mid-plane sliced view plots and vector plots.

6.2 Problem specification

The present problem considers a three-dimensional duct having a groove on its one of the walls. The analysis of the present problem is based on the assumption that a major fraction of droplet fluid is already trapped inside the groove as shown in the previous study. The main aim of the present work is to sweep-out this trapped droplet fluid inside the groove. To sweeping the trapped fluid out of the groove, we have used a larger size droplet adhering to the outer surface of the grooved wall as shown in Fig. 6.1. The size of the domain is considered as 81 lu, 61 lu and 320 lu in x-, y- and z-directions, respectively. It is also considered that outer surface of the grooved wall is hydrophilic wettable, $g_{2w} = -0.02$ ($\theta = 78°$) whereas the inside surface of the groove is considered to be of hydrophobic, $g_{2w} = 0.05$ ($\theta = 118°$) and neutrally wet, $g_{2w} = 0.0$ ($\theta = 90°$) in two different cases. The width of the groove is taken as 30 lu and height (H) is varied from 60-80 lu for different cases of parametric study and the larger droplet is placed at z=271 lu. The initial density of carrier fluid (ρ_1) and droplet fluid (ρ_2) are taken as 0.035 and 0.965 lu, respectively and the relaxation parameters which define the kinematic viscosities are taken as τ_1=τ_2=1. The fluid or droplet motion has been governed by the gravitational force that is applied in the negative z-direction. A periodic boundary condition is applied in the z-direction and no-slip (i.e., bounce back) boundary condition has been applied at all walls located in x- and y-directions.

6.3 Results and discussion

In this section, the results are presented to show that the entrapped fluid inside groove on the duct wall can be swept-out with the help of a larger size droplet. It is important to mention here that when a droplet moves over a wall having groove on it, a fraction of the droplet fluid is entrapped inside the groove which depends on the size of the groove. This entrapped fluid is not desirable in many industrial applications, e.g., inkjet printing, spray painting etc. The entrapment of droplet fluid is well explained by Son et al. [46]. The present work is an attempt to analyze the sweeping-out phenomenon of entrapped fluid with the motion of a larger size droplet. It is found that no work has been reported till now which shows the sweeping-out phenomenon of this entrapped fluid inside wetted groove. A parametric analysis has been done to see the effect of groove size and capillary number (Ca)

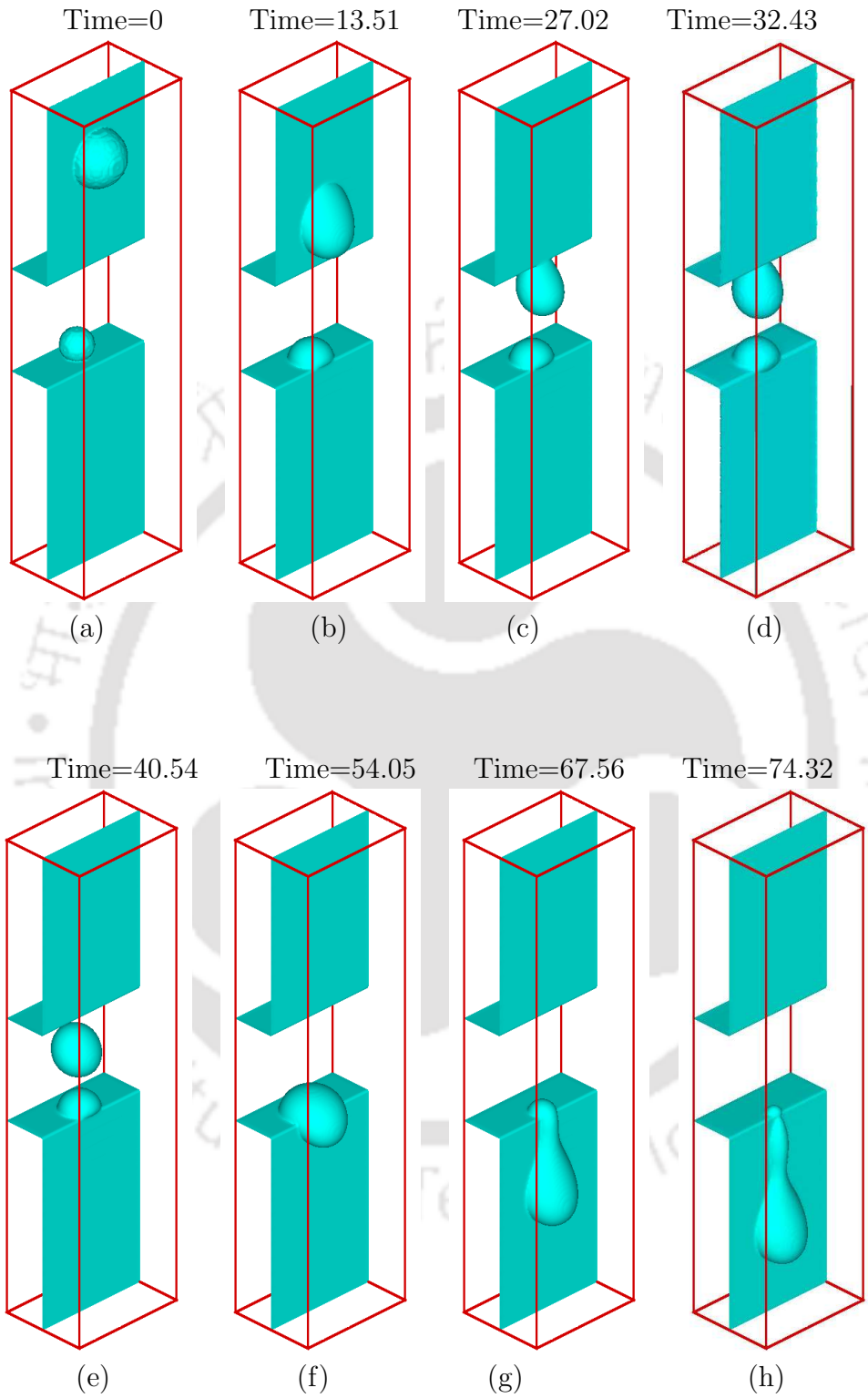

Figure 6.2: The isosurface plots of the droplet in 3D-plane for hydrophobic (g_{2w} = 0.05) groove surface at Ca = 0.25, groove height, H=70 lu and at various lattice time

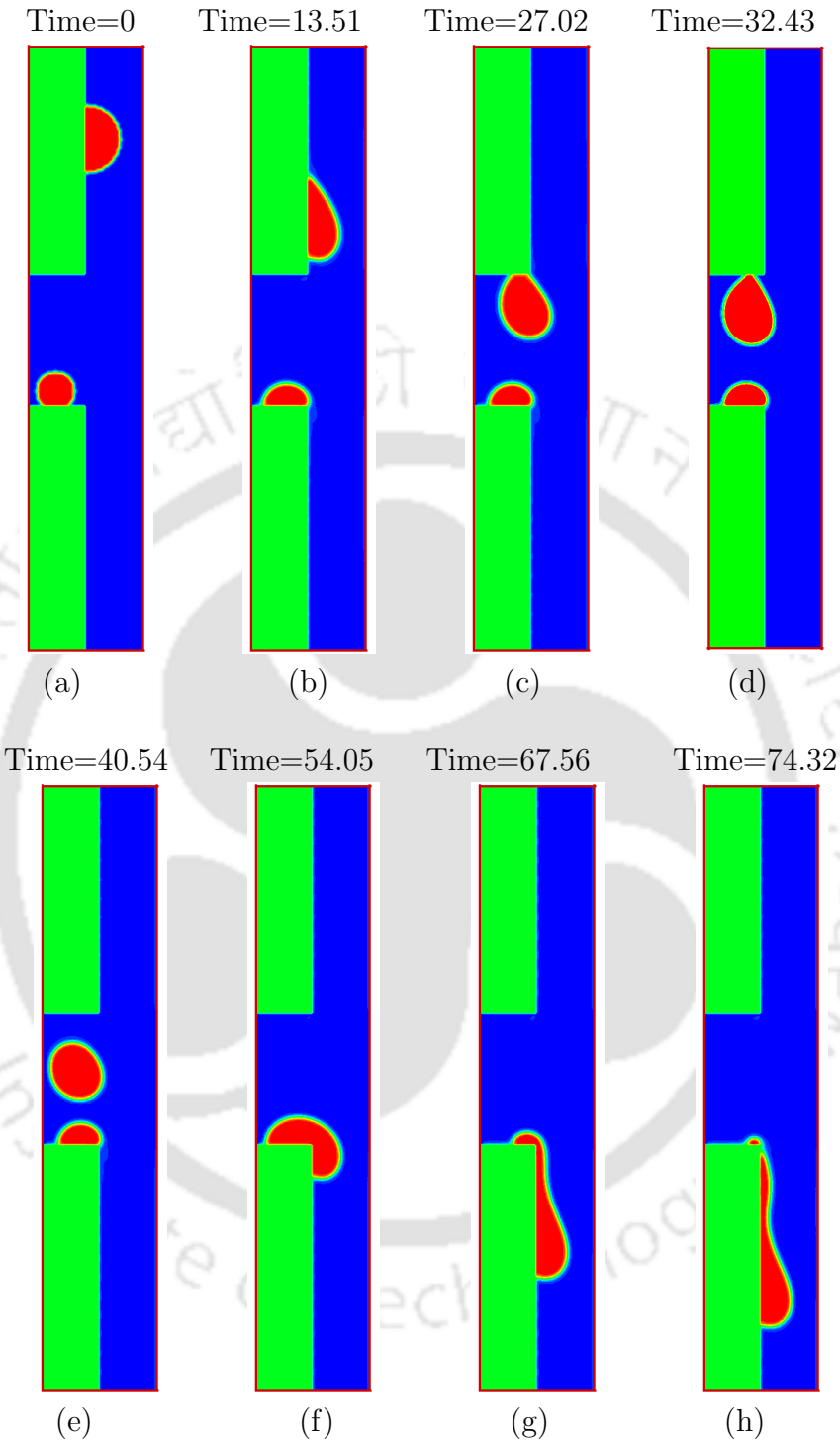

Figure 6.3: The shape of the droplet in $y-z$ plane at x=40 lu for hydrophobic ($g_{2w} = 0.05$) groove surface at Ca = 0.25, groove height, H=70 lu and at various lattice time

which depends on the radius of larger droplet.

The entrapped fluid inside the groove is assumed to be a small size droplet (R=10 lu) which is sitting on the lower surface of the groove in all cases. The groove size is considered to be 80 lu, 30 lu and 70 lu in x-, y- and z-directions, respectively. The capillary number is taken as 0.25 which is based on large droplet having a radius, R=18 lu in the present case. It is important to mention here that in reality the groove wettability plays a major role in entrapment of the fluid and it is not necessary that the wettability of the groove should be same as outer surface wettability. Based on this fact, in the present study, the wettability of the groove is considered as uniform hydrophobic and outer surface is considered to be of uniform hydrophilic. Time is made dimensionless by characteristic time $\frac{l}{U}$, where l is characteristic length and U is defined as characteristic velocity, $U = \frac{\rho_2 g h^2}{\mu_2}$ [101].

6.3.1 Droplet dynamics on a grooved wall

The three-dimensional isosurface plots of dynamic droplet behaviour at Ca=0.25 and at groove height, H=70 lu at various time have been shown in Figs. 6.2(a)-(h). From these plots, it is clearly visible that initially, the droplet is completely hemispherical at Time=0 as shown in Fig. 6.2(a) but as time progresses the droplet area, as well as droplet length, starts increasing on the wall surface above to the groove. This is because of the fact that as time progresses, the droplet fluid tries to make a bond with the surface in the presence of high adhesive forces as the surface has uniform hydrophilic wetting. However, the gravitational forces acting on the droplet tries to displace the droplet in a negative z-direction as shown in Fig. 6.2(b). The effect of this gravitational force can be seen in the change of shape of the droplet as well as the fluid entrapped inside the groove (Figs. 6.2(a)-(d)). As the groove is hydrophobically wet, it does not allow the droplet to spread over it and due to low surface energy, the surface area of the droplet contracted and finally, the droplet detaches from the groove upper surface. Beyond this instant, the sole effect of gravity, inertia of the droplet and groove surface wettability play a vital role in the sweeping of the entrapped fluid that can be seen in Figs. 6.2(e)-(h).

Figure 6.3 illustrates the dynamic behavior of sweeping-out entrapped fluid with the motion of large size droplet in $y-z$ plane view at x=40 lu. As it is seen in

Fig. 6.3, the large droplet slides down on the channel wall under the action of gravitational force as time progresses and because of the larger adhesive force due to hydrophilic nature of surface, the wetted area and wetted length of the droplet increase. In the mean time, the entrapped fluid starts settling down on the groove surface and due to hydrophobic nature of the groove surface, the fluid tries to move out of the groove but the velocity field acting on entrapped fluid is not that strong which allows it to completely sweep out of the groove itself. When the large droplet reaches the upper surface of the groove, the droplet tries to stick on the upper surface but due to hydrophobicity the upper surface of the groove repels the droplet fluid and droplet pinches off the groove surface. As the droplet detaches from the surface with a finite velocity under gravity, it falls inside the groove and coalesces with the entrapped fluid inside the groove. Thus, the volume of the total fluid has been increased. It is clearly seen in the figure that after coalescence of the large droplet with entrapped fluid, the large inertia force on the total fluid of the droplet tries to pull the entrapped fluid out of the groove.

Figure 6.4 depicts the zoomed view of vector fields near to the groove in $y - z$ plane at x=40 lu for Ca = 0.25, groove height, H=70 lu and at various lattice times. It is to mention that the no-slip boundary condition is fully satisfied at the wall which can be visualized by the very low intensity of velocity vectors near to the walls. However, the velocity vectors inside the droplet are not straight and take a curved shape. When the droplet reaches the groove, the velocity vectors are such that it tries to slide the droplet inside the groove as shown in Fig. 6.4(a). At Time=32.43 as shown in Fig. 6.4(b), a vortex is generated inside the droplet. It is also observed that the velocity in the downstream side of the droplet is larger than the upstream side and due to high shear stress between droplet and groove surface, the droplet pinches off the surface as shown in Figs. 6.4(b)-(c). In the same instant, a weak velocity vortex is also generated inside the previously entrapped fluid on the lower surface of the groove. This weak vortex tries to slide the fluid out of the groove but it is not able to break the resistance provided by the carrier fluid. In Fig. 6.4(d), it is seen that after the coalescence of the droplet and entrapped fluid, the total volume of the fluid increases and hence, the inertia force also increases. Due to the combined effect of inertia, gravity and wetting force, the velocity of the droplet increases and hence, the droplet slides down on the duct wall out of the groove as shown in Figs. 6.4(e)-(f).

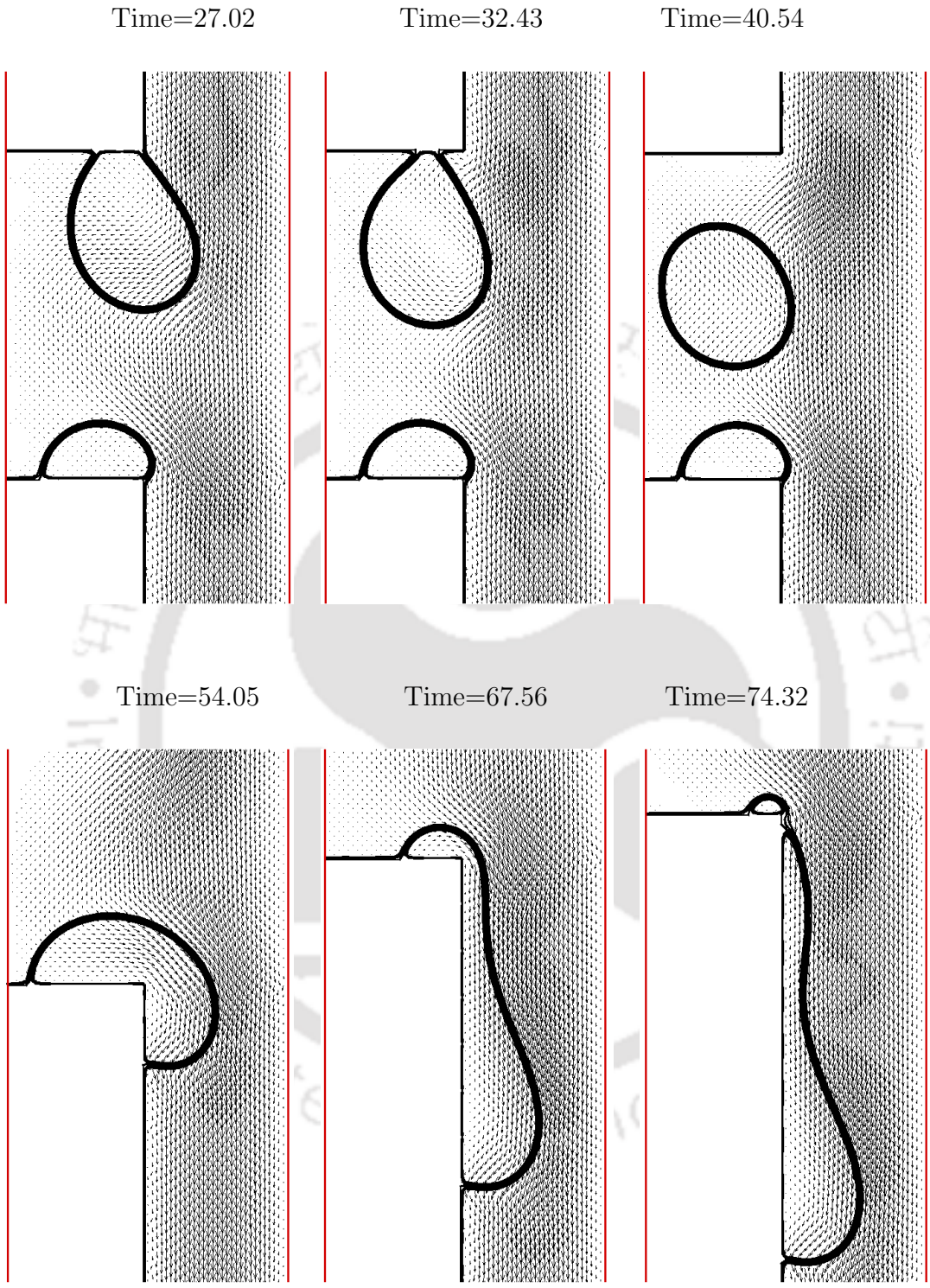

Figure 6.4: The zoomed view of vector fields inside channel in $y-z$ plane at x=40 lu for Ca = 0.25, groove height, H=70 lu at various lattice time

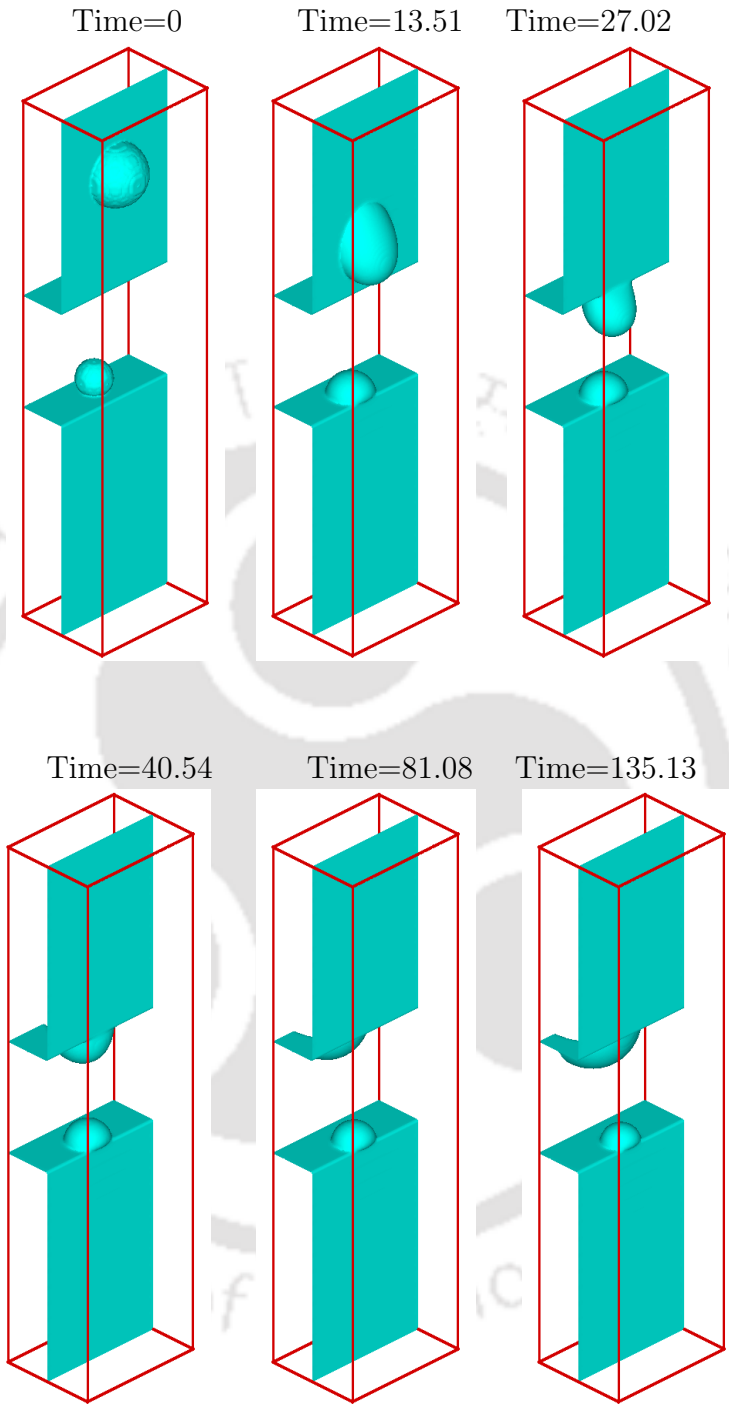

Figure 6.5: The isosurface plots of the droplet in 3D-plane for neutral ($g_{2w} = 0.0$) groove surface at Ca = 0.25, groove height, H=70 lu and at various lattice time

6.3.2 Effect of wettability on the sweep out behaviour

A set of numerical experiments has also been performed to see the effect of wettability of the groove surface on the sweeping of entrapped fluid out of the groove. In

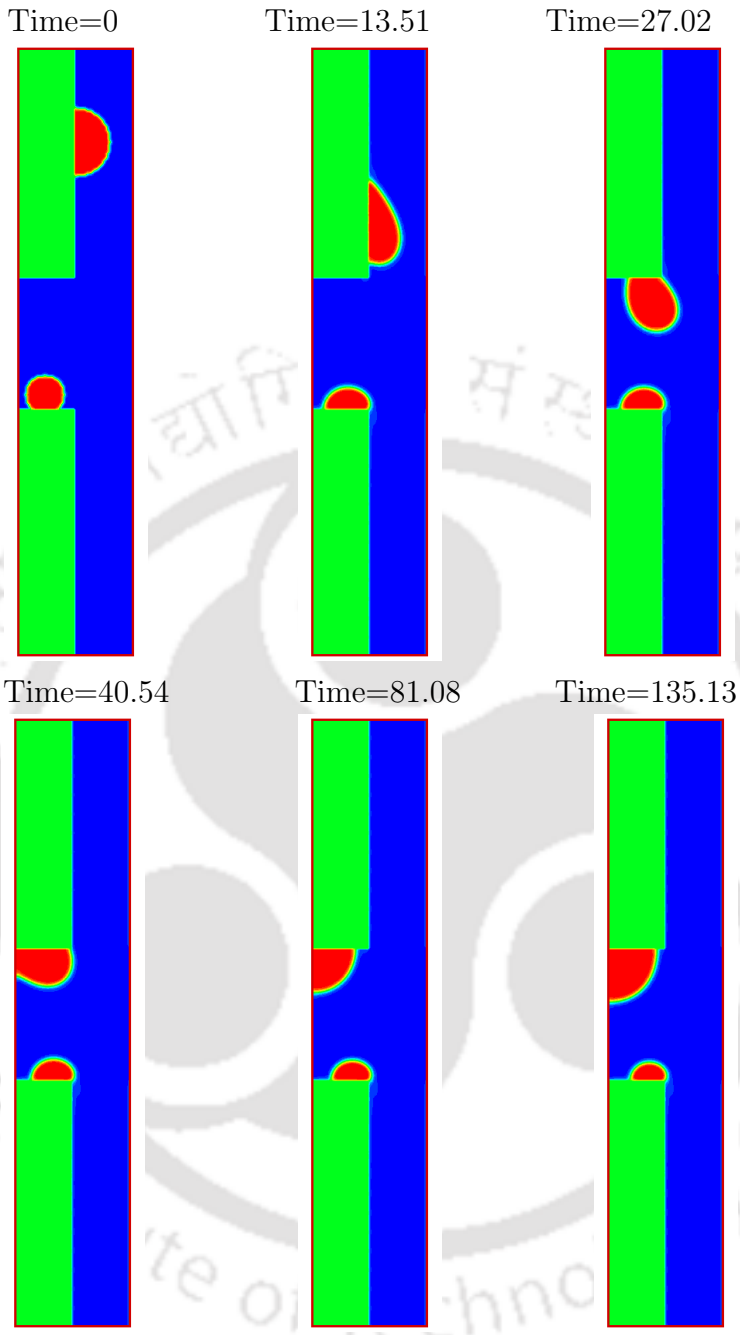

Figure 6.6: The shape of the droplet in $y-z$ plane at x=40 lu for neutral ($g_{2w} = 0.0$) groove surface at Ca = 0.25, groove height, H=70 lu and at various lattice time

the present study, a neutral surface of the groove has also been considered to see the effect of wettability. Figure 6.5 shows the dynamic droplet behaviour at various lattice time in the form of isosurface plots keeping other parameters same as in the

case shown in Fig. 6.2 except groove wettability. The behaviour of the movement of a droplet on the surface of the wall above groove is exactly the same as previously explained for the hydrophobic groove case. The physics has been changed once the droplet reaches to the groove. Unlike the hydrophobic groove, neutrally wet groove surface does not allow the droplet fluid to contract on the surface but it makes a strong bond and the droplet fluid partially wet the groove surface. In this case, the velocity inside the droplet and inertia force are not that strong to detach the droplet fluid from the groove surface. This phenomenon can also be seen in $y-z$ plane sliced view at x=40 lu in Fig. 6.6. In the sliced view, we can clearly see that the droplet after reaching the groove, spreads on the surface and slides deep down inside the groove.

Figure 6.7 shows the evolution of wetted area (A/A_0) and wetted length (b/b_0) at Ca=0.25 and at groove height, H=70 lu for both hydrophobic as well as neutral groove surfaces where A_0 is the initial area of the hemispherical large droplet and b_0 is the initial length of the droplet at Time=0. In Figs. 6.7(a)-(b), wetted area and wetted length are plotted against time at g_{2w}=0.05 and 0, respectively. It is observed in the plots that initially, both wetted area and wetted length increase till Time=18 (approximately) for both wetting condition (i.e., g_{2w}=0.05 & 0). This is due to the fact that the droplet is sliding on the hydrophilic surface and the droplet spreads and tries to wet the surface. This spreading gives rise in the wetted area and as droplet displaces under gravitational acceleration, its length also increases. But beyond Time=18, both wetted area and wetted length start decreasing monotonically for neutrally wet groove case but for hydrophobic groove, both wetted area and wetted length decrease till Time=44 and again start increasing. This behavior is observed due to the presence of groove cavity. It is important to mention here that both the quantities i.e., wetted area and wetted length, are calculated on the surface of the channel wall on which the groove is created. In case of neutrally wet groove, the wetted area and wetted length after initial increase, decrease monotonically and reach almost equal to zero. This is because of the fact that once the droplet reaches the groove, it completely gets entrapped inside the groove and there is no sweeping of previously entrapped fluid out of the groove. But in case of hydrophobic groove, as the droplet reaches the groove and past through the groove surface, the wetted area and wetted length on the duct wall decrease. Beyond the time at which the coalescence of droplet and entrapped fluid take place, both the wetted area and

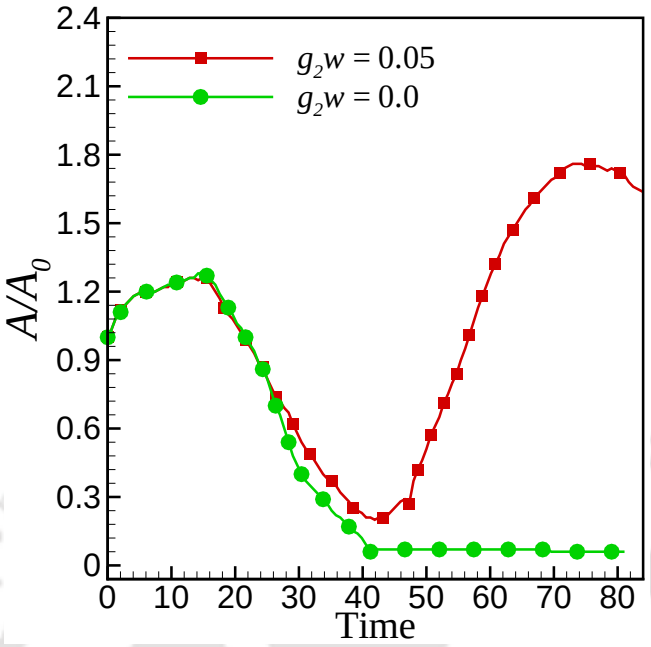

(a)

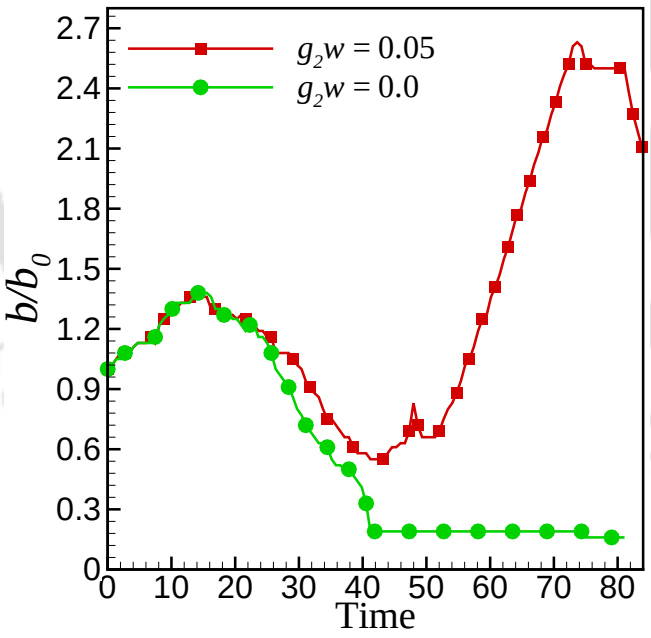

(b)

Figure 6.7: Evolution of wetted area and wetted length of the large droplet on the wetted duct wall. The plots are obtained at capillary number, Ca=0.25 and groove height, H=70 lu

wetted length start increasing and the value goes beyond the initial increase in area because now the combined volume of the droplet has increased. In later stages when the combined droplet translates on the duct wall below the groove, the droplet itself breaks into two parts and hence, the wetted area and wetted length are found to be decreasing as shown in Figs. 6.7(a)-(b).

6.3.3 Effect of the capillary number and groove height

In the previous studies of droplet flow, it is found that there are few parameters which majorly affect the flow of droplet on the wall of the channel. One of the prime parameters is capillary number, Ca which is defined as the ratio of viscous to surface tension force across an interface, Ca=$\frac{\rho_2 g V}{\sigma h}$ where ρ_2 is the density of fluid 2, g represents the gravitational acceleration, V is volume of spherical droplet, σ is surface tension and h is the width of the rectangular microchannel. There are three parameters either of which can be varied to get different capillary numbers; these are the gravitational factor (g), surface tension (σ) and droplet radius (R). In the present analysis, different capillary numbers are obtained by varying large droplet radius (R). In the present study different capillary numbers, Ca=0.07, 0.15, 0.25 and 0.40 are obtained for droplet radius, R=12, 15, 18 and 21 lu keeping gravitational factor, $g = 1 \times 10^{-4}$. In this analysis, it is observed that as capillary number increases, i.e., the radius of the large droplet increases, the sweeping of the entrapped fluid inside the groove is faster. It is also observed that at Ca=0.40 (i.e., R=21 lu) the percentage fraction of the sweeping of entrapped fluid is maximum as shown in Fig. 6.8. The cause of this maximum sweeping of the entrapped fluid is majorly the combined effect of inertia and interfacial interaction force due to the large volume of the droplet. Figure 6.8 clearly depicts that at small capillary numbers (Ca=0.07 and 0.15), the volume of the droplet is not that large which can allow the droplet to detach from the upper surface of the groove, Thus the total volume of the droplet is entrapped itself inside the groove which is highly undesirable.

Figure 6.9 shows the effect of the height of the groove on the sweeping out of the entrapped fluid inside the groove at the fixed capillary number, (Ca=0.25) and different time steps. In the present study, the three different heights, i.e., 60, 70 and 80 lu, of the groove are considered for the analysis. The height of the groove is an important parameter for such studies because the droplet has to travel along a path

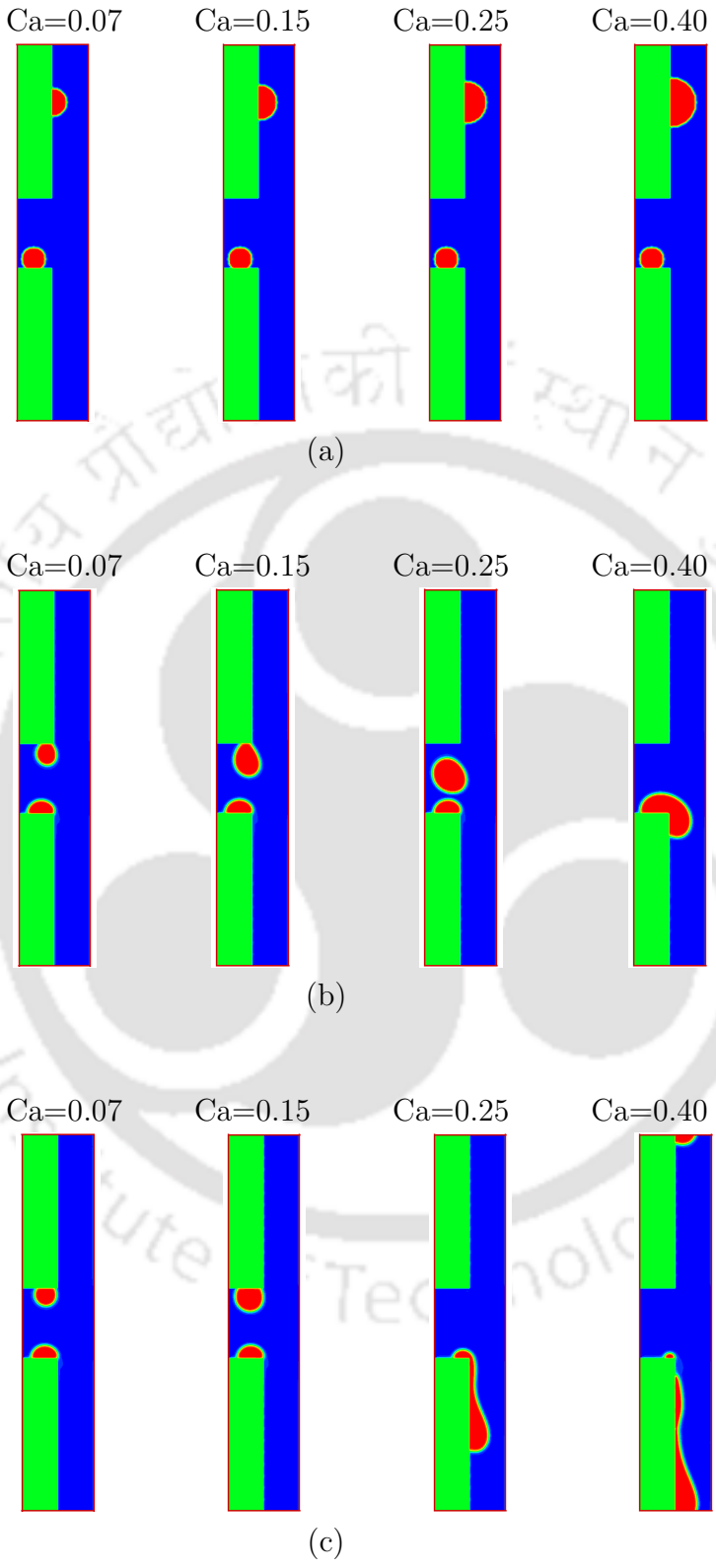

Figure 6.8: The shape of the droplet in case of hydrophobically wetted groove in $y-z$ plane at x=40 lu, groove height H=60 lu and at lattice times, (a) Time=0, (b) Time=40.54 and (c) Time=67.56

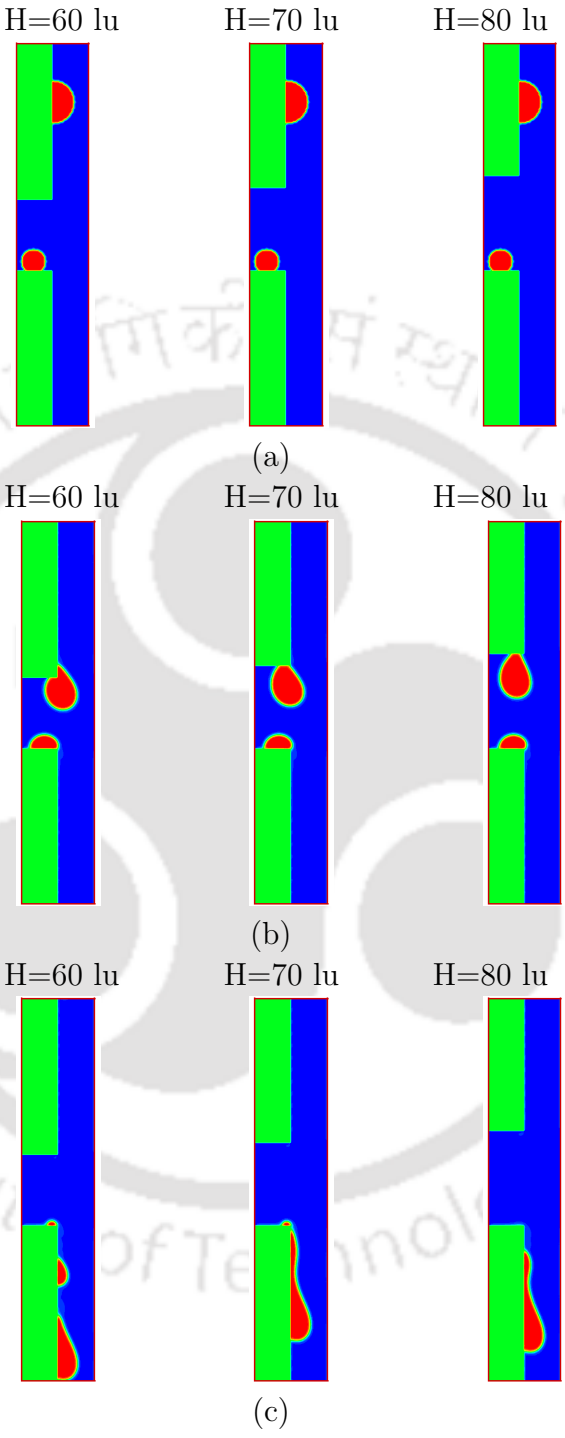

Figure 6.9: The shape of the droplet in case of hydrophobically wetted groove in $y-z$ plane at x=40 lu, Ca=0.25 and lattice time, (a) Time=0, (b) Time=27.02 and (c)Time=74.32

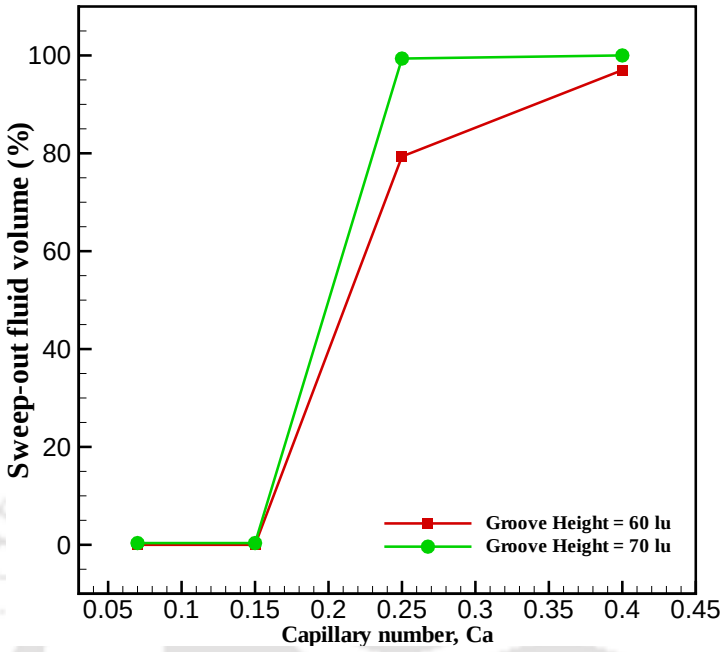

(a)

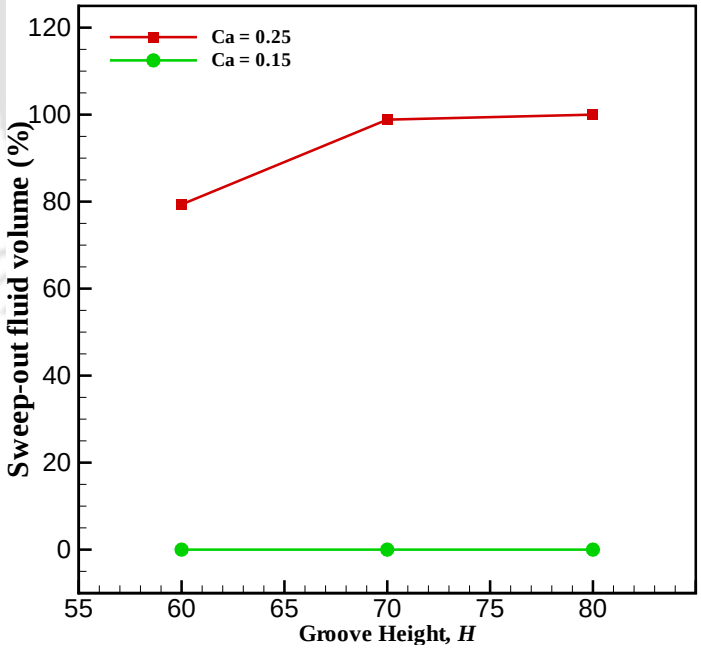

(a)

Figure 6.10: Plot showing the fraction (%) of sweep out fluid volume against (a) capillary number, (b) groove height,

inside a groove after the detachment from the upper surface of the groove. As shown in Fig. 6.9, when the height of the groove is 60 or 70 lu, the droplet is not able to completely sweep out entrapped fluid inside the groove and a very small fraction of entrapped fluid still remains on the lower surface of the groove. But when the groove height is equal to 80 lu which is comparatively larger, the droplet detaches from the upper surface of the groove with a large velocity and has travelled deep inside the groove. Therefore, the droplet completely coalesce with the entrapped fluid and sweep it out of the groove.

Figures 6.10(a)-(b) show the percentage (%) fraction of sweep out fluid volume at the particular capillary number and groove height. From this analyses, it is found that at capillary numbers, Ca=0.07 and 1.5, there is no sweeping for all three groove heights (H=60, 70 and 80 lu). The complete sweeping (100 %) of entrapped fluid out of the groove is achieved for the set of Ca=0.25, H=80 lu and Ca=0.40, H=70 lu. There are few combinations of Ca and H for which little less than 100 % sweeping of entrapped fluid is achieved. For Ca=0.25 and groove height, H equal to 60 and 70 lu, a fraction of swept volume is 79.35 % and 98.85 %, respectively and for Ca=0.40 and H=60 lu, the fraction of swept volume is found to be equal to 97 %.

6.4 Summary

The present study was focused on the method of sweeping the entrapped fluid out of the groove with the help of a large size three-dimensional immiscible droplet under gravity. The problem considered a single grooved wetted wall of a rectangular three-dimensional channel. The wettability of the groove surface was considered as neutral and uniform hydrophobic whereas the wettability of three-dimensional channel walls outside of the groove is considered as uniform hydrophilic. The analysis showed that the sweeping of entrapped fluid out of the groove largely depends on the capillary number and groove height. It was also observed that sweeping of entrapped fluid takes place only for the uniform hydrophobic surface of the groove. In case of the neutral surface of the groove, the large size droplet itself completely trapped inside the groove and does not able to sweep the previously entrapped fluid.

Chapter 7

Analysis of Deformation and Breakup of a Three-dimensional Droplet Past a Solid Spherical Obstruction

7.1 Introduction

The distortion of an immiscible liquid droplet in a stream of another liquid has been a major fluid mechanics issue for roughly about 100 years. It is to be noted that in a wide range of industrial applications, the phenomenon of droplet dynamics past solid obstacles can be found very frequently. The most common applications can be found in oil recovery, inkjet printing, droplet-based microfluidics, and so on. In these types of systems, the dynamics of drop deformation and breakup are usually very complicated for the complex interactions between components. On the other hand, the study of the droplet past a solid target has recently been an active field of research for its great importance in many fields.

Recently, a detailed two-dimensional study was conducted by Li et al. [102] to explore the phenomena of deformation and breakup of a liquid droplet passing through a solid circular cylinder in a confined microchannel using lattice Boltzmann

method. In this investigation, Li et al. [102] focused on the effect of eccentric ratio, Bond number, viscosity ratio and surface wettability to show that there are two typical patterns i.e., breakup or no breakup. It was also found that the viscosity ratio is an important parameter which strongly affects the droplet dynamics. But the study lacks in the more detailed study in three-dimension; the study was only focused on the two-dimensional assumption.

The prime objective of the present study is to numerically investigate the dynamic behaviour of droplet moving under gravity in a three-dimensional channel. The path of the droplet is restricted by wetted solid spherical obstruction. Therefore, the study also considers the direct impact of droplet and obstruction as well as the spreading behaviour of droplet fluid over the solid obstruction. To explore the complex physics of the present problem, a parametric study is conducted to analyze the effects of capillary number, surface wettability, obstruction size and structure.

7.2 Problem specification

A schematic diagram of the droplet flow in a confined microchannel with a solid spherical obstruction is provided in Fig. 7.1. The lattice size of the physical domain is considered to be of 150 $\times$ 150 $\times$ 900 in x-, y- and z-directions (all dimensions are used in LB units). For the analyses of droplet dynamics, initially an immiscible fluid droplet of radius R=50 is placed at z=750 and the centre of the droplet lies in the central axis of the channel. In order to provide a restricted passage to the droplet, a solid spherical obstruction with a characteristic size d is placed at z=450 and aligned at the centre of the channel. The main driving force which provides the movement to the droplet is gravitational acceleration, g that is applied in the negative z-direction. In the present numerical simulations, the periodic boundary condition is implemented at the inlet and outlet of the channel, and a simple bounce-back scheme is applied to all solid walls including solid spherical obstruction. The initial density of carrier fluid (ρ_1) and droplet fluid (ρ_2) are taken as 0.035 and 0.965 lu, respectively.

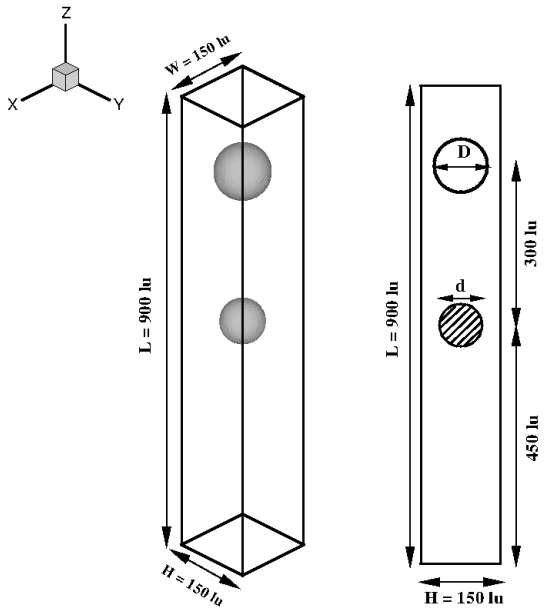

Figure 7.1: Schematic diagram of computational domain

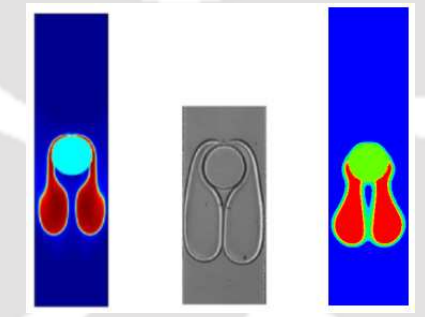

(a) (b) (c)

Figure 7.2: The comparison of present LBM formulation results with the available literature, (a) Numerical [102], (b) Experimental [64], (c) Present LBM result

7.3 Results and discussion

Before commencing the numerical simulation using current flow-solver, it is important to test the accuracy of the LBM code. Therefore, the two most important parameters, namely the fluid-fluid and fluid-solid interaction parameter are to be inspected critically. The significance of fluid-fluid interaction parameter lies in surface tension force and the fluid-solid interaction parameter gives rise to the wall adhesion force. A detailed description of the validation of the solver and the behaviour of

the above-mentioned parameters have already been reported in our previous studies [37, 103]. Therefore, a detailed description of validation has not been included for brevity. However, to show that the in-house LBM code has the capability to solve such a complex problem, a comparison of LBM results with the previously reported experimental results [64] has been carried out and presented in Fig. 7.2. Based on this comparison, it can be inferred that the LBM results are promising and agree qualitatively with the reported experimental results [64]. In conclusion, it can be said that the present LBM code can handle a complex phenomenon of impact and breakup of the droplet on a solid obstacle.

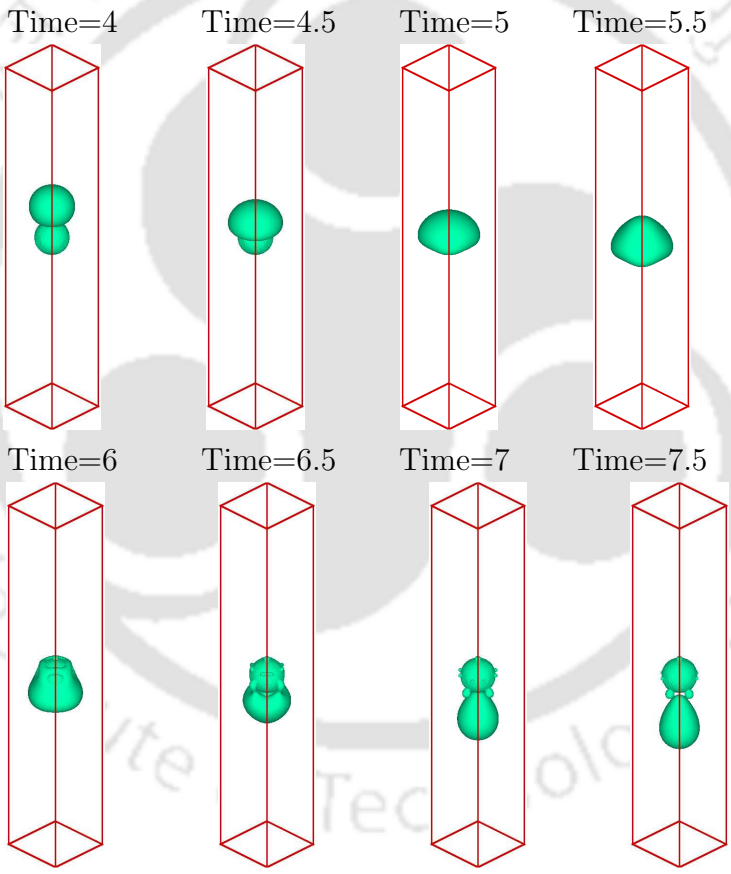

Figure 7.3: The isosurface plots of the time evolution of the droplet past a spherical obstruction at Ca=0.407, M=1 and $\theta = 120^{\circ}$

The present investigation is solely based upon the droplet dynamics past a solid spherical obstruction. It is to be noted that a few studies of droplet past a solid

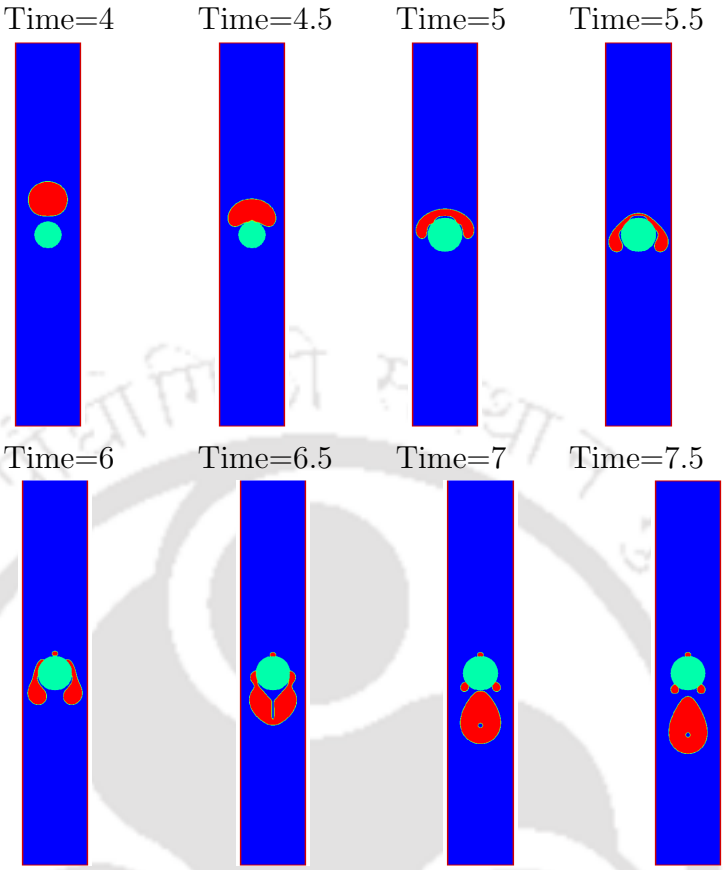

Figure 7.4: The $y-z$ sliced view (at mid plane of x) of the time evolution of the droplet past a spherical obstruction at Ca=0.407, M=1 and $\theta = 120°$

cylinder in a two-dimensional domain have been performed in the past but the analysis of such problem in a three-dimensional channel has heretofore not been reported. Therefore, to bridge this gap and understand the flow physics in the three-dimensional scenario, a comprehensive parametric study has been carried out to determine the effect of different parameters and factors on the droplet dynamics past a spherical obstruction in a three-dimensional channel. In order to investigate the droplet flow dynamics and impact of the droplet with the solid spherical obstruction, the effect of capillary number (Ca), surface wettability (θ), size of solid spherical obstruction and structure of obstruction has been performed by varying a number of parameters. The capillary number, Ca is defined as the ratio of viscous to surface tension force across an interface, Ca=$\rho_2 gV/\sigma h$ where, ρ_2 is the density of fluid 2, g represents the gravitational acceleration, V is volume of spherical droplet,

σ is surface tension and h is the width of the rectangular microchannel. There are three parameters either of which can be varied to get different capillary numbers; these are the gravitational factor (g), surface tension (σ) and droplet radius (R). In the present analysis, different capillary numbers are obtained by varying gravitational factor g. Time is made dimensionless by characteristic time $\frac{l}{U}$, where l is characteristic length and U is defined [101] as characteristic velocity, $U = \rho_2 g h^2/\mu_2$.

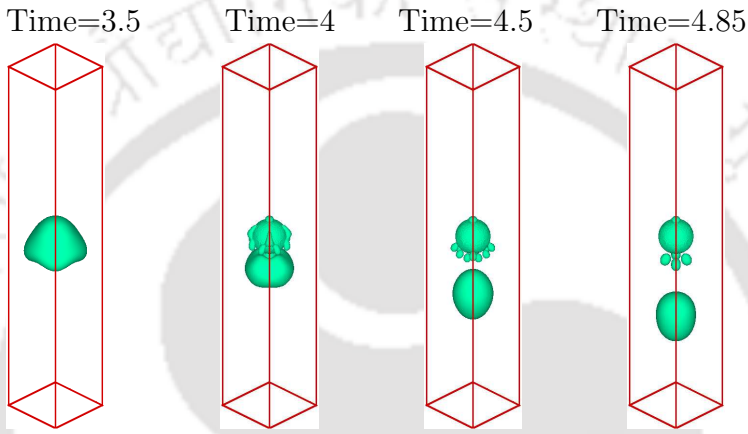

Figure 7.5: The isosurface plots of the time evolution of the droplet past a spherical obstruction at Ca=0.814, M=1 and $\theta = 120°$

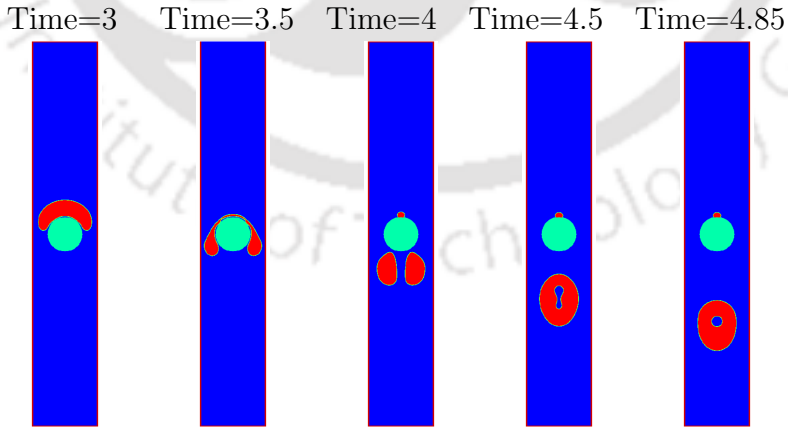

Figure 7.6: The $y-z$ sliced view (at mid plane of x) of the time evolution of the droplet past a spherical obstruction at Ca=0.814 , M=1 and $\theta = 120°$

7.3.1 Effect of capillary number

The numerical simulations are performed to understand the effect of the capillary number on the droplet dynamics and breakup past the solid spherical obstruction and the time taken to cross past the obstruction. As it is reported earlier that the capillary number represents the relative magnitude of the viscous force and surface tension force; therefore this investigation reveals the combined effect of viscous, surface tension and adhesive forces on droplet deformation and breakup. In the present section, we first report the droplet dynamics at Ca=0.407, viscosity ratio, M=1 and surface wettability, $\theta = 120^{\circ}$ and then the value of the capillary number is doubled, i.e., Ca=0.814 to show the effect of the higher capillary number. Figures 7.3-7.4 illustrate the isosurface and $y - z$ plane slice view plots, respectively at Ca=0.417. The droplet falls under the action of gravity and the deformation commences once it reaches near the solid obstruction at Time=4. As soon as the droplet makes contact with the obstruction at Time=4.5, continuous fluid in the form of the bubble is entrapped inside the fluid covering the obstruction's upper half. The droplet fluid film breaks at the upper surface of the obstruction due to the curvature of the obstruction as shown in Figs. 7.3-7.4 at Time=6. Later, the meniscus owing to gravity tries to fill the gap between obstruction and the side walls and finally slides down. If we closely look at the bottom side of the solid obstruction, the spherical obstruction due to its hydrophobic nature of the surface starts repelling the droplet fluid. This gives rise to a dead zone at the bottom of the obstruction. The dead zone is defined as the area under the obstruction where the droplet fluid is not in contact with the obstruction. This is owing to the fact that droplet fluid follows the path along the streamline close to the obstruction. The combined effect of viscous drag and surface tension force result in the generation of daughter droplets which are adhered on the surface of the solid obstruction. These daughter droplets under the action of gravity and hydrophobic surface morphology slide down and merge into a single droplet that is detached from the surface. However, a small fraction of droplet fluid remains attached on the upper surface of the obstruction.

As the capillary number increases to Ca=0.814, the droplet quickly reaches the solid obstruction with more deformation due to high gravitational force as shown in Figs. 7.5-7.6. The effect of high gravitational force also affects the time taken by the droplet to pass the solid obstruction. The droplet, when collides with the

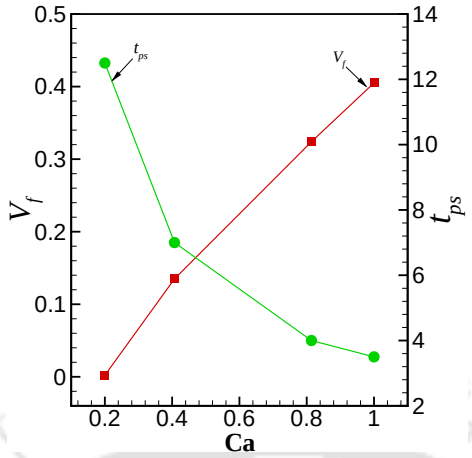

Figure 7.7: Effect of the capillary number on passing time and fraction of deposited volume on the upper surface of obstruction at Ca=0.407 and $\theta = 120°$

obstruction, starts deforming and the liquid film at the upper surface of the obstruction becomes thin. At an early stage of deformation, the droplet fluid eventually breaks and detaches from the surface of the obstruction. Similar to the case of Ca=0.407, here also few daughter droplets have formed which after passing through the obstruction merge into a single droplet. At the later stages when the droplet fluid merges after detachment, the continuous phase in the form of the bubble is entrapped inside the merged droplet. This may be the effect of surface tension force which tends to contract the droplet fluid into a circular shape. To further investigate the droplet dynamics process, passing time (t_{ps}) and the fraction (%) of droplet fluid attached on the upper surface of the solid obstruction have been measured. The passing time (t_{ps}) can be defined as the time taken by the bulk of the droplet fluid to cross the solid spherical obstruction. Figure 7.7 shows the various passing time and % volume fraction for different capillary number at $g_{2w} = 0.06$ and viscosity ratio, M=1. The results clearly reveal that as capillary number increases, the passing time (t_{ps}) decreases and the fraction of droplet volume left attached on the upper surface increases. It can be explained as the capillary number increases, the gravitational acceleration also increases which ultimately makes the movement of droplet faster. Figure 7.7 also depicts that the % volume of the remaining fluid on the upper surface of the obstruction is less than 1% for all capillary numbers, this is owing to the hydrophobicity of the spherical obstruction surface which makes most of the fluid non-wetting.

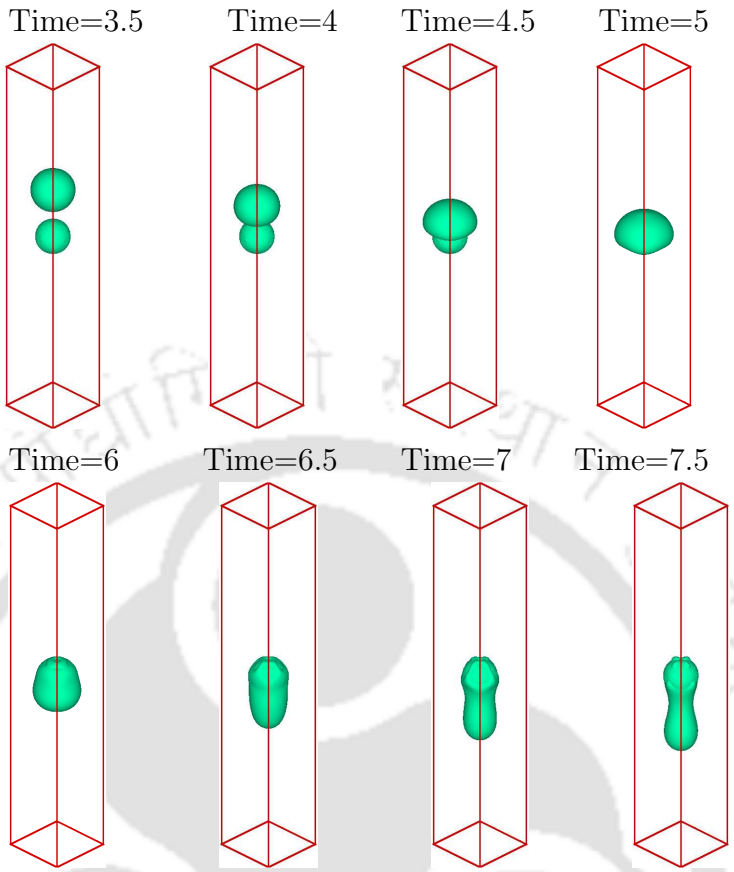

Figure 7.8: The isosurface plots of the time evolution of the droplet past a spherical obstruction at Ca=0.407, M=1 and $\theta = 60°$

7.3.2 Effect of surface wettability on droplet dynamics

The droplet flow past a solid obstruction includes a direct contact of obstruction surface and droplet fluid. Therefore, the surface characteristics of the obstruction largely affect the dynamics of droplet when it crosses past the obstruction. Thus, to investigate the droplet dynamics, various wetting conditions of the solid walls of the channel and the surface of the solid obstruction have been considered in the present section. Basically, wetting or wettability is the property of the surface which defines the ability of fluid to spread over the solid surface. In nature, different types of wetting patterns are found, uniformly hydrophobic (non-wetting) and hydrophilic (wetting) are two of them. In the case of uniformly hydrophobic surface, the surface tries to repel the mass of fluid and in the case of hydrophilic wettability, the surface tries to attract and makes bond with the mass of fluid. However, it is reported in

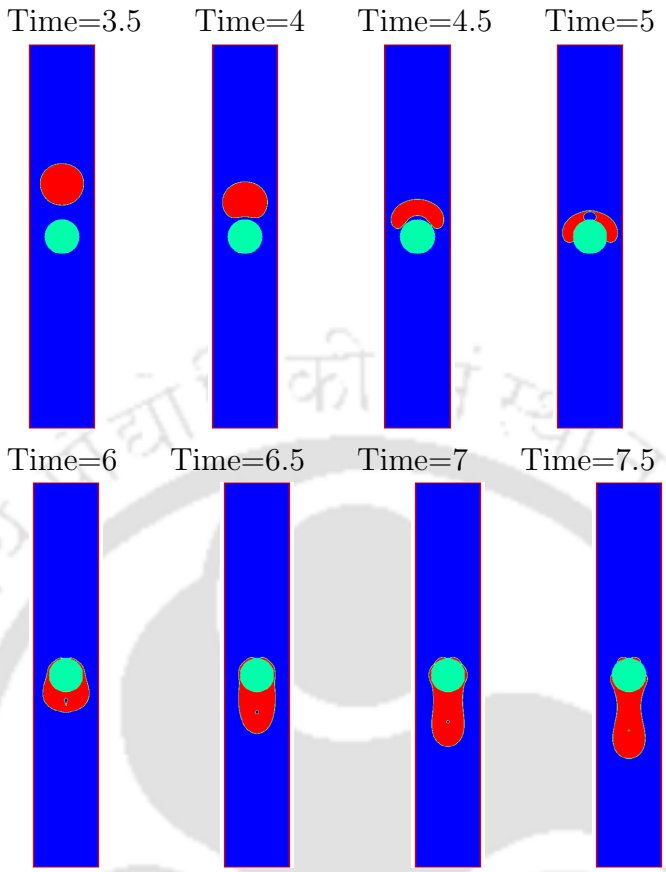

Figure 7.9: The $y-z$ sliced view (at mid plane of x) of the time evolution of the droplet past a spherical obstruction at Ca=0.407, M=1 and $\theta = 60°$

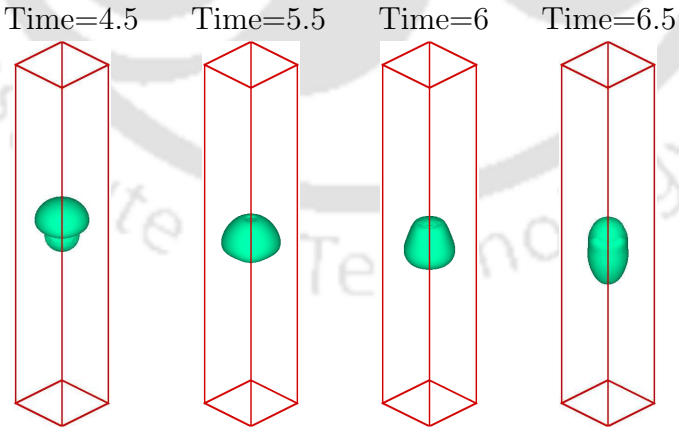

Figure 7.10: The isosurface plots of the time evolution of the droplet past a spherical obstruction at Ca=0.407, M=1 and $\theta = 90°$

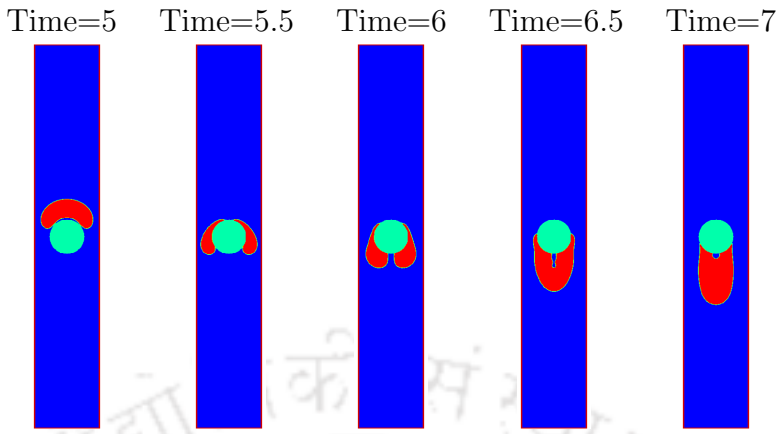

Figure 7.11: The $y-z$ sliced view (at mid plane of x) of the time evolution of the droplet past a spherical obstruction at Ca=0.407, M=1 and $\theta = 90°$

literature that the dynamics of wetting surfaces are more complicated compared to non-wetting surfaces.

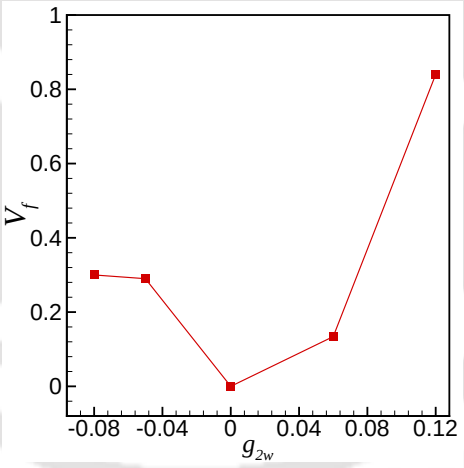

Figure 7.12: Effect of surface wettability on fraction of deposited volume on the upper surface of obstruction at Ca=0.407 and obstruction radius, r=40 lu

The dynamics of the droplet in hydrophobic surface of obstruction are well explained in the section 7.3.1; results shown in Figs. 7.3-7.4. The discussions are herein focused on the hydrophilic surface of the solid obstruction. As illustrated in Figs. 7.8-7.9, when there is head to head impact of the droplet with the obstruction, the surface attracts most of the fluid to adhere on it owing to its high adhesive property. During this process, a continuous phase fluid is entrapped when the droplet

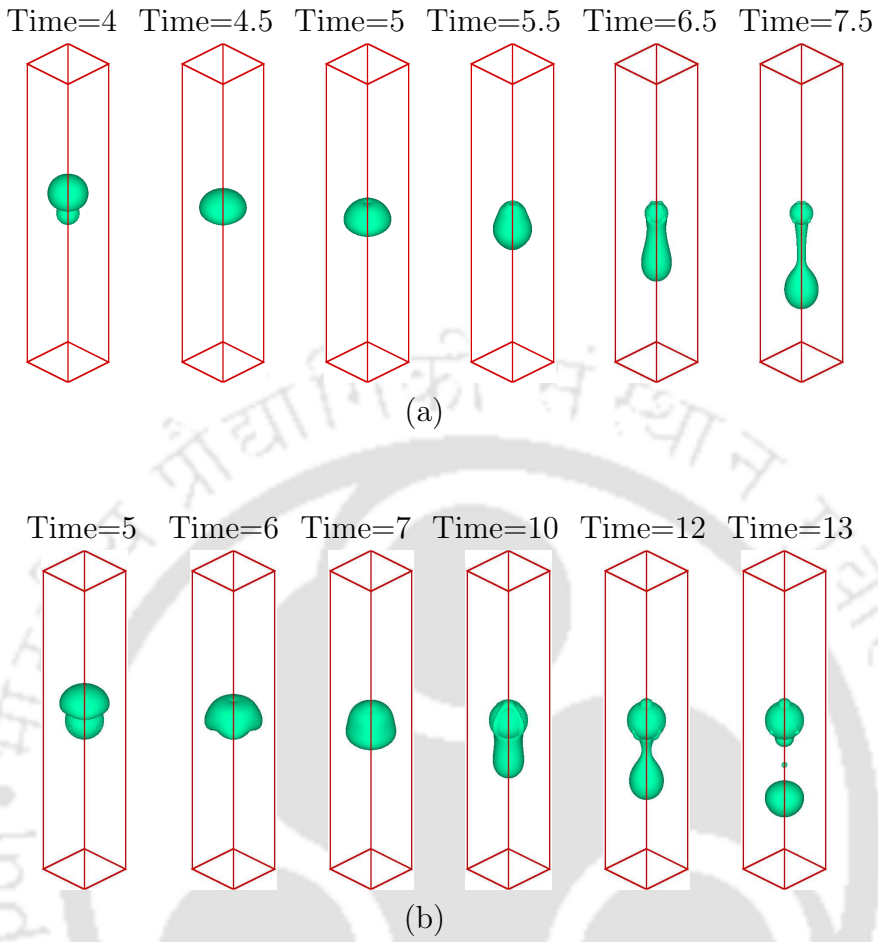

Figure 7.13: The isosurface plots of the time evolution of the droplet past a spherical obstruction at Ca=0.407, M=1 and $\theta = 60°$ for spherical obstruction radius, (a) r=30 lu, (b) r=50 lu

makes an envelope over the obstruction. However, the combined effect of adhesion and gravity tries to make the droplet layer thinner and hence, the droplet fluid layer breaks at the top surface of the obstruction. It is observed that the high philicity of the surface creates difficulty for the droplet to flow down on the surface and hence, it completely wets the surface of the obstruction. When the droplet fluid moves down the obstruction surface, it assumes a bullet like shape and then the fluid, owing to gravity, elongates further whereas adhesion tries to get the fluid attached on the surface. The investigation also shows that the deposition of the droplet fluid, in the case of a hydrophobic wetting surface, is brought about on the upper surface of the obstruction. In the case of hydrophilic wetting, deposition is less on the upper

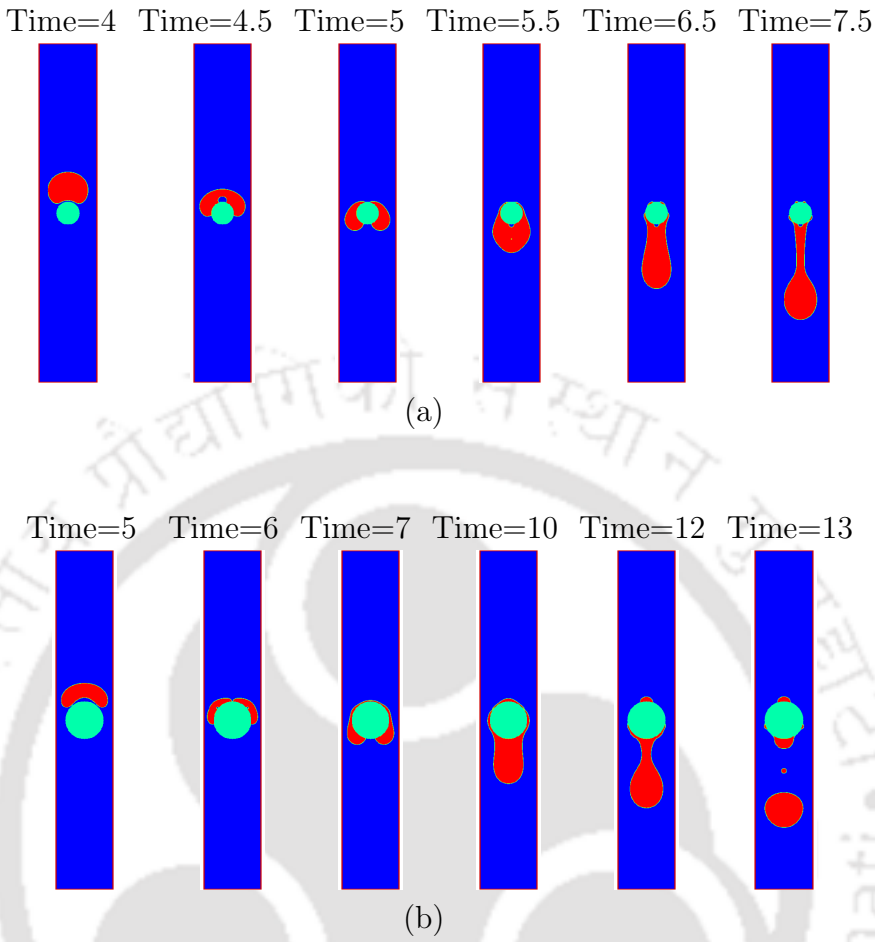

Figure 7.14: The $y-z$ sliced view (at mid plane of x) of the time evolution of the droplet past a spherical obstruction at Ca=0.407, M=1 and $\theta = 60^{\circ}$ for spherical obstruction radius, (a) r=30 lu, (b) r=50 lu

surface and more on the downward side of the obstruction. In the case of the neutral wetting surface (Figs. 7.10-7.11), it is found that the deposition of the droplet is only on the downward side of the obstruction. We further conducted simulations over a wide range of the contact angles and found that the location of deposition is changed from the upward to downward along the cylinder surface with the decrease in contact angle. This happens as the wetting droplet tends to get attached to the surface tightly, and the thin layer of liquid deposition is dragged away by the gravity force. The effect of surface wettability on the fraction of the deposited volume of droplet fluid on the upper surface of the obstruction has been illustrated in Fig. 7.12. The results are shown at Ca=0.407 and r=40 lu for various surface wettabil-

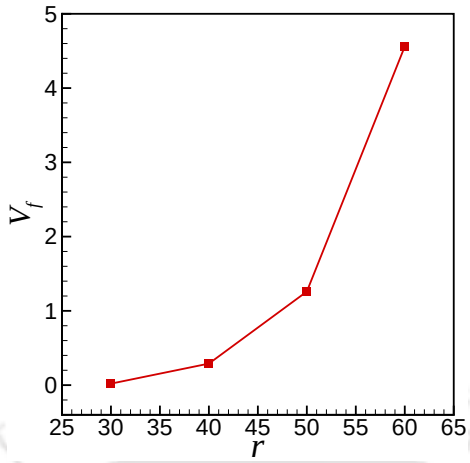

Figure 7.15: Effect of obstruction size (i.e., radius, r) on fraction of deposited volume on the upper surface of obstruction at Ca=0.407 and $\theta = 60°$

ities. The study shows that the fraction of deposited volume of droplet fluid first decreases (in the case of hydrophilic wettability) and then increases (in the case of hydrophilic wettability) with the increasing value of θ. It is interesting to see that the deposition of droplet fluid on the upper surface of the obstruction is found to be zero in the case of neutral wetting ($\theta = 0°$).

7.3.3 Effect of the size of the obstruction

It is evident that in most of the industrial applications where the droplet is moving inside a channel, it may encounter obstructions of various sizes. Therefore, it is important to carry out a parametric study of droplet impact with various size of solid spherical obstruction. In the present section, four different values of the radius of the solid spherical obstruction, i.e., r=30, 40, 50 and 60 lu have been considered. Here, it is necessary to mention that the different radii of the obstruction represent the different surface areas of the obstruction which may affect the droplet dynamics. Figures 7.13 and 7.14 depict the isosurface views and its corresponding $y - z$ plane views at mid-x plane, respectively for different diameters of obstruction having hydrophilic wettability (i.e., $\theta = 60°$). The investigation reveals that at r=30 lu the droplet is comparatively larger in size than that of the obstruction, which allows the droplet to completely overlap the obstruction and a large fraction of droplet fluid is deposited on the downward side of the obstruction. This deposition of the fluid

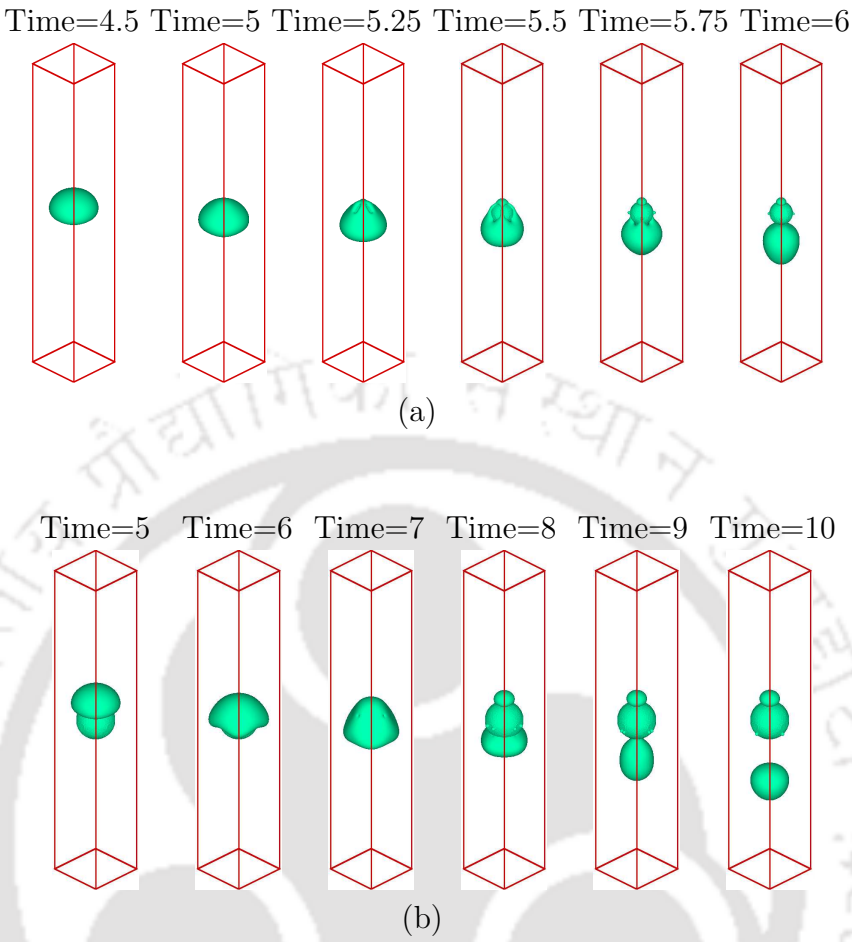

Figure 7.16: The isosurface plots of the time evolution of the droplet past a spherical obstruction at Ca=0.407, M=1 and $\theta = 120^{\circ}$ for spherical obstruction radius, (a) r=30 lu, (b) r=50 lu

is dragged by smaller adhesive force owing to low contact surface area. However, the deposited fluid elongates more in length because the gravitational force is larger than the surface adhesion force as shown in Figs. 7.13(a) and 7.14(a). As we increase the radius of obstruction, the contact surface area and hence, the magnitude of the surface adhesion force increases. As shown in Figs. 7.13(b) and 7.14(b), increasing radius of the obstruction also increases the volume of entrapped continuous phase fluid inside droplet fluid at the upper surface of the obstruction. As a result, the breakup of liquid film at the upper surface of the obstruction takes place rapidly.

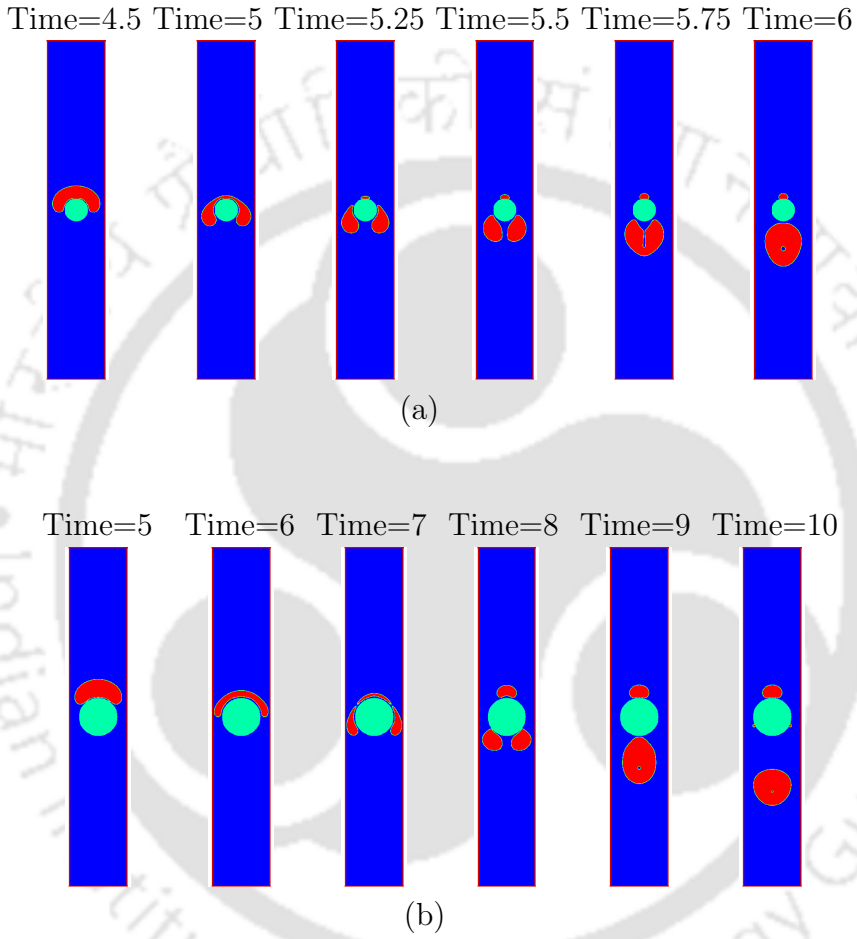

Figure 7.17: The $y-z$ sliced view (at midplane of x) of the time evolution of the droplet past a spherical obstruction at Ca=0.407, M=1 and $\theta = 120°$ for spherical obstruction radius, (a) r=30 lu, (b) r=50 lu

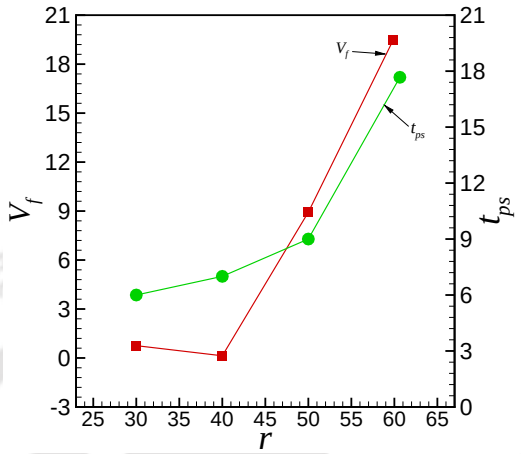

Figure 7.18: Effect of obstruction size (r) on passing time and fraction of deposited volume on the upper surface of obstruction at Ca=0.407 and $\theta = 120°$

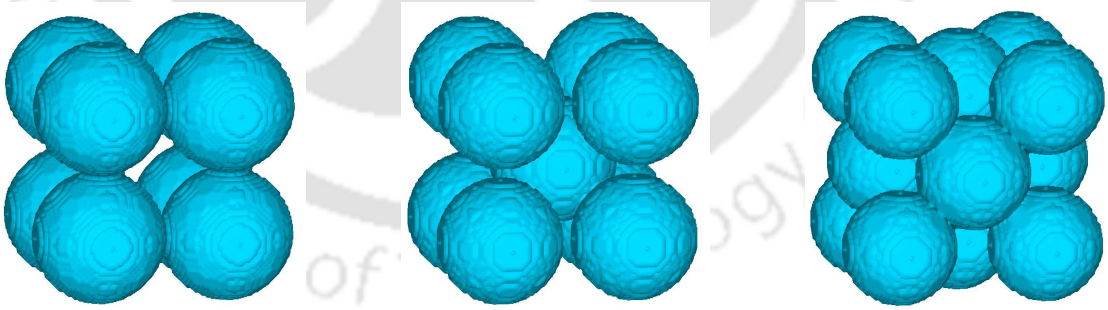

(a) (b) (c)

Figure 7.19: The different spherical obstruction arrangements (a) SC, (b) BCC, and (c) FCC

In the case of hydrophobic wettability i.e., $\theta = 120°$ as shown in Figs. 7.16 and 7.17, the obstruction with small radius (r=30 lu) provides less contact surface area to the droplet fluid. Moreover, the presence of gravity and hydrophobic wetting force allows the droplet fluid to quickly pass the obstruction compared to the case, where the radius of the obstruction is equal to 60 lu. When r=60 lu, the droplet makes contact with the large surface area of the obstruction. It is to be noted that the breaking of the droplet fluid at the upper surface of the obstruction occurs under the influence of curvature of the spherical obstruction. Owing to that the large surface area allows the droplet fluid to deposit more fluid on the upper surface of the obstruction in the case of r=60 lu (as compared to r=30 lu). It is also observed that the time taken by the bulk of the fluid to cross past the obstruction in the case of r=60 lu is more (Time=10) compared to the case of r=30 lu where the residence time is equal to 6. The effect of different obstruction radii on the deposited volume of the droplet fluid on the upper surface of the obstruction at Ca=0.407 and $\theta = 120°$ is also shown in Fig. 7.15. The deposition of fluid is found to be more at a higher radius compared to the lower radius of the obstruction. This might be due to the effect of the surface area of impact between droplet and obstruction. In the case of hydrophobic wettability, $\theta = 120°$, the deposition of the droplet fluid is greatly increased for r=50 lu and r=60 lu as shown in Fig. 7.18. The hydrophilic wetting case has already been shown in Fig. 7.15. Another parameter which is calculated for $\theta = 120°$ is the time duration for crossing past the obstacle with respect to obstruction radius. It is observed that as we increase the radius of the obstruction, the residence time also increases. It is noted that the passing time or residence time in case of r=60 lu is almost double as compared to the case with r=50 lu.

7.3.4 Effect of obstruction structure

The droplet dynamics past a solid obstruction strongly depend on the structure or arrangements of the obstruction particles. In the previous sections, a single spherical particle is considered as an obstruction in the path of droplet movement inside a confined channel. In this section, different spherical agglomerate structures are considered as obstruction architectures. These three agglomerate structures are known as simple cubic (SC), body centered cubic (BCC) and face centered cubic (FCC) structures as shown in Fig. 7.19. To keep the unit cell size same as in the case of single spherical particle, the radii of the spherical particles in SC, BCC and

FCC have been adjusted. The values of radii of spherical particles in SC, BCC and FCC are taken as 20 lu, 18 lu and 16 lu, respectively. It is important to mention here that the numbers of spherical particles in each arrangement are 8, 9 and 14 in SC, BCC and FCC, respectively. The obstruction of such type provides more restriction and viscous drag to the droplet compared to only one spherical particle obstruction.

Figures 7.20-7.21 illustrate the isosurface and sliced view plots of a droplet past an obstruction with different agglomerate structures (i.e., SC, BCC and FCC) at Ca=0.407 and $\theta = 120°$. Initially as discussed earlier, a droplet moves under gravity until it impacts on the obstruction and gets deformed slightly. Once it touches the obstruction, the structure of the obstruction plays a significant role in the deformation and breakup of the droplet. In the case of SC structure, there is space between eight spherical particles which is generally called as throat area. The droplet after colliding with obstruction completely covers the obstruction upper surface at Time=5.5 and lately due to the gravitational force and surface tension effect, the fluid film gets thinner. As time progresses, the gaps which are created between the spherical particles have been occupied by the droplet fluid and a small fraction of fluid remains attached on the top of the obstruction. The fraction of total volume remains attached on the surface of the spherical particles are found to be equal to 8.47%, 6.27% and 4.93% in SC, BCC and FCC structures, respectively. This shows that although the total number of particles is more in the FCC structure the fraction of droplet volume captured by it is less compared to SC and BCC structures.

In the case of hydrophilic wetting (i.e., $\theta = 60°$) of solid spherical particles of different structures as shown in Figs. 7.22-7.23, the droplet fluid makes a strong bond with the obstruction surface and tries to wet the complete surface area of the obstruction. However, it is observed that in SC structure obstruction, the droplet fluid at the top centre of the obstruction gets entrapped due to the presence of a throat area as shown in Fig. 7.22(a) and 7.23(a). However, in BCC and FCC structures, the droplet films break at the top surface of the obstruction owing to the presence of solid particles at the middle and upper side of the obstructions as shown in Figs. 7.22(b-c) and 7.23(b-c). In later stages when the droplet fluid elongates on the sides of the obstruction, gets entrapped in the gaps generated between solid particles in all three structures. It is also found that hydrophilic surface of the

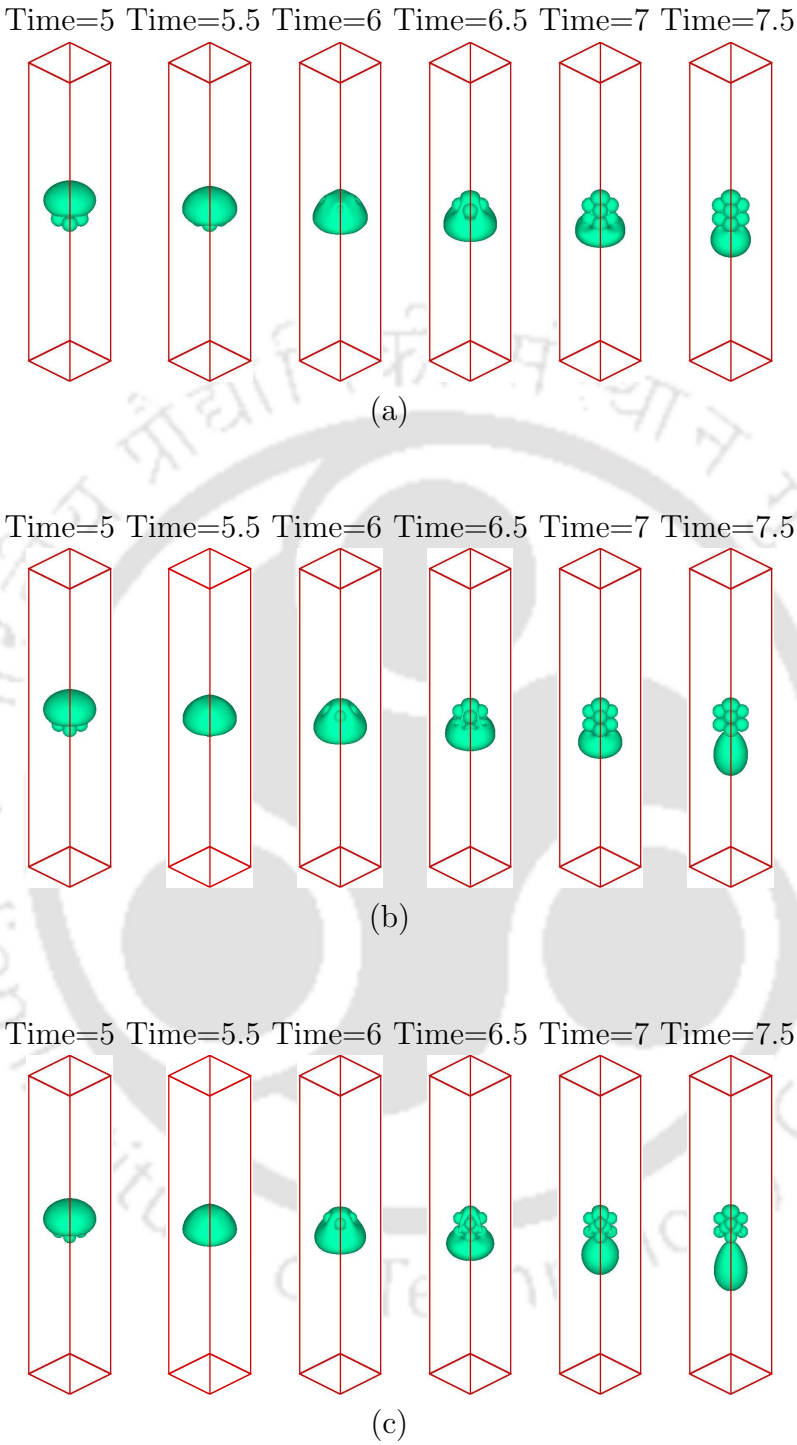

Figure 7.20: The isosurface plots of the time evolution of the droplet past an obstruction at Ca=0.407, M=1 and $\theta = 120^{\circ}$ for spherical obstruction structure, (a) SC, (b) BCC, and (c) FCC

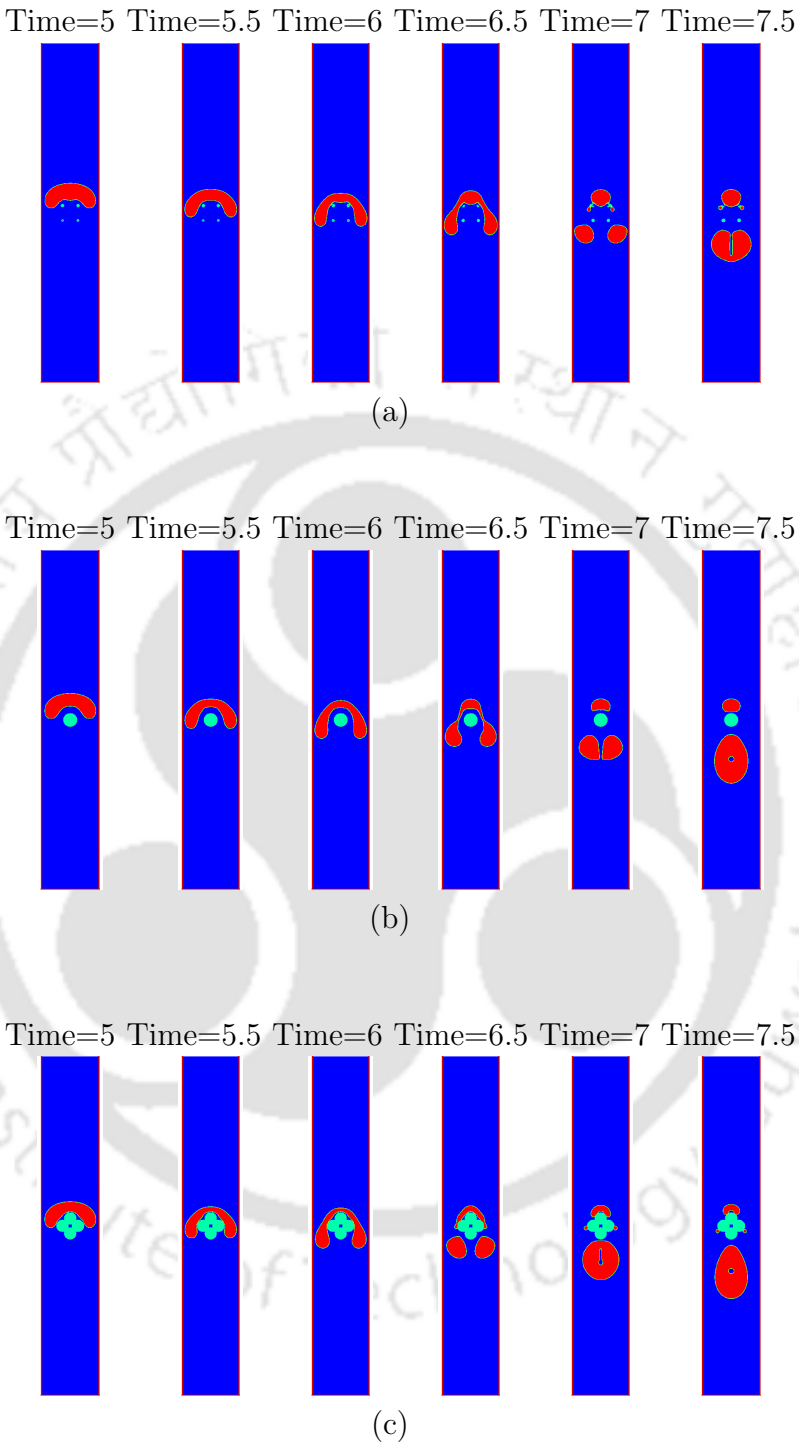

Figure 7.21: The $y-z$ sliced view (at midplane of x) of the time evolution of the droplet past an obstruction at Ca=0.407, M=1 and $\theta = 120°$ for spherical obstruction structure, (a) SC, (b) BCC, and (c) FCC

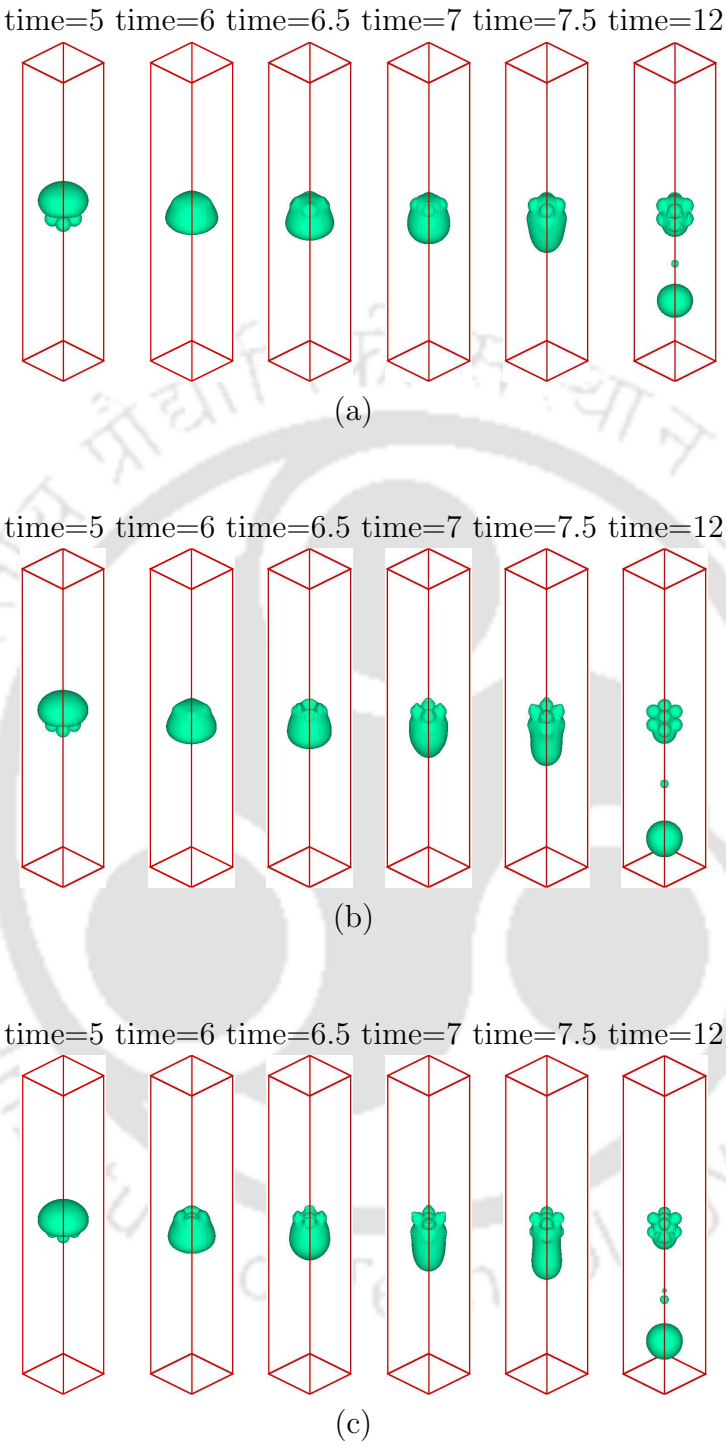

Figure 7.22: The isosurface plots of the time evolution of the droplet past an obstruction at Ca=0.407, M=1 and $\theta = 60^{\circ}$ for spherical obstruction structure, (a) SC, (b) BCC, and (c) FCC

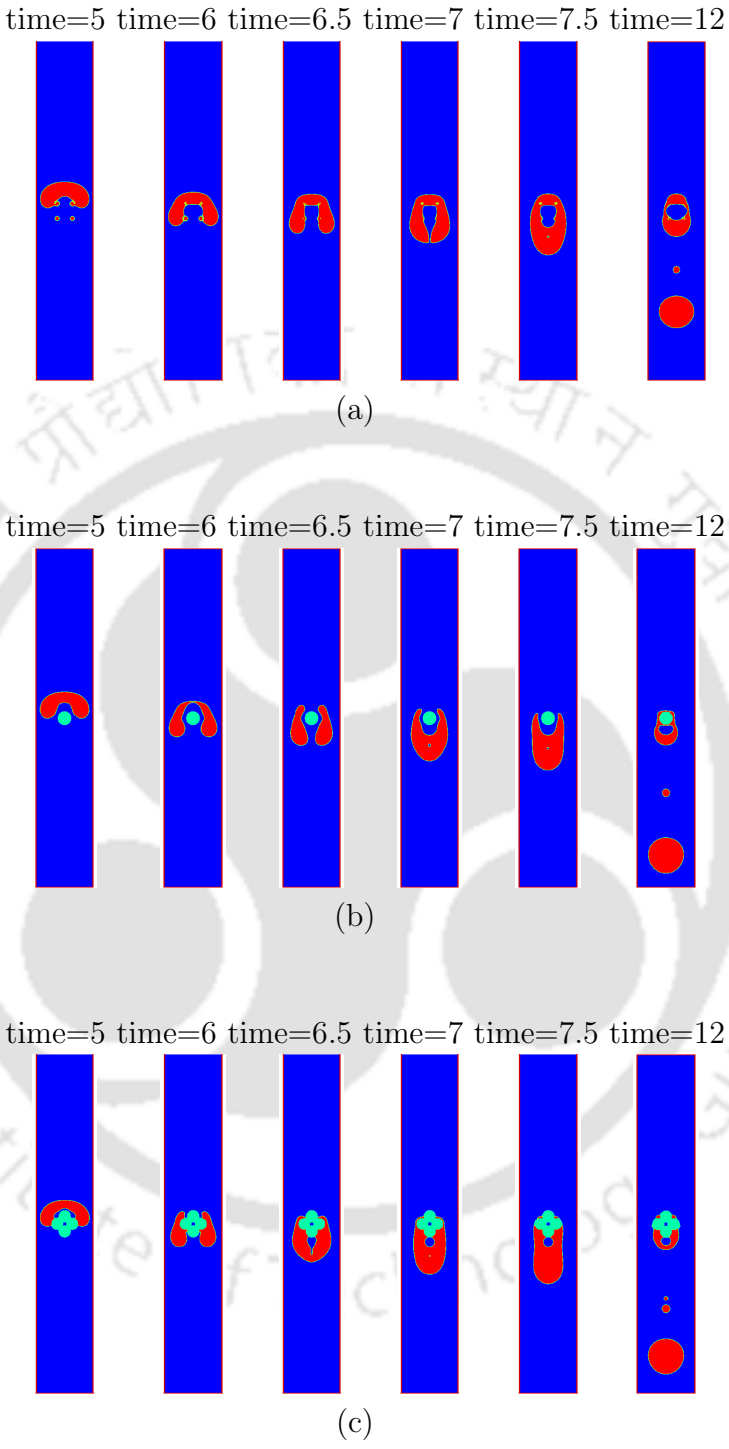

Figure 7.23: The $y-z$ sliced view (at mid-plane of x) of the time evolution of the droplet past an obstruction at Ca=0.407, M=1 and $\theta = 60°$ for spherical obstruction structure, (a) SC, (b) BCC, and (c) FCC

obstructions tries to hold the droplet fluid at the downward side of the obstruction and the combined effect of gravity and inertia tries to elongate the droplet fluid further which triggers the detachment of droplet from the obstruction surface. For a better understanding of the deposition of the droplet fluid on the obstruction surface, the fraction of deposited volume has been measured and it is found to be equal to 22.65%, 16.12% and 15.50% for SC, BCC and FCC structures, respectively. By this analysis, it is further observed that the deposition of droplet fluid in the case of the hydrophilic wetting surface of the SC type obstruction is 167% more than the hydrophobically wetted SC obstruction.

7.4 Summary

This study presented droplet dynamics due to the capillarity-wettability interaction through a partially obstructed pore channel confinement based on a mesoscopic, two-phase lattice Boltzmann model. To explore the dynamic behaviour of droplet motion past an obstruction with or without pores, the effect of capillary number and surface wettability, including obstruction size and architecture, were elucidated. In this work, single spherical obstruction, and different spherical porous agglomerate structures were considered. The mesoscale simulations exhibit interesting two-phase flow physics and pattern formations due to droplet pinching, break up, and surface adherence owing to the underlying wettability-capillarity characteristics. This study further reveals an interesting trade-off, between the time required for the bulk droplet fluid to pass by and/or through the obstruction and the fraction of droplet fluid volume adhering to the surface, depending on the combination of the capillary number and surface wettability.

Chapter 8

Mesoscopic Pore-Scale Study of Fluid Flow Through Porous Medium

8.1 Introduction

An understanding of porous media flows is important because it is found everywhere in nature, in technology and in daily life. A general definition of a porous material or medium can be defined as a material or structure which is having spaces or so-called voids or pores and also it must be permeable to a variety of fluids. The skeletal portion of the material is often called the matrix or frame. The pores are typically filled with a fluid (liquid or gas). In a natural porous medium (e.g. beach sand, sandstone, limestone, wood etc) the distribution of pores with respect to shape and size is irregular. A porous medium is most often characterized by its porosity. The porosity of a porous medium is defined as the fraction of the total volume of the medium that is occupied by void space. Other properties of the medium (e.g., permeability, tensile strength, electrical conductivity) can sometimes be derived from the respective properties of its constituents (solid matrix and fluid). The flow in porous media can be characterized on two bases, i.e., either as a flow-through (inside) very small and complex conduits or as a flow around many and random obstacles. It is important to note that the former approach is more

suited for low porosities, while, the latter is more appropriate for porous media with high porosities. The application areas, where fluid flow in porous media can be found specifically, are hydrocarbon production, catalysis, groundwater flow, or the gas diffusion layers in fuel cells, Oil and gas transport in porous rock, and permeation of ink on paper. Most of these examples involve not only single-phase flows but multiple phases or fluid components. As such, a thorough understanding of the underlying physical processes by means of computer simulations requires accurate and reliable numerical tools. The immiscible flow of multiple-phase fluids through porous media, as compared with single-phase flow, is much more complicated and is still not well understood in many areas due to the complex interactions of different fluid phases in porous media.

8.2 Problem specification

In the present problem, the two immiscible fluid flow through a porous media is considered for the analysis to explore the physics associated with a complex porous domain. To conduct the numerical simulation of immiscible, two-phase transport through the porous structure, Fig. 8.1 depicts the computational domain and setup of the displacement simulation generally known as primary drainage experiment. To provide continuous flow through the domain, a non-wetting phase (NWP) reservoir is provided to the porous structure at the inlet side (i.e., x=0) and a wetting phase (WP) reservoir is added at the outlet side (i.e., $x = lx$) [80, 85]. In the present primary drainage (PD) simulation, it is to be noted that the NWP liquid is denoted as fluid 2 and WP liquid is denoted as fluid 1. The fluid flow in the domain is achieved by imposing the fixed pressure boundary conditions, which are equivalent to fixed densities in LB modelling. This fixed pressure boundary condition is applied to the first layer of the NWP reservoir and the last layer of the WP reservoir. From the modelling point of view, the fixed pressure boundary conditions are implemented by assigning the equilibrium distribution functions to the distribution functions; the equilibrium distribution functions are computed with specified density and zero velocity at the reservoirs. In the other two directions, the periodic boundary conditions are applied. To get a no-slip boundary condition on all solid walls, a particle distribution function bounce-back scheme [104] is used. The primary drainage process is simulated starting with zero capillary pressure which is achieved by fixing

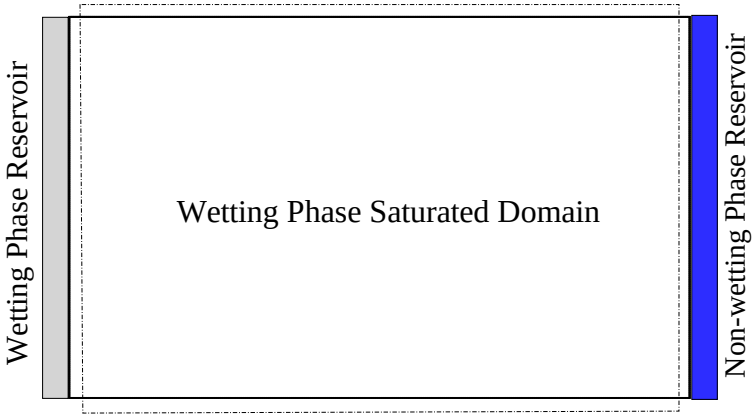

Figure 8.1: Schematic diagram of immiscible two-fluid displacement experiment setup

the NWP and WP reservoir pressures to be equal. Then the capillary pressure is increased gradually by decreasing the WP reservoir pressure while maintaining the NWP reservoir pressure at the fixed initial value. The pressure gradient drives NWP liquid into the initially saturated porous medium by displacing it. It should be noted that a lattice site is assumed occupied by the NWP if the NWP density at that node is larger than half of the fixed NWP density; otherwise, the node is assumed to be occupied by the WP.

For the simulation, a three-dimensional channel is considered which is having solid spherical particles as porous structure as shown in Fig. 8.2. The size of the domain is considered as 325 lu, 200 lu and 200 lu in x-, y- and z-directions, respectively. It is to be noted that all the solid walls are considered to be wetted and three different wetting conditions are taken for the study. The three different wetting conditions which are considered for the study are uniform hydrophobic, $g_{2w} = 0.05$ ($\theta = 118°$), uniform hydrophilic, $g_{2w} = -0.05$ ($\theta = 60°$) and mixed wettability, $g_{2w} = \pm 0.05$. The initial densities of fluid 1 and fluid 2 at inlet are taken as 10^{-5} and 150 whereas the densities of fluid 1 and fluid 2 at outlet are 150 and 10^{-5}, respectively. The relaxation parameters for fluid 1 (WP) and fluid 2 (NWP) are considered to be equal to 1 and 1.42 which gives a dynamic viscosity ratio approximately equal to 2. An idealized porous medium is generated inside the domain which consists of equal diameter spherical particles of radius equal to 20 lu as shown in Fig. 8.2. The structure and volume of the pores between the spherical

particles can be seen in Fig. 8.3.

8.3 Results and discussion

In the present study, a straight three dimensional channel is considered to simulate the two immiscible fluid liquid transport through porous structure with the effect of different porosity, wettability of the solid surfaces and the pressure gradient. It should be noted that the structure of porous media is important here because in place of reconstructed randomly distributed porous media, we have considered here a systematic sphere pack porous medium which creates capillary tubes like pores as shown in Fig. 8.3. The primary aim of the present study is to explore the methodology and physics of the capillary pressure behavior as a function of NWP liquid saturation in the pore structure. For such a complex problem, it is very difficult to correctly capture the physics associated with the fluid flow through porous medium. Therefore, in order to simulate efficiently such a complex problem, a large number of lattice points are considered. Another difficulty lies in the handling of such a large number of lattice points computationally.

8.3.1 Effect of wettability on liquid transport

In this section, the effect of different wettability on the NWP liquid transport in primary drainage experiment through sphere pack porous medium is studied. The wettability means the characteristic of the solid surface to allow the fluid to spread or contract on it. In context to porous medium, wettability plays an important role because the fluid has to pass through the pore surface which is having strong influence of wetting conditions and thus, influences the fluid front movement [105]. In the present analysis, three different wetting conditions are considered; hydrophobic, hydrophilic and mixed-wettability.

Figures 8.4-8.5 illustrate the three-dimensional isosurface contour plots and two-dimensional cross-sectional view of saturation fluid front invasion patterns of non-wetting phase (NWP) for porosity, $\phi = 0.48$ and hydrophobic wettability, $g_{2w} = 0.05$ ($\theta = 118^{\circ}$) of the pore surface at different timesteps. It should be noted that in cross-sectional view, the sharp interfaces between two fluids or between fluid and solid have

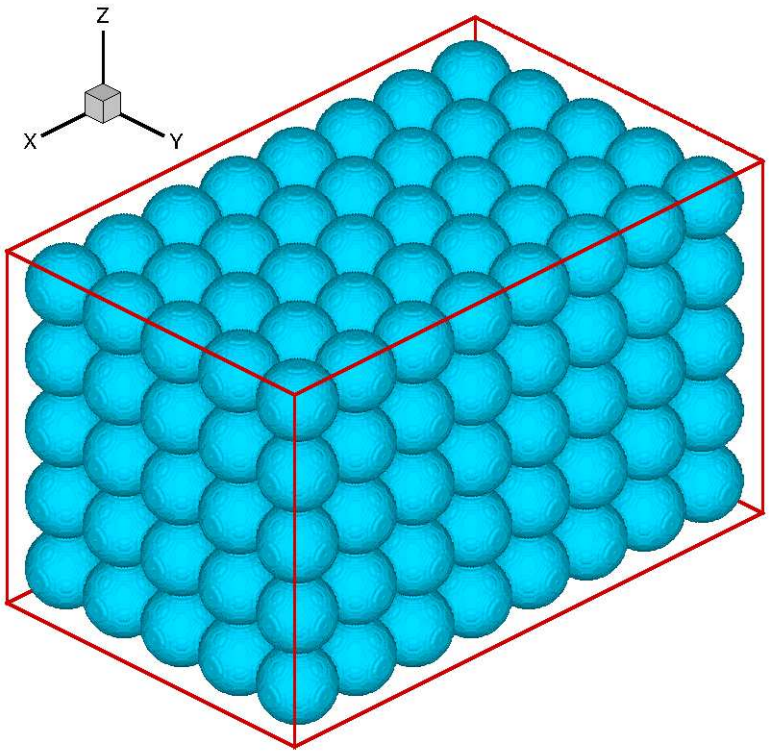

(a)

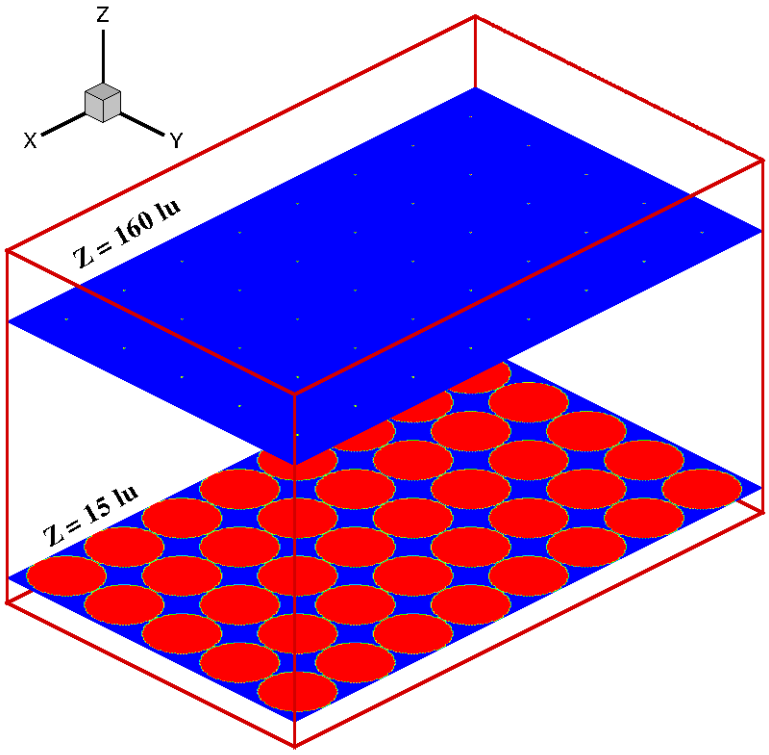

(b)

Figure 8.2: Schematic computational domain, (a) isosurface view, (b) cross-sectional view.

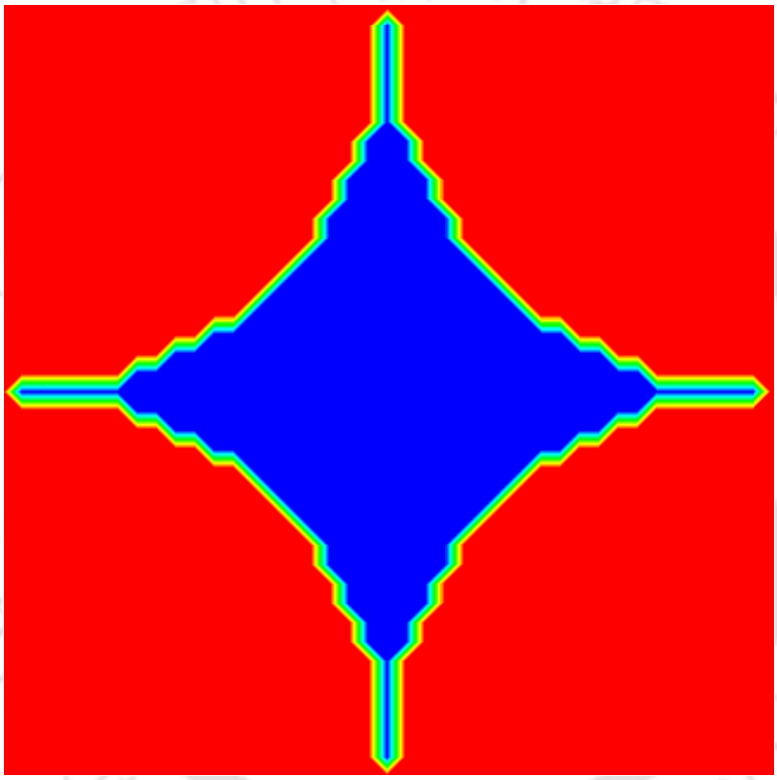

Figure 8.3: The structure of the pore created between spherical particles

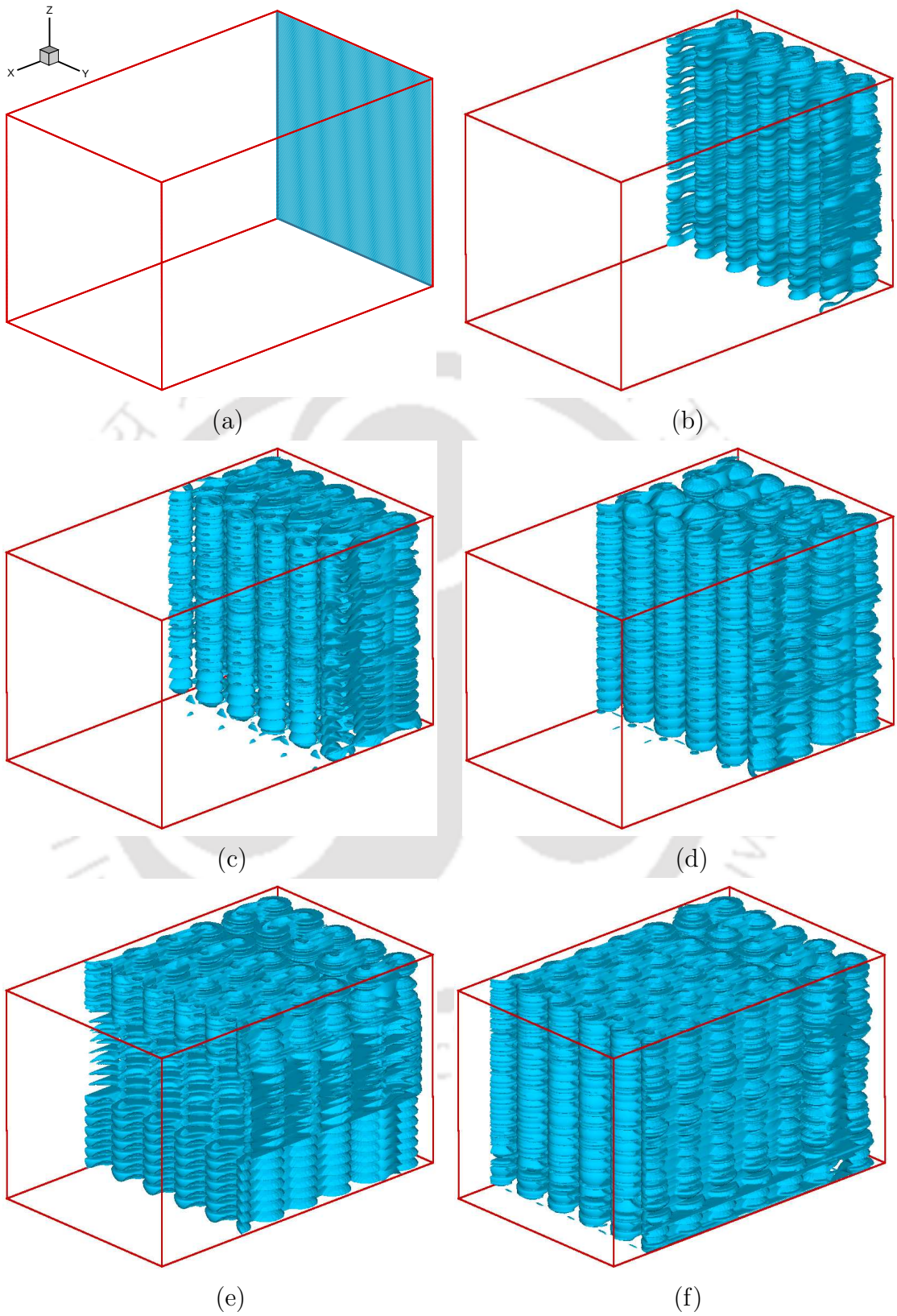

Figure 8.4: Advancement of the liquid front through the initially saturated porous medium with increasing capillary pressure at porosity, $\phi = 0.48$ and hydrophobic wettability, $g_{2w} = 0.05$

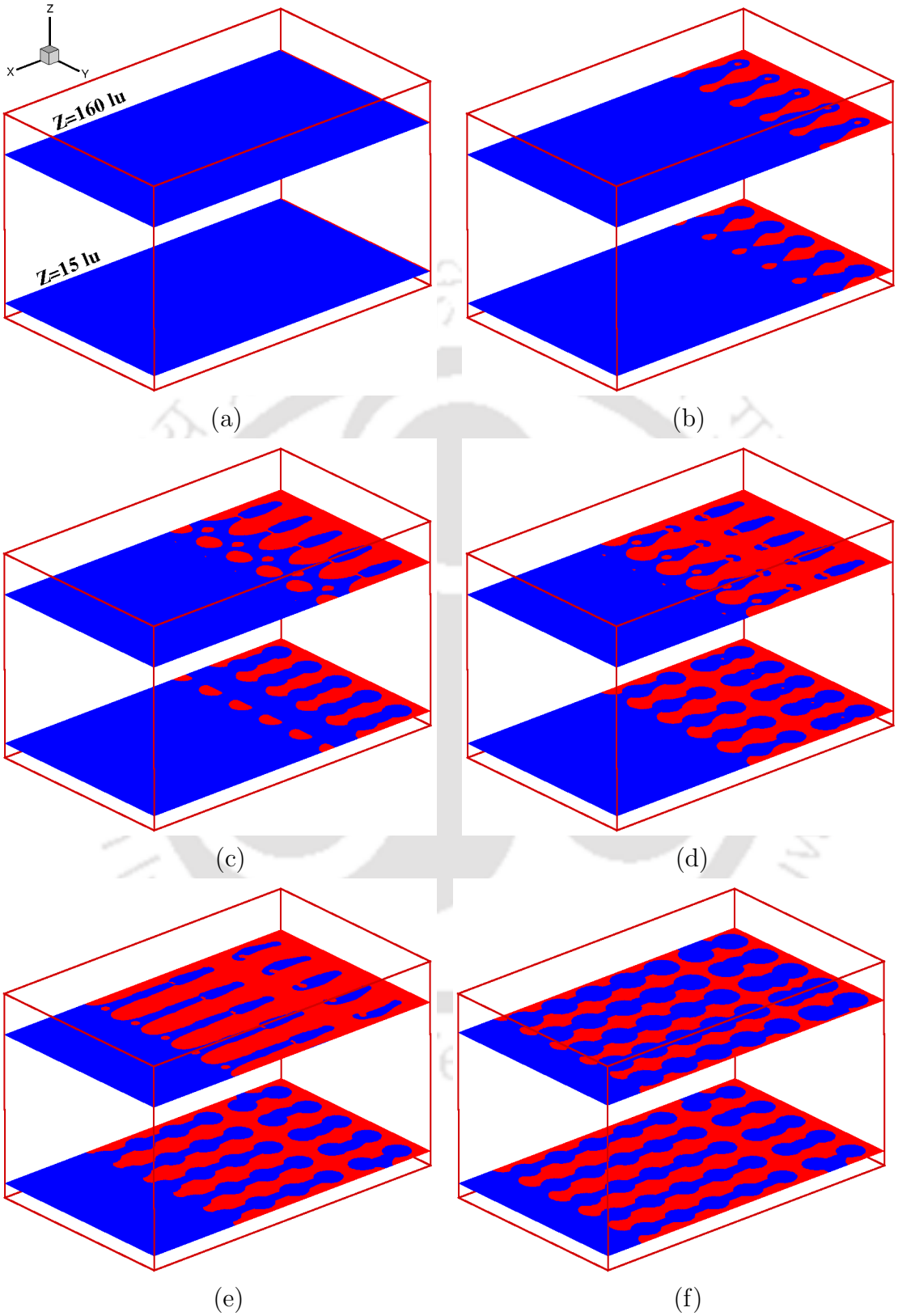

Figure 8.5: Two-dimensional cross-sectional view of advancement of liquid front for porosity, $\phi = 0.48$ and hydrophobic wettability, $g_{2w} = 0.05$

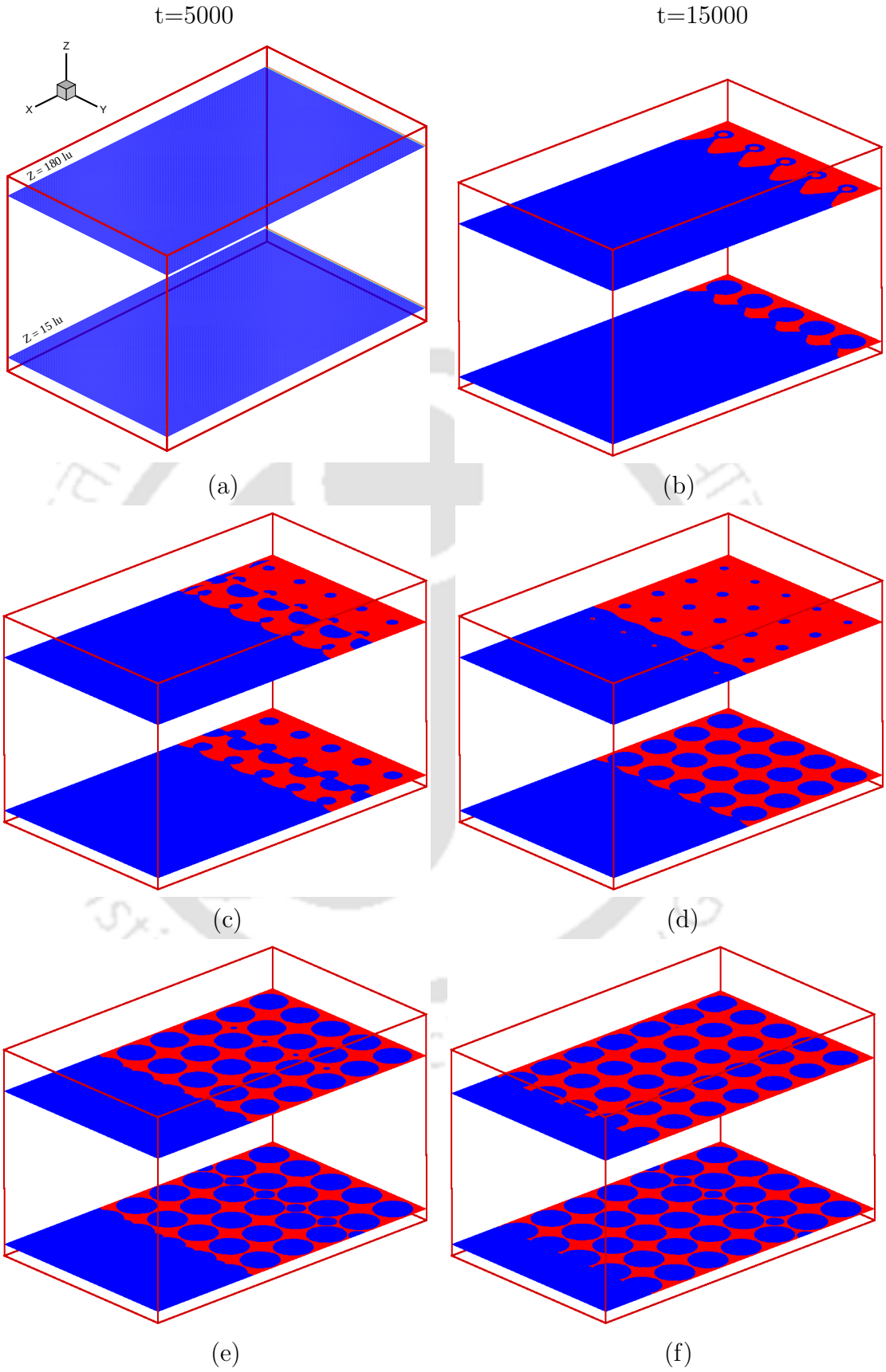

Figure 8.6: Two-dimensional cross-sectional view of advancement of liquid front at porosity, $\phi = 0.48$ and hydrophilic wettability, $g_{2w} = -0.05$

been shown for the sake of proper understanding but in reality, as Shan-Chen LBM is used for incorporating the multiphase-multicomponent effect in present analysis, the interface between two fluid or between solid-fluid is diffuse with finite width. As shown in Fig. 8.4, at initial timesteps when the capillary pressure is low, the invading liquid shows a finger like pattern. The wetting fluid i.e., air, is already occupying the space available in the pores. As the pore surface is hydrophobic wetted, the NWP liquid penetrates into the pore area and try to displace the WP air due to the surface tension force. As time increases, these finger like invading fluid penetrates deep inside the pores and shows a flat and stable advancing front with increasing capillary pressure. In Fig. 8.5, two cross-sectional views have been taken in z-direction at $z = 15$ lu & $z = 160$ lu as shown in Fig. 8.2 also. These cross-sectional views have been taken to show the behavior of invading liquid transport at two different location. It can be seen from cross-sectional view that the liquid penetrates inside the pores in the form of fingers and its front moves parallelly in the whole domain. This may be due to the combined effect of hydrophobic wettability-capillarity force. As the pore surface is non-wetting, it does not allow the liquid to spread over it and block the path of further invading fluid. However, in case of hydrophilic wettability of the pore surface, the invading liquid drain-out the WP fluid which occupies the volume of the pores and starts spreading over the pore surfaces as shown in Fig. 8.6. This spreading of the NWP liquid on the pore surface blocks the path of the further invading fluid and the fluid moves in forward direction bit slowly compared to hydrophobic wet pores. Figure 8.7 depicts the effect of wettability on the liquid saturation against normalized time. The time is being normalized to provide a consistency in liquid transport time for different simulation cases for different parameters. Here, it is clearly visible that the liquid saturation is more in less time for the case of hydrophilic wetting compared to hydrophobic case. It is interesting to note that in case of mixed wettability, the saturation curve falls between hydrophobic and hydrophilic case. This is due to the fact that as explained earlier mixed wetting is the combination of hydrophobic and hydrophilic wettability of the solid spherical particles in the domain which signifies that half of the pore surfaces are hydrophobically wet and other half are hydrophilically wet.

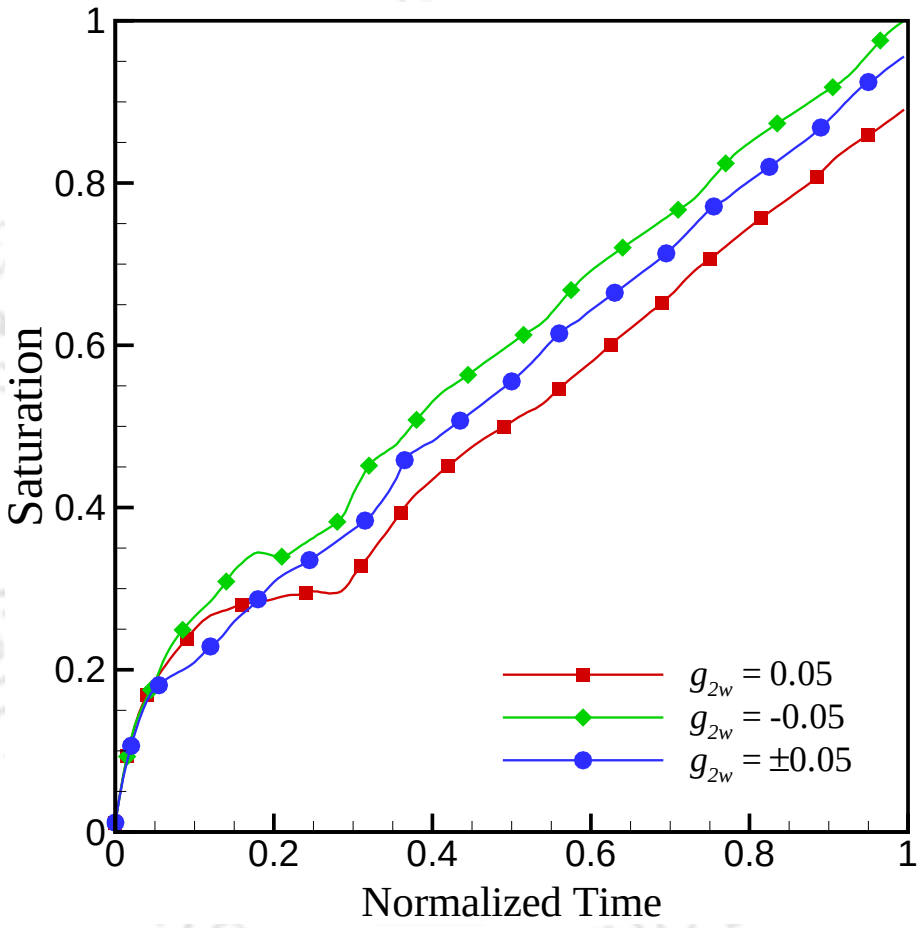

Figure 8.7: Effect of wettability on the liquid transport

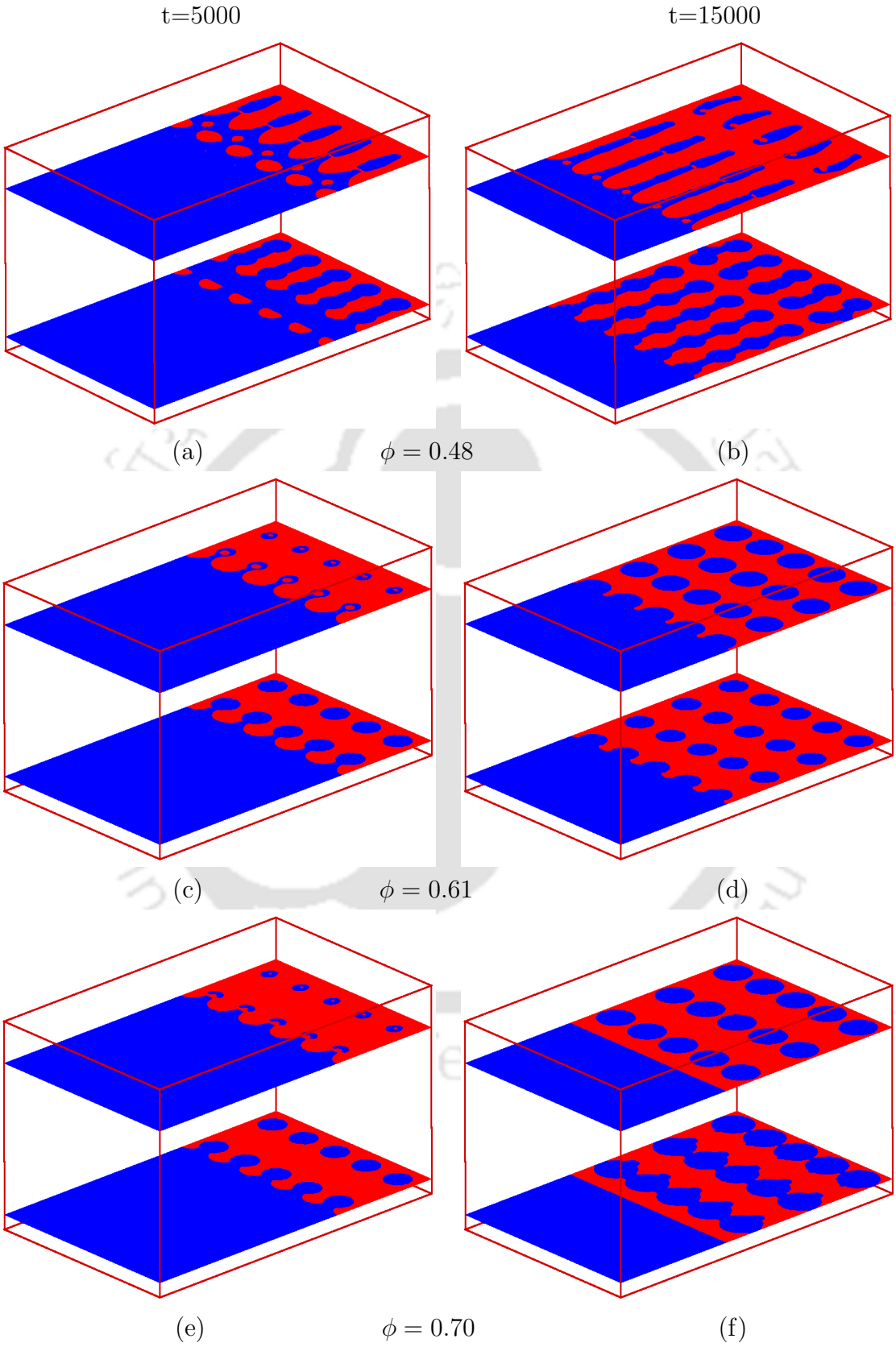

Figure 8.8: Two-dimensional cross-sectional view of advancement of liquid front at different porosity for NWP density equal to 150 and hydrophobic wettability, $g_{2w} = 0.05$

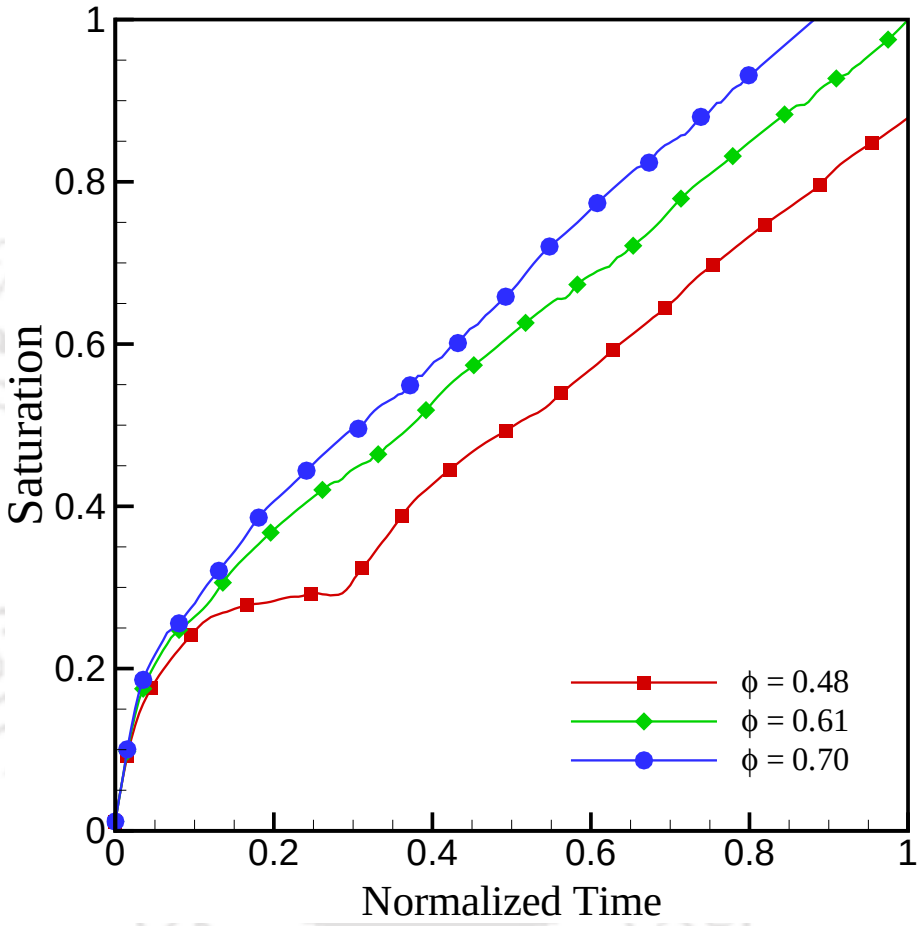

Figure 8.9: Effect of porosity on the liquid transport for hydrophobic wettability, g_{2w}=0.05

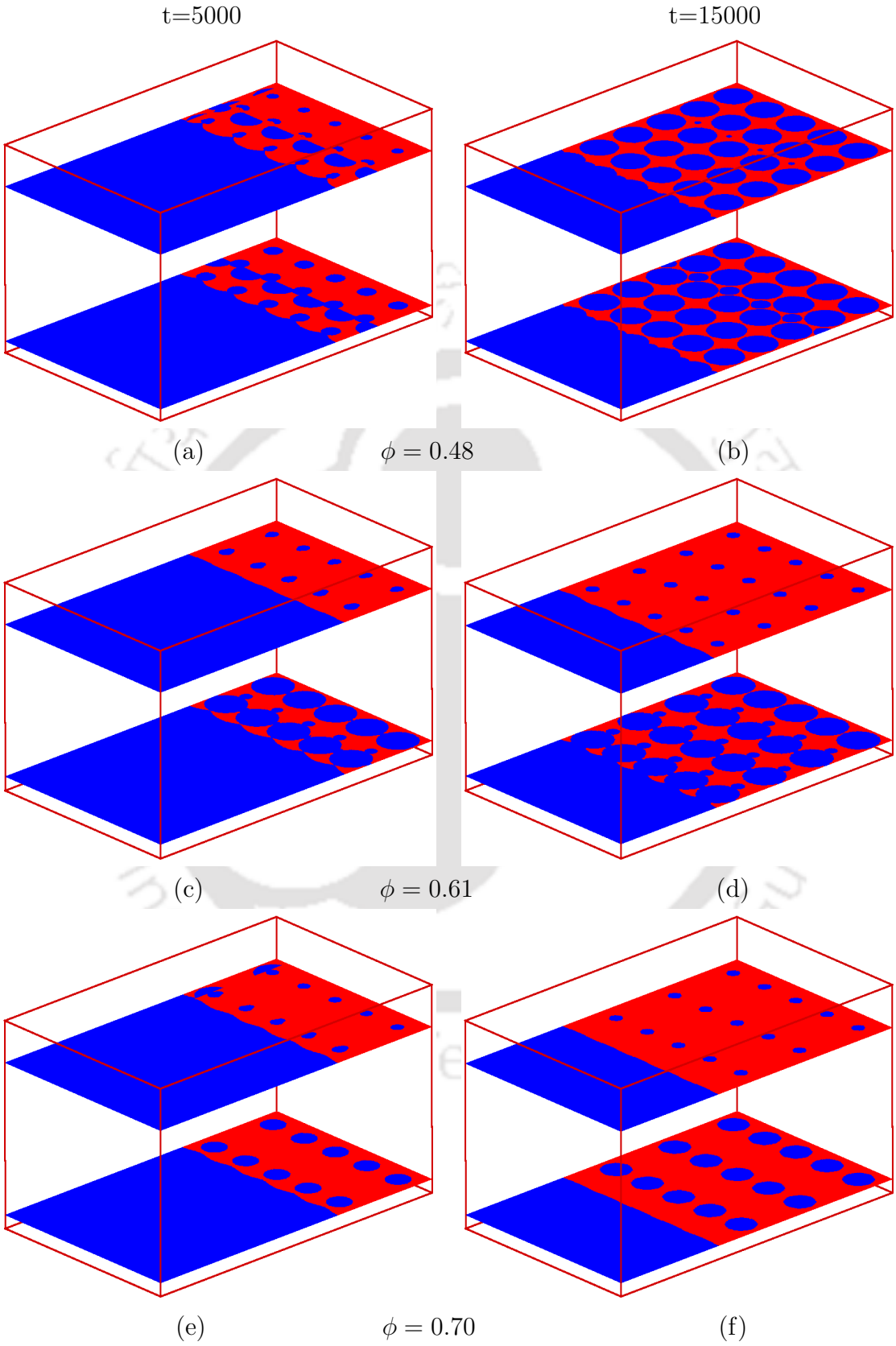

Figure 8.10: Two-dimensional cross-sectional view of advancement of liquid front at different porosity for NWP density equal to 150 and hydrophilic wettability, g_{2w}=-0.05

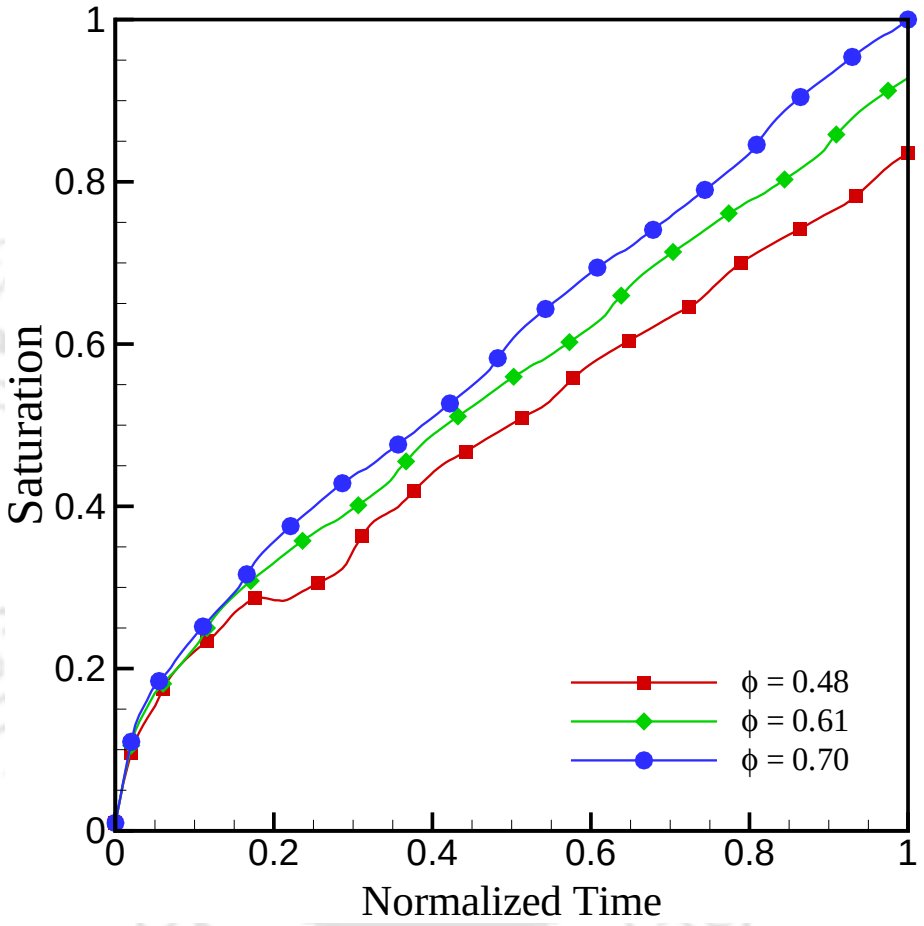

Figure 8.11: Effect of porosity on the liquid transport for hydrophilic wettability, g_{2w}=-0.05

8.3.2 Effect of porosity on liquid transport

Porosity being an important parameter of any porous structure forms the basis of a necessary analysis of fluid flow through porous medium. It is defined as the space or gap generated between the solid structure. Quantitatively, porosity can be represented as the ratio of the pore volume to the total volume (bulk volume) of a porous domain. It should be noted that transportation of fluids is controlled mainly by these connected pores in the domain. The porosity of a rock or any other porous medium depends on many factors, including the arrangement of rock grains and the type of a rock. For the better understanding of porosity, it can be described with an example of granite which is a crystalline rock has a very low porosity ($< 1\%$) since the only pore spaces are the tiny, long, thin cracks between the individual mineral grains. Sandstones, typically, have much higher porosities (10-35%) because the individual sand or mineral grains do not fit together closely, allowing larger pore spaces. In the present study, three cases with porosity, ϕ= 0.48, 0.61 and 0.7 have been studied to show the effect of porosity on the liquid transport in porous domain.

Figure 8.8 shows the cross-sectional views of advancement of liquid front at timestep equal to 5000 and 15000 for the contact angle, $\theta = 118°$. It is found in the analysis that the liquid front movement is faster and the more saturation achieved in the shorter time for higher porosity. It is due to the fact that the large value of porosity provides more passage to the NWP liquid to flow owing to the fact that the resistance to the flow decreases as the value of porosity increases. It is also observed that in case of porosity ϕ= 0.48 for contact angle $\theta = 118°$, the advancement of NWP liquid is in the form of liquid fingering throughout the domain. However, a stable liquid front advancement is achieved for large values of porosity. The liquid saturation for different porosities at hydrophobically wetted ($\theta = 118°$) pore surfaces is illustrated in Fig. 8.9. From the figure, it can be clearly observed that as porosity increases, the liquid saturation also increases and also it takes less time to achieve complete saturation in case of large porosity.

It is interesting to see the effects of porosity on NWP fluid front advancement and saturation for hydrophilic wetted ($\theta = 60°$) pore surfaces. Figures 8.10-8.11 illustrate that in case of hydrophilic wetted pore surfaces, the advancement of NWP liquid is not like fingers but it behaves like a stable fluid movement at low porosity

which is entirely different from the case of hydrophobic wetted pores. It is also observed that as porosity increases, the NWP fluid try to completely wet the pore surface and flush out the WP liquid completely from the pores. The fluid front, in the case of hydrophobic wetted pores, while passing through the pores, first generates a small finger but later moves as a stable flow. However, in hydrophilic wetted pores case, no finger-like structure is observed even for higher values of porosity.

8.4 Effect of pressure gradient on liquid transport

The liquid transport in the present analysis is achieved by providing a pressure gradient in terms of density difference. In previous sections, the density of NWP liquid inlet density is taken equal to 150 and investigations have been performed. However, it is possible to change the pressure gradient keeping all other parameters fixed by changing the NWP liquid inlet density and analyze the behaviour of liquid transport. In the present section, three different values of inlet density of NWP liquid are considered and taken equal to 150, 200 and 250. As it is understood that increasing the inlet density of NWP liquid, keeping the outlet density of NWP liquid fixed in addition to the same value of WP liquid density, increases the driving force of NWP liquid. For the present analysis, the wettability of the pore surface is considered to be hydrophobic ($\theta = 118^{\circ}$) and porosity, ϕ= 0.48. The analysis shows that the NWP liquid front advances more quickly as pressure gradient increases owing to increased driving force. Figure 8.12 depicts that as time increases, the liquid front moves quickly towards the outlet as well as the NWP saturation in the pores increases. As the density of NWP liquid increases from 150 to 250 with an intermediate value of 200, it is observed that the saturation of pores with NWP liquid increases quickly and more saturation is achieved.

8.5 Summary

In the present study, an immiscible fluid flow and liquid transport inside a sphere packed porous domain are analyzed for various physicochemical conditions. The investigation is aimed to explore the physics associated with the displacement of NWP fluid draining out the WP fluid initially saturating the pores. The effects of different pore surface wettability, porosity and pressure gradient have been studied

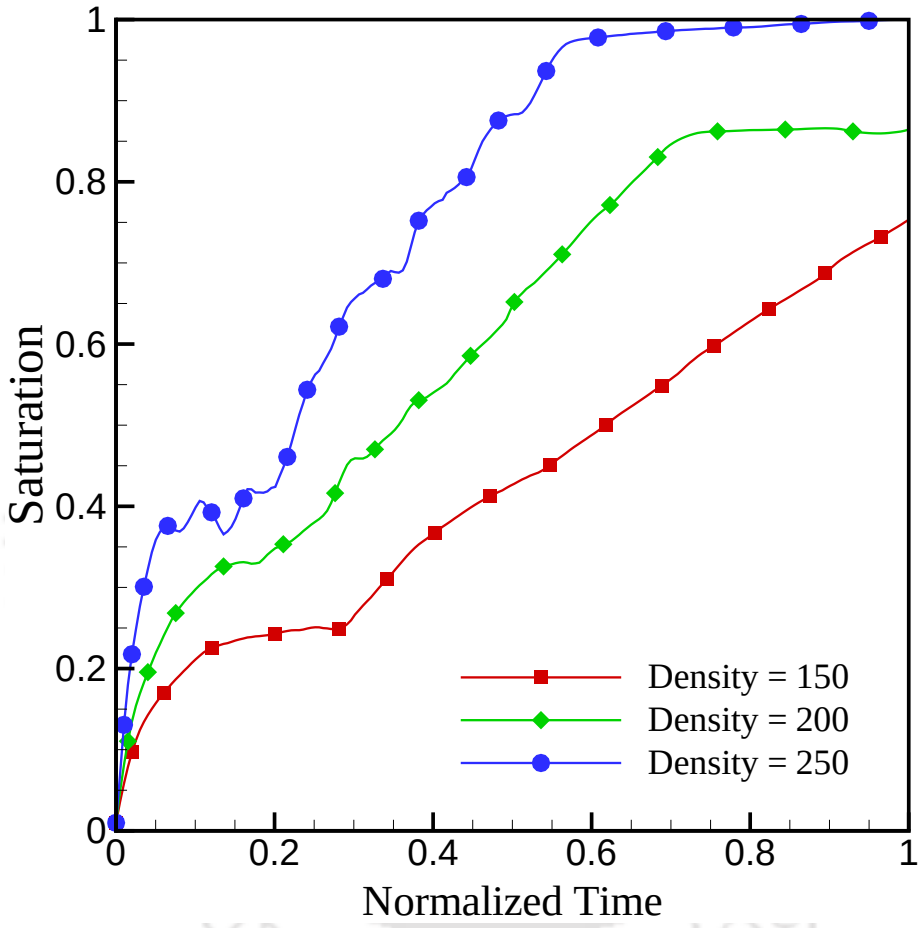

Figure 8.12: Effect of pressure gradient on the liquid transport for hydrophobic wettability, g_{2w}=0.05

on fluid flow behaviour. The study reveals that the fluid saturation is more for high values of porosity and for hydrophilic wettability of the pore surface. It is also observed that the fluid saturation and fluid front advancement is more for large pressure gradients.

Chapter 9

Conclusions and Scope of Future Work

9.1 Conclusions

The present thesis deals with the immiscible fluid flow dynamics in confinements and porous media flows considering surface wettabilities using S-C lattice Boltzmann method. The present numerical work is conducted with the goal of understanding the behaviour of the interaction of two immiscible liquids inside a three-dimensional channel. In literature, a large amount of work has been dedicated to the understanding of a droplet displacement and spreading in a confined channel as well as immiscible fluid flow through porous media. The formulation and capabilities of the LBM and Shan-Chen model have been discussed in details and found to be a promising tool for analyzing immiscible fluid flow dynamics. The validation of the present code is found to be in a good agreement with the available literature. The present thesis, in particular, presents the detailed insight of the capillarity-wettability interactions on droplet displacement and spreading on the channel walls and immiscible fluid flow through sphere pack porous media.

Firstly, an attempt has been made to explore the physics of two droplet coalescence on a wetted channel wall. A numerical analysis has been carried out to investigate the implications of the dynamic behaviour of the coalescence of two droplets placed on a rectangular channel wall considering wetting effects. In order

to asses the effects of centre distance between the droplets ranging from 47 lu to 55 lu on the displacement in the form of wetted area and wetted length, a study has been performed to analyze the time taken by two droplets to merge into a single droplet. Three capillary numbers i.e., Ca=0.35, 0.50 and 0.81 have been considered for the present study. It is noteworthy to mention that the time of coalescence of droplets is sometimes a major factor in several engineering and nature applications. In the present study, it is revealed that the type of wettability plays a crucial role in the coalescence of two droplets in a channel wall. In addition to this, it is also noticed that the two droplets coalesce more quickly in case of mixed wettability compared to uniform hydrophilic wettability for a certain capillary number. This is due to the fact that the alternately placed hydrophobic and hydrophilic nature of the surface leads to elongation of the droplet, especially when it travels in between these surfaces. Here, it is found that the wetted length and area keep changing with time between maximum and minimum values. In addition to that, an interesting feature has been observed. The increase in capillary number increases the time taken by the droplets to start merging in mixed wettability case. Another investigation which is carried out is to examine the effect of centre distance between droplets and concluded that an increase in centre distance increases the time of coalescence.

Next, a parametric study has been conducted to analyze the dynamic droplet behaviour on a wetted flat as well as a grooved wall of a rectangular microchannel. The main focus is to investigate the effect of viscosity ratio and wettability-capillarity interaction on droplet displacement under gravitational acceleration. Two wetting conditions, i.e., hydrophobic and hydrophilic, are considered for the study. It is observed that in case of a flat vertical wall, as the viscosity ratio increases, the displacement of a droplet on the hydrophobic surface becomes faster and more deformation of the droplet occurs, and finally droplet gets detached from the wall. It is also found that the wetted area and the wetted length on hydrophobic surface decrease monotonically with time. A reverse effect is observed in the case of the hydrophilic wall surface. As the viscosity ratio increases from 0.7 to 1.0, more spreading of the droplet on the wall surface and an increase in wetted area and wetted length are observed. In addition to that, the investigation shows that as the capillary number increases, the displacement of a droplet on the surface is much faster than the low capillary number. The presence of the groove on the vertical wall does not affect the dynamic droplet displacement in the case of the hydropho-

bic nature of the surface as the droplet gets detached before reaching the groove. However, the fraction of droplet liquid gets entrapped into the groove in case of the hydrophilic surface. It is found that the height of the groove affects the dynamic behaviour of the droplet greatly. It is observed from the present study that there is a lower limit on viscosity ratio, i.e., $M = 0.7$ below which this model does not work well and give an erroneous and unphysical result.

Then the numerical simulations are carried out to investigate the effect of surface roughness in terms of a groove on the droplet displacement. A rectangular channel is considered for the study in which grooves have been created on one of the channel walls on which droplet moves under the action of gravity. The periodic boundary has been considered in z-direction and bounce back scheme is used for all solid walls. The two different cases i.e., single groove on the wall and two grooves on the wall, are considered wherein single groove case, the location of the groove is also varied. In this investigation, it is revealed that the wettability of the groove plays a major role in the displacement and entrapment of the droplet fluid in the groove. Among the three different wetting conditions of the groove, the hydrophilic wettability of the groove allows more droplet fluid to entrap inside the groove due to more adhesion. It is further observed that the location of the groove also affects the entrapment of the droplet fluid inside the groove. In this study, the groove located on the upper side of the domain entraps more fluid compared to the groove created on the middle and lower side of the domain. In case of the hydrophilic groove, the % fraction of the entrapped fluid is about 10.96%, 8.17% and 7.17% in upper, middle and lower groove, respectively. In case of two grooves on the wall, the lower groove does not allow the droplet to entrap more inside the upper groove but the entrapment of fluid in the two grooves collectively is almost double of the single groove.

In the next problem, the physics of sweeping the previously entrapped fluid out of the groove created on one of the walls of a three-dimensional duct under gravitational acceleration has been explored. All the walls of the duct are considered to be uniform hydrophobically wetted and the surface of the groove is having uniform hydrophobic and neutrally wet surfaces in two different cases. The analyses have been done to see the effect of capillary number and groove height on the sweeping phenomenon. To explain all aspects of physics, the results are presented in the form of isosurface plots, mid-plane sliced view plots, vector plots and the plots showing

the wetted area and wetted length. In the analysis, it is found that there is a possibility to sweep out the previously entrapped fluid which is undesirable in many engineering applications, out of the groove with the help of sliding down the large size droplet. It is also observed that the wetting characteristics of the groove surface also play a major role in the sweeping phenomena. The hydrophobic surface of the groove in some cases allows the entrapped fluid to sweep out whereas neutrally wet groove surface does not allow the sweeping. In the parametric study of capillary number and groove height, it is found that the fraction of swept volume of the entrapped fluid varies from 0% to 100% for different sets of Ca and H. A 100% sweeping of entrapped fluid out of the groove is achieved for Ca=0.25, H=80 lu and Ca=0.40, H=80 lu.

Another study considers a three-dimensional confined wetted channel having an obstruction in the flow path of a spherical immiscible droplet. A rigorous study has been carried out to show the deformation and breakup dynamics of the droplet when it passes over the obstruction. The effects of capillary number, surface wettabilities, single spherical obstruction size and the pore structure of obstruction on the droplet deformation and breakup dynamics have been discussed in detail. The present results reveal that the dynamics of the droplet is largely affected by the capillary number. It is observed that the capillary number determines the passing time and deposited volume of the droplet on the obstruction upper surface. It is further observed that an increase in capillary number increases the deposited volume fraction whereas decreases the passing time in the case of hydrophobic wettability. Additionally, the morphology of the droplet changes when the surface wettability of the obstruction surface as well as channel walls changes. The deposited volume on obstruction upper surface is found to be decreasing when contact angle increases up to $\theta = 0^\circ$ (i.e., neutral wetting) and after that, it starts increasing. Moreover, the deposition of droplet fluid changes from upward to downward side of the obstruction as the wettability changes from hydrophobic to hydrophilic. The structure of the solid obstruction also plays a major role in the deformation and breakup of the droplet. The deposition of the droplet fluid is more in hydrophilic wetting of the obstruction surface compared to hydrophobic wettability of the obstruction in different agglomerate structures. It is also found that different agglomerate structures provide more restriction to the flow of droplet.

Finally, an investigation has been done to explore the behaviour of immiscible fluid flow through a porous media. The three-dimensional domain with periodic boundaries in span-wise directions has been considered and the domain is embedded with sphere pack solid particles that are continuous and connected to each other. The fluid flow through the porous media has been achieved by providing a pressure difference in the x-direction. The effects of different pore surface wettabilities, different porosities of the porous structure and changed pressure differences have been analyzed. The study reveals that the wettability of the pore surface affected the NWP fluid flow through the porous medium. The finger-like fluid front advancement is observed in case of hydrophobic wetting pore surface whereas more stable advancement of the fluid front is achieved in case of hydrophilic wetting of the pore surface at low porosity, $\phi = 0.48$. It is further explored that the NWP saturation in the pore volume is more for hydrophilic wettability compared to mixed and hydrophobic wettability of the pores. The advancement of fluid front and saturation have also been affected much by porosity. The porosity, which has a large dependence on the porous structure, is the prime parameter and primarily defines the behaviour of the fluid flow. In the present investigation, it is found that the large value of porosity gives rise to the NWP fluid saturation in the pores for all types of wettabilities of the pores. Similarly, an increase in the pressure difference, acting as a driving force, increases the movement of the fluid front advancement along with more saturation of the NWP fluid inside the pores.

9.2 Scope of future work

The present thesis gives an insight into the mesoscopic analysis of two immiscible fluid interaction under the action of gravitational acceleration inside a three-dimensional channel considering wetting characteristics of solid walls as well as the two-phase flow through a sphere pack porous media. The analyses explore the complex wettability-capillarity interaction physics associated with the immiscible liquids under various physicochemical conditions. To gain more insight into the multiphase-multicomponent flows with or without porous media, the following recommendations for future study may be suggested.

- The present Shan-Chen LBM code is developed with the assumption of the isothermal condition i.e., the temperature remains constant throughout the numerical experiment. However, there may be temperature change in the system which may affect the properties and behaviour of the system. Therefore, it is important to analyze the behaviour of the interaction of two immiscible fluids considering temperature change. This can be achieved by solving energy equation using thermal lattice Boltzmann methodology [106–114].

- In the present thesis, the analysis has been done using periodic boundary conditions in the flow direction for showing the droplet spreading and displacement on the channel wall. In all cases, a straight three-dimensional channel has been considered. As a scope of future study, the present code can also be modified to analyze the droplet formation and breaking in the junction type microchannel (e.g., T-type and cross junction channels) which is an important topic of research in biomedical field, e.g., drug delivery, as well as industrial application, e.g., emulsification. To numerically simulate this problem, the present code can be modified for velocity boundary conditions in the flow direction so that the flow boundary conditions can be applied for different fluids [115–119].

- The present code can be extended to study the effect of different porous structure on the liquid water transport experiment. In one of the problems, a regular sphere pack porous structure is considered for the two-phase liquid transport. For further study, the simple cubic, body-centred cubic and face-centred cubic spherical particle structures can be considered as a porous medium. Considering these porous structures, investigations can be performed to see the effect of wettability, porosity, pressure gradient and relative permeability on the liquid water transport or primary drainage experiment. For an industrial application like polymer electrolyte fuel cells, the effect of wettability-capillarity interaction on liquid water transport through the catalyst layer structure needs to be further explored considering different pore structures.

- In nature or industrial applications, the density and viscosity ratio of two-phase flow can be found equal to around 1000 and 20, respectively. The most common application is air-water two-phase flow in a fuel cell where density ratio can be around 1000 and viscosity ratio equal to 18. In literature, it is found that most of the basic LB models including Shan-chan model cannot handle such a large density and viscosity ratio alone. Therefore, other LB models [33, 34, 120] which can handle the issue of high density and viscosity ratio can be implemented.

References

[1] Brennen C.E. (2005) 'Fundamentals of Multiphase Flows', *Cambridge University Press.*

[2] Huang H., Sukop M.C., and Lu X. (2015) 'Multiphase Lattice Boltzmann Methods: Theory and Application', *WILEY Blackwell.*

[3] Dullien F. (1991) 'Porous media, fluid transport and pore structure', *Academic Press, Inc, San Diego.*

[4] Ingham D. and Pop I. (2002) 'Transport Phenomena in Porous Media II', *Pergamon, Oxford.*

[5] Broadwell J.E. (1964) 'Shock structure in a simple discrete velocity gas', *Physics of Fluids*, vol. 7, pp. 1243–1247.

[6] Kadanoff L. and Swift J. (1968) 'Transport coefficients near the critical point: A master-equation approach', *Physical Review A*, vol. 165, pp. 310–322.

[7] Hardy J., Pomeau Y., and de Pazzis O. (1973) 'Time evolution of a two dimensional model system. i. invariant states and time correlation functions', *Journal of Mathematical Physics*, vol. 14, pp. 1746–1759.

[8] Hardy J., de Pazzis O., and Pomeau Y. (1976) 'Molecular dynamics of a classical lattice gas: Transport properties and time correlation functions', *Physical Review A*, vol. 13, pp. 1949–1961.

[9] Frisch U., Hasslacher B., and Pomeau Y. (1986) 'Lattice-gas automata for the navier-stokes equation', *Physical Review Letters*, vol. 56, pp. 1505–1508.

[10] d'Humires D., Lallemand P., and Frisch U. (1986) 'Lattice gas models for 3d hydrodynamics', *Europhysics Letters*, vol. 2, pp. 291–297.

[11] Wolfram S. (1986) 'Theory and applications of cellular automata', *World Scientific, Singapore.*

[12] MacNamara G.R. and Zanetti G. (1988) 'Use of the Boltzmann equation to simulate lattice-gas automata', *Physical Review Letters*, vol. 61, pp. 2332–2335.

[13] Dahlburg J.P. and Montgomery D. (1987) 'Noise and compressibility in lattice-gas fluids', *Physical Review A*, vol. 36, pp. 2471–2474.

[14] Succi S. (2001) 'The lattice Boltzmann equation for fluid dynamics and beyond', *Oxford University Press.*

[15] Bhatnagar P., Gross P., and Krook M. (1954) 'A model for collision processes in gases. i. small amplitude processes in charged and neutral one-component systems.', *Physical Review E*, vol. 94, pp. 511–525.

[16] He X. and Luo L.S. (1997) 'A priori derivation of the lattice Boltzmann equation', *Physical Review E,*, vol. 55, pp. R6333–R6336.

[17] He X. and Luo L.S. (1997) 'Theory of the lattice Boltzmann method: From the Boltzmann equation to the lattice Boltzmann equation', *Physical Review E,*, vol. 56, pp. 6811–6817.

[18] Chapman S. and Cowling T. (1970) 'The mathematical theory of nonuniform gases', *Cambridge University Press, Cambridge.*

[19] Gunstensen A.K., Rothman D.H., Zaleski S., and Zanetti G. (1991) 'Lattice Boltzmann model of immiscible fluids', *Physical Review A*, vol. 43, pp. 4320–43 27.

[20] Rothman D.H. and Keller J.M. (1988) 'Immiscible cellular-automaton fluids', *Journal of Statistical Physics*, vol. 52, pp. 1119–1127.

[21] Grunau D., Chen S., and Eggert K. (1993) 'A lattice Boltzmann model for multiphase fluid flows', *Physics of Fluids A*, vol. 5, pp. 2557–2562.

[22] Dortona U., Salin D., Cieplak M., and Banavar J.R. (1994) 'Interfacial phenomena in Boltzmann cellular automata', *Europhysics Letters*, vol. 28, pp. 317–322.

[23] Shan X. and Chen H. (1993) 'Lattice Boltzmann model for simulating flows with multiple phases and components', *Physical Review E*, vol. 47, pp. 1815–1819.

[24] Shan X. and Doolen G. (1995) 'Multicomponent lattice-Boltzmann model with interparticle interaction', *Journal of Statistical Physics*, vol. 81, pp. 379–393.

[25] Chen H. (1993) 'Discrete Boltzmann systems and fluid flows', *Computational Physics*, vol. 7, pp. 632–637.

[26] Swift M.R., Osborn W.R., and Yeomans J.M. (1995) 'Lattice Boltzmann simulation of nonideal fluids', *Physical Review Letters*, vol. 75, pp. 830–833.

[27] Swift M.R., Orlandini S.E., Osborn W.R., and Yeomans J.M. (1996) 'Lattice Boltzmann simulations of liquid-gas and binary-fluid systems', *Physical Review E*, vol. 54, pp. 5041–5052.

[28] Sbragaglia M., Benzi R., Biferale L., Succi S., Sugiyama K., and Toschi F. (2007) 'Generalized lattice Boltzmann method with multirange pseudopotential', *Physical Review E*, vol. 75, p. 026702.

[29] Yuan P. and Schaefer L. (2006) 'Equations of state in a lattice Boltzmann model', *Physics of Fluids*, vol. 18, p. 042101.

[30] Zheng H., Shu C., and Zhang R. (2006) 'A lattice Boltzmann model for multiphase flows with large density ratio', *Journal of Computational Physics*, vol. 218, pp. 352–371.

[31] He X.Y., Shan X., and Doolen G.D. (1998) 'A discrete Boltzmann equation model for non-ideal gases', *Physical Review E*, vol. 57, p. R13.

[32] X. Y. He S.Y.C. and Zhang R.Y. (1999) 'A lattice Boltzmann scheme for incompressible multiphase flow and its application in simulation of rayleightaylor instability', *Journal of Computational Physics*, vol. 152, pp. 642–663.

[33] Inamuro T., Ogata T., Tajima S., and Konishi N. (2004) 'A lattice Boltzmann method for incompressible two-phase flows with large density differences', *Journal of Computational Physics*, vol. 198, pp. 628–644.

[34] Lee T. and Lin C.L. (2005) 'A stable discretization of the lattice Boltzmann equation for simulation of incompressible two-phase flows at high density ratio', *Journal of Computational Physics*, vol. 206, pp. 16–47.

[35] Dimitrakopoulos P. and Higdon J.J.L. (2001) 'On the displacement of three-dimensional fluid droplets adhering to a plane wall in viscous pressure-driven flows', *Journal of Fluid Mechanics*, vol. 435, pp. 327–350.

[36] Schleizer A.D. and Bonnecaze R.T. (1999) 'Displacement of a two-dimensional immiscible droplet adhering to a wall in shear and pressure-driven flows', *Journal of Fluid Mechanics*, vol. 383, pp. 29–54.

[37] Randive P. (2014) 'Mesoscopic modeling of capillarity-wettability interaction', *Ph.D. Thesis Department of Mechanical Engineering Indian Institute of Technology Guwahati, India.*

[38] Kang Q., Zhang D., and Chen S. (2002) 'Displacement of a two dimensional immiscible droplet in a channel', *Physics of Fluids*, vol. 40, pp. 3203–3214.

[39] Dupuis A. and Yeomans J.M. (2005) 'Modeling droplets on superhydrophobic surfaces: Equilibrium states and transitions', *Langmuir*, vol. 21, pp. 2624–2629.

[40] Zu Y.Q. and Yan Y.Y. (2010) 'Wetting behaviours of a single droplet on biomimetic micro structured surfaces', *Journal of Bionic Engineering*, vol. 7, pp. 191–198.

[41] Zu Y.Q. and Yan Y.Y. (2011) 'Lattice Boltzmann method for modelling droplets on chemically heterogeneous and microstructured surfaces with large liquidgas density ratio', *Journal of Applied Mathematics*, vol. 76(5), pp. 743–760.

[42] Kumar A., Williams S.J., Chuang H., Greend N.G., and Wereleye S.T. (2011) 'Hybrid opto-electric manipulation in microfluidicsopportunities and challenges', *Lab on a Chip*, vol. 11, pp. 2135–2148.

[43] Vananroye A., Cardinael R., Puyvelde P.V., and Moldenaers P. (2008) 'Effect of confinement and viscosity ratio on the dynamics of single droplets during transient shear flow', *Journal of Rheology*, vol. 52, pp. 1459–1475.

[44] Chang Q. and Alexander J.I.D. (2006) 'Analysis of single droplet dynamics on striped surface domains using a lattice Boltzmann method', *Microfluidics and Nanofluidics*, vol. 2(4), pp. 309–326.

[45] Huang J.J., Shu C., and Chew Y.T. (2009) 'Lattice Boltzmann study of droplet motion inside a grooved channel', *Physics of Fluids*, vol. 21, p. 022103.

[46] Son S., Chen L., Derome D., and Carmeliet J. (2015) 'Numerical study of gravity-driven droplet displacement on a surface using the pseudopotential multiphase lattice Boltzmann model with high density ratio', *Computers and Fluids*, vol. 117, pp. 42–53.

[47] Wang Q., Li Y., Yu Z., and Guo B. (2016) 'Numerical simulation of gravity-driven droplet displacement on an inclined micro-grooved surface', *ASME 2016 5th International Conference on Micro/Nanoscale Heat and Mass Transfer*, p. V001T01A006.

[48] Fan L., Fang H., and Lin Z. (2001) 'Simulation of contact line dynamics in a two-dimensional capillary tube by the lattice Boltzmann model', *Physical Review E*, vol. 63, p. 051603.

[49] Watanabe T. and Ebihara K. (2002) 'Numerical simulation of droplet flows and evaluation of interfacial area', *Journal of Fluids Engineering*, vol. 124, pp. 576–583.

[50] Ristenpart W.D., McCalla P.M., Roy R.V., and Stone H.A. (2006) 'Coalescence of spreading droplets on a wettable substrate', *Physical Review Letters*, vol. 97, p. 064501.

[51] Xing X.Q., Butler D.L., Ng S.H., Wang Z., Danyluk S., and Yang C. (2007) 'Simulation of droplet formation and coalescence using lattice Boltzmann-based single-phase model', *Journal of Colloid and Interface Science*, vol. 311, pp. 609–618.

[52] Nilsson M.A. and Rothstein J.P. (2011) 'The effect of contact angle hysteresis on droplet coalescence and mixing', *Journal of Colloid and Interface Science*, vol. 363, pp. 646–654.

[53] Xie G., Luo J., Yang Y., Guo D., and Si L. (2012) 'Water droplets on a hydrophobic insulator surface under high voltages: A thermal perspective', *Applied Physics Letters*, vol. 101, p. 131602.

[54] Yeh S., Fang W., Sheen H., and Yang J. (2013) 'Droplets coalescence and mixing with identical and distinct surface tension on a wettability gradient surface', *Microfluidics and Nanofluidicsics*, vol. 14, pp. 785–795.

[55] Moghtadernejad S., Jadidi M., Tembely M., Esmail N., and Dolatabadi A. (2015) 'Concurrent droplet coalescence and solidification on surfaces with various wettabilities', *Journal of Fluids Engineering*, vol. 137, p. 071302.

[56] Fakhari A. and Rahimian M.H. (2009) 'Simulation of falling droplet by the lattice Boltzmann method', *Communications in Nonlinear Science and Numerical Simulation*, vol. 14, pp. 3046–3055.

[57] Li Q., He Y.L., Tang G.H., and Tao W.Q. (2011) 'Lattice Boltzmann modeling of microchannel flows in the transition flow regime', *Microfluidics and Nanofluidics*, vol. 10, pp. 607–618.

[58] Fei K., Chen W.H., and Hong C.W. (2008) 'Microfluidic analysis of co2 bubble dynamics using thermal lattice-Boltzmann method', *Microfluidics and Nanofluidics*, vol. 5, pp. 119–129.

[59] Zhang J. (2011) 'Lattice Boltzmann method for microfluidics: models and applications', *Microfluidics and Nanofluidics*, vol. 10, pp. 1–28.

[60] Passandideh M., Bussmann M., Chandra S., and Mostaghimi J. (2001) '*s*imulating droplet impact on a substrate of arbitrary shape', *Atomization Sprays*, vol. 11, pp. 397–414.

[61] Link D.R., Anna S.L., Weitz D.A., and Stone H.A. (2004) 'Geometrically mediated breakup of drops in microfluidic devices', *Physical Review Letters*, vol. 92, p. 054503.

[62] Bakshi S., Roisman I.V., and Tropea C. (2007) 'Investigations on the impact of a drop onto a small spherical target', *Physics of Fluids*, vol. 19, p. 032102.

[63] Chung C., Ahn K.H., and Lee S.J. (2009) 'Numerical study on the dynamics of droplet passing through a cylinder obstruction in confined microchannel flow', *Journal of Non-Newtonian Fluid Mechanics*, vol. 162, pp. 38–44.

[64] Chung C., Lee M., Char K., Ahn K.H., and Lee S.J. (2010) 'Droplet dynamics passing through obstructions in confined microchannel flow', *Microfluid Nanofluid*, vol. 9, p. 1151.

[65] Protiere S., Bazant M.Z., Weitz D.A., and Stone H.A. (2010) 'Droplet breakup in flow past an obstacle: A capillary instability due to permeability variations', *Europhysics Letters*, vol. 92, p. 54002.

[66] Do-Quang M., Carlson A., and Amberg G. (2011) 'The impact of ink-jet droplets on a paper-like structure', *Fluid Dynamics and Materials Processing*, vol. 7, pp. 389–402.

[67] Gac J.M. and L.G. (2014) 'Lattice-Boltzmann modeling of collisions between droplets and particles', *Colloids and Surfaces A: Physicochemical and Engineering Aspects*, vol. 441, pp. 831–836.

[68] Juarez G., Gastopoulos T., Zhang Y., Siegel M.L., , and Arratia P.E. (2012) 'Splash control of drop impacts with geometric targets', *Physical Review E*, vol. 85, p. 026319.

[69] Salkin L., Courbin L., and Panizza P. (2012) 'Microfluidic breakups of confined droplets against a linear obstacle: The importance of the viscosity contrast', *Physical Review E*, vol. 86, p. 036317.

[70] Chakraborty S. (2015) 'Droplet dynamics in microchannels', *Encyclopedia of Microfluidics and Nanofluidics*, pp. 411–418.

[71] Chaudhury K., Mandal S., and Chakraborty S. (2016) 'Droplet migration characteristics in confined oscillatory microflows', *Physical Review E*, vol. 93, p. 023106.

[72] Hao L. and Cheng P. (2010) 'Pore-scale simulations on relative permeability of porous media by lattice Boltzmann method', *International Journal of Heat and Mass Transfer*, vol. 53, pp. 1908–1913.

[73] Buckles J.J., Hazlett R.D., Chen S., Eggert K.G., Grunau D.W., and Soll W.E. (1994) 'Toward improved prediction of reservoir flow performance: simulating oil and water flows at the pore scale', *Los Alamos Science*, (22), pp. 112–121.

[74] Xu R.N., Luo S., and Jiang P.X. (2011) 'Pore scale numerical simulation of supercritical co2 injecting into porous media containing water', *Energy Procedia*, vol. 4, pp. 4418–4424.

[75] Lawry M.I. and Miller C.T. (1995) 'Pore-scale modeling of nonwetting phase residual in porous media', *Water Resources Research*, vol. 31, pp. 455–473.

[76] Owens W.W. and Archer D.L. (1971) 'The effect of rock wettability on oil-water reiative permeability relationships', *Journal of Petroleum Technology*, pp. 873–878.

[77] Jerauld G.R. and Salter S.J. (1990) 'The effect of pore-structure on hysteresis in relative permeability and capillary pressure: Pore-level modeling', *Transport in Porous Media*, vol. 5, pp. 103–151.

[78] Oostrom M. and Lenhard R.J. (1998) 'Comparison of relative permeability-saturation- pressure parametric models for infiltration and redistribution of a light nonaqueous-phase liquid in sandy porous media', *Advanced Water Resources*, vol. 21, pp. 145–157.

[79] Kang Q., Zhang D., and Chen S. (2003) 'Simulation of dissolution and precipitation in porous media', *Journal of Geophysical Research*, vol. 108, pp. 2505 (1–9).

[80] Pan C., Hilpert M., and Miller C.T. (2004) 'Lattice-Boltzmann simulation of two-phase flow in porous media', *Water Resources Research*, vol. 40, p. W01501.

[81] Wang C., in: W. Vielstich, Lamm A., and (Eds.) H.G. (2003) 'Handbook of fuel cellsfundamentals, technology and applications', *John Wiley and Sons, Chichester*, vol. 3, p. 337 (Chapter 29).

[82] Wang C. (2004) 'Fundamental models for fuel cell engineering', *Chemical Reviews*, vol. 104, pp. 4727–4766.

[83] Zhu X., Sui P.C., and Djilali N. (2007) 'Dynamic behaviour of liquid water emerging from a gdl pore into a pemfc gas flow channel', *Journal of Power Sources*, vol. 172, pp. 287–295.

[84] Gostick J.T., Ioannidis M., Fowler M.W., and Pritzker M.D. (2007) 'Pore network modeling of fibrous gas diffusion layers for polymer electrolyte membrane fuel cells', *Journal of Power Sources*, vol. 173, pp. 277–290.

[85] Mukherjee P.P., Wang C.Y., and Kang Q. (2009) 'Mesoscopic modeling of two-phase behavior and flooding phenomena in polymer electrolyte fuel cells', *Electrochimica Acta*, vol. 54, pp. 6861–6875.

[86] Hao L. and Cheng P. (2009) 'Lattice Boltzmann simulations of liquid droplet dynamic behavior on a hydrophobic surface of a gas flow channel', *Journal of Power Sources*, vol. 190, pp. 435–446.

[87] Hao L. and Cheng P. (2009) 'Lattice Boltzmann simulations of anisotropic permeabilities in carbon paper gas diffusion layers', *Journal of Power Sources*, vol. 186, pp. 104–114.

[88] Hao L. and Cheng P. (2010) 'Lattice Boltzmann simulations of water transport in gas diffusion layer of a polymer electrolyte membrane fuel cell', *Journal of Power Sources*, vol. 195, pp. 3870–3881.

[89] Salah Y., Tabe Y., and Chikahisa T. (2012) 'Two phase flow simulation in a channel of a polymer electrolyte membrane fuel cell using the lattice Boltzmann method', *Journal of Power Sources*, vol. 199, pp. 85–93.

[90] Cho S.C., Wang Y., and Chen K.S. (2012) 'Droplet dynamics in a polymer electrolyte fuel cell gas flow channel: Forces, deformation, and detachment. i: Theoretical and numerical analyses', *Journal of Power Sources*, vol. 206, pp. 119–128.

[91] Cho S.C., Wang Y., and Chen K.S. (2012) 'Droplet dynamics in a polymer electrolyte fuel cell gas flow channel: Forces, deformation and detachment. ii: Comparisons of analytical solution with numerical and experimental results', *Journal of Power Sources*, vol. 210, pp. 191–197.

[92] Chukwudozie C. and Tyagi M. (2013) 'Pore scale inertial flow simulations in 3-d smooth and rough sphere packs using lattice Boltzmann method', *AIChE Journal*, vol. 59, pp. 4858–4870.

[93] Liu H., Valocchi A.J., Kang Q., and Werth C. (2013) 'Pore-scale simulations of gas displacing liquid in a homogeneous pore network using the lattice Boltzmann method', *Transport in Porous Media*, vol. 99, pp. 555–580.

[94] Wang A., Husar T., and Zhou H.L. (2003) 'A parametric study of PEM fuel cell performances', *J. hydrogen Energy*, vol. 28, pp. 1263–1272.

[95] Wolf-Gladrow D.A., *Lattice Gas Cellular Automata and Lattice Boltzmann Model: An Introduction* (Springer, 2000).

[96] Chen H., Chen S., Doolen G.D., Lee Y.C., and Rose H.A. (1989) 'Multithermodynamic phase lattice-gas automata incorporating interparticle potentials', *Physical Review A*, vol. 40, p. 2850.

[97] Young T. (1805) 'An essay on cohesion of fluids', *Philosophical Transactions of the Royal Society*, vol. 95, pp. 65–87.

[98] Mukherjee P. (2007) 'Pore-scale modeling and analysis of the polymer electrolyte fuel cell catalyst layer', *Ph.D. Thesis Department of Mechanical Engineering Pennsylvania State University,USA*.

[99] Dullien F.A.L., *Porous Media: Fluid Transport and Pore Structure* (Academic Press, San Diego, CA, 1992).

[100] Farhangi M.M. (2012) *Numerical study of droplet coalescence and droplet shedding on surfaces with various wettabilities*, Master's thesis, Master of Applied Sciences Thesis, Concordia University Montreal, Quebec, Canada.

[101] Kang Q., Zhang D., and Chen S. (2005) 'Displacement of a two dimensional immiscible droplet in a channel', *Journal of Fluid Mechanics*, vol. 545, pp. 41–66.

[102] Li Q., Chai Z., Shi B., and Liang H. (2014) 'Deformation and breakup of a liquid droplet past a solid circular cylinder: A lattice *b*oltzmann study', *Physical Review E*, vol. 90, p. 043015.

[103] Randive P., Dalal A., and Mukherjee P. (2014) 'Probing the influence of superhydrophobicity and mixed wettability on droplet displacement behavior', *Microfluidics and Nanofluidics*, vol. 17, pp. 657–674.

[104] Lavallee P., Boon J., and Noullez A. (1991) 'Boundaries in lattice gas flows', *Physica D: Nonlinear Phenomena*, vol. 47, pp. 233–240.

[105] Laroche C., Vizika O., and Kalaydjian F. (1999) 'Network modeling as a tool to predict three-phase gas injection in heterogeneous wettability porous media', *Journal of Petroleum Science and Engineering*, vol. 24, pp. 155–168.

[106] Alexander F.J., Chen S., and Sterling J.D. (1993) 'Lattice Boltzmann thermohydrodynamics', *Physical Review E*, vol. 47, pp. R2249–R2252.

[107] Qian. Y.H. (1993) 'Simulating thermohydrodynamics with lattice BGK models', *Journal of Scientific Computing*, vol. 8, pp. 231–242.

[108] Chen Y., Ohashi H., and Akiyama. M. (1994) 'Thermal lattice Bhatnagar-Gross-Krook model without nonlinear deviations in macrodynamical equations', *Physical Review E*, vol. 50, pp. 2776–2783.

[109] Renda A., Bella G., Succi S., and Karlin I.V. (1998) 'Thermohydrodynamic lattice BGK schemes with non-perturbative equilibria', *Europhysics Letters*, vol. 41, pp. 279–283.

[110] Zhang R. and Chen H. (2003) 'Lattice Boltzmann method for simulations of liquid-vapor thermal flows', *Physical Review E*, vol. 67, p. 066711.

[111] He X., Chen S., and Doolen G.D. (1998) 'A novel thermal model for the lattice Boltzmann method in incompressible limit', *Journal of Computational Physics*, vol. 146, pp. 282–300.

[112] Kupershtokh A.L., Medvedev D.A., and Gribanov I.I. (2017) 'Thermal lattice Boltzmann method for multiphase flows', *arXiv:1705.10045v2 [physics.flu-dyn]*.

[113] Yuan P. (2005) 'Thermal lattice Boltzmann two-phase flow model for fluid dynamics', *PhD Thesis, Department of Mechanical Engineering, School of Engineering, University of Pittsburgh*.

[114] Peng Y., Shu C., and Chew Y.T. (2003) 'Simplified thermal lattice Boltzmann model for incompressible thermal flows', *Physical Review E*, vol. 68, p. 026701.

[115] Gupta A. and Kumar R. (2010) 'Effect of geometry on droplet formation in the squeezing regime in a microfluidic T-junction', *Microfluidics and Nanofluidics*, vol. 8, p. 799812.

[116] Li Z., Kang J., Park J.H., and Suh Y.K. (2007) 'Numerical simulation of the droplet formation in a cross-junction microchannel using the lattice Boltzmann method', *Journal of Mechanical Science and Technology*, vol. 21, pp. 162–173.

[117] Yu Z. and Fan O.H.L. (2007) 'Experiment and lattice Boltzmann simulation of two-phase gasliquid flows in microchannels', *Chemical Engineering Science*, vol. 62, pp. 7172–7183.

[118] Alapati S., Kang S., and Suh Y.K. (2009) 'Parallel computation of two-phase flow in a microchannel using the lattice Boltzmann method', *Journal of Mechanical Science and Technology*, vol. 23, pp. 2492–2501.

[119] Liu H. and Zhang Y. (2011) 'Lattice Boltzmann simulation of droplet generation in a microfluidic cross-junction', *Communications in Computational Physics*, vol. 9, pp. 1235–1256.

[120] Zheng H., Shu C., and Chew Y. (2006) 'A lattice Boltzmann model for multiphase flows with large density ratio', *Journal of Computational Physics*, vol. 218, pp. 353–371.

Appendix A

Conversion of Units from Physical System to Lattice Boltzmann System

In real physical system, the parameters are defined based on SI units whereas in LBM lattice units are considered to define any parameter for simulation. This change in units of parameters sometime creates confusion. This description may resolve this confusion by explaining the conversion of units from physical to lattice systems. For the proper understanding, here the basic units considered in SI system are meter (m) for length, second (s) for time and kilogram (kg) for mass whereas in LBM, units can be defined as lattice length unit (lu) for length, lattice time unit (lt) for time and lattice mass unit (lm) for mass. In the below given procedure for conversion, subscript p stands for physical system and lb stands for lattice Boltzmann (LB) system.

Let us take an example where fluid flow takes place with the physical velocity, u_p. Now, to convert this physical velocity to lattice Boltzmann velocity, (u_{lb}), the following points can be considered. The first step is to choose the size of mesh in LB units and find the conversion parameters, C_l for length and time conversion parameter, C_t.

$$C_l = \frac{L_p}{L_{lb}} \tag{A.1}$$

Now, select the value of relaxation parameter, τ in the range of $0.5 \leq \tau \leq 2$ for minimizing the errors and achieving the stability. After selecting this value, kinematic viscosity in LBM can be calculated as

$$\nu_{lb} = C_s^2(\tau - \frac{1}{2}) \tag{A.2}$$

$$\nu_{lb} = \nu_p \frac{C_t}{C_l^2} \tag{A.3}$$

$$C_t = \frac{\nu_{lb}}{\nu_p} C_l^2 \tag{A.4}$$

After finding the primary conversion factors, C_l and C_t, the secondary conversion parameters for velocity, C_v can be found from the definition of velocity as

$$C_v = \frac{C_l}{C_t} \tag{A.5}$$

The LB velocity can be calculated as.

$$u_{lb} = \frac{u_p}{C_v} \tag{A.6}$$

Similarly, to calculate lattice Boltzmann pressure, the conversion parameter for density can be defined as.

$$C_\rho = \frac{\rho_p}{\rho_{lb}} \tag{A.7}$$

$$P_{lb} = \rho_{lb} C_s^2 \tag{A.8}$$

$$P_{lb} = \frac{\rho_p C_s^2}{C_\rho} \tag{A.9}$$

In this way, the units of different parameters can be converted from physical to lattice Boltzmann system or vice-versa. For example, based on the above mentioned conversion criteria, the physical dimensions of the domain chosen based on the polymer electrolyte fuel cell experiment [94] as given in Table A.1 can be converted in lattice units.

The physical dimensions are first converted to lattice units to carry out simula-

Table A.1: Physical dimensions of a typical polymer electrolyte fuel cell channel

Parameter	Values (m)
Channel length	0.07
Channel height	0.0061
Channel width	0.001

Table A.2: Physical and Lattice Units for droplet dynamics simulation

Physical units	Lattice units
ρ=965 kg/m^2	ρ=0.965
R=1.8mm=18$\times10^{-4}$	R=18
h=6.1mm	h=61

tions, with typical ranges for the governing parameters and the corresponding lattice unit values used in the present simulations shown in Table A.2.

LIST OF PUBLICATIONS

International Journal

1. **Bhardwaj, S.**, Randive, P. and Dalal, A., 2017, Lattice Boltzmann Simulations of Coalescence of Two Droplets on a Rectangular Channel Wall Considering Wetting Effects, Progress in Computational Fluid Dynamics, vol. 17(5), pp. 281-289.

2. **Bhardwaj, S.**, and Dalal, A., 2017, Mesoscopic Analysis of Dynamic Droplet Behavior on Wetted Flat and Grooved Surface for Low Viscosity Ratio, ASME Journal of Heat Transfer, vol. 139, No. 5, pp. 052002 (1-11).

3. **Bhardwaj, S.**, and Dalal, A., 2018, Mesoscopic Analysis of Three-dimensional Droplet Displacement on Wetted Grooved Wall of a Rectangular Channel, European Journal of Mechanics, B/Fluids, vol. 67, pp. 35-53.

4. **Bhardwaj, S.**, and Dalal, A., 2018, Sweeping of the Entrapped Fluid Out of the Groove in a Three-Dimensional Channel Using Lattice Boltzmann Method, European Journal of Mechanics, B/Fluids, vol. 72, pp. 328-339.

5. **Bhardwaj, S.**, Dalal, A., Biswas G., and Mukherjee P. P., 2018, Analysis of Droplet Dynamics in a Partially Obstructed Confinement in a Three-Dimensional Channel, Physics of Fluids, vol. 30, p. 102102

6. **Bhardwaj, S.**, Dalal, A., and Mukherjee P. P., Mesoscale Understanding of Capillarity Driven Two-Phase Flow in a Packed Bed Architecture, International Journal of Heat and Mass Transfer (Under Review)

International Conference

1. Randive, P., **Bhardwaj, S.**, and Dalal, A., Lattice Boltzmann Modelling of Capillarity-Induced Resonance of Blob inside a Circular Tube, Paper No: 526, 5th International and 41th National Conference on Fluid Mechanics and Fluid Power, December 12-14, 2014, IIT Kanpur, India.

2. **Bhardwaj, S.** and Dalal, A., 2016, Three-Dimensional Deformation of a Droplet on a Square Duct Wall Considering Wetting Effects, Paper No:289, 6th International Congress on Computational Mechanics and Simulation, IIT Bombay, India.

3. **Bhardwaj, S.**, and Dalal, A., 2016, Mesoscopic Analysis of Droplet Spreading Behaviour on Wetted Surface for Low Viscosity Ratio, Paper No: MNHMT2016-6492, ASME 2016 5th Micro/Nanoscale Heat and Mass Transfer International Conference, Biopolis, Singapore.

Book Chapters

1. Randive, P., **Bhardwaj, S.**, and Dalal, A., 2017, Lattice Boltzmann Modelling of Capillarity-Induced Resonance of Blob inside a Circular Tube, Fluid Mechanics and Fluid Power Contemporary Research, Lecture Notes in Mechanical Engineering, Springer.